

## ASTRONOMICAL ELECTRONOGRAPHIC PHOTOMETRY

by

SUSAN PATRICIA WORSWICK, B.Sc., A.R.C.S.

March 1975

A thesis submitted for the degree  
of Doctor of Philosophy of the  
University of London and for  
the Diploma of Imperial College.

Astronomy Group  
Physics Department  
Imperial College  
London S.W.7.

ABSTRACT

An outline is given of the various systems that have been developed for the production and reduction of electronographic exposures. The typical limits to photometric accuracy are discussed.

The performance of the individual constituents of a particular system consisting of a Spectracon image tube, nuclear emulsion and Joyce-Loebl MkIII CS microdensitometer is described.

The problems of mounting the image tube on a telescope are discussed and are illustrated by a description of a camera design for the Cassegrain focus of the 60-inch reflector at Boyden Observatory.

The computing procedures followed for the extraction of morphological and photometric data are given and are illustrated by some of the data produced so far. The need for monochromatic photometry of planetary nebulae is outlined and the suitability of electronography is shown by preliminary results from an ongoing observation programme.

The problem of the removal of photocathode non-uniformities is tackled and the limitations set by this procedure are discussed together with the implications for astronomical photometry.

Some improvements are proposed which might be made to existing systems and which should be considered in setting up new equipment.

### ACKNOWLEDGEMENTS

I would like to express my thanks to Professor J. Ring for his supervision and his continued interest in this work. I am also grateful for the help extended by many members of the Astronomy Group, both past and present, in particular Dr C.I. Coleman, Mr M.J. Cullum, Dr B.L. Morgan, Dr N.K. Reay and Mr C.L. Stephens.

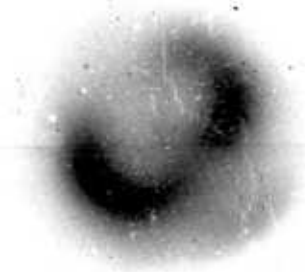
My thanks go to Messrs. Jack Crabtree and Roy Barr for trying to instil in me some understanding of mechanical design and to Mr Peter Sharp whose patient assistance has ensured that the microdensitometer has been kept in working order.

The 60-inch Boyden telescope was used by kind permission of the Director, Professor A.H. Jarrett. Time on the Isaac Newton telescope was allocated by the Large Telescope Users Panel; I am grateful to the staff of the Royal Greenwich Observatory for their assistance during these observing periods.

From October 1971 to October 1974 I was in grateful receipt of a Science Research Council studentship.

My thanks also go to Miss Y. Dearlove for typing this thesis.

Finally, I would like to dedicate this volume to my parents, whose support and encouragement have helped me throughout my studies.



NGC 7662



NGC 3242

v

"I at last deliver to the world a Work which I have long promised, and of which, I am afraid, too high expectations have been raised....

The labour and anxious attention with which I have collected and arranged the materials of which these volumes are composed, will hardly be conceived by those who read them with careless facility."

James Boswell

Advertisement to the First Edition  
of Boswell's Life of Johnson

## PREFACE

The only method by which information can be obtained about astronomical objects is by careful observation of that proportion of their radiation which reaches us. There is no way in which we can affect the processes within these objects and indeed, unless one restricts observations to the very closest of our neighbouring stars, all the photons that we are likely to detect in our lifetime have already left their sources.

Therefore the astronomer must rely on collecting as large a fraction as possible of the incoming light and on processing it to yield spectral, spatial and photometric information. To undertake this sort of work one must always be aware of the improvements in detection techniques and their possible application to both old and new problems.

For over one hundred years the predominant tool for optical observations has been the photographic plate which provides a practical means of integrating and storing the incoming light. The "two-dimensional" nature of this detector means that accurate relative positions can be obtained while a knowledge of the characteristic curve, relating density to exposure, for each plate yields photometric data. Over the years emulsions have been tailored to the needs of the astronomer so that long exposures of fairly faint objects may be undertaken. The detection efficiency of the plates has also been improved by various techniques such as baking and nitrogen flushing which increase the sensitivity.

The inability of the emulsion to record incident fluxes lower than a certain threshold value, coupled with limited storage of the plate, requires that exposures be tailored to specifically faint or bright features within any given field. Then a cross-calibration between plates

is required. However, for survey work, where a detector of very large surface area is required, the photographic plate remains the only practical solution.

The photoelectric effect is a process which has true linearity; it is also more efficient than photography. If the electrons released from a photocathode can be detected and stored a fairly straightforward method for photometry can be obtained. Originally the process was employed in single channel detectors (using photomultipliers) for photometry of stars and for the measurement of integrated fluxes from objects. The area of sky from which the light is being collected is defined by a diaphragm and the total amount of light which falls within this aperture is measured. The signal from the photomultiplier can either be recorded in analogue form or the amplified pulses from individual photo-electrons can be counted. The severe drawback of this method is its single channel nature which necessitates the use of a large amount of telescope time if a large area is to be covered. Very often photoelectric measurements are used to calibrate photographic photometry which can cover a much larger field.

Obviously if the advantages of linearity and high sensitivity of the photoelectric process are coupled to a two-dimensional form of image recording an improvement in detection limits should be expected.

The development of image tubes which retain spatial information within a focussed electron image has produced several variants, each with different read-out systems. Cascade devices simply act as image intensifiers, the final stage having a phosphor screen at the output end, the light being focussed onto a photographic emulsion using a coupling lens or more recently, a fibre-optic plate. Electronographic detectors, which are single stage devices, use nuclear track emulsions to register

the electron image directly. Television-type systems, where charge is stored in a target, produce an analogue signal using an electron beam read-out. Finally there are photon counting systems or more strictly photoelectron counting systems which use computer memory or magnetic tape as the storage medium. These latter devices have only produced one-dimensional information (e.g. Spectra) so far but two-dimensional read-out with about  $10^5$  picture points is now technically feasible.

In each of these types of systems it is necessary to evaluate the efficiency of the detection process and the amount of noise that is introduced by the detector. This has led to the concept of detective quantum efficiency (DQE) as a figure of merit. This compares the performance of the measuring device with a so-called "perfect" detector which would register every incoming photon with equal weight. If the measured signal-to-noise ratio of the detected signal is  $|S/N|_{OUT}$  and the incoming signal-to-noise ratio is  $|S/N|_{IN}$  then the DQE(E) is given by

$$E = \frac{|S/N|_{OUT}^2}{|S/N|_{IN}^2}$$

The incoming signal-to-noise ratio is just the photon flux (M) divided by its shot noise ( $\sqrt{M}$ ); thus the DQE is given by

$$E = \frac{|S/N|_{OUT}^2}{M}$$

It can be seen that to maximise this quantity it is necessary to detect as many of the incident photons as possible with an equal weighting.



Photoelectron counting, when available in two dimensions, will provide the nearest approximation to this process. However, at the moment other forms of detection must be investigated. They are all analogue techniques and therefore each photoelectron event will not be given equal weighting in the read-out process.

Another important consideration is the dynamic range of the device which is basically limited by the amount of storage available per picture element. With image intensifier systems this limit is set by the photographic emulsion. In electronographic systems again it is emulsion which provides the limitation but the grain size of the nuclear track emulsions is small; thus the storage per picture element is larger than for photographic plates. Television-type systems can be limited by the charge that can be stored on the target while a photoelectron counting system will have virtually unlimited storage for any single element but the range of brightness within a single exposure is governed by the maximum data rate that can be handled by the system.

If a useful comparison is to be made between the various methods of detection the data have to be compared at a comparable point. That is the stage where one has extracted the numerical information that is going to be processed to produce the final photometric and spatial data. Thus, in the case of emulsions being used as an intermediate store, the method by which the density data is obtained becomes an integral part of the overall system.

Therefore, it is only by a knowledge of the interaction of the various parts of the system of image tube, emulsion and microdensitometer that the true limiting performance can be defined.

Part of the work for this thesis has been to undertake a study of the interaction of various parts of a specific electronographic system and to understand the resultant limitations to photometric accuracy.

At the same time the application of the system to astronomical problems has led to a clearer understanding of the practical aspects of operating an image tube on a telescope and the areas where minor modifications would greatly assist the observer and would help to obtain the best performance from the device.

LIST OF CONTENTS

<u>Chapter I: Electronographic Photometry.</u>	1
Spectra	7
Star Fields	10
Extended Objects	19
<u>Chapter II: The Photometric System</u>	26
2.1 The Spectracon	26
2.2 Nuclear Track Emulsion	31
2.3 The Microdensitometer	38
2.3.1 The Joyce-Loebl Mk III CS Microdensitometer	39
2.3.2 Accuracy of Spatial Sampling	46
2.3.3 Linearity	56
2.3.4 Microdensitometer Noise	63
<u>Chapter III: Astronomical Observations</u>	69
3.1 Spectracon Cameras	69
3.1.1 Weight and Dimensions	69
3.1.2 Cooling	71
3.1.3 Power Supplies	72
3.1.4 Adjustments to Position Angle and Focus	72

3.1.5 Aquisition and Setting	73
3.1.6 Additional Requirements	73
3.1.7 Spectracon Camera for a 60 inch Reflector	75
3.2 Observing Procedures	78
3.3 Scanning and Computer Processing of Electronographs	79
3.3.1 Scanning	79
3.3.2 Computer Processing	81
3.4 Astronomical Observations	89
3.4.1 Planetary Nebulae	90
3.4.1.1 Formation	90
3.4.1.2 Spectra	93
3.4.1.3 Structure	99
3.4.2 Monochromatic Photometry	102
3.4.3 Spectracon Observations	104
3.4.3.1 Nebular Dimensions	106
3.4.3.2 NGC 6543	108
3.4.3.3 NGC 7662	112
3.4.3.4 NGC 3242	117
<u>Chapter IV</u> : Limitations set by Photocathode Non-uniformities	127
4.1 The Calibration Process	127
4.1.1 Location	128
4.1.2 Matching	131
4.1.3 Correction of Data	133
4.2 Practical Limitations of the Calibration Process	133
4.3 Noise Power Spectra	141
4.4 Limitation to Photometric Accuracy	153

<u>Chapter V: Conclusions and Future Work</u>	159
APPENDICES	165
<u>Appendix I: Processing of Electronographic Emulsions</u>	166
<u>Appendix II: Computer Programs</u>	167
<u>REFERENCES</u>	203

CHAPTER 1

ELECTRNOGRAPHIC PHOTOMETRY

"The naked papers, without an historical treatise interwoven, require some other book to make them understood."

Samuel Johnson (1709-1784)

The original concept behind the electronographic process was put forward by Kiepenheuer in 1934 (1). Despite the simplicity of the idea of using the quantum efficiency and linearity of the photoelectric process coupled to the information storage capabilities of an emulsion, the development of viable detectors has been a long and involved process.

The present-day devices fall into two main categories, those in which the emulsion and the photocathode are contained within the same envelope for the duration of the exposure, as in the Kron camera (2), or for longer periods, as in the Lallemand camera (3), and the devices such as the Spectracon (4) and the McMullan wide-field camera (5) where a permanent thin mica membrane is placed between the emulsion and the main part of the tube containing the photocathode and electron optics. The latter devices require a higher operating potential to ensure that a substantial proportion of the electrons released from the photocathode pass through the mica membrane, while retaining sufficient energy to leave tracks in the emulsion. The typical operating voltage for the Kron and Lallemand devices is about 25 → 30 KV, whereas for the Spectracon and McMullan cameras a voltage of 40 KV is required. Due to scattering within the mica the emergent photoelectrons (about 75% of the incident electron flux) have an energy distribution which peaks at about 28 KV

### ELECTRON ENERGY DISTRIBUTION IMPOSED BY MICA WINDOW

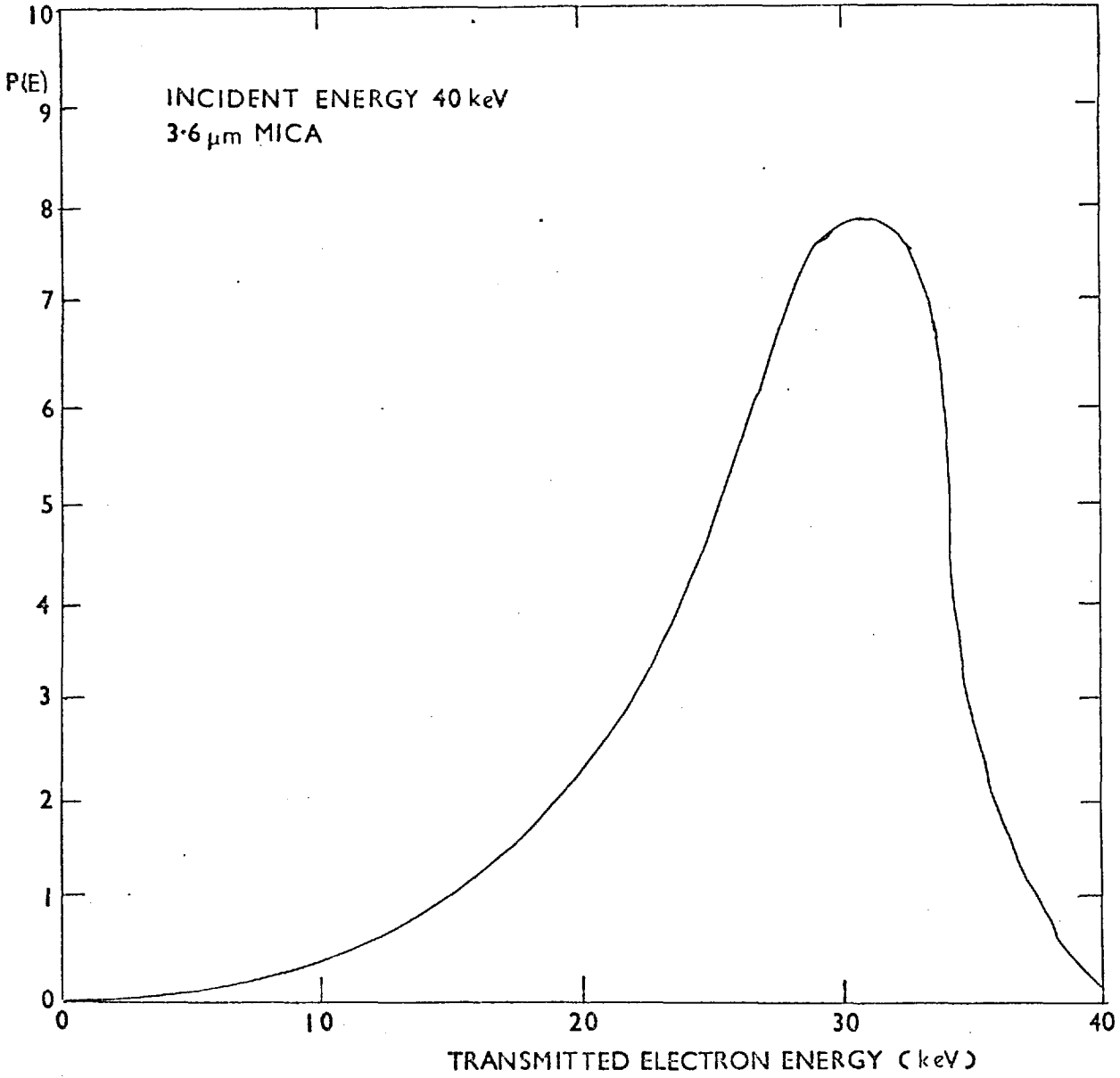


FIGURE 1-1

(see Fig. 1.1). Thus, although a thin membrane output window improves the potential shelf life of the device by preventing contamination of the photocathode by substances outgassed from the emulsion and, in the case of the Spectracon, means that the unit can be used without complicated auxiliary vacuum equipment, its effects on the photoelectrons can also have a bearing on the overall photometric performance of the device. Since each photoelectron reaching the emulsion leaves a track, the length of which is energy-dependent, the higher working voltage and the energy distribution of emergent electrons can affect both the storage capabilities of the emulsion and the "weighting" given to the individual tracks. Coleman (6) has shown that these are important considerations when making an assessment of the detective quantum efficiency (DQE) of a device such as the Spectracon.

Three of the devices mentioned, the Lallemand camera, the Kron camera and the Spectracon are in regular use on telescopes. Thus substantial quantities of electronographic data are becoming available to the general astronomical community, and the emphasis is moving towards the development of methods for the efficient retrieval of the large amount of information stored on each exposure.

Due to the high storage capacity of fine-grain nuclear track emulsions, such as Ilford L4, used for electronography and the linear relationship between the density and exposure which has been shown to hold to densities of the order of  $5D$  (7), any measuring machine used for data retrieval must be capable of accurate and linear measurement over this whole range. Since density can be related to the transmission of a sample in the following way

$$D = -\log_{10} T$$



it can be seen that the measuring system, which responds to the light transmitted by the plate, will have to cope with incident fluxes varying by about five orders of magnitude.

The resolution of electronographic devices is high - the electrostatically-focussed Lallemand and Kron cameras reach about 70  $\mu\text{p}/\text{mm}$  as does the magnetically-focussed Spectracon when operated at single-loop focus. Higher resolutions have been obtained using magnetically-focussed devices, for example of the order of 120  $\mu\text{p}/\text{mm}$  at two-loop focus for the Spectracon. In most cases the resolution of the astronomical exposure will be set by the size of the "seeing" disc and the spatial sampling rate required will be similar to that for a photographic plate. However, in certain cases, where either the optics have been designed to match the resolution of the device, or where measurements for accurate photometry in regions of rapidly changing density are needed, samples may be required at separations amounting to only a few microns.

Since each photoelectron is capable of leaving a track in the emulsion the electronographic process does not suffer from reciprocity failure. That is to say, there is no "threshold" incident photon flux required before an image starts to build up. The only effects that have to be taken into account when measuring plates at low density are those of plate fog which can be very low (less than 0.03 D for L4 (8)) and those arising from any dirt picked up on the emulsion during processing. Due to the fine grain and high storage of the emulsions such as L4 the human eye is totally incapable of assessing the information stored in the exposure, and, even for straightforward morphological studies, contour maps produced from density measurements of the plates are required to reveal the structure present in the object. Therefore, when using electronographic techniques, the measuring machine

and the subsequent data processing are equally as important as the primary detector.

As with many new astronomical techniques, some of the first work done using electronography was to take spectra (9,10). When working with spectral data the reduction of the exposures can be straightforward and the amount of data fairly small if it is possible to reduce the information to "one dimension". This is true where the spectrum has been artificially broadened and where the image geometry is good. In this case the measuring aperture of the machine can be extended perpendicular to the dispersion and a fairly slow scan along the length of the spectrum can be used, thus allowing a larger "dwell time" per sample point. Both of these methods serve to improve measurements of high density where the microdensitometer may be photon noise-limited and, since only a few scans are required, without making the measuring time prohibitively long. If, however, one is dealing with time-resolved spectra (11), or spectra containing spatial information (for example across the diameter of a galaxy), or distorted spectra, then the sampling aperture must be made small and thus the number of sample points becomes large. The problems are then the same as those of the extraction of spatial information from direct exposures.

For two-dimensional data, whether it be from star fields, extended objects or spectra, it is necessary to be able to produce accurate density measurements from samples taken at small intervals and at fairly high rates if the scan time is not to be too long. Of late several scanning machines which are capable of high-speed sampling have been developed, mainly for work on aerial survey photographs. Since many of the problems of information retrieval

and data handling are common to the fine-grain, high-storage, astronomical, photographic emulsions such as IIIaJ, these devices are finding their way into use by astronomers. However, photographic emulsions generally saturate at a density not much greater than 2D. With this limited density range fast scanning machines can be used to good advantage but, with the high densities present in electronographs and the short sampling periods dictated by high-speed scanning, the measurement of density may become very inaccurate due to the low photon-flux reaching the microdensitometer detector. Also, due to the linear density-exposure relationship, a stringent set of conditions are set on the inherent linearity of the measuring machine.

Therefore, when studying the limiting photometric accuracy of observations, it is necessary to consider the overall performance of a system comprised of the image tube, the emulsion and the scanning machine. The final results will obviously be peculiar to a particular set of equipment, but it should be possible to outline general trends which have a bearing on other systems.

Once having obtained numerical data from electronographic exposures the subsequent processing is usually tailored to the specific problem being studied. However, in some cases the problems that have been tackled have been dictated by the form in which data can be extracted. The rest of this chapter is taken up with a brief description of some of the methods used so far for processing of electronographic exposures and an outline of the advantages and limitations of various systems.

Broadly speaking, the photometry that has been undertaken using electronography can be split into three main categories:

- 1) Spectra
- 2) Starfields
- 3) Extended Sources

This roughly follows the chronological order in which electronography was first usefully applied in each branch. The sequence stems partly from the availability of detectors and partly from the development of the necessary tools for extracting the information from the exposures.

#### 1) Spectra

The first electronographic camera that was available for use on a telescope was the one developed by Lallemand in France. Work on this device was first started in 1936 (12) but it was not until the early sixties that it really came into regular use. It was originally mounted at the Coudé focus of the Lick 120-inch reflector in 1959. It was used with a grating giving a dispersion of  $48 \text{ \AA}/\text{mm}$  at the photocathode, which corresponds to a dispersion of about  $64 \text{ \AA}/\text{mm}$  at the plate since there is a demagnification of about 0.75 produced by the electron optics. The first result from this device was obtained on the nucleus of M31 (13). This was shown to be in rapid rotation by the curvature of the lines that showed up due to the large scale of the Coudé spectrograph perpendicular to the dispersion. Mainly, this was a case of utilising the speed of the device to register an image that could not be easily obtained using a photographic plate. Ilford G5, a fairly fast emulsion, was used, and the data reduction took the form of accurate positional measurement of the lines rather than that of accurate densitometry. As well as applying this device

to other problems involving the dynamics of objects as derived from their spectra (14,15) it has been turned to the problem of time resolved spectra of variables (16). The star is trailed along the slit manually, giving a time resolution of the order of a few minutes. As well as obtaining relative fluxes by scanning along the spectrum, a scan along a line perpendicular to the dispersion will yield a record of the variations within one line. Again it is a case of utilising the speed of the device to obtain information that could not be registered using a photographic plate.

The linear response has been used to derive energy distributions of stars and nuclei of galaxies (15,17,18) and to study the intensities of emission lines in planetary nebulae (19,20). In these cases the photometry is of more importance. However, in all these observations the information which has been extracted has been in the form of single scans and, perhaps of necessity, only portions of the total information present have been selected. Similar work is now being undertaken with the Spectracon on the same telescope and using identical techniques (21,22). For both the Lallemand camera and the Spectracon, Walker has found that the limitations on positional measurement are set by the accuracy of the measuring engine and that the wavelength resolution is equal to, or better than, that normally obtained with photographic spectra of the same dispersion.

The Spectracon, as its name implies, was originally considered as a device for studying spectra. The output mica window was made long and narrow (30 mm x 5 mm) since it was thought necessary to keep to this sort of configuration to retain sufficient strength in the 4  $\mu$ m mica sheet to withstand atmospheric pressure. Being a fairly compact

sealed unit the Spectracon has been used as a primary detector in two astronomical spectrographs designed to accommodate image tubes (23). In both cases special optics were required (24) together with a focussing solenoid designed to give the required uniformity of field at the focal plane. Once designed, these spectrographs will accept standard Spectracon image tubes which may have photocathodes of different types and therefore differing spectral responses. The focussing solenoid is provided with scan coils so that the image may be trailed electronically in a direction perpendicular to the dispersion. Thus the spectrum may be artificially broadened without movement of the telescope or instrument. The two spectrographs have been used regularly on the 98" Isaac Newton Telescope and 36" telescope at the Royal Greenwich Observatory, Herstmonceux, and on the 74" reflector which, until recently, was sited at Pretoria, South Africa and is now being moved to a better site at Sutherland.

Being "user instruments" the spectrographs have been used on many different problems of both stellar spectra (25,26) and studies of extended objects (27). Again in some cases accurate photometry has only been obtained for what is virtually "one-dimensional information" and the faster electronographic emulsions have been used to obtain spectra in fairly short exposure times for the purposes of line identification rather than photometry. Using the linear response, coupled with fairly simple reduction methods, it is possible to obtain information which would not be readily available from a single photographic plate.

## 2) Starfields

It is perhaps in the study of star clusters that electronography has one of its primary applications and also where the most difficulties in data reduction arise. The advantages of the process are threefold:

- a) The large dynamic range of the process means that both bright and faint stars can be registered on the same plate. Therefore it is possible to measure stars in the very bright central regions of the cluster and relate them to those in outer regions that are easy to measure as standards using conventional photoelectric techniques.
- b) The linearity of the process makes the transference of magnitudes from the standards to the rest of the cluster easy. Only a few standards are required and there is no need to set up different sequences for different magnitude regions as is required for photographic photometry.
- c) Basically one is performing photoelectric photometry in two dimensions. Since the data is recorded on emulsion the "diaphragm" through which one makes a measurement of the stellar magnitude can be set during data reduction and thus effects such as crowding of the field can be taken into account. Also one is simultaneously measuring many stars so that the telescope time required is greatly reduced.

However, the rapid extraction of data from such plates is still not a routine process, although various methods have been tried.

Table 1.1Errors obtained from profile method of magnitude determination

Magnitude Interval	Probable Error	
	Observed (mag)	Predicted (mag)
16.0<m<16.9	±0.020	±0.001
17.0<m<17.9	±0.023	±0.002
18.0<m<18.9	±0.028	±0.005
19.0<m<19.9	±0.035	±0.010
20.0<m<20.9	±0.050	±0.028
21.0<m<21.9	±0.072	±0.062
22.0<m<22.9	±0.146*	±0.161

\* Small sample

Measurements taken from a 180 minute exposure using a Spectracon plus L4 emulsion on a 60-inch reflector. Half-height diameter of image =  $2.1^{\circ}$  (110 $\mu$ m).



The most regular production of results has come from Walker (28,29,30,31,32), who used the Spectracon on the 60" reflector at Cerro Tololo to obtain B and V observations of 13 clusters in the Magellanic Clouds. The method used for extracting the data is simple but slow, and only a fraction of that present on the plate is used. Walker and Kron (33) showed that magnitudes of stars could be determined by using the profiles of stellar images on in-focus electronographic exposures over a range of 5 magnitudes up from the plate limit. To extract the full information the density volume of the image should be taken, and using an integrating microdensitometer designed by Hewitt (34), the range can be pushed to 7 magnitudes (35). Walker found that the use of the volume method in the crowded regions of the cluster led to a larger scatter in the magnitudes obtained <sup>than</sup> when the profile method was used (28). To obtain the profile the image is scanned using a Joyce-Loebl microdensitometer operated as a simple manually-controlled device. Using a measuring aperture of  $12.5 \times 12.5 \mu\text{m}$  the image is moved back and forth until centred in the "Y" direction, and then a scan is made across the diameter. Variations in local sensitivity of the photocathode are corrected by using a map obtained from an exposure of the dawn sky.

Table 1.1 shows the errors obtained using this method for different magnitude regions (36). These are compared with the error one would expect from an ideal detector registering sources of differing brightness against a fixed background which is the predominant source of noise (37). It can be seen for the brighter stars a limiting accuracy of about  $0.02^m$  is reached. Walker attributes this effect to the grain structure of L4 emulsion, since using a volume-integral method on a small sample of the stars produces a drop in the error.

However, apart from the random effects of grain statistics one must take into account microdensitometer noise at the bright magnitudes and residual effects of local variations in sensitivity due to both photocathode and emulsion.

Wlérick et al (38) have undertaken stellar photometry using the Lallemand camera and methods that are somewhat similar to those used by Walker. The reduction of the data is limited to manual scanning of the images and several procedures have been investigated. They have found local variations in sensitivity across both the photocathode and the emulsion of the order of 20% over distances of 20 mm and 8 mm respectively. Therefore they use the night sky background around an object as a measure of the sensitivity of the overall system from point to point within the exposure. There are certain limitations to this method. Since one is using the night sky as a uniform light source emulsion fog must be low, as must the tube background. Also, scattered light and reflections within the optical system must be removed, since all these may produce effects which are not uniform across the image plane. Also this method will only work with those objects that are small as compared with the scale of the sensitivity variations.

Four methods of measuring stellar magnitudes have been studied. Low scattering in nuclear emulsion means that bright star images do not tend to spread as they do in photographic plates. Therefore, assuming that the image diameter is the same for a bright or faint star, the peak density of the image can be taken as a measure of the magnitude. Wlérick et al have also used the profile method of Walker, a variant on this where three sections are used, the central one and one either side spaced by approximately the width of the measuring slit, and finally the density volume of the object obtained from the areas of several profiles across the whole star. With the Lallemand camera

there is a pincushion distortion produced by the electron optics, which leads to an increase in the size of the images at the edge of the field. Since the sky background and the stellar image are spread in the same way there is no need to correct the measures made using the maximum density measurement. For the other methods corrections must be put in for the effect of image spreading on the measurement of local sensitivity. More important in the outer regions of the photocathode are astigmatism and field curvature, which distort the image - in these cases the density volume method is the one most easily applied. Practically, the simpler and faster methods are limited to the region of the exposure where these distortions are small as compared with the image sizes (typically  $60\ \mu\text{m}$  to  $80\ \mu\text{m}$ , corresponding to  $1.5''$  to  $2''$ ); this area is a circle of about 12 mm diameter. To obtain 1% accuracy on the stellar images it is necessary to allow for the effects from pincushion distortion right across the field. Using these methods a study of stars in the field of BL Lacertae was undertaken; the sample contained about 15 stars which had been measured photoelectrically. Using both the density volume method and the three-area method an accuracy of approximately 2% has been obtained on stars in the region  $14^{\text{m}} < B < 19.3^{\text{m}}$ .

All the methods described so far are slow and, apart from the integrating microdensitometer used by Ables et al (35), all the data is obtained by manual scanning. With the general use of measuring systems which produce digital output, the application of computer processing to the large amounts of data has been investigated. The scanning of the plate need not now be selective, providing that either the program is sufficiently "intelligent" to recognise a star, or there is some form of interaction between the system and the user. However,

to store digital data of a whole starfield, even from tubes of fairly restricted image area, over a million picture points must be kept so that they are readily available to the computer. Also, to produce such large amounts of data, there is a minimum speed required of the measuring machine if problems of long-term stability are not to be important.

An interactive program for the processing of star fields has been produced at Imperial College (39). Data produced by a Joyce-Loebl microdensitometer is stored on magnetic tape and is subsequently processed using a CDC 6600 computer coupled to an interactive graphics terminal. The magnitude of the star is estimated by making repetitive fits of two orthogonal gaussian profiles to the raw data and then using these to calculate the density volume of the image. The various stars can be "called up" by using rough coordinates obtained from a CALCOMP plot of the whole field. The area around the stellar image is displayed and the position of the window over which the fit is to be performed can be changed. Residuals between the gaussian fit and the raw data can then be displayed.

In the method mentioned above the locations of the stars have to be fed into the program by the user. A system developed by Newell and O'Neill (40,41,42) for ESP (Electrographic Stellar Photometry) has a data "thresholding" procedure for searching large arrays of data. This locates a peak by two criteria:

- 1) It must have a density greater than, or equal to, that of the surrounding eight points.
- 2) It must lie above a preset threshold density level.

These peaks are plotted on a map. Those that are due to dirt and non-stellar objects are rejected and then small subsets of data centred on the remaining peaks are retrieved from the random access disc, where the main scan is stored, and are processed using the main photometric reduction routines.

The density volume of the star is extracted by using either curve-fitting routines or a numerical integration technique which is faster than the curve-fitting and therefore used for large amounts of data. The method does not require that a zero level be set for each star and so can be used in fairly crowded fields. In effect, a variable diaphragm is used on the stellar image and the optimum size of this window, for a numerical integration, is determined by the variation of the difference in magnitudes obtained by integrating in two orthogonal directions with the different window sizes. When this difference reaches a minimum the window size can be set. This is obviously dependent on the crowding of the field and the seeing conditions, and so it can be tailored to a particular group of stars. Once a pseudo-magnitude of the star is found by one, or an average of several, integrations the whole field is calibrated by comparing the measured magnitudes with established magnitudes of standard stars. Using this method a curved magnitude calibration curve has been obtained. The curvature is attributed to two main causes:

- 1) The effects of transmission averaging in the microdensitometer on the measured density.
- 2) The effects of the upper density limit of the microdensitometer at the centres of dense images.

Table 1.2

Plate-to-Plate agreement of Electronographic Stellar Magnitudes  
obtained from the cluster M13

Magnitude $m_V$	Error in magnitude determination $\Delta m_V$
12.76	$\pm 0.037$
13.51	$\pm 0.034$
14.58	$\pm 0.015$
15.45	$\pm 0.013$
16.30	$\pm 0.014$
17.43	$\pm 0.035$
18.47	$\pm 0.066$
19.07	$\pm 0.100$

Both effects cause an underestimation of the magnitudes of the bright stars. The former can be minimised by using as small an aperture as possible, and the latter can be improved by increasing the area of integration. However, departures from linearity then occur in the faint stars due to the inclusion of parts of surrounding objects, and the fainter objects are systematically measured too bright. In practice it has been found that the calibration curve maintains its shape from plate to plate and is wavelength-independent. Thus it can be used for all plates obtained and reduced under the same conditions.

In a study of two short-exposure plates of M13 Newell and O'Neill have shown that this method can provide accurate photometry. Using a PDS microphotometer to produce digital data with a raster scan of  $10\ \mu\text{m}$  in X and Y and a projected measuring aperture of  $20\ \mu\text{m}$ , which corresponds to 1 arcsec on the plate, a whole exposure of  $1.8\ \overset{\text{cm}}{\mu\text{m}} \times 1.8\ \overset{\text{cm}}{\mu\text{m}}$  was measured producing about  $3\frac{1}{2}$  million densities. The integration for the magnitude determination was carried out over an effective aperture of 8.5 arcsecs. This method of integration suffers from centring errors. The machine can accurately repeat measurements to about  $\pm 0.003^{\text{m}}$ , but if the scan pattern is shifted across the image a variation of about  $\pm 0.01^{\text{m}}$  can arise in the magnitude obtained. This is for images of about  $40\ \mu\text{m}$  diameter scanned at  $10\ \mu\text{m}$  intervals. Reducing these effects by reducing the step length, or increasing the aperture over which the integration is made, results in greatly increased computing time and data storage problems in the first case, and effects arising from background crowding in the latter. A plate-to-plate agreement test was then undertaken using two exposures of different length. The results are shown in Table 1.2. The increase

in standard error in the magnitudes of the brighter stars is attributed to calibration errors as the microdensitometer upper density limit was approached for stars brighter than  $14^m$ .

It can be seen that for regular reduction of large numbers of cluster plates methods such as the one above have to be used. To be able to employ these sorts of techniques one needs not only the machine to extract the data from the plate but also the availability of fairly sophisticated computing facilities. Investigations into similar techniques are being undertaken by Heckathorn and Chincarini (43) and Purgathofer (44a).

### 3) Extended Objects

The study of extended objects by electronographic means has mainly come into its own with the availability of digital output from microdensitometers. As pointed out previously an electronographic image does not reveal much when visually inspected and it is necessary to produce some sort of contour map to study the morphology of the source. Machines such as the Joyce-Loebl isodensitracer will produce maps with a varying number of grey levels, but the one scan of the object will present spatial details at the expense of photometric information. Equally well, manual scans across sections within the object, or the use of an integrating microdensitometer such as that used by Ables and Kron (44), will extract photometric information while losing a fair proportion of the morphological detail. By scanning the image and storing the data in digital form it is possible to process the results from one scan in several ways to yield the required spatial and photometric information.



Using a Joyce-Loebl isodensitracer, Walker (22,45) has undertaken morphological studies of both planetary nebulae and extra-galactic nebulae from exposures taken with Spectracon image tubes. Various emission lines from the planetaries are isolated using narrow-band filters, and the subsequently-produced contour maps reveal the varying structure of these objects in the light of particular ions. Broad-band observations have been made of QSOs and compact radio sources to investigate the faint outer structure of these objects and to look for the existence of luminous bridges between galaxies of different red-shift. On these sorts of exposures structure has been revealed by contours set at about 1% above the night sky brightness.

Ables and Ables (46,47) used narrowly-spaced contours of the sort described above to obtain the luminosity profile of the galaxy NGC 4881, from exposures using the Kron camera. Several maps were made and the density-above-sky for the outer isophote was estimated for each map. The profile was plotted by taking the dimensions of each contour; circular symmetry was assumed so that the data was presented as a single profile. To extract photometric information in this manner is a long process and also is subject to difficulties arising from the quantised density levels. As mentioned before, Hewitt (34) has modified an isodensitracer to produce an integrated density along one line of a raster scan. A potentiometer driven by the density-wedge carriage provides a voltage (which is proportional to the density) that is integrated using analogue techniques and displayed on a chart recorder. Measuring errors are estimated at less than 1% for this method. The application of this device can be somewhat limited since spatial information is only retained in one direction, but it has been used to good advantage by Ables and Kron (44) and Kron et al (48) on the photometry of jets in M87 and 3C273 where they retained spatial

Table 1.3

	Colour	Seeing arcsec	Night Sky Brightness mag/arcsec <sup>2</sup>	Limiting Stellar Magnitude	Limiting Isophotal Magnitude Used mag/arcsec <sup>2</sup>	Emulsion	Exposure Time Mins
	V	3.7	21.3	24.1	26.0	L4	165
Lelièvre	B	2.7	22.2	24.4	26.8	L4	95
	U	2.3	21.4	22.9	24.8	G5	45
Wlérick	V	-	20.1	-	26.2	L4	80

Plate scale 1" = 40 $\mu$ m

information across the width or along the length of the jet.

Similar integration techniques can be performed by using several manual scans across an object. These methods have been used by Wlérick (49) for work on BL Lacertae and by Lelièvre (50) in a study of N Galaxies. With a single scan across an exposure of BL Lacertae, taken using the Lallemand camera, nebulosity round the object has been detected down to a level that is about 6 magnitudes down on night sky brightness. This result was obtained using a measuring aperture of 25  $\mu\text{m}$  by 25  $\mu\text{m}$ . To increase the size of the measuring aperture would improve the emulsion noise, but limitations to accuracy are set below this level by the residual effects of variations of sensitivity within both the emulsion and photocathode. Separating BL Lacertae into a bright central core and an outer faint nebulosity the magnitude of the latter has been estimated out to the contour at  $V = 26.2^{\text{m}}$  arcsec<sup>-2</sup> to an accuracy of 0.2<sup>m</sup>. Lelièvre has estimated magnitudes of galaxies and stellar-like objects in the field of 3C303 to an accuracy of 0.05<sup>m</sup> and 0.10<sup>m</sup> respectively. The galactic magnitudes are assessed within a "diaphragm" set by an outer isophote of given brightness per square arcsec. Table 1.3 summarises the detection limits of Lelièvre and Wlérick. Lelièvre comments that the larger granularity of the G5 emulsion served to reduce the overall photometric performance of the system.

The application of scanning machines producing digital data has meant that not only can a larger volume of data be handled but the reduction routines can be more sophisticated and varied.

A whole series of routines for studying the structure of galaxies has been developed at the University of Texas and the Johnson Space-Craft Centre for the analysis of data produced by a Boller and Chivens PDS 1010A microdensitometer (43,51,52,53). The system is used on exposures obtained with the Kron camera. The microdensitometer is operated under computer control (from a PDP-8/e with 20K memory) and the data may be stored on either disc or magnetic tape. The system is also supplied with a high-speed teletype, a paper tape reader/punch and a precision CRT plotter. The data can be processed in two ways, either using a quick-look facility on the PDP which can produce density profiles, dummy contours and a playback of the raster, and display them on the CRT, or by using a larger computing facility to handle scans read from magnetic tape. Some of the routines used for the handling of large data arrays are based on methods outlined by Jones et al (54). This includes a program for fitting a polynomial to the sky background surrounding an object and interpolating over the object so that the sky background can be subtracted. The data can be corrected for non-linearity in the camera-emulsion-microdensitometer system and emulsion defects can be removed, as are stellar images that are superimposed on the nebulosity under study. The corrected data is then used to produce isophotes and integrated magnitudes (53). An investigation into the performance of the microdensitometer shows that slow scanning speeds are required for images with high peak densities (51) since there is an apparent shift in position of the measured image due to the response time of the photometric system. Benedict et al (52) calculate a limiting surface brightness at  $3\sigma_D$  above the background density, which would be 3.8 magnitudes down on the sky background. This is based purely on the microdensitometer noise at high density which amounts to about 1% of the measured density.

Gull (55), in an assessment of the performance of various emulsion and image intensifier combinations, has shown that L4 emulsion noise is swamped by the machine noise of the PDS over most of its density range for measuring apertures larger than  $10 \mu\text{m} \times 10 \mu\text{m}$ . To obtain results on a  $40 \mu\text{m} \times 40 \mu\text{m}$  aperture it was necessary to make measurements of the plates taken on the Kron camera using a  $10 \mu\text{m} \times 10 \mu\text{m}$  aperture and then to add them to produce the given resolution. Even so, the effects of microdensitometer noise were seen for densities in excess of 2.4 D as measured on the PDS. The peak signal-to-noise performance of the system was found to be about 150:1. This would give a limiting surface brightness about  $5.4^{\text{m}}$  down on the sky background with an exposure taken to a background density of 2.4 D and an analysing aperture of  $40 \mu\text{m} \times 40 \mu\text{m}$ . Gull has used the Kron camera to take narrow-band exposures of the Orion Nebula to produce both straight isophotes and also maps of the ratio of continuum emission to  $\text{H}\beta$ .

It is the large dynamic range of the electronographic process which is probably of the greatest importance in surface photometry. The ability to record, on the same exposure, both bright central regions and faint outer extensions of an object and thus to relate the relative fluxes accurately provides a powerful tool for both general morphology and luminosity studies.

It can be seen that the general trend in electronography has been to move toward more automated methods of reduction as the machines have become available. At the moment most of the astronomy is still coming from fairly simple measurements made with unsophisticated equipment. This partly stems from the complexity of an automated photometric system as such. Since no one part can be considered totally in isolation, it is only by studying interaction of the constituent elements that the final

overall performance can be defined. However, once such a system is established it should be possible to process large amounts of data on a routine basis.

## CHAPTER II

### THE PHOTOMETRIC SYSTEM

"Observe how system into system runs,"

Alexander Pope (1688-1744)

As outlined in Chapter I, it is necessary to consider the photometric limitations of a complete system. Each constituent part will contribute to the overall performance and, by a knowledge of the role that each one plays, areas for improvement can be defined.

The system under study consists of the following components:

- 1) The Spectracon electronographic image tube
- 2) L4 nuclear track emulsion
- 3) A Mk III CS Joyce-Loebl microdensitometer,  
producing digital output on magnetic tape.

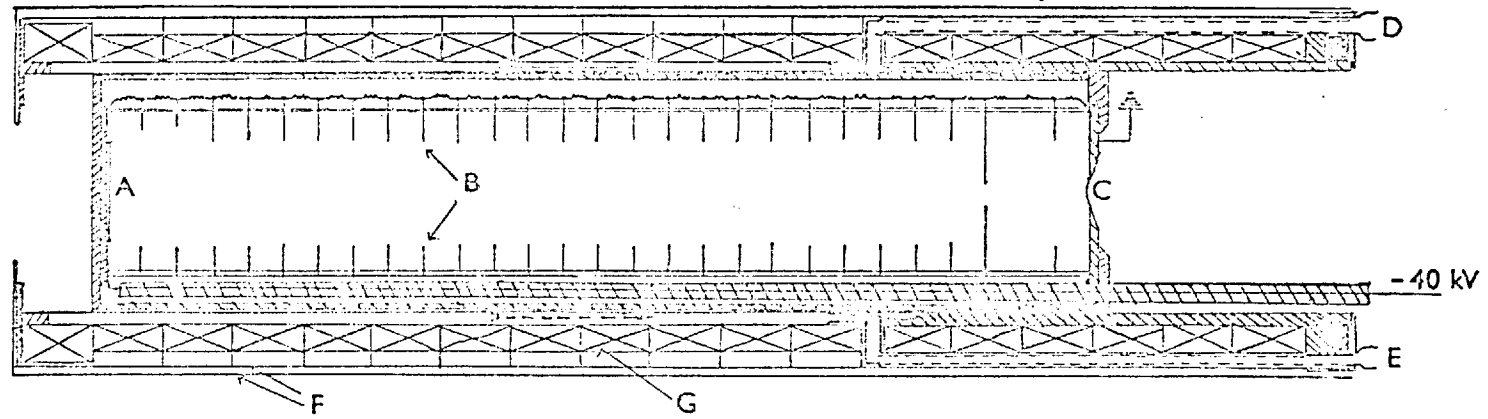
This sequence basically deals with the incoming data, from the image at the focal plane of the telescope to the scan data on magnetic tape. The computer processing is tailored to a particular type of observation and will be dealt with in a later chapter.

#### 2.1 The Spectracon

The design and operating characteristics of this device have been described in full detail in many publications (4,6,56,57).

Therefore an outline will be given of those features of the instrument which have a bearing on its photometric performance.

FIG 2-1-1: SPECTRACON AND SOLENOID



- A Photocathode
- B Annular electrodes
- C Mica window
- D Coolant inlet
- E Coolant outlet
- F Mu-metal screens
- G Focussing coil



Fig. 2.1.1 is a cross-sectional diagram of the encapsulated tube sitting inside the focussing solenoid. The standard photocathode size is 10 mm x 30 mm, although tubes of larger image area have been built by placing two such cathodes side by side (58). The photocathode is processed in a separate cell and transferred to the main tube through a side arm. Careful handling is required during this transfer to avoid scratching the photocathode surface. The plate is manoeuvred down the tube and is locked in place in a metal frame which is mounted inside the glass tube-window. To a certain extent a pre-selection process can be used to find photocathodes of fairly high sensitivity before the transfer is undertaken. Using this technique cathodes with S-9, S-10, S-11, S-20 and S-25 responses have been successfully put into Spectracons. However, there has been little success with cathodes of the S-1 type (56) which tend to lose up to 50% of their efficiency during transfer. Typical photocathode sensitivities are 50 - 70  $\mu\text{A}/\text{lumen}$  for S-11 and 90 - 120  $\mu\text{A}/\text{lumen}$  for S-20. These white light responses correspond to quantum efficiencies of approximately 14% at  $4200\text{\AA}$  and 15% at  $4900\text{\AA}$  respectively.

Obviously the speed of the device will be governed by the quantum efficiency of the photocathode. Coleman (59) has calculated the detective quantum efficiency (DQE) of the Spectracon used in conjunction with various different methods for recording the photoelectrons. The overall DQE ranges from about 70% of the quantum efficiency of the photocathode for track counting in emulsions and diode detection of photoelectrons, to 30% to 50% of the cathode efficiency for different electron-sensitive emulsions scanned using a microdensitometer. The primary mechanism which reduces the performance is the effect of the

output mica window, which transmits about 75% of the incident electrons and imposes an energy distribution on those emerging from it (see Fig. 1.1).

The overall sensitivity of the photocathode affects the speed of the Spectracon, but of equal importance, from the point of view of relative photometry within a field, are the changes in sensitivity across the cathode surface. Peak-to-peak variations of the order of 50% of the overall sensitivity have been measured over the whole photocathode by Smyth and Brand (60). Typical measurements over areas of about 2 mm by 2 mm give variations ranging between 2% and 7% depending on the photocathode quality. These fairly low spatial frequency effects arise from non-uniform deposition of the photosensitive layer during manufacture, possibly due to varying temperature along the surface of the plate or poor geometry within the cell. There are also photocathode defects, which are small areas of zero-sensitivity and can take the form of pinholes or fine scratches. These are produced by dust particles masking part of the cathode plate during evaporation, and scratches may occur as the photocathode is manoeuvred into the tube.

When the tube is in focus these dead spots are indistinguishable from dust specks on the outside of the mica window. However, on an out-of-focus exposure the latter show up as in-focus spots on the plate. Any dust lying on the surface of the window can be removed using a soft brush. Usually the output window of the Spectracon consists of a uniform cleaved sheet of mica about 4  $\mu\text{m}$  thick. Windows ranging from 5 mm x 30 mm to 20 mm x 25 mm have been constructed and used on Spectracons. Sometimes, during use, some of the mica may be removed by contact with moist emulsion. The resulting structure in the mica window is then revealed by a change in sensitivity across the image

area of the tube. This usually leads to a step-function in sensitivity and this has to be compensated for if accurate relative photometry across the field is required.

The resolution of the Spectracon is dependent on the emulsion that is used with it. When operated at two-loop focus, resolutions of 70  $\mu\text{p}/\text{mm}$  have been obtained with Ilford XM, 90  $\mu\text{p}/\text{mm}$  with G5 and 120  $\mu\text{p}/\text{mm}$  with L4. Since this greatly exceeds the resolution required for most astronomical optical systems and, by going to single-loop focus the heat output of the solenoid can be reduced by a factor of four, the tube is normally operated at single-loop focus for astronomical exposures. The limiting resolution is then 70  $\mu\text{p}/\text{mm}$  to 80  $\mu\text{p}/\text{mm}$  on L4 over the whole field. The resolution limit of the tube itself is set by the electron optics and scattering of the electrons within the mica and is about 150  $\mu\text{p}/\text{mm}$ .

The image geometry of the Spectracon is generally good. Distortions of the order of 5  $\mu\text{m}$  or less occur between the centre of the photocathode and a radius of 2 mm. Over the usual extent of most of the astronomical images obtained with this device no correction is required. The emulsion is on a Melinex backing of 25  $\mu\text{m}$  or 50  $\mu\text{m}$  thickness, which provides dimensional stability.

For the photometry of faint objects, and narrow-band observations, the background of the tube must be low. Extremely high values of dark current stem from electrical breakdown within the tube and the subsequent corona being detected at the photocathode. These sources can of course be non-uniform. There will also be thermionic emission from the photocathode. Oliver (61,62) has investigated another source of background which is only important for tubes with S-20 cathodes. This is the occurrence of multiple-electron events (ion spots) where groups

of 10 to 20 electrons are released from the photocathode by  $\text{Cs}^+$  ions. These ions are formed by the evaporation of caesium from the tri-alkali photocathode to the tube electrodes and its subsequent field desorption from these as  $\text{Cs}^+$  ions.

With careful encapsulation and cooling of the photocathode dark currents in the range of 50 to 500 electrons/cm<sup>2</sup>/sec have been obtained for both S-11's and S-20's (56,57). This upper level amounts to a density increment of about 0.002D/hr on L4 and 0.02D/hr on G5.

Signal-induced background (SIB) can also serve to reduce the performance of the device. Coleman (6,59) has investigated the various sources of SIB in the Spectracon and has shown that the predominant effects are from light scatter within the face plates of the tube (there are five glass-air or glass-vacuum surfaces), and reflection of transmitted light by the electrode structure. The effect appears to be fairly uniform over most of the image surface but rises at the extreme ends of the photocathode due to almost specular reflection from the first electrode. Coleman gives a value for the SIB of  $(10 \pm 2)\%$ . This would lead to a loss of limiting magnitude of  $0.05^m$  for stellar photometry.

As can be seen from the figures presented so far, the performance of the Spectracon cannot be defined in isolation from the method that is used to detect the electrons. Therefore the next stage in the assessment of the system is the storage medium.

## 2.2 Nuclear Track Emulsion

Over the past few years extensive work has been carried out on the various nuclear track emulsions used for electronography (Brand (63), Cohen (64), Harwood (65), Kahan and Cohen (7), Cohen and

Kahan (66), Coleman (6,59), Griboval et al (8), Kron and Papiashvili (67), Ables and Kron (68)). One of the prime areas of investigation has been the linearity of the response of the detector-emulsion combination. Valentine (69) has proposed that the linear density versus exposure response of electronography comes from the single hit nature of the process (that is, one electron producing one registered "event" in the emulsion).

Considering the definition of optical density (D)

$$D = \log_{10} \frac{1}{T}$$

where T is the transmission and is given by

$$T = 1 - S$$

S is the total projective area of all the blackened grains per unit area of the emulsion. Thus the relation between D and S is

$$D = -\log_{10} (1-S)$$

Silberstein and Trivelli (70) have taken the shielding effect of the grains into account and replaced S by S', the effective projective area of the blackened grains per unit area. S' is related to S by the following means

$$S' = 1 - e^{-S}$$

$$\text{Hence } D = -\log_{10} (1-S') = \log_{10} e^S$$

S can in turn be replaced by the product of the number of developed grains per unit area (N) and the effective area of each grain (a).

$$D = 0.434 N a$$

This is Nuttings Formula. Therefore it can be seen that if, as Valentine suggests, a single hit process is taking place with a mean

\*

The grain area  $a'$  is the effective cross-section of the undeveloped grain and is associated with the scattering and detection of incident electrons. The effective grain area  $a$  is related to the size of the developed grain and is involved with the measurement of the density of the emulsion.

number of electrons/track and the number of tracks in the emulsion proportional to the incident flux, that a linear density versus exposure relationship should follow. However, in expressing the number of grains/unit volume ( $N$ ) rendered developable by an exposure to  $E$  electrons/unit area, one must take into account the probability of a grain being hit. With an electron range of  $R$  and a total number of halide grains per unit volume of  $N'$ , each of area  $a'$ , the number of exposed grains ( $N$ ), assuming a single hit law, is given by the following expression:

$$N = N' R (1 - e^{-Ea'})$$

Therefore the density  $D$  can be related to the exposure  $E$  in the following manner

$$D = 0.434 Na = 0.434 N'Ra (1 - e^{-Ea'}) \quad *$$

When  $E$  is infinitely large the saturation density of the emulsion is reached.

$$D = D_{SAT} = 0.434 N'Ra$$

Thus

$$D = D_{SAT} (1 - e^{-Ea'})$$

and for  $D \ll D_{SAT}$

$$D = D_{SAT} Ea'$$

and the linear density versus exposure relationship holds. Cohen (64) has shown that at densities which are a substantial proportion of the saturation density of the emulsion ( $D > D_{SAT}$ ), the linearity of the single hit process breaks down, departing  $\frac{4}{4}$  by more than 15%. However, the saturation density of nuclear track emulsion is high and thus linearity is still maintained over a useful density range.

Table 2.2.1

Emulsion/type	Mean Grain Size $\mu\text{m}$	Thickness of Emulsion Layer $\mu\text{m}$	Relative Speed at Unit Density	Useful Linear Range	Reference
XM, Fast speed	1.5	10	110	$\sim 1.3D$	(64)
G5, Medium speed	0.27	10	22	$\sim 2.3D$ $\sim 4D$	(64) (69)
L4, Slow speed	0.14	5	1.5	$> 5.6D$ $\sim 6D$	(64) (69)



Varying degrees of linearity have been found for different emulsions. The most consistent results come from Ilford L4, a slow fine-grain emulsion, when exposed either to mono-energetic electrons (69) or to the range of electron energies present from the Spectracon (6,59). Most measurements have been taken to densities in excess of 5. The useful linear range of an emulsion seems to some extent to decrease with increasing speed (see Table 2.2.1). This will be due, at least in part, to the lower storage of the coarser grained emulsions. Exposures to test the linearity of G5 were undertaken by several workers (67) in an attempt to verify the relationship. An identical method of development was used for all the exposures, and measurements were made on both the experimenter's own measuring machines and the Joyce-Loebl microdensitometer at Imperial College. Substantial agreement was found except for the results from Griboval, the disparity being attributed to the performance of the different measuring devices.

Coleman (59) has tested the linearity of L4 using three different developers and has found that the emulsion was linear up to densities in excess of 5 for all three. However, stringent precautions were taken to ensure rapid and even development. The methods used for processing these exposures, and all those taken by the author for experimental work and observations, are described in Appendix I.

As well as considerations of linearity and speed the noise of the emulsions is important when accurate photometry is required. In this respect L4 produces by far the best results. The zero frequency noise power of the emulsion has been found to be proportional to density up to about  $4.5D$  (67). This relationship implies that the distribution of the developed grains in the emulsion is still random at high density. This can be compared with similar measures made for G5 (64) which show some evidence for grain clumping at higher densities. Cohen (64) has

shown that despite the lower speed of L4, the signal-to-noise performance of L4 and G5 is similar for an exposure of fixed level. Coleman (6) has explained this better performance in terms of the higher uniformity of the dimensions of the L4 emulsion crystals.

The zero frequency noise power is given by the following expression

$$n(0) = \sigma_D^2 A$$

where A is the area of the measuring aperture and  $\sigma_D$  is the r.m.s. density variation obtained with that aperture. Providing the noise-power spectrum of the emulsion is flat over the range in spatial frequencies to which the measuring machine is capable of responding, this value is independent of scanning <sup>aperture</sup> area. Since a linear relationship between  $n(0)$  and density implies a random distribution of grains at quite high density an assumption of a flat noise-power spectrum for L4 would seem justified. Simple checks using different-sized apertures bear this out (6).

The zero frequency noise power can in turn be related to the Selwyn granularity,  $S(A)$

$$n(0) = \frac{1}{2} S^2(A)$$

Shaw (71) has related the granularity to the distribution in developed track areas by the following expression

$$\frac{1}{2} S^2(A) = 0.434 \left( \overline{\alpha_D^2} / \overline{\alpha_D} \right) D$$

where  $\overline{\alpha_D}$  is the mean area of a developed track at density D. Thus

$$n(0) = 0.434 \left( \overline{\alpha_D^2} / \overline{\alpha_D} \right) D$$

This may be rewritten as

$$n(0) = 0.434 \overline{D\alpha_D} \left( 1 + \frac{\overline{\sigma^2}}{\alpha_D} / \frac{\overline{\sigma^2}}{\alpha_D} - 2 \right)$$

The two sources of density noise are as follows. The first term in the bracket arises from the random variation of the number of tracks within the area A of the aperture. The second term indicates the increase in noise over that obtained if all the tracks were of equal area. For a narrow distribution in track areas  $n(0)$  will be proportional to D, a result that has been found experimentally for L4.

The signal-to-noise power ratio  $\left| \frac{S(0)}{n(0)} \right|^2$  at zero frequency is given by  $D^2/n(0)$  - thus  $\left| \frac{S(0)}{n(0)} \right|^2$  should also be proportional to density.

The detective quantum efficiency of the emulsion at zero spatial frequency can be defined as follows

$$E_D(0) = \frac{\left| \frac{S(0)}{n(0)} \right|_{\text{OUT}}^2}{\left| \frac{S(0)}{n(0)} \right|_{\text{IN}}^2}$$

$\left| \frac{S(0)}{n(0)} \right|_{\text{IN}}^2$  is simply the number of electrons E impinging on unit area of the emulsion.

The density for a given number of tracks per unit area ( $N_T$ ) is given by

$$D = 0.434 N_T \overline{\alpha_D}$$

Thus the zero-frequency DQE is given by

$$E_D(0) = \frac{D^2}{0.434 \overline{D\alpha_D} \left( 1 + \frac{\overline{\sigma^2}}{\alpha_D} / \frac{\overline{\sigma^2}}{\alpha_D} - 2 \right) E}$$

$$= \frac{0.434 \overline{N_T \alpha_D}}{0.434 \overline{\alpha_D} E \left( \frac{1 + \overline{\sigma_{\alpha_D}^2}}{\overline{\alpha_D}^2} \right)}$$

$$E_D (0) = \frac{N_T}{E} \left( \frac{1 + \overline{\sigma_{\alpha_D}^2}}{\overline{\alpha_D}^2} \right)^{-1}$$

where  $\frac{N_T}{E}$  is the fraction of electrons which form tracks and the other term  $\frac{N_T}{E}$  arises from the non-equal weighting of tracks. Obviously this last term requires to be kept as small as possible. Coleman (6) has investigated the various factors affecting this spread in track area. One of the prime requirements is a low spread in the dimensions of the undeveloped halide grains. Again L4 is shown to have the advantage of a fairly low spread (6).

Therefore it seems that, for performing accurate photometry, L4 is the prime candidate as far as emulsions go. XM and G5 still have their applications in the detection of faint images that would be below the measuring capabilities of the microdensitometer on L4, and for positional rather than photometric work.

### 2.3 The Microdensitometer

As stated in Chapter I the full detail of the electronographic image can only be revealed by using a microdensitometer to scan the plate. Electronographic data impose rigorous conditions on the performance of any measuring machine (Pilkington (72)). The requirements are not only the accurate representation of spatial

information, which is necessary for any high-resolution emulsion, but also the accurate measurement of densities that may be much higher than those that are useful for photographic emulsions and also, for applications where large areas of plate must be digitised, speed is important. The microdensitometer is the final link in the chain from photon image to numerical data. The three primary areas of investigation to define its performance are:

- 1) Accuracy of spatial sampling
- 2) Linearity
- 3) Noise levels at high density.

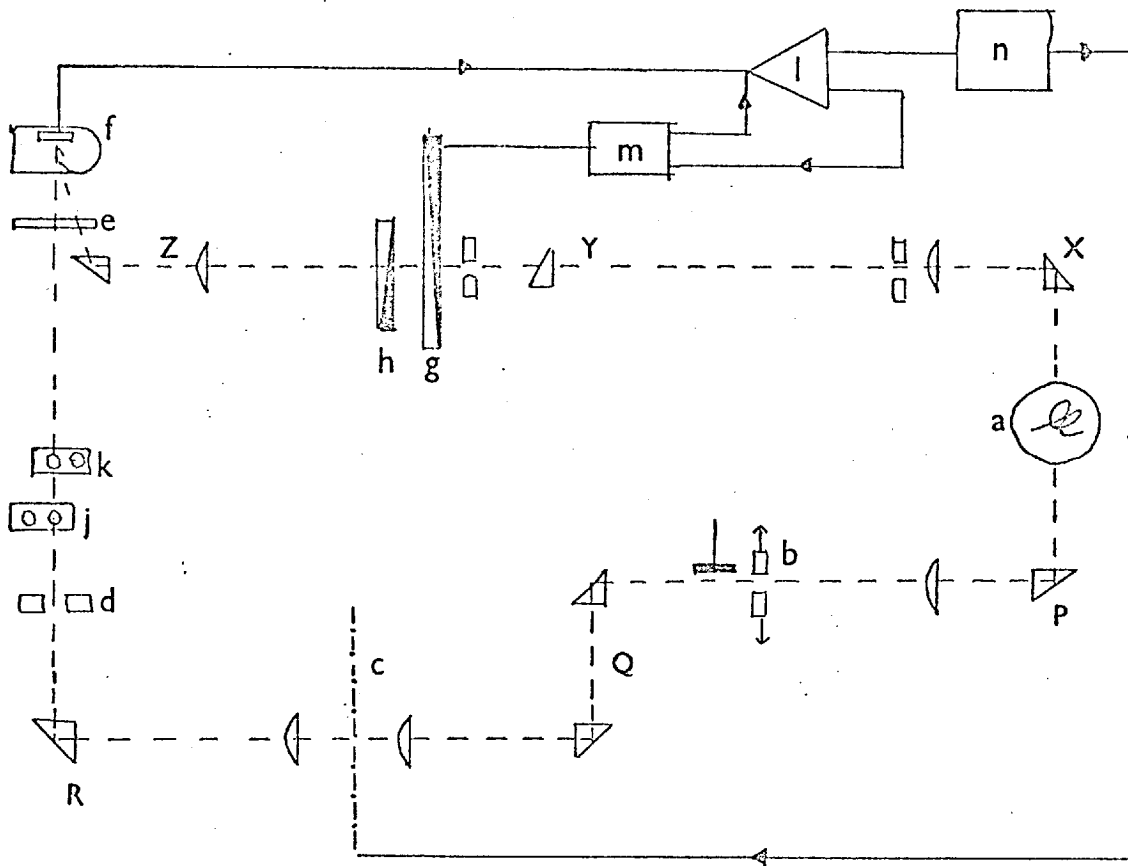
Before discussing these in detail, the general properties of the Joyce-Loebl machine used for the work presented in this thesis will be outlined.

### 2.3.1 The Joyce-Loebl Mk III CS Microdensitometer

The microdensitometer consists of two elements - the density measuring device and the control and digitisation electronics.

The system for the measurement of density was originally designed to operate as a one-dimensional scanner for spectra with fixed pre- and post-slits and the sample table being moved through the measuring beam. The sample table can be coupled to the recording table by various ratio arms which will give a sample travel ranging from 25 cm down to 125  $\mu\text{m}$  for one complete stroke of the recording table. In this simple form the "Y" position of the table can be adjusted to about 1/10 mm. In order to use the machine for two-dimensional scanning, stepping motors and lead-screws are added to both X and Y motions, the smallest increment in each direction being 5  $\mu\text{m}$ . These motors can be disengaged

FIGURE 2-3-1: SCHEMATIC DIAGRAM OF JOYCE LOEBL MICRODENSITOMETER



- PQR    measuring beam  
 XYZ    reference beam  
 a      lamp  
 b      pre-slit  
 c      sample plane  
 d      post-slit  
 e      synchronous motor and chopper  
 f      photomultiplier  
 g      density wedge  
 h      zero-effect wedge  
 j      neutral density filter  
 k      filter to prevent light from red glass jaws of  
       pre-slit system from reaching the photomultiplier  
 l      amplifier  
 m      wedge servo motor  
 n      specimen table servo system
- electrical connections  
 - - - -    light paths

for manual scans. The position angle of the specimen can be altered by about  $\pm 20^\circ$ .

The measurement of density is made using a two beam optical system (see Fig. 2.3.1). Measuring and reference beams are taken from either side of the quartz iodine lamp (a). The measurement beam passes through the sample (c) while the reference beam is diverted through the motor-driven grey wedge (g). Both beams are brought together and are mechanically chopped so that they fall alternately onto a photomultiplier. The signal from this detector is used to drive the grey wedge carriage, thus a servo-loop is formed that balances the attenuation in both beams. The position of the wedge is then taken as a measure of the density. When the sample is being manually scanned a second servo-system drives the recording table so that it moves at a slower speed when high density gradients are present. When operated in manual mode, a pen is connected to the wedge carriage to provide density output, when digital data is required a 100 K $\Omega$  potentiometer is driven by the carriage and provides a voltage input for an A/D converter. The density range and resolution of the device can be changed by using different wedges (see Table 2.3.1). There is also a facility for providing zero level density offsets. Tests have been made of the stability of the photometric system. It has been found that, after a warm-up period of about two hours during which density measurements change due to mechanical drift of the optics arising from temperature changes, residual drifts in density of the order of 0.002 D/hr remain. One cause of this may be the fact that the two beams are taken from opposite sides of the lamp and are looking at different parts of the filament. However, the effect is small for the typical duration of scans and as compared with the density content of the exposures.

Table 2.3.1Density Ranges and Resolution of Joyce-Loebl

Wedge	Density Range	Density Resolution of Digital Output
A	.39	0.00022
B	.79	0.00048
D	1.67	0.001
F	2.5	0.0015
J	3.9	0.0022



The optical system has both pre- and post- slits which serve to reduce scattered light. Since the machine was originally designed for spectrum scanning the Y slit control is not quite as accurate as the X. With care, the area of the pre-slit can be set so that it differs from that of the post-slit by less than 50% for a 10  $\mu\text{m}$  aperture and by less than 10% for a 40  $\mu\text{m}$  aperture. There is a facility for changing the objective; for electronography those of magnifications x10 and x20 are most frequently used, having numerical apertures of 0.25 and 0.5 respectively. The exposures are sometimes mounted on glass plates and are measured with the emulsion face-up and uncovered. However, most of the emulsion is on a Melinex backing and during scanning these exposures are held between two glass plates of about 1 mm thickness.

The design of the control electronics has been described by Cullum and Stephens (39). The table can be moved under manual control (using a joystick) or in an automatic raster scan. The output of the potentiometer is fed to the A/D converter when a "wedge balanced" signal is received. The table is then stepped and another measurement is made. The scan rate is slow, basically limited by the response of the mechanical system and the wedge-servo balance time at high density. The maximum sample rate is 18 samples/sec; an average figure obtained from exposures of varying density content is about 10 samples/sec.

Any wedge range can be divided into about 1,700 levels and the density increment per level can be found by simple calibration techniques. There is a small keyboard to write numerical identifications at the head of a scan and the facility for writing single densities onto the magnetic tape. The scan data is written to tape with "beginning of scan line" and "beginning of density-word" characters. The structure

FIGURE 2-3-2: STRUCTURE OF SCAN

Header Record

```

AA|BBBBB|C|WDDD|WDDD|. . . .
                                     .....|0000|EOR

```

Scan

```

LDDD|WDDD| . . . .
                                     .....|WDDD|EOR

```

```

WDDD|WDDD|LDDD|WDDD| . . . .
                                     .....|WDDD|EOR

```

```

.
.
.
.
.

```

Last Record

```

WDDD|WDDD|0000| . . . .
                                     . . . |0000|EOF

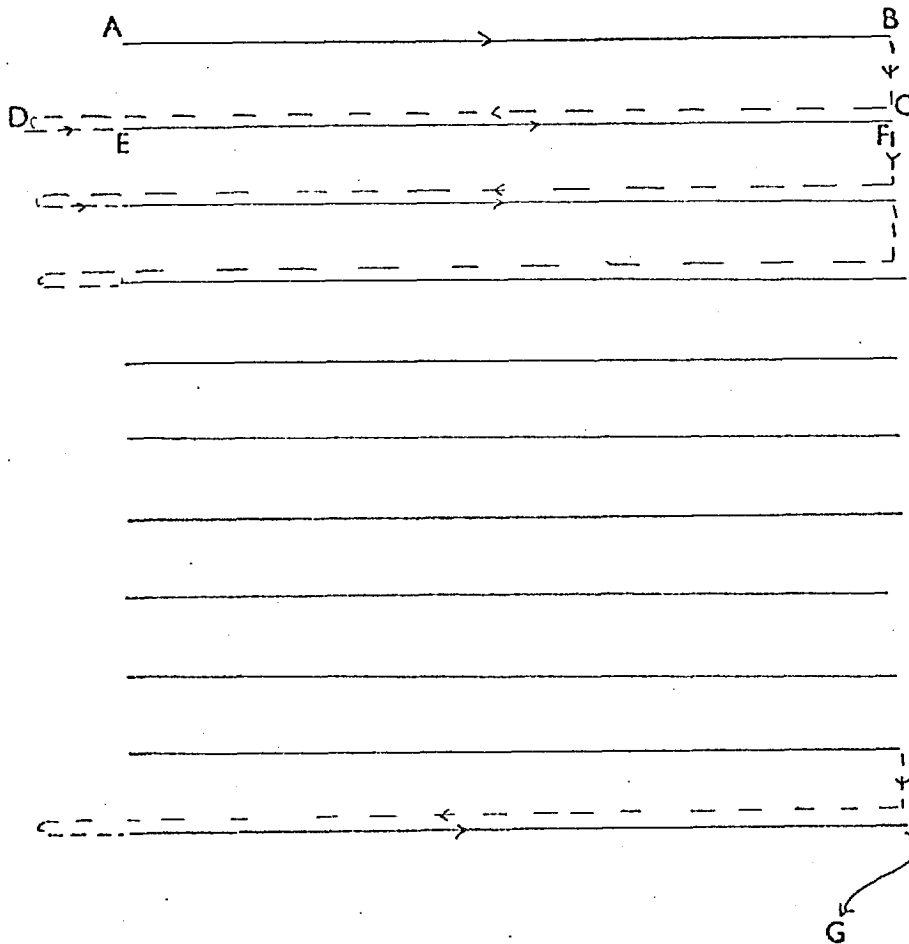
```

End of Scan

---

AA User Identity	W Beginning of Density Word
BBBBB Scan Identity	L Beginning of Line
C Number of Standard Densities	EOR End of Record
D Density	EOF End of File

## PROJECTION OF SCAN PATTERN ON SAMPLE



- A → B      Samples
- B → C      Steps in Y direction
- C → D      Flyback
- D → E      Takes up backlash
- E → F      Samples
- G          Returns to zero taking up backlash

FIGURE 2-3-3

of a typical scan is shown in Fig. 2.3.2. The 7-track magnetic tape produced by the machine is processed on a CDC 6400 computer at the College computer centre.

### 2.3.2 Accuracy of Spatial Sampling

For mapping and photometry it is necessary to have an accurate representation of the spatial distribution of the emission from any object. Also, if comparison or matching of two scans is required, there must be good repeatability of a given scan pattern.

Positional information used for the mapping of images scanned with the Joyce-Loebl is based on the assumption of equal spacing between samples within the raster. The stepping motors and lead-screws providing the X and Y motions of the table have a minimum step length of 5  $\mu\text{m}$  and the scan length and sampling interval are set up as multiples of this dimension. Since there is no check on absolute or relative position during scanning some general investigations have been made into the table motion.

There is a certain amount of backlash between the sample table and the lead-screw and this was taken into account when the control of the automatic scan was designed. During scanning a pattern is followed as shown in Fig. 2.3.3. The table overshoots on the flyback and sampling commences as the stepping motors return the table to the zero point. Of course, if the backlash is not taken up before starting there will be errors in the first few data points. However, it is a fairly simple matter to perform a short scan, which will automatically take up the backlash, or to position the table correctly using the joystick.

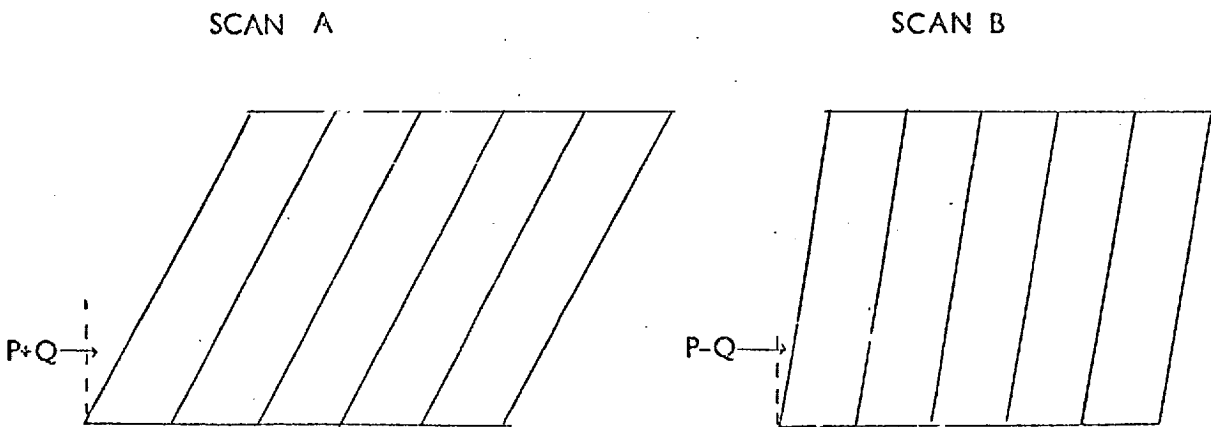
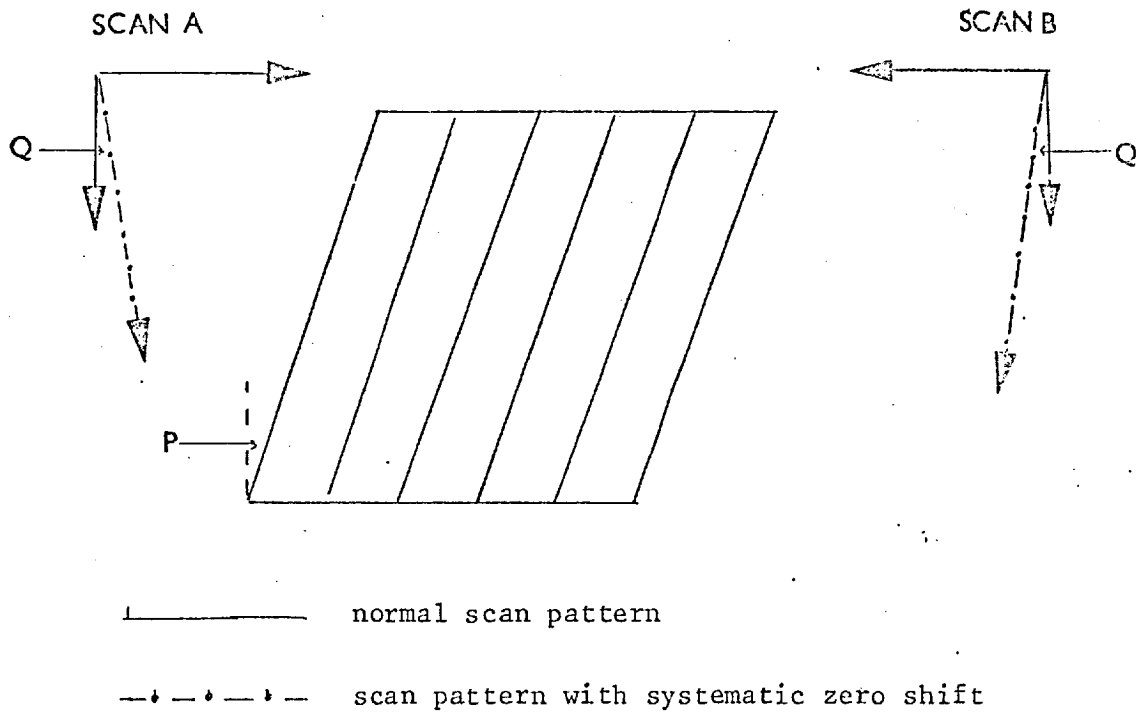
FIGURE 2-3-4 : SCAN OF BAR PATTERN



50μm

12.6 INS.

FIGURE 2-3-5: CHECK FOR ZERO-SHIFT IN SCAN PATTERN



Form of the plots of scans of a bar pattern  
with a systematic shift in the zero position

Cullum (73) has made some measurements of the cumulative error obtained on a 25 mm stroke of the sample table (25 mm is about the longest length of scan required for a Spectracon exposure). The r.m.s. error was found to amount to  $\pm 6 \mu\text{m}$  in the Y direction and slightly better than this in X.

To look for effects arising from individual sample intervals being of non-standard length a check can be made by scanning a pattern of equi-spaced lines with a fairly close separation. A diffraction grating of 250  $\mu\text{p}/\text{inch}$  was used for this test. Obviously the edges of the bars will be smoothed out by the finite width of the slit, but it is possible to check the length of the dark and bright bars and look for gross irregularities (a typical scan is shown in Fig. 2.3.4). On measurements made so far, no evidence for large differences in sample interval has been found. Another effect that can be checked is a systematic shift in zero position. To do this one must eliminate effects due to the grating being at an angle to the direction of the scan (see Fig. 2.3.5). If the sense of the scan is reversed in the X-direction and then the two scans are plotted so that the data represents the same spatial orientation, the bars in the two plots should be at the same angle unless the zero position shifts. This has been checked and again a null result obtained.

Thus, with care, it is possible to obtain quite good positional accuracy within a set of scan data, and if the same features are visible within two scans it should be possible to match them.

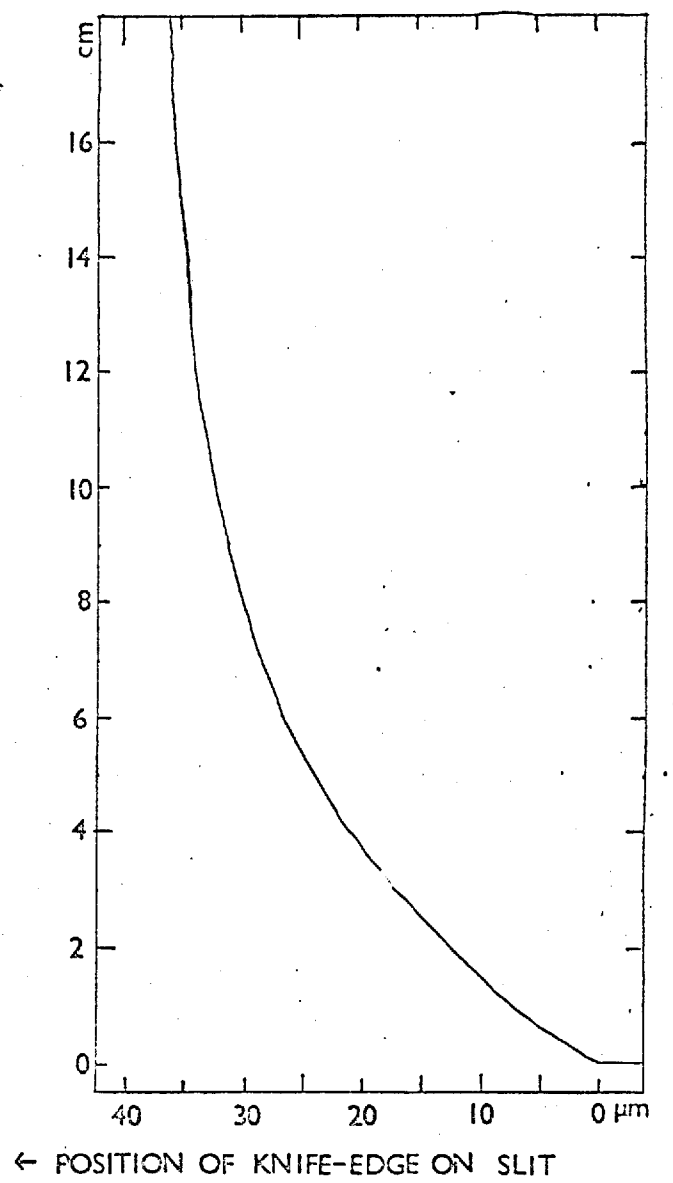
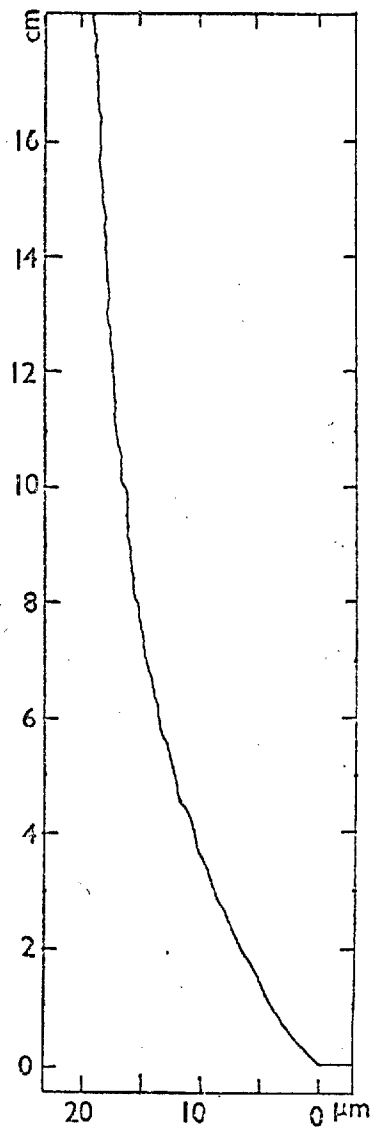
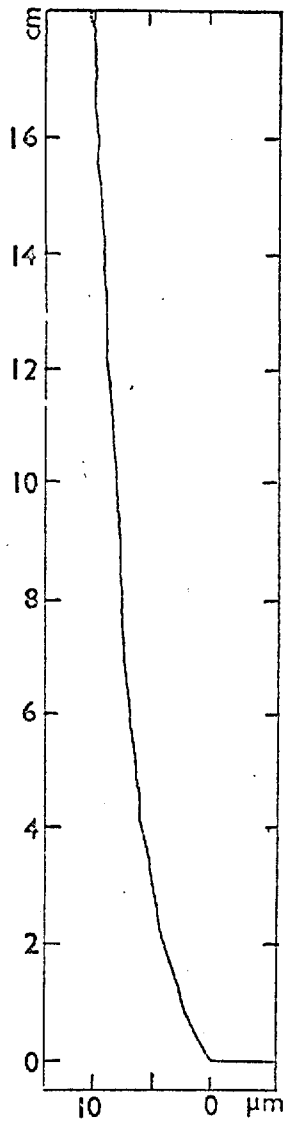
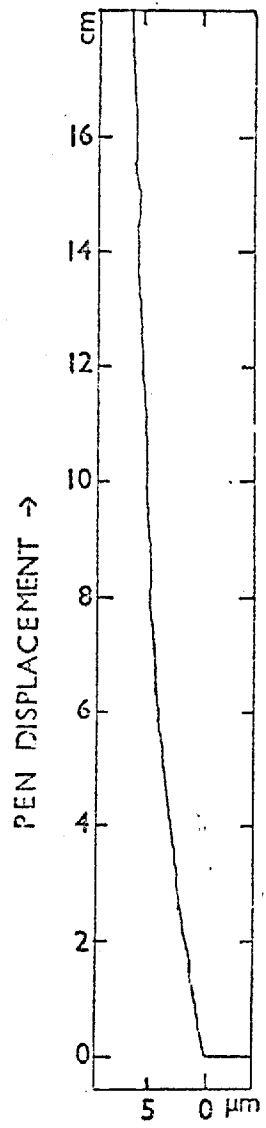


FIGURE 2-3-6 : TYPICAL KNIFE-EDGE TRACES

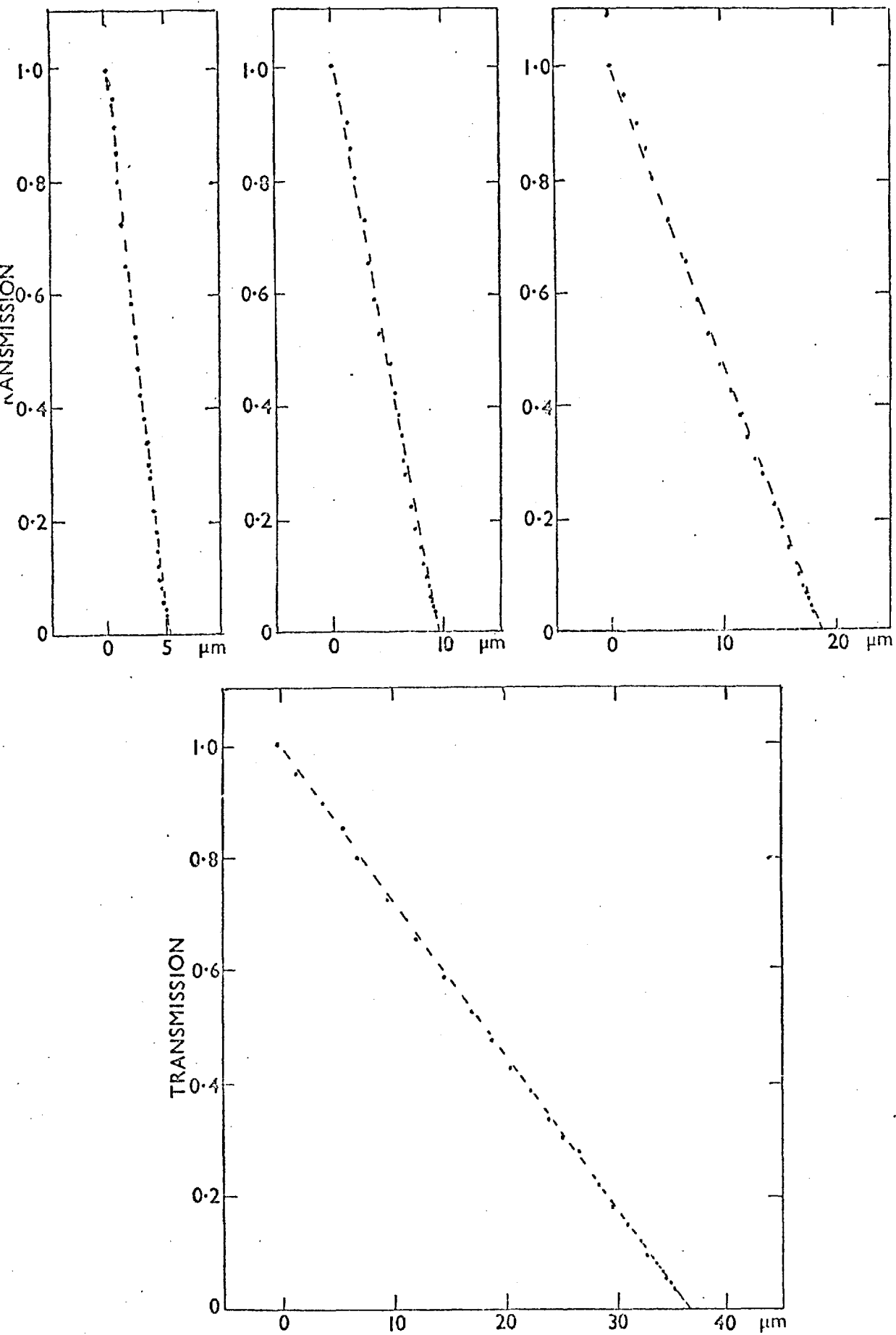


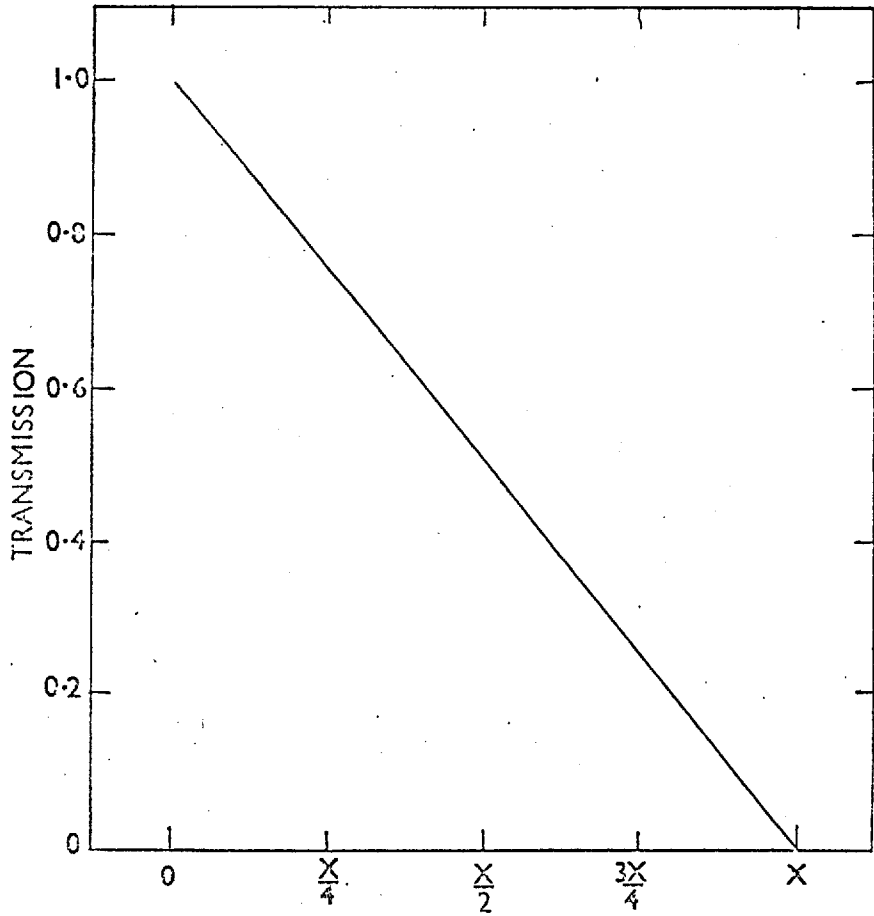
Table 2.3.2

Objective	N.A.	Actual Slit Width	Projected Slit Width at Sample*	Slit Width Obtained from Edge Trace
		$\mu\text{m}$	$\mu\text{m}$	$\mu\text{m}$
x20	.5	200	4.55	5
		400	9.0	9.5
		800	18.25	18.75
		1600	36.4	36.5

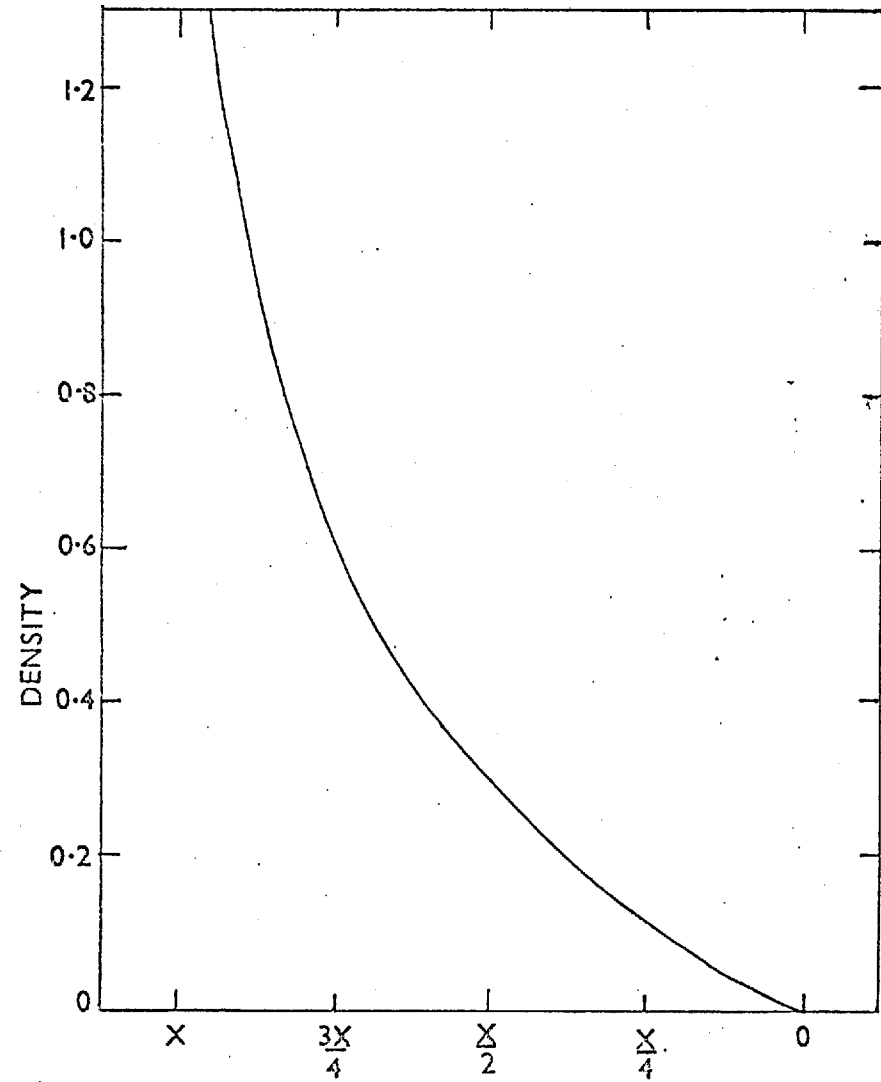
\* Allowing for a projection factor of 2.2 between the sample and the measuring aperture.

FIGURE 2.3.7 : TRANSMISSION VERSUS POSITION OF KNIFE-EDGE ACROSS THE SLIT





POSITION OF KNIFE-EDGE ACROSS SLIT →



← POSITION OF KNIFE-EDGE ACROSS SLIT

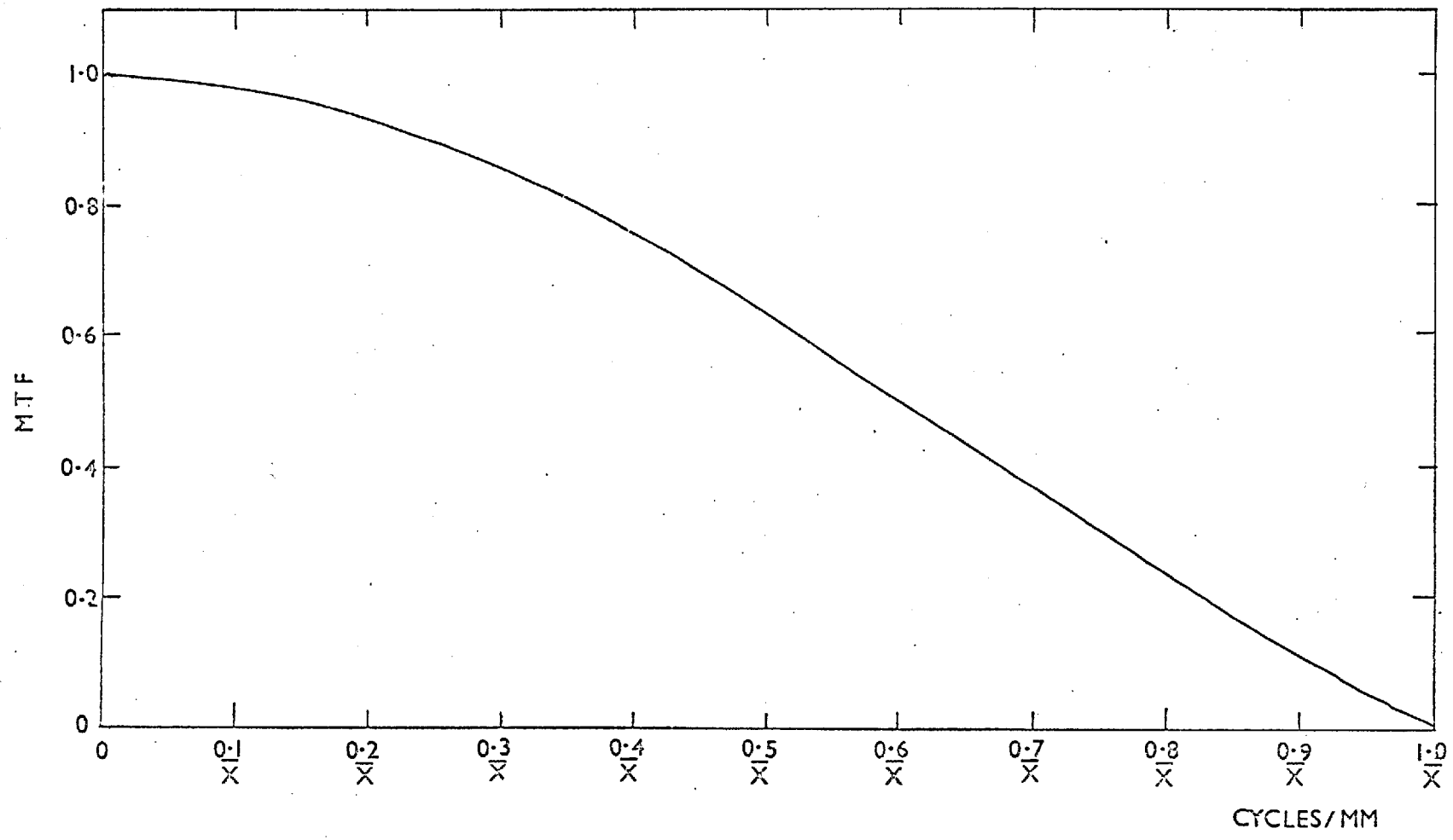
FIGURE 2-3-8: CALCULATED TRANSMISSION AND DENSITY CURVES FOR KNIFE-EDGE TRACES USING A SLIT X MM WIDE

### Microdensitometer Modulation-Transfer Function

As well as considering the effects of positional accuracy on the representation of the distribution of the data on the plate, one has to take into account the effects of the microdensitometer in filtering the spatial frequencies of the measured image. The modulation-transfer function (MTF) of the device gives a measure of these effects. The MTF of the microdensitometer can be measured from traces of a knife-edge either by obtaining the line-spread function and performing a Fourier transform, or by using a method described by Scott, Scott and Shack (74) which yields the square-wave response of the system, which is then converted to the sine-wave response or MTF. For this latter method the output of the microdensitometer in terms of the measured relative brightness is required. Therefore the density measurements must be converted to transmission.

Scans of a knife-edge were undertaken using the range of aperture widths most likely to be used for digitisation of electronographs. Thus the smallest slit used was about 5  $\mu\text{m}$  wide, coinciding with the minimum available step length of the stepping motor. Table 2.3.2 gives the details of the scans and Fig. 2.3.6 shows the typical edge traces. When these traces are converted into plots of transmission versus the position of the knife-edge across the slit a series of straight lines are obtained, Fig. 2.3.7. This is the result one would expect if the MTF of the microdensitometer is predominantly the filter function of the slit rather than stemming from any limitation of the optical system. Fig. 2.3.8 shows the calculated variation of density and transmission with displacement for a knife-edge being drawn across a slit. Thus it seems, in the range of slit widths likely to be used for digitisation purposes, that the MTF of the microdensitometer can be adequately described by the slit function alone. This takes the

FIGURE 2-3-9: MODULATION TRANSFER FUNCTION FOR A SLIT X MM WIDE



form of a sinc function so that the MTF  $M(f)$  is given by

$$M(f) = \frac{\sin \pi f x}{\pi f x}$$

where  $f$  is the spatial frequency in cycles/mm and  $x$  is the width of the slit in mm. A plot of the function is shown in Fig. 2.3.9.

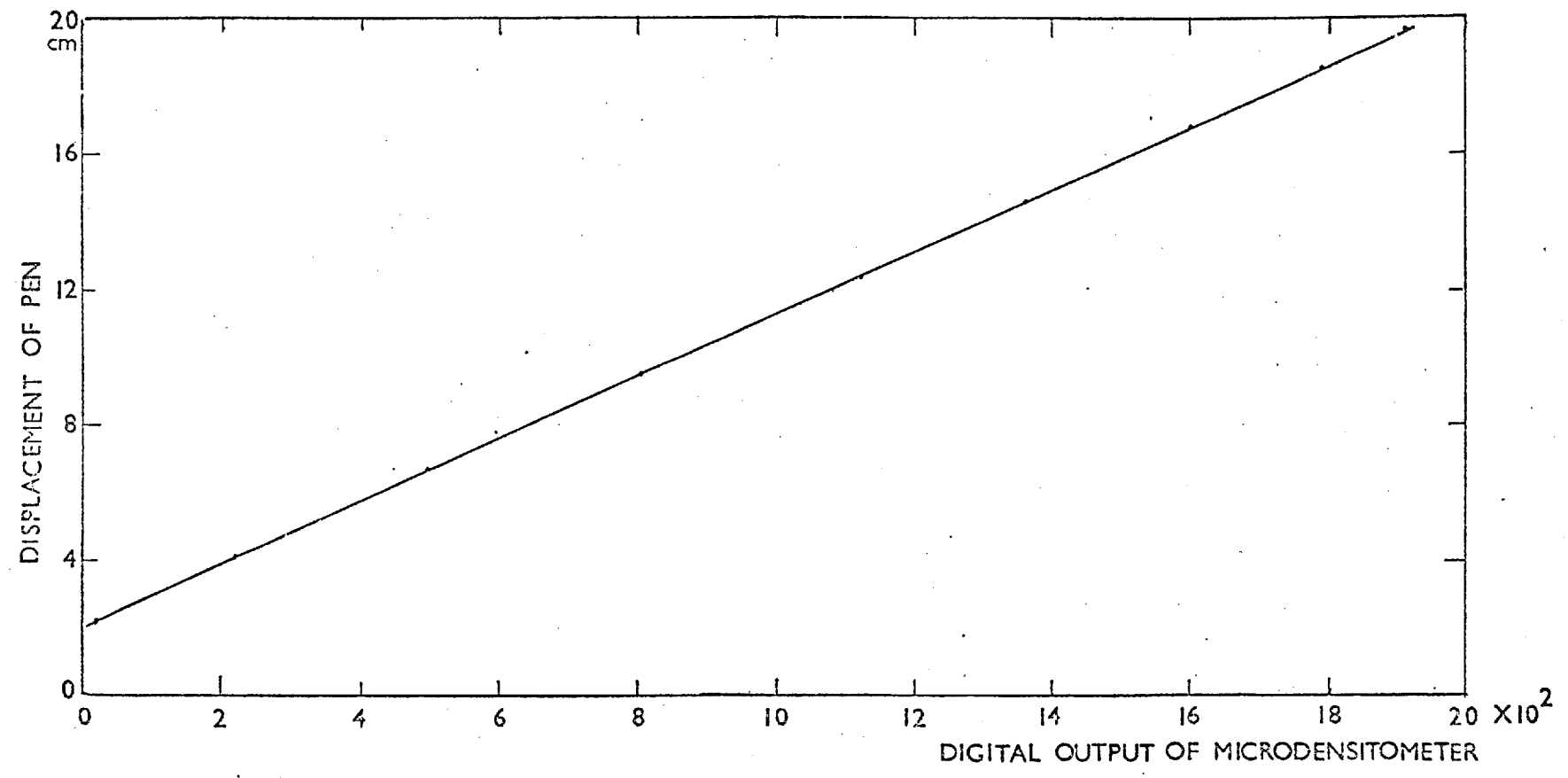
### 2.3.3 Linearity

The linear response of the electronographic process requires that the microdensitometer itself be highly linear. Certainly the combination of the Joyce-Loebl plus L4 has been shown to be linear over a large range in density (Kahan and Cohen (7), Ables and Kron (68)), and it would seem fortuitous if this arose from mutually compensating non-linearities in the two components.

With the two-beam system used in the Joyce-Loebl, one possible source of non-linearity is the grey wedge. Cohen (64) reports small scale departures of 2% or less due to inhomogeneities in the wedge and states that these cancel out over the full wedge range. Two methods can be used to remove these effects, either to calibrate the wedge (Ables and Ables (47) have used the electronograph itself to do this) or to scan twice using a small zero offset so that densities are measured at slightly different parts of the wedge. It is also fairly simple to check the relationship between the position of the wedge and the output that is written onto the magnetic tape (see Fig. 2.3.10) to look for non-linearities in the potentiometer.

A problem with all microdensitometers, and probably the major source of non-linearity with the Joyce-Loebl, is the low assessment of true density due to transmission averaging across the measuring slit. The machine is balancing the amount of light passing through the sample against that coming through the grey wedge, and has no means of

FIGURE 2-3-10 : LINEARITY OF DIGITISATION PROCESS



compensating for the density structure across the measuring aperture. Taking a trivial example of a slit, half of which contains zero density and the other half contains density  $1D$ , it can be shown that the true average density is  $0.5 D$  while the measured density from the average transmission is  $0.26 D$ . Pilkington (72) has calculated these effects for stellar images with a gaussian profile of half density width  $W$  and peak density  $D_0$  above background, scanned with a square aperture of side  $L$ . He has shown that the error ( $\Delta_m$ ) in the magnitude derived from the density solid of the image is given by

$$\Delta_m = 0.29 D_0 \left(\frac{L}{W}\right)^2$$

Thus for an image peak density 3 an error of  $0.1^m$  requires a slit of  $\frac{1}{3}$  the <sup>width at</sup> half density height of the image ( $W$ ) and an error of  $0.01^m$  (about 1% accuracy) requires a slit of approximately  $\frac{1}{10} W$ .

Taking a fairly simple case of a linear density gradient across the measuring slit it is possible to do some order-of-magnitude calculations on the change in density across the slit that is tolerable for a given percentage error in density measurement.

Using the relationship between density ( $D$ ) and transmission ( $T$ )

$$D = -\log_{10} T$$

it can be shown that

$$T = 10^{-D} = e^{-KD} \quad \text{where } K = \log_e 10$$

if  $D$  is of the form that

$$D = Gx + C$$

where  $x$  is the displacement across the aperture and  $C$  is the background density level, then the average transmission  $T$  across a slit of width



'a' is given by

$$\begin{aligned}\bar{T} &= \frac{1}{a} \int_0^a T dx \\ &= \frac{1}{a} \int_0^a e^{-K(Gx+C)} dx \\ &= \frac{-e^{-KC}}{KGa} \left[ e^{-KGx} \right]_0^a \\ \bar{T} &= \frac{e^{-KC}}{KGa} \left[ 1 - e^{-KGa} \right]\end{aligned}$$

Therefore if we now turn this into the measured density  $D^*$

$$\begin{aligned}D^* &= -\log_{10} \bar{T} = \frac{1}{K} \log_e \frac{1}{\bar{T}} \\ D^* &= C + Ga + \log_{10} \frac{KGa}{(10^{Ga} - 1)}\end{aligned}$$

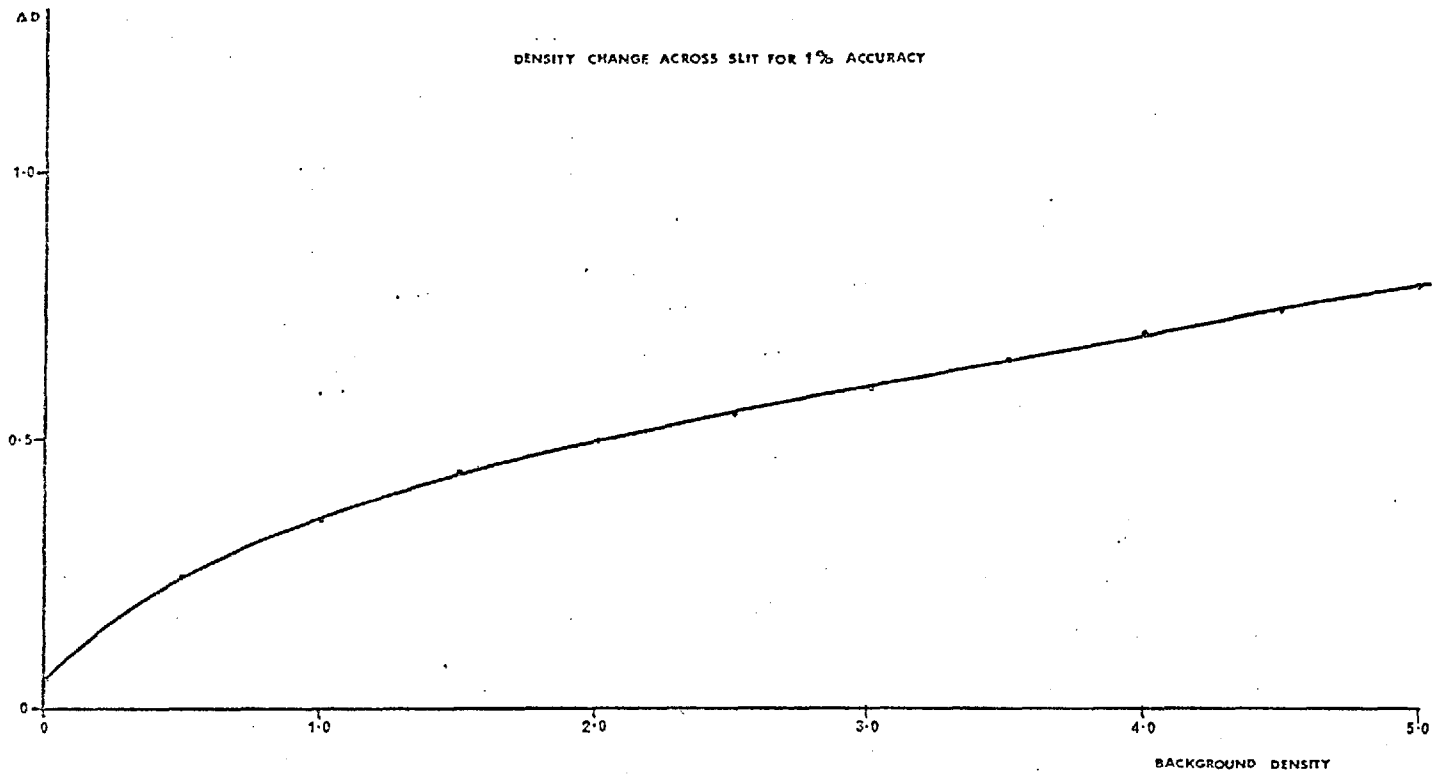
But  $\bar{D}$  is the true average density

$$\bar{D} = C + \frac{Ga}{2}$$

Therefore the percentage departure from the true density  $\Delta\%$  is given by

$$\Delta\% = \frac{\bar{D} - D^*}{\bar{D}} \times 100 = \left( \frac{-\log_{10} \frac{KGa}{(10^{Ga} - 1)} - \frac{Ga}{2}}{\frac{Ga}{2} + C} \right) \times 100$$

FIGURE 2-3-11



Ga is simply the density change across the slit. Let this be equal to  $\Delta D$ , then  $\Delta\%$  is given by the following expression

$$\Delta\% = \frac{100}{\frac{\Delta D + C}{2}} \left( -\log_{10} \frac{K\Delta D}{10^{\Delta D} - 1} - \frac{\Delta D}{2} \right)$$

A Hewlett Packard calculator was used to evaluate  $\Delta D$  for different values of background density C for a  $\Delta\%$  of 1. The results are shown in Fig. 2.3.11.

It is very simple to extend the treatment to two gradients in both x and y directions across a slit of side 'a' such that the density (D) at any given point is

$$D = Ax + By + C$$

D\* the measured density is then given by

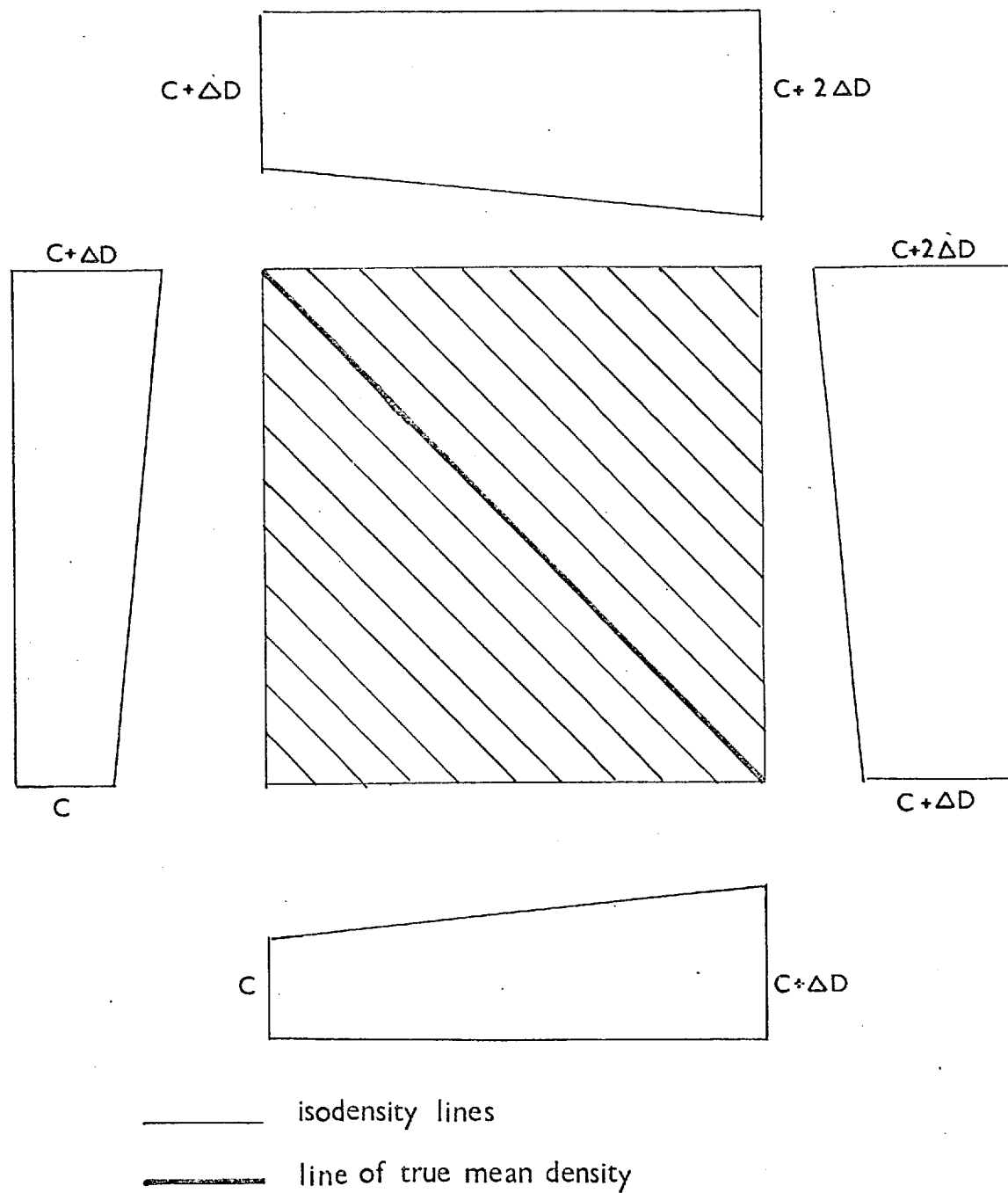
$$D^* = C + Aa + Ba + \log_{10} \frac{K^2 ABa^2}{(10^{Ba} - 1)(10^{Aa} - 1)}$$

now if  $A = B = G$  the percentage density change ( $\Delta\%$ ) is given by

$$\begin{aligned} \Delta\% &= \frac{100}{Ga + C} \left( -2\log_{10} \frac{KGa}{(10^{Ga} - 1)} - Ga \right) \\ &\approx \frac{100}{\Delta D + C} \left( -2\log_{10} \frac{K\Delta D}{(10^{\Delta D} - 1)} - \Delta D \right) \end{aligned}$$

which at zero background density yields the same limit as the one-dimensional treatment. This may at first seem odd since there is a total change of  $2\Delta D$  across the diagonal of the aperture. However, by considering the aperture split up into strips of equal density (see Fig. 2.3.12) one can see that a heavier weighting is given to those areas clustered round the true mean density.

FIGURE 2-3-12: VARIATION OF DENSITY ACROSS MEASURING SLIT

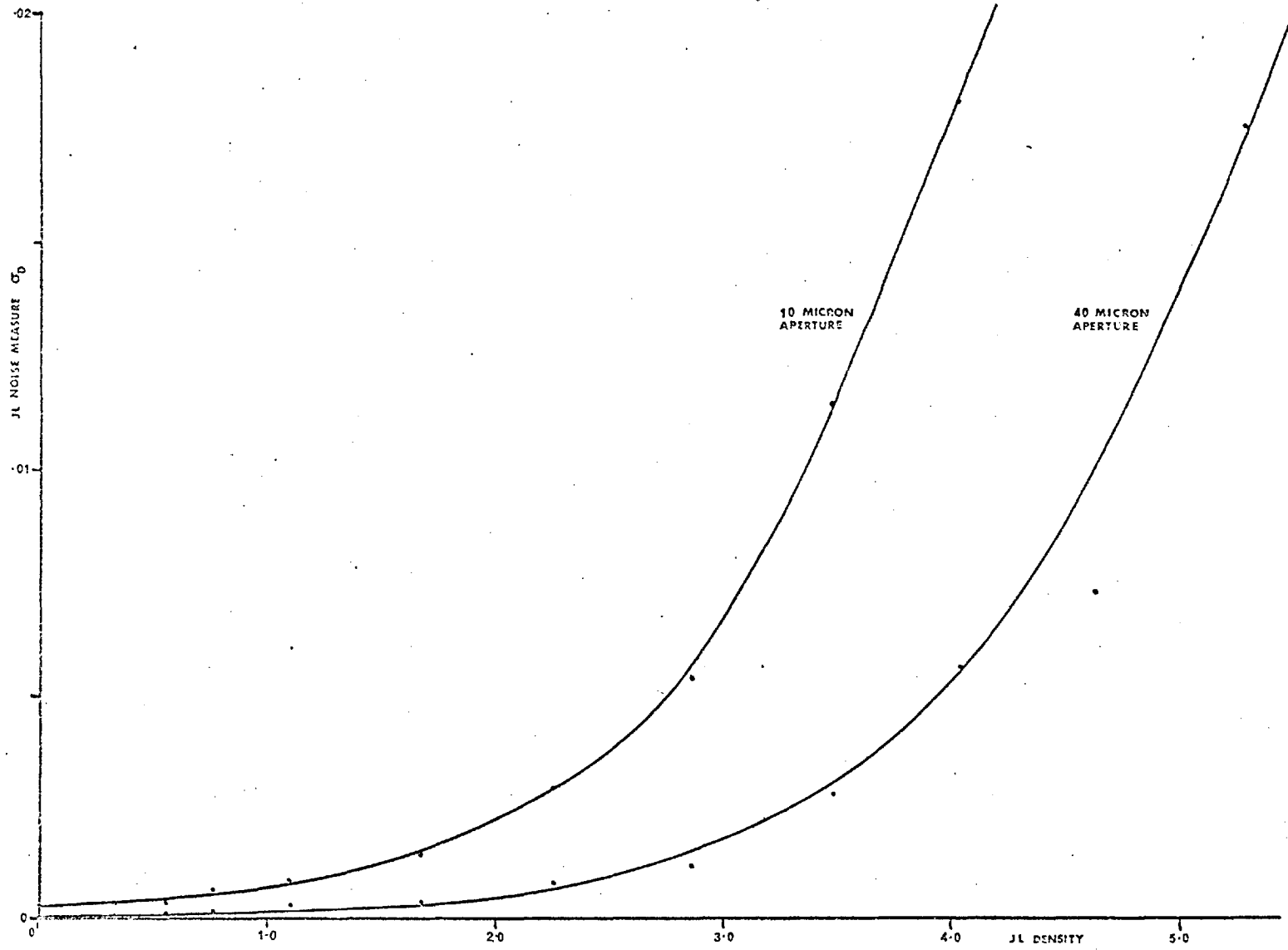


Therefore, for given image content, these figures can be used as a guide to the maximum size of measuring aperture that can be used. At this point it might be valuable to stress the distinction between the "measuring aperture" and the "analysing aperture". In the first case one is considering the effective size, at the emulsion surface, of the measuring slit of the microdensitometer. In the second case the analysing aperture is the area which is considered as a single element in the numerical analysis undertaken using computer programs. It can be the same size as the measuring slit or an integer multiple of it. This effect is achieved by adding adjacent samples from a scan to form a new array of data for processing. Experiments have shown that, for emulsion noise data, the noise scales down with the addition of samples, as would be expected. That is, the noise is reduced by  $\sqrt{N}$  where  $N$  is the number of samples added together. However, for systematic rather than random fluctuations this addition does not reduce the noise. Therefore, even if a fairly large analysing aperture is required, sampling must still be undertaken with the size of aperture dictated by linearity and accuracy considerations and the data then added together to give the required resolution element.

#### 2.3.4 Microdensitometer Noise

Having considered the systematic errors of the microdensitometer it is necessary to deal with the random noise arising from both the photometric system and the digitising electronics. Since the digitisation process is used purely to register the position of the grey wedge, the noise arising from this source should not change over the different density ranges. It should only be of importance at low densities since at high density the predominant effect should arise from photon shot noise within the photometric system.

FIGURE 2-3-13



Measurements of system noise have been made for the Joyce-Loebl by holding neutral density filters fixed in the measuring beam while scanning the table in the normal manner. The densities produced were written to magnetic tape and were subsequently processed on an INTERDATA 70 minicomputer to produce r.m.s. noise values. For each density, 5 scans of 1,000 points were taken, each scan on a different part of the grey wedge. Fig. 2.3.13 shows results for 10  $\mu\text{m}$  and 40  $\mu\text{m}$  square measuring apertures. The r.m.s. density noise ( $\sigma_D$ ) is plotted against the density of the neutral filters as measured on the Joyce-Loebl. Using the relationship between density (D) and transmission (T)

$$D = -\log_{10} T \quad (\text{i})$$

one can relate the density variation ( $\sigma_D$ ) to the change in transmission  $dT$

$$\sigma_D = dD = -\frac{1}{\log_e 10} \frac{dT}{T} \quad (\text{ii})$$

If  $N^*$  is the number of photons passing through the slit at zero density, in the time it takes to make a measurement, then the number of photons (N) passing through the slit at transmission T are given by

$$N = TN^*$$

Thus

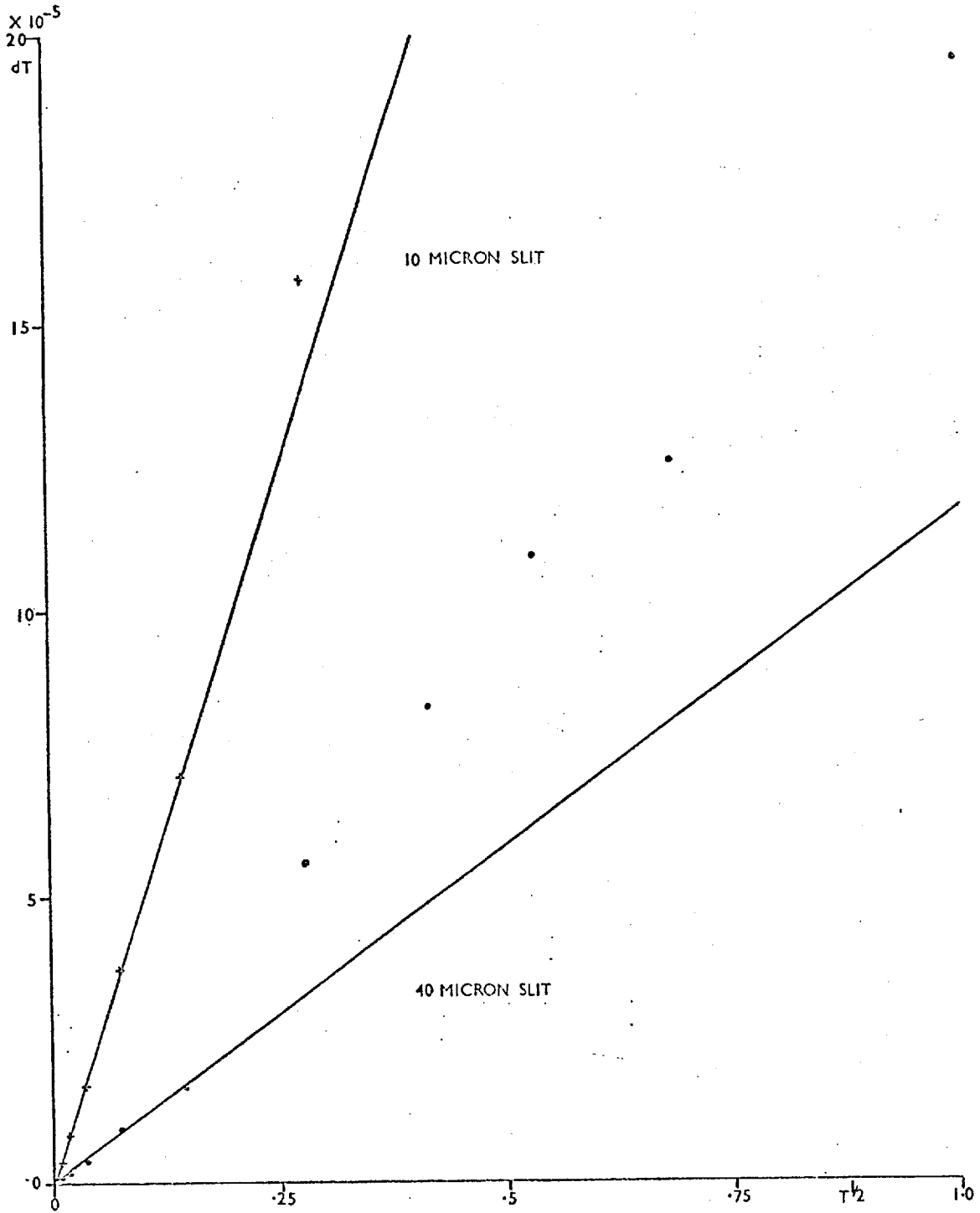
$$dN = N^* dT \quad (\text{iii})$$

and so

$$\frac{N}{dN} = \frac{T}{dT} \quad (\text{iv})$$

Therefore  $\frac{N}{dN}$ , which is the photon signal-to-noise ratio of the photometric system of the machine, can be related to the density fluctuation  $\sigma_D$

FIGURE 2-3-14





$$\frac{N}{dN} = \left| \frac{1}{\sigma_D \log_e 10} \right| \quad (v)$$

However, since photons obey Poissonian statistics

$$dN = \sqrt{N^*T} \quad (vi)$$

substituting (vi) in (iii)

$$dT = \frac{1}{\sqrt{N^*}} \sqrt{T}$$

Therefore a plot of  $dT$  versus  $\sqrt{T}$  should yield a straight line if the machine is limited by the photon shot noise of the system. Fig. 2.3.14 shows the plots for different slit widths. It can be seen for the 40  $\mu\text{m}$  aperture that there are two distinct parts to the plot. It must be remembered that what is actually being measured is  $\sigma_D$ , which from equation (ii) is proportional to  $\frac{dT}{T}$ . This quantity, which in turn is proportional to  $\frac{1}{\sqrt{N}}$ , will decrease at high transmissions and so eventually the limiting electronic noise of the digitisation system will begin to dominate, resulting in an over-assessment of photon noise at low density. One can also argue that at higher transmission the closer spacing of points serves to give a better fit for a straight line. However, if the slopes of the two lines, taken from the low transmission measurement, are used to make an estimate of the number of photons passing through the slit at zero density, a factor of 16.2 is found between the two results. This is in good agreement with the factor of 16 one would expect from the difference in areas of the measuring apertures.

The useful working density range of the microdensitometer can be defined by comparing its own noise with that of the emulsion for the same given measuring aperture. The machine should always be operated so that it is the emulsion noise that dominates - then one obtains the correct reduction in emulsion noise when samples are added together

to provide a given analysing aperture. This limiting density will then define the highest accuracy that can be reached for a given resolution element. (Referring to section 2.2, for L4 emulsion, where the zero frequency noise power  $n(0)$  is proportional to density, then the signal-to-noise power ratio  $\left| \frac{s(0)}{n(0)} \right|^2$  should also be proportional to density.)

Having outlined the general properties of the photometric system, the next process is to examine its use and performance in astronomical observations.

## CHAPTER III

### ASTRONOMICAL OBSERVATIONS

"The universe is full of magical things,  
patiently waiting for our wits to grow sharper."

Eden Phillpots

This chapter deals with the acquisition of astronomical exposures and their subsequent reduction to useful information. There are three main aspects to be considered - the mounting of the image tube on the telescope and the observational procedures, the scanning and processing of the exposures and the interpretation of the results obtained.

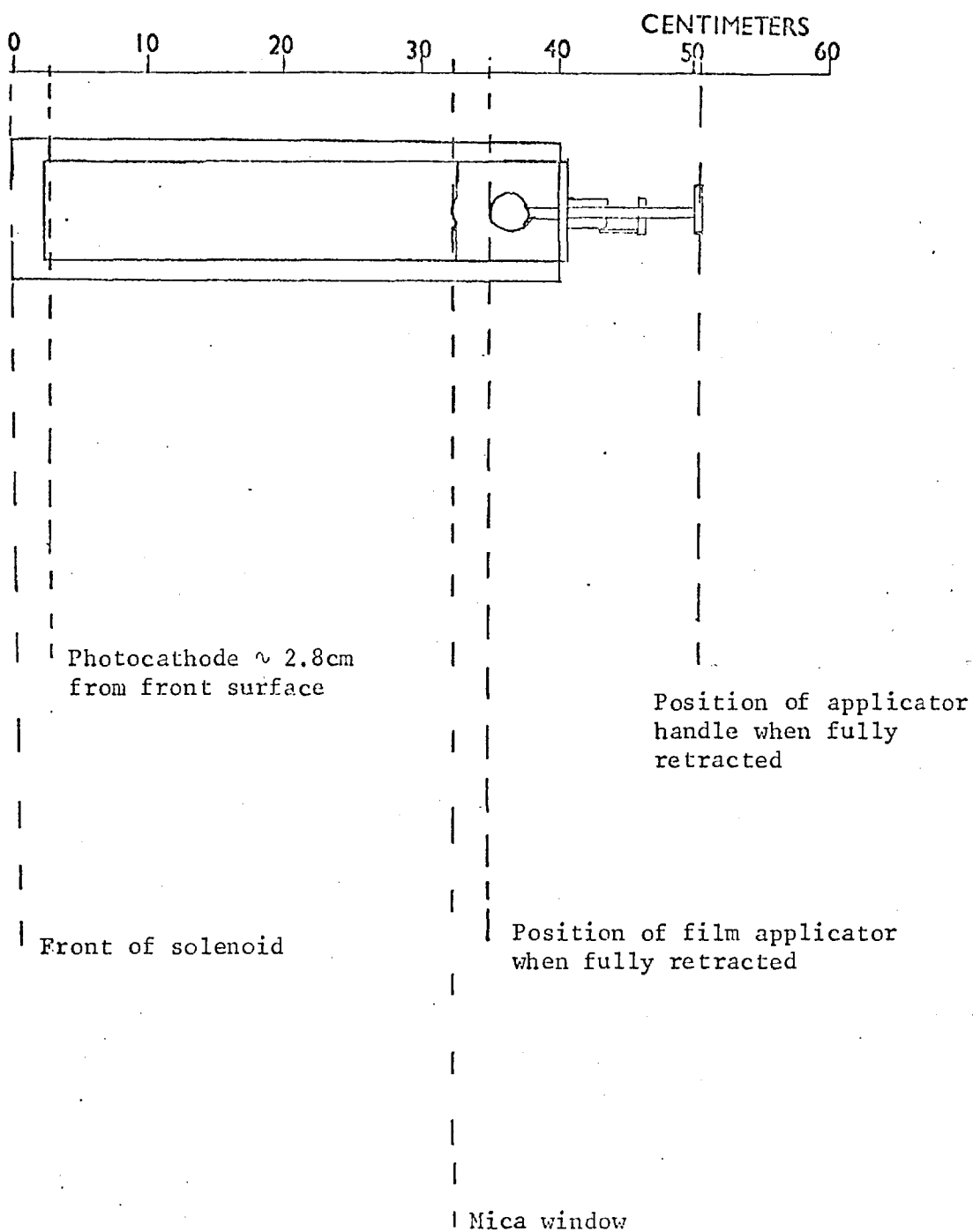
#### 3.1 Spectracon Cameras

This section deals with some of the general aspects of mounting a Spectracon on a telescope, together with a description of a simple camera developed by the author.

##### 3.1.1 Weight and Dimensions

The present-day Spectracon solenoid (see Fig. 2.1.1) was specifically designed to be as light and compact as possible while maintaining an adequately uniform magnetic field. The use of mu-metal shields ensures that the effects of stray magnetic fields external to the coil (such as the earth's magnetic field) are reduced below the level that would cause a serious shift in the image. (A shift of 5  $\mu$ m occurs for a transverse field of 0.003 oersted at double-loop focussing. (Bacik (56).) The solenoid has been described in full detail by McCee et al (75) and a variation of that design, not requiring liquid cooling,

FIGURE 3-1-1 : DIMENSIONS AND CLEARANCES FOR SOLENOID



has been produced for operation at the prime focus of a large telescope (McGee et al (4)).

The outer diameter of the solenoid is about 10 cm and the length is approximately 40 cm. When the tube and film holder are in place a further clearance at the back end of about 20 cm is required if the film is to be loaded and retracted without undue damage (see Fig. 3.1.1). The entrance aperture of the solenoid is about 4 cm diameter and the tube sits well back so that the photocathode lies about 28 mm inside the solenoid. The total weight of the combination of Spectracon plus focussing coil is about 11 kg to 12 kg. Thus, with design of a sufficiently-rigid, light-weight support, this device can be mounted on a fairly small telescope (76).

### 3.1.2 Cooling

The solenoid can be operated at 1 or 2-loop focussing, producing 16W and 65W respectively. When located at Cassegrain and Coudé foci, liquid coolant can be circulated through the solenoid. This liquid can be either tap water or anti-freeze circulated by a cooler. As has been mentioned previously a solenoid has been developed for operation at the prime focus, where it is not feasible to use liquids. In this case four Peltier coolers are located at the front of the coil to cool the photocathode. This system is only operated at single-loop focus and good thermal contact with a large heat sink is required. A temperature differential of about 20°C is maintained between the photocathode and ambient temperature.

In both solenoids the cooling is concentrated towards the photocathode end of the tube while the mica window is allowed to warm up. This prevents condensation on the window and problems with the emulsion becoming sticky.

### 3.1.3 Power Supplies

Two sets of cabling must be run to the camera, a high voltage cable carrying the 40 KV supply to the Spectracon and a 12-way low voltage cable which supplies the solenoid. A high voltage connector is usually located close to the solenoid and an adequate form of clamping and support must be provided to stop the cable shifting when the telescope is moved. A good earth return is absolutely essential.

### 3.1.4 Adjustments to Position Angle and Focus

The number of degrees of freedom which have to be built into the camera depends very much on the properties of the mounting flange and telescope to which it is being matched.

Because of the rectangular shape of the image area of the Spectracon an adjustment of position-angle is necessary so that objects which are greatly extended in one direction can be accommodated. This rotation need only have a complete range of  $180^{\circ}$  and is fairly easy to provide by rotating the assembly of solenoid and tube in its mounting.

The position of the focal plane of the telescope can usually be set with sufficient accuracy using the telescope controls and only a coarse location adjustment need be built into the camera.

The location of the photocathode 28 mm inside the solenoid causes no problems when there is a large back focal-distance to play with. However, some difficulties can arise at the prime focus. For example there is approximately 75 mm between the surface of the Wynne corrector and the focal plane at the prime focus of the Isaac Newton Telescope. This is sufficient space to fit in a filter holder and shutter arrangement but not enough for any form of reflex viewer or field finder.

### 3.1.5 Acquisition and Setting

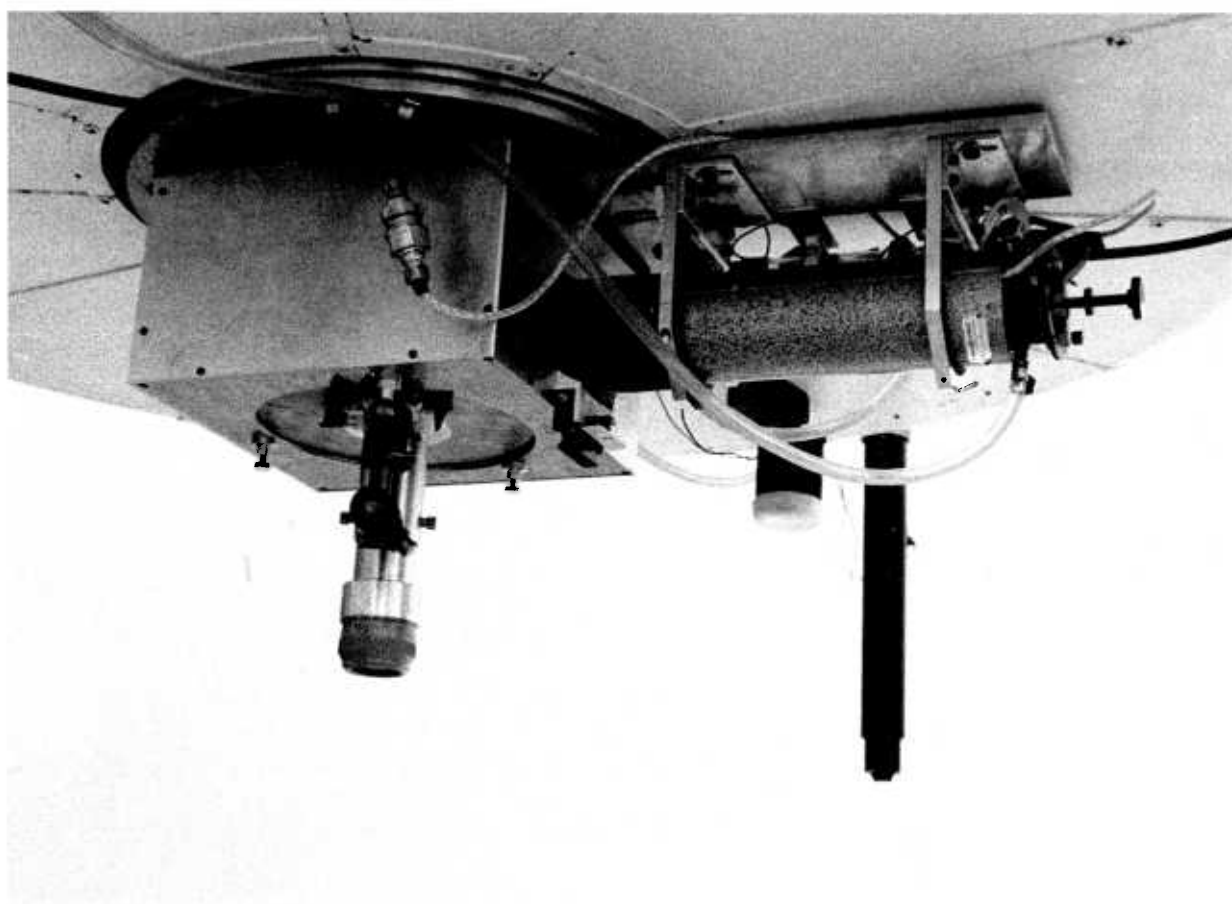
The limited image area of the Spectracon is often cited as a disadvantage in astronomical observations (Walker (9)). Certainly for work on large star clusters this can be a drawback, but there is quite a substantial class of objects that can be easily fitted onto the photocathode provided that they can be set with a fairly high accuracy.

The general problem of acquiring an object obviously varies in nature with the complexity of the telescope. With a mechanically accurate and fairly sophisticated instrument such as the Isaac Newton Telescope accurate co-ordinates and off-setting techniques can be used to good advantage. If such co-ordinates are not available or if the telescope cannot be set to within the accuracy required, then some form of field viewing device and a means of relating the photocathode position to that field are needed. This can range from a television finding system, if it is already available, to a simple combination of cross-wire and eyepiece. Certainly it is an advantage to be able to view the field as seen by the photocathode and very often the efficiency of an observing programme will be governed by the ease of acquisition and setting of the objects.

### 3.1.6 Additional Requirements

As with any instrument there must be provision for some sort of guiding eyepiece, a shutter mechanism and filters. Also care must be taken to exclude stray light. This is particularly important when the observing floor is illuminated with red lamps and a S-20 response tube is being used. Light levels that are not visible when a phosphor screen is placed near the mica window can still produce clearly visible background within an hour on L4.

FIGURE 3-1-2 : BOYDEN CAMERA





### 3.1.7 Spectracon Camera for a 60" Reflector

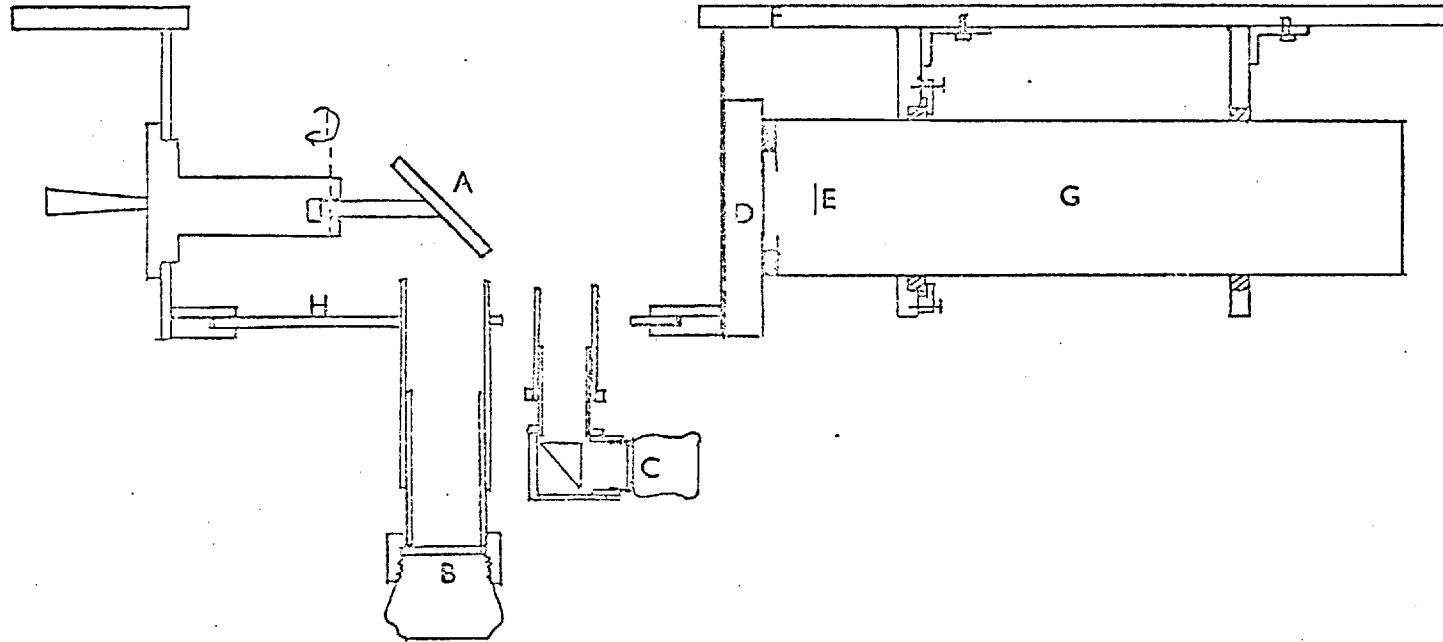
During April 1973 observations of some southern radio sources and planetary nebulae were undertaken using a Spectracon on the 60" reflector at the Boyden Observatory, Bloemfontein, South Africa. The camera that was built for the Cassegrain focus of this instrument is shown in Fig. 3.1.2 and a cross-sectional diagram is shown in Fig. 3.1.3.

The camera was to be mated to a fixed mounting flange so a facility for adjusting the position angle had to be provided. The setting accuracy of the telescope was known to be worse than  $2'$  and, since the Spectracon photocathode represented a field of  $1 \frac{1}{3}' \times 4'$ , it was necessary to provide an adequate field-finding eyepiece for acquisition and setting. The telescope was provided with only a 4-inch finder so that a guiding eyepiece also had to be built into the camera. Focusing was achieved using movements of the secondary mirror of the telescope, although positional adjustment of the solenoid was built in.

When working on certain parts of the sky the back of the 60" mirror-cell comes within a couple of feet of the floor. Since the focal plane lies in a range between 14" and 18" from the back of the cell, a "straight through" system for the Spectracon was clearly not feasible. Therefore, it was decided to use an accurately locating  $45^\circ$  mirror to deflect the image onto the tube, this mirror being moved to one side of the beam when the field finder was being used. The system had been used before at the Cassegrain focus of the Isaac Newton Telescope (INT) with satisfactory results.

The finding and guiding eyepieces were mounted on a circular plate; this could be rotated through a full  $360^\circ$  and clamped in position. The guiding eyepiece was also provided with a radial motion by being

FIGURE 3-1-3 : CROSS-SECTION OF 60 INCH CASSEGRAIN CAMERA



- |   |                                  |   |   |
|---|----------------------------------|---|---|
| A | 45° flip-in mirror               | E | Position of photocathode                |
| B | Finder eyepiece                  | F | Base plate                              |
| C | Guider eyepiece                  | G | Solenoid                                |
| D | Filter holder + shutter assembly | H | Top plate providing rotation for guider |

mounted on a dovetail slide. This provided a total search area for the guider of a little under 500 square arcmins. The guider eyepiece was provided with a graticule with a guiding box of  $2'' \times 2''$ . The unvignetted field of view of the finder eyepiece was about  $5'$  in diameter and a graticule with a central box of  $5 \text{ mm} \times 5 \text{ mm}$  ( $44'' \times 44''$ ) was fitted. The camera was built so that the finder eyepiece could be adjusted to be confocal with the photocathode. Therefore, by setting the object using the main finder graticule it was possible to make it fall on the photocathode when the  $45^\circ$  mirror was put into the beam. The whole top plate assembly was supported from the base plate by four pillars. The  $45^\circ$  mirror-mount was attached to one wall of the camera, which was made of  $\frac{1}{4}''$  dural plate, while the remaining three sides of the box were made from light-weight cladding.

Since water cooling was used there was no need to provide a large heat sink at the front end of the solenoid. Therefore a layer of black rubber was used between the solenoid and the filter holder and shutter assembly to provide a light seal. As an added precaution a hood was fitted over the front part of the tube. Light leaks through the slot in the guider plate were reduced by fitting a strip of black paper which was free to move back and forth with the guider and which was held down on the plate by light-weight runners made from small strips of plastic.

The total weight of the finished camera plus solenoid came to about 40 kg. Various parts of it have since been incorporated in a slightly heavier version for use on the Isaac Newton Telescope. This latter arrangement can also accommodate a narrow-gap Fabry-Perot interferometer which can be used as a tunable filter (Reay, Ring and Scaddan (77)).

Further descriptions of the mountings for the Spectracon are given by Walker (22,78), McGee et al (4) and Coleman et al (76). The tube and solenoid has also been incorporated as the detector in a coherence interferometer described by Dainty and Scaddan (79).

### 3.2 OBSERVING PROCEDURES

The Spectracon system is fairly easy to set up and run and only simple precautions are necessary.

1) The EHT connections to the tube should be checked to ensure good contacts throughout, and the tube should be properly earthed. The most common cause of corona in the connectors is bad contact between the plug and socket. However, high humidity can cause trouble, and in this case dessicant can be packed round the mouth of the EHT junction box and an extra seal added.

2) The cooling, focussing current and EHT should be run up well before observing is started to allow time for both thermal and electrical stabilisation of the tube. The EHT should be applied fairly slowly (over 1 minute minimum) to allow for the gradual charging up of the glass spacers.

3) The mica window of the tube is surprisingly strong and it should not implode unless treated carelessly. Any dust should be removed from it using a soft brush. These small particles are unlikely to break it but will mask the emulsion and mar the exposure. The main trouble will arise if the window becomes damp, because the emulsion will stick to it when put in contact and will pull the mica away when removed.

4) To obtain good exposures care must be taken to ensure that the emulsion remains clean during processing (see Appendix I). Small pieces of dirt can usually be recognised when the plates are measured, but

smears and patches due to uneven drying will look like features of the object, particularly in the very low contrast images.

With very elementary care the Spectracon can be mounted and operated on many different sorts of telescopes and sites. For example, during the past three years, as well as being used at both the prime and Cassegrain foci of the INT, it has been used for observations in South Africa, Tenerife and Hawaii, on telescope apertures ranging from 20" to 60".

### 3.3 SCANNING AND COMPUTER PROCESSING OF ELECTRONOGRAPHS

Once having obtained an electronograph one has to set about producing useful information from it. The exposure must be scanned and the resultant data processed to produce the required output. The Joyce-Loebl microdensitometer (described in Chapter II) was designed to produce magnetic tape in a format that could be easily handled by the CDC 6400 computer at the College computer centre, and most of the reduction routines have been developed using this machine. However, it is a fairly simple matter to transfer them to the CDC 6600 that is available at the University of London computer centre. Some of the programs that will be described were originally used on data produced by a Joyce-Loebl Autodensidater at the Royal Greenwich Observatory, Herstmonceux. In these cases the author has had a hand in modifying them and getting them to work with the data produced by the Imperial College densitometer.

#### 3.3.1 Scanning

When scanning the exposure the following parameters have to be chosen: slit width, sample step length, extent of scan and angle of scan. The slit width and sample length are normally chosen to be the same. The slit width is set by linearity considerations (see Chapter II)

combined with the density content of the object and the plate scale of the exposure. The scan area is usually chosen to be somewhat larger than the visible object since, through experience, it has been found there can be extensions to the object which are not apparent to the eye. The angle of scan can be easily adjusted and is usually set up to be E-W or N-S for convenience. The density range of the object can be assessed by moving the sample back and forth in the measuring beam and the appropriate grey wedge is chosen.

The data is written onto magnetic tape with a header record containing scan identification and standard densities. The magnetic tape records are made up of 256, 60 bit words, each word representing ten characters. Each density word is made up of four characters, thus a full record holds 640 densities. The header record is filled up with zeros after the last standard density has been written, and the scan is started at the beginning of a new record. All the records are filled up, the beginning of a new line being represented by a different leading character from the one used for the beginning of a density word. The last record of the scan is filled up with zeros after the last measured density and then a file mark is put on automatically. After a scan is completed the machine returns to the starting point and the tape is ready to receive a new scan.

This binary tape produced by the machine can be read into the CDC 6400 computer; it is then possible to translate it into a format that is readable using FORTRAN programs. It is in this form that all the scans are stored for archive purposes, the scan tapes being re-used once the data has been translated.

### 3.3.2 Computer Processing

Listings of the computer programs referred to in this section are to be found in Appendix II.

#### JLTRAN (Translation Program)

The advantage of producing digital data on magnetic tape is that it can be processed in many different ways. Since the output from the microdensitometer is used by a lot of people it is necessary to get it into a form that can be handled using a high level language like FORTRAN. Thus, if all users adhere to the same data format on the tape, a pool of programs, that can be used on all tapes, can be built up.

The original translation routine was written by C.L. Stephens (80) and has been modified by the author. The data can be handled in three ways:

- 1) The tape can be dumped in Octal onto the line printer.
- 2) The tape, with a header, can be translated and written to an archive file in "standard format".
- 3) The tape, without a header, can be translated and then an addition to the program must be made to write the data to a given output device.

The archive format stores all the information considered necessary to identify the scan and to retain its usefulness if the original log data for the scan has been lost. The header consists of identifying characters for the user and scan number, the number of lines in the scan and number of points along a line, two 80-character alphanumeric arrays containing exposure and scan parameters and two arrays containing the values of standard densities and their corresponding measured values on the machine.

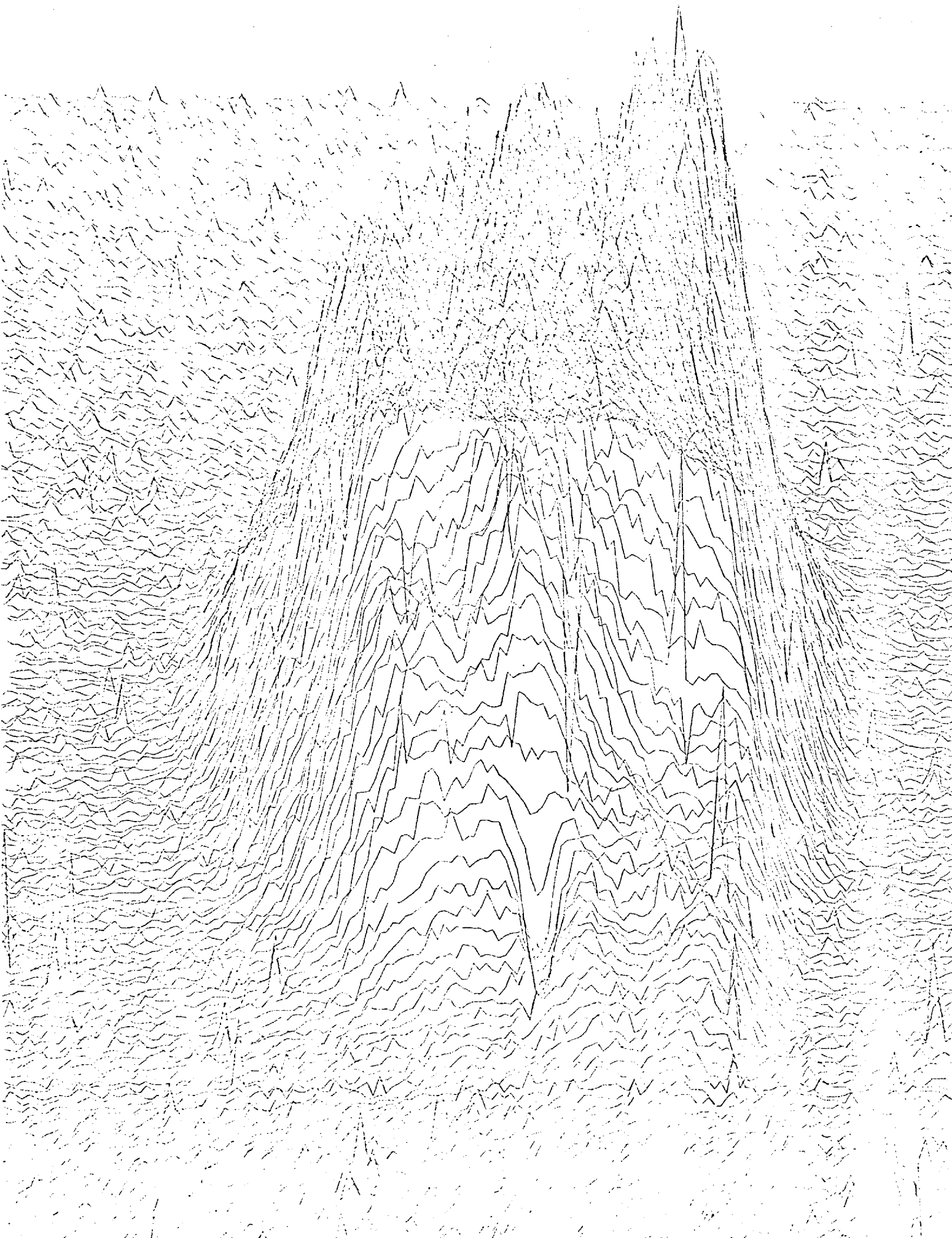


FIGURE 3-3-1: LARD DISPLAY FOR NGC 3918



The identifying characters, the measured densities and the number of points in the scan are all obtained from the tape produced on the Joyce-Loebl. The other data are read-in from cards. If there is a fault with the tape, so that it does not translate properly, the scan is not written to the archive and a message is put out on the line printer. The program is capable of translating several files and if one is faulty it will proceed to the next scan.

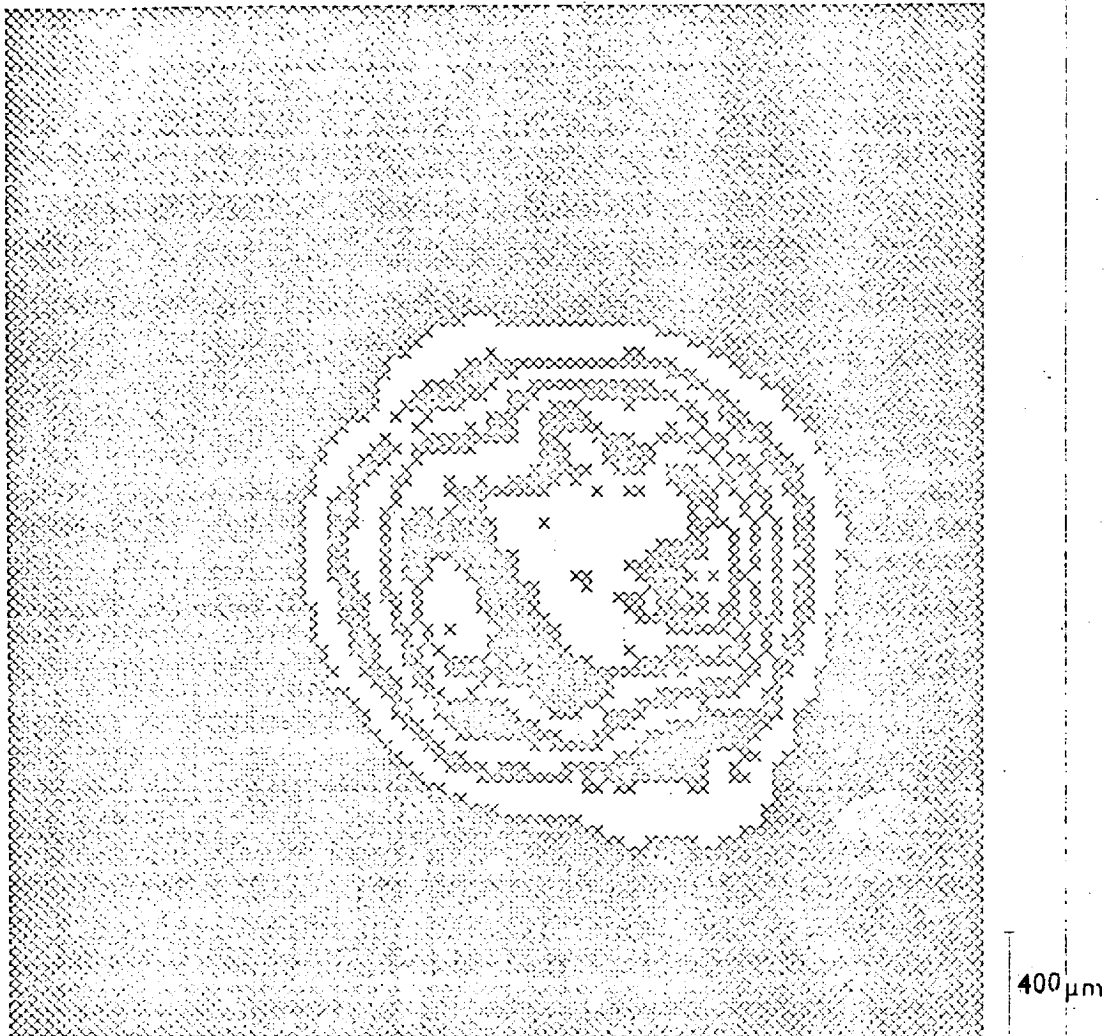
### Display Programs

Having obtained a translated scan some form of display routine is required. Most of the programs have been designed to use the plotting package, available at Imperial College, for the CALCOMP incremental plotter. These routines are easily transferred to the MICROFILM plotter available at the University of London computer centre.

#### 1) "Quick Look" Programs (LARD and MICSIT)

The first plot of any scan is used to get a general idea of the quality of the data and also of the position of the object within the scan. Two programs exist to do this job. The first, LARD, was written by C.L. Stephens (80) for use on data from scans of star fields produced by the Joyce-Loebl Autodensidater at Herstmonceux. It has since been modified to take the standard format tapes produced at Imperial College. A plot array is formed from either the complete scan or part of it, each plotting point being a single sample or an addition of adjacent samples. As this array is formed it is searched for its maximum and minimum value. This range in the data is then set equal to a given value of the plot "height". The array is drawn out line by line, the variations in density being represented by changes in the height of the plot from a given base line. Although this routine is economical in computer time the plot time can be fairly long when large arrays are being handled. An example of this form of display is shown in Fig. 3.3.1.

FIGURE 3-3-2: MICSIT DISPLAY



MENIZE 74 (NGC 3919) PLANETARY 5 MINS 0 111 13 APR 73 B 27E

SCAN IN AREA OF NEBULA USING WEDGE D 20 MIC BOYDEN B 27S L4 MELNX

PLOT OF COMPLETE SCAN WITH A BLOCKING FACTOR OF TWO

The LARD display has certain drawbacks in that it is not very easy to see "behind" the object, therefore a program working on similar principles (MICSIT) was written for the microfilm plotter. This again forms a plotting array from the same data, but the range in data is divided into a given number of grey levels. These grey levels are displayed by using a single character in an on/off mode to produce a set of dummy contours. This is a fairly crude form of display but has sufficient accuracy to locate the object and to give an idea of its extent for subsequent plotting by contour routines (see Fig. 3.3.2).

Each plot is labelled with the two alphanumeric arrays on the archive tape plus an array fed in from cards giving details about the area of the scan used. A scale marker, 10 plot steps in length, is also drawn on.

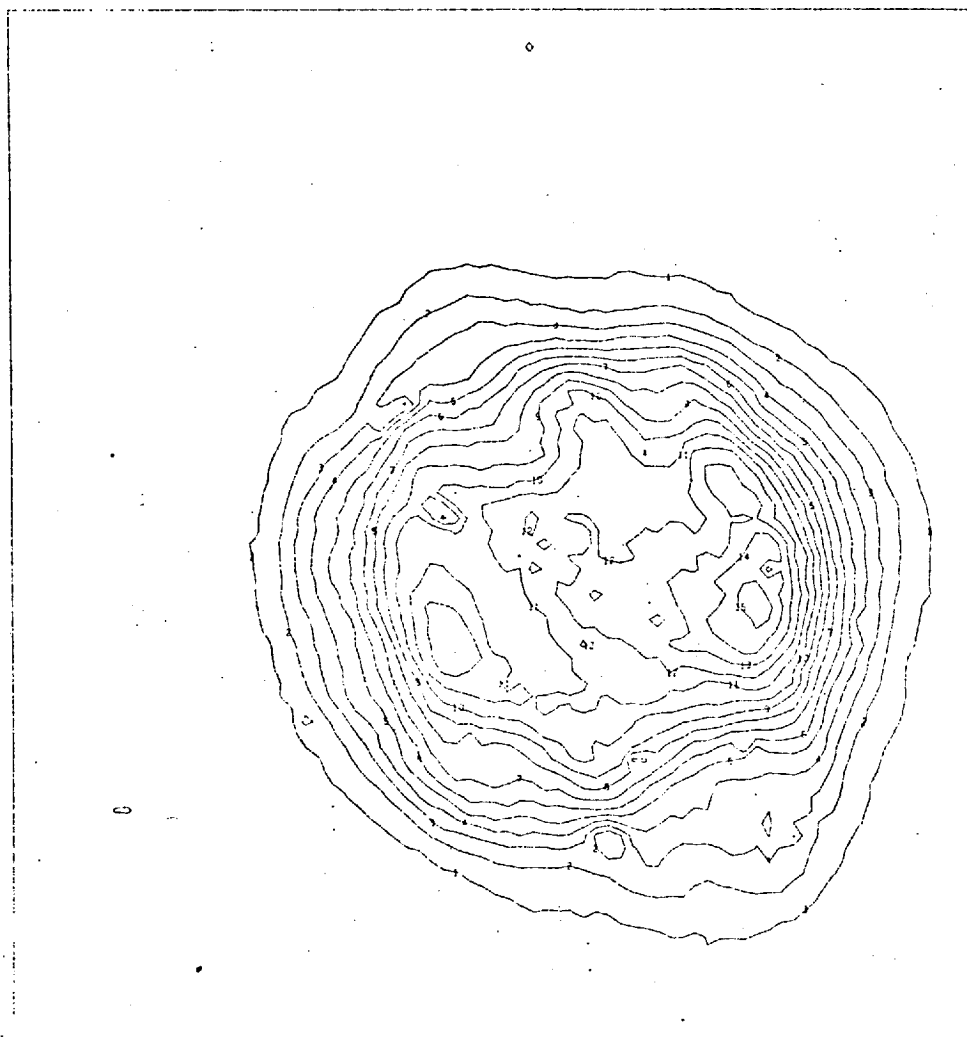
## 2) Contour Program (DSPLY) (C.L. Stephens (80))

Again a plot array is formed from the scan data (since this job has to be performed in many programs it was written as a sub-routine (SECTN)). The major sub-program (CONT) finds and draws a contour at a given level within the data array. The contour heights can be set to fixed levels, or a number of contours can be equispaced within the range of data. There is also a facility for logarithmic contour levels if required. The search mode of the contouring routine requires that the complete plot array be stored in the computer. To reduce the storage required, the "Quick Look" programs are used to select the minimum area of the plot required to obtain contours of the complete object. An example of the contouring routine producing 15 equispaced contours is shown in Fig. 3.3.3.

### Photometric Routines

The display routines, as such, reveal the general morphology of the object. Thus one obtains results that are available from machines such

FIGURE 3-3-3 : CONTOUR DISPLAY



ME174-04 (100 8418) PLURINARY 5 MINS 0 111 13 APR 73 B 275  
24. IN DEEP OF NEP-A USING WEDGE D 30 MIC 5020N B 275 L4 MELNY  
POINT 05 A 10.11 TO B 170.1441 WITH A BLOCKING FACTOR OF 1.63

400  $\mu$ m

as the Joyce-Loebl isodensitracer which use the exposure as a read-only memory to produce isodensity maps. Therefore one also needs routines which will produce information about fluxes from the object and which can be used to obtain more information from the contour maps. Most of the simple jobs have been written into one program (VOL) which is used in conjunction with the "Quick Look" routines.

a) Background level assessment

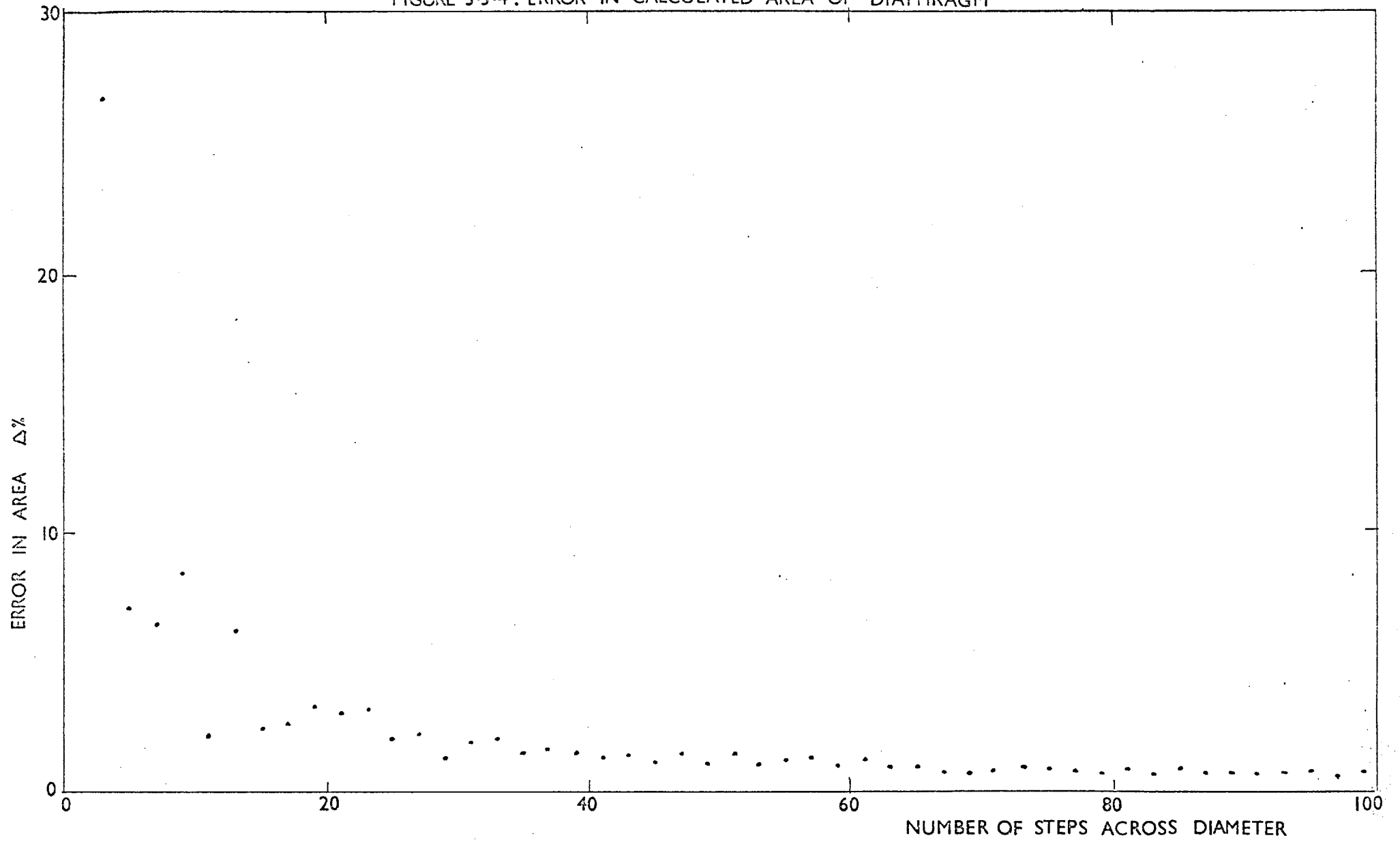
Using a display of the scan, to locate the object, areas of background can be selected. The co-ordinates of these areas are fed into the program and the background level and the noise on that background are assessed for each area. An average value is also calculated. The r.m.s. noise can be used to set the level of the outermost contour of the object.

b) Density volume assessment

The raster scan-pattern of the Joyce-Loebl most readily accommodates a rectangular or square "window" over which to make an assessment of the density volume, particularly if the size of the window is an integer multiple of the step length. At present an average value of the background level is subtracted since the program has been used on narrow band observations where the background level is very low and predominantly set by the plate fog.

For the total flux from the object the rectangular window is probably quite sufficient. However, it is useful to compare data from electronographs with integrated fluxes measured using circular diaphragms of different sizes with a photomultiplier. This will also provide a method for absolute calibration of contour levels. Therefore a sub-routine has been written into VOL which will take the density volume within a dummy circular aperture projected in the scan. Again, at the moment, it works with an integer number of samples, the data being read-in line by line. The difference in the value of the area of the "diaphragm"

FIGURE 3-3-4: ERROR IN CALCULATED AREA OF DIAPHRAGM



as compared with the actual area required is plotted against the number of steps across a diameter (see Fig. 3.3.4). Since most diaphragms used for astronomical photoelectric observations are in excess of  $5''$  across and the image scales used for the exposures such that at least 15 samples may be put across a diameter, this leads to an accuracy of at least 3%. If a higher accuracy is required two assessments of the volume can be made with two different diameters straddling the required value and the average volume can be found.

The programs as a whole tend to be changed and modified by different users to produce an output to suit themselves. The basic routines described here have served as general building blocks from which many variants have arisen.

#### 3.4 ASTRONOMICAL OBSERVATIONS

During the past three years the author has been associated with Spectracon observations of several types of objects including radio-galaxies, pulsars and planetary nebulae. This has afforded opportunities for working with the device at different telescope foci and for learning about the requirements of different observing programmes. However, the main area of interest, where the majority of the data reduction has been undertaken, has been in the narrow-band photometry of planetary nebulae.

In many ways the Spectracon is well suited to the study of these objects since they exhibit a wide range of surface-brightness which can be accommodated by the high dynamic-range of the electronographic process. Also the majority of the nebulae are of fairly limited angular extent; thus the small image area of the tube does not serve as a limitation.

### 3.4.1 Planetary Nebulae

#### 3.4.1.1 Formation

At present, it is believed that planetary nebulae represent a fairly common phase in the evolution of a large number of stars (Miller (85)). The most likely progenitors seem to be the red giants. These objects satisfy the mass (about  $1.5M_{\odot}$  (Liller and Aller (82))) and distribution requirements (Perek (86)) set by the nebulae. Also, studies of the structure of the atmospheres of these stars show that there are processes which can provide natural ejection mechanisms.

From observations of spectra of both the central stars and the surrounding nebulae, there seems to be a clear distinction between the hydrogen-deficient nucleus and the outer envelope which, being predominantly hydrogen, has a composition similar to Population I objects. This requires an ejection process which will produce a clear separation between an outer, largely unprocessed, stellar-envelope and a highly evolved core containing helium and heavier elements. There are three, not necessarily mutually exclusive, models that have been considered.

#### 1) Ionisation instability (Lucy (88), Paczynski and Ziolkowski (89)).

This is based on the fact that high-luminosity red giants can have envelopes with net positive energy if ionisation energy is taken into account. If this energy is converted to a motion of the outer envelope, the latter will escape from the nucleus with a terminal velocity of about 30 km/sec. This is close to typical observed expansion velocities of planetaries (Wilson (90)). So far the full dynamics of this mechanism has not been worked out and the instability has only been shown to exist. However, it is an attractive proposition in that it is associated with stars slightly more luminous than the long-period variables and would come as a result of evolution up the asymptotic red-giant branch of the



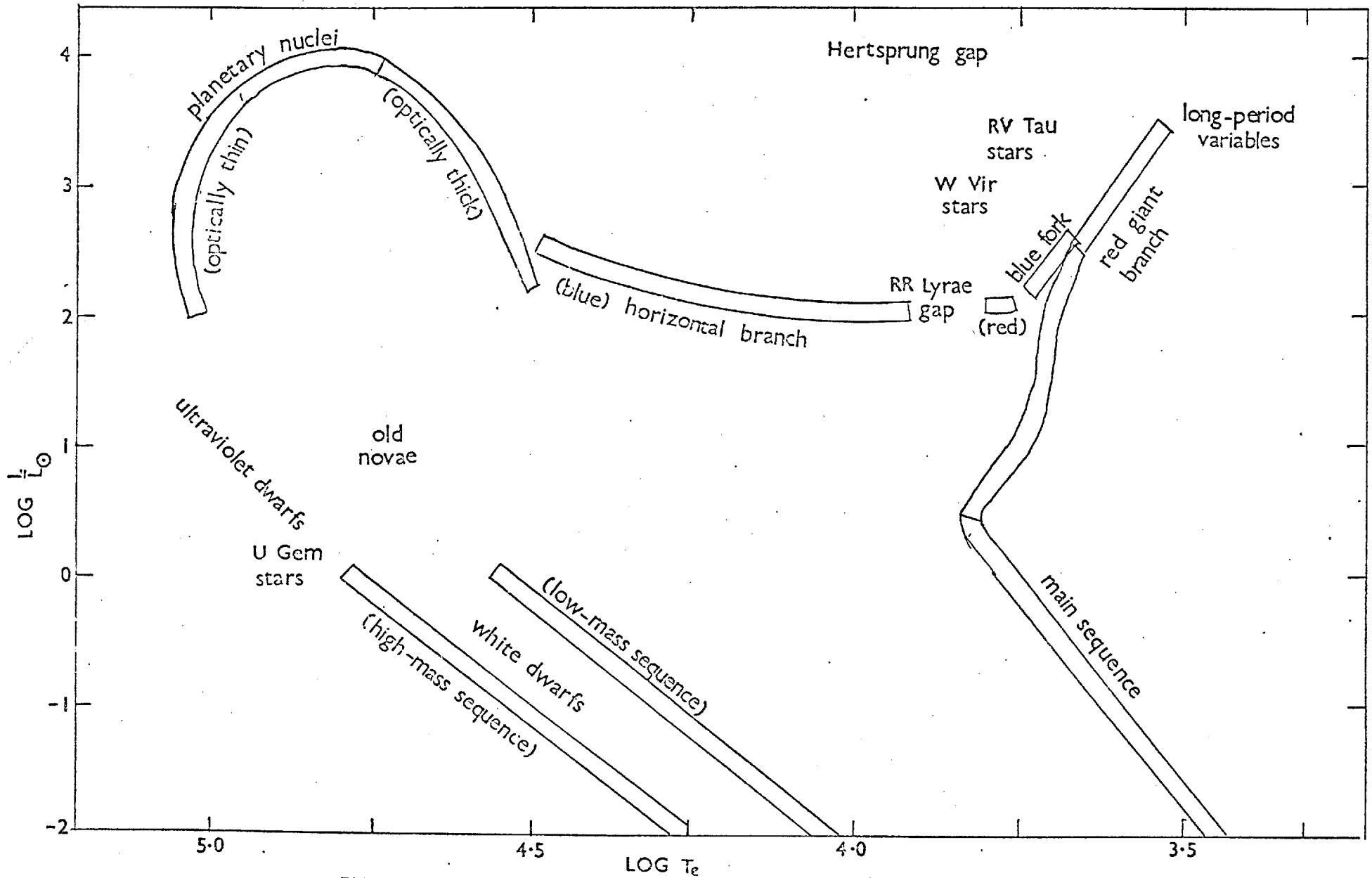


FIGURE 3.4.1: SCHEMATIC COLOUR-MAGNITUDE DIAGRAM

H-R diagram (see Fig. 3.4.1).

2) Helium-burning-shell instability (Rose (91), Smith and Rose (92))

In this case ejection of the envelope results from relaxation oscillations caused by instability in the helium-burning shell. Calculations for models of helium-shell-burning stars have been made showing that, in the unstable cases, the rate of nuclear-energy generation attains a high value for a short interval during each relaxation oscillation, the highest rate being obtained in the last oscillation, that is at the end of the helium burning and before the star starts to contract towards the white-dwarf stage. Cahn and Kaler (82) have shown that the local birth rate of planetary nebulae ( $3.2 \times 10^{-3} \text{ kpc}^{-3} \text{ year}^{-1}$ ) tallies quite closely with the local birth rate of white dwarfs ( $1.6 \rightarrow 5 \times 10^{-3} \text{ kpc}^{-3} \text{ year}^{-1}$ ) (Weidemann (83,84)). Therefore it is possible that planetary nebulae account for the production of a large proportion of white dwarfs.

3) Radiation-pressure forced ejection (e.g. Faulkner (93), Finzi and Wolf (94)).

Given the correct set of initial conditions radiation pressure can directly force the ejection of a stellar envelope. However, it is not clear how these conditions are reached during stellar evolution (Osterbrock (81)).

Of all these processes the ionisation instability mechanism seems the most likely but the link between the formation and the observed structure of nebulae has not yet been made. If multiple shell objects (Gurzadian (95), Kaler (96)) result from successive ejections of envelopes, some mechanism must be found to account for this process. One object which has a possible bearing on planetary evolution is F G Sge which is located in the centre of a fairly old planetary, Hz 1-5

(Faulkner and Bessel (97)). This star has been steadily brightening since the turn of the century, and certain spectral features show evidence of expansion velocities in the envelope of the order of 70 km/sec. Herbig and Boyarchuk (95,99) have proposed that F G Sge could be in the process of producing a second planetary shell. From measurements of the expansion velocity Flannery and Herbig (100) have set the age of the surrounding nebula at about 6,000 years.

#### 3.4.1.2 Spectra

Whatever the details are of the mechanism for the production of planetary nebulae, observations can provide us with an idea of the general properties of the well evolved nebula.

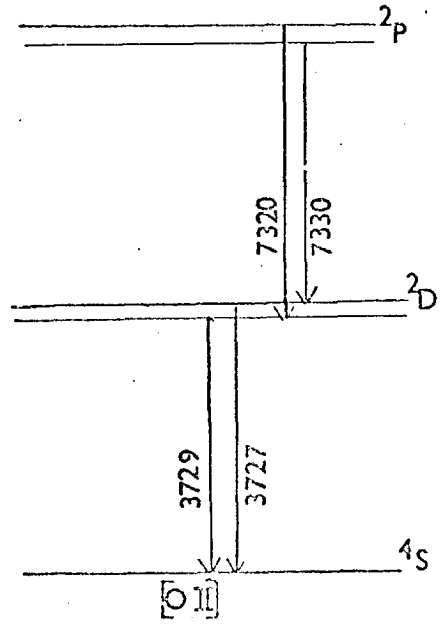
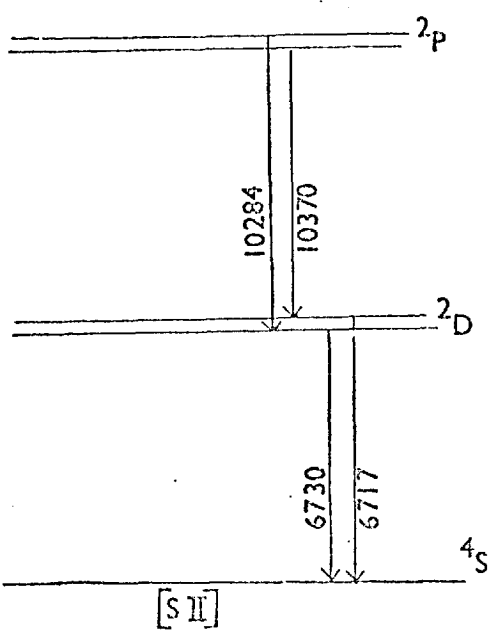
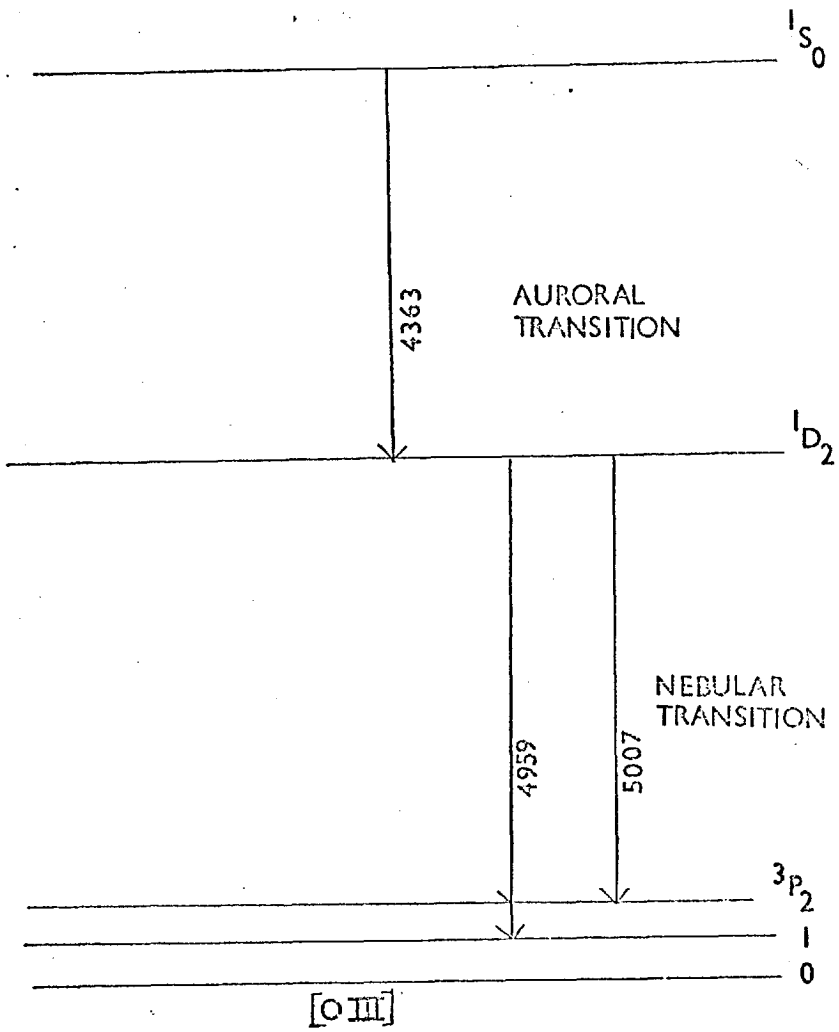
The nebulae are characterised by an emission line spectrum with a background continuum in the visible. The central star is of high temperature ( $30,000 \rightarrow 100,000^{\circ}\text{K}$  depending on the stage of evolution (87)) and emits mainly in the ultra-violet. Observations of these stars are to some extent hindered by the bright surrounding nebulosity which derives its emission from the degradation of the ultra-violet photons. The primary process within the nebula is photo-ionisation of atoms from the ground state. There are three main mechanisms which explain the observed emission line spectrum:

- 1) Recombination
- 2) Forbidden line emission
- 3) Fluorescence

#### 1) Recombination

When an electron is recaptured into a highly excited level of an atom or ion it can cascade to lower levels emitting permitted lines. The most abundant element in the nebula is hydrogen, while there are about

FIGURE 3-4.2: TRANSITION SCHEME FORBIDDEN LINES



one-fifth that number of helium atoms. The strengths of the recombination lines are dependent on the element abundances, so that the spectra due to hydrogen and helium predominate. However, weak recombination lines may be observed for ions of other atoms, for example carbon, nitrogen, oxygen and neon (Seaton (101)). Extensive calculations on the recombination spectrum of hydrogen have been undertaken and now there is substantial agreement between calculated and observed values (Miller (85)). This means that the comparison of observed Balmer decrements with theory can be used to evaluate interstellar reddening effects.

## 2) Forbidden line emission

The photo-ionisation process provides a source of random kinetic energy in the nebula. This energy may be lost in inelastic collisions and subsequent radiations. The most important inelastic collisions are those which produce excitation of low-lying metastable states of various atoms and ions. These states have lifetimes that are long (a few seconds) as compared with those of non-metastable states ( $10^{-8}$  sec). However, if there is a sufficiently low material density within the nebula, there will be enough time between collisions for these states to decay, emitting "forbidden lines" by magnetic-dipole or electric quadrupole transitions. In practice, collisional deactivation is by no means negligible as compared with forbidden line emission, and both collisional effects as well as transition probabilities have to be considered when making calculations of line strengths.

Physical conditions within the nebula can be inferred from ratios of forbidden lines emitted by the same ion (see Fig. 3.4.2). For example, the ratio of the intensities of the nebular lines to the auroral line of [OIII] is found to be heavily dependent on the electron temperature ( $T_e$ ) of the nebula (Seaton (101)). Ratios of doublets from nebular transitions in [SII] and [OII] will give values for the electron density ( $N_e$ ) while

remaining fairly insensitive to the electron temperature.

The strength of the forbidden line emission from the nebula stems from two main sources. First, the lack of high energy electrons (15-30 e.v.) that can excite the higher configurations that lead to the emission of permitted lines and, secondly, the vast extent of the nebula, which permits the surface brightness in the forbidden radiation to build up.

The optical depth of the nebula, for the forbidden line radiation, is very small. Thus, once emitted, the energy contained in this radiation is lost to the nebula. This provides a mechanism by which the gas may be "cooled".

### 3) Bowen Fluorescence (Bowen 102)

The effects of this mechanism can be seen in the spectra of many high-excitation planetaries. Certain permitted lines of OIII and NIII are observed to be of high intensity while other lines, which under laboratory conditions would be as strong or even stronger, are missing. Bowen (102) showed that all the OIII lines could be produced by atoms cascading from a given level ( $2p3d^3P_2$ ) and that there was a near coincidence in the energy required for a transition, within OIII, to this level ( $2p^2\ ^3P_2 \rightarrow 2p3d^3P_2$ ) and that associated with the resonance Ly $\alpha$  transition of the ionised helium. Therefore, in high-excitation planetaries, where there is a high proportion of doubly-ionised helium, the Ly $\alpha$  of ionised helium is strong and the OIII fluorescence is triggered. The final transition in this cycle has a wavelength that is, in turn, nearly coincident with a resonance line of NIII, setting up a somewhat similar cycle in that ion.

## Continuum Emission

Continuum emission from planetaries originates from the following mechanisms:

a) The recombination of electrons to excited levels of hydrogen and helium

The intensity jump in the continuum at the head of the Balmer series is produced by recombination into the second level of hydrogen. These second level recombinations contribute to the continuum for wavelengths shorter than  $3650\text{\AA}$ . Recombination into higher levels will produce continuum emission in the visible and near infrared regions. Similar processes for ionised helium will be of importance in high-excitation planetaries.

b) Free-Free Transitions

These involve a loss of kinetic energy by free electrons moving in an electro-static field produced by the ions. This is the predominant source of the radio continuum emission from planetary nebulae.

c) 2-photon emission

This is produced by hydrogen atoms escaping from the 2s metastable level by jumping to a fictitious p-level and then to the 1s ground level, releasing two photons (Mayer (103), Spitzer and Greenstein (104)). This process is only important under low density conditions, since at high density the 2s-level is collisionally depopulated.

d) Emission from dust

This process has been invoked to explain the high fluxes found in the infrared spectra of planetary nebulae. The continuum levels in this region are well above those that would be expected from the other processes mentioned above. At the moment the heating mechanism for the grains is not fully understood. However, at least part of the energy comes from Ly $\alpha$  radiation (Miller (85)).

Using the data obtained from spectra of nebulae it is possible to extract information about the physical conditions of density and temperature and the chemical abundances within those objects. However, one major factor, which can produce anomalous results, is the effect of the structure of the nebula on the values obtained.

For calculations on chemical abundances, made using model atmospheres, assumptions have to be made about the dilution of the radiation of the central star; this requires information about the geometry and the stratification of the nebula. Also the effects of inhomogeneities in temperature and density and the distribution of the atoms causing the various states of ionisation must be taken into account (Aller and Czyzak (105)). Several models have produced too low a flux in the lines of  $[\text{OII}]$  and  $[\text{NII}]$  (Williams (106), Flower (107), Harrington (108)). Both Flower and Harrington were attempting models of the fairly regular planetary nebula NGC 7662. To explain the low fluxes in the forbidden lines Flower invokes higher temperatures in the areas where the lines are formed, and Harrington explains the effects in terms of neglected density fluctuations. Kirkpatrick (109) produced a better agreement between the observed and modelled spectra by taking into account optically thick condensations and by adjusting the central star energy distribution.

Boeshaar (110) has taken spectra of different regions of nebulae and has shown that, using ratios of the  $[\text{SII}]$  and  $[\text{NII}]$  lines, the filamentary areas have a generally higher electron density and lower temperature than the surrounding nebula. This leads to increased fluxes in the forbidden lines from these areas. Thus, when integrated fluxes are taken either from spectral lines or from the whole nebula, the filaments are given a heavier weighting in subsequent temperature and density calculations. To some extent this explains the discrepancy between temperatures obtained from forbidden line emission and from radio fluxes.



Thus it is only with a general picture of the morphology of the nebula that accurate abundances and physical parameters can be determined.

#### 3.4.1.3 Structure

When viewed through a telescope planetary nebulae appear as pale green discs resembling the planets Neptune and Uranus, hence the name. As has been explained, their spectra are composed of a series of emission lines, the predominant ones arising from hydrogen and the forbidden lines of  $[OIII]$ . Much of the classification of the various forms of nebula has been made from either white light photographs or exposures of the bright emission lines. However, their structure can appear strikingly different when observed in the light of different atoms and stages of ionisation. One well-known example of this is the so-called stratification of radiation, where the image of the nebula appears smaller in the light of ions of higher ionisation potential.

Several classification systems for the various observed forms have been used (Curtis (111), Stoy (112), Vorontsov-Velyaminov (113), Thackeray and Evans (114), Westerlund and Henize (115), Hromov and Kohoutek (116), Gurzadian (117)). The proliferation of these different systems reflects the wide range of forms that have to be included within the one general term planetary nebula. The different groups range from stellar-like objects, through various kinds of discs to helical, annular and irregular or amorphous structures. Also, a high proportion of the observed nebulae exhibit some symmetry about an axis lying in the plane of the sky; these objects are classified as bi-polar.

Apart from the single-envelope objects there are those classified as double-envelope nebulae (e.g. NGC 3242, NGC 7009) and there is also evidence for other forms of peripheral structure and possibly third envelopes (Duncan (117), Kaler (96)).

There have been several attempts to explain the observed intensity distributions in terms of the two-dimensional projection of a three-dimensional structure. By far the largest classes of planetary nebulae are the stellar and disc-like objects. Some of these will be young planetaries but a large proportion are obviously well-evolved objects at large distances. Of the remaining groups, the ring nebulae predominate; various different models have been suggested for this configuration:

- 1) A hollow shell of low opacity
- 2) A toroid viewed normally
- 3) A uniform sphere or cylinder with decreased emission in the central regions
- 4) A uniform sphere or cylinder with increased opacity in the central regions

Wilson (118) has ruled out the last model on the basis of the intensities of the Doppler-separated emission-line components arising from the "back" and the "front" of the nebula. Since the two components of the lines appear to be of equal intensity for several nebulae there can be very little absorption in the central regions of these objects. The three remaining models are possible. Hromov and Kohoutek (119) have managed to explain other than annular forms in terms of a right-angled toroid inclined at different angles to the line of sight, and have produced calculated isophotes of the resulting structures. From observations of IC 418 (120), IC 3568 (121), NGC 650-1 and NGC 6720 (122) and IC 4660 (123, 124) it has been found that IC 418 and IC 3568 can be explained by spherical or ellipsoidal shells, while the others require some sort of cylindrical symmetry. More recently the radio structure of NGC 7027 has been explained in terms of a cylindrical shell (125) although the visible object is largely obscured by dust.

Obviously these models are only a rough approximation to the real nebulae, and it is only with the extremely regular objects that comparisons can be made. However, a knowledge of the three-dimensional structure of the envelope, when coupled with the gas dynamics, can give more insight into the formation of the nebula.

An important problem in the small-scale structure of the nebulae is the formation of and maintenance of density fluctuations in the envelopes. These filaments are most obvious in the nearest planetary nebula, NGC 7293. Van Blerkom and Army (126) have explained the low excitation of these features in terms of the shielding effect of optically-thick knots which prevent the radiation from the central star from ionising the filaments. Thus they are only subject to the diffuse radiation field present in the nebula. Capriotti (127) has suggested a mechanism for the formation of such condensations. He has shown that a dynamical instability can be set up in the ionisation front of the expanding nebula. This front distorts around spikes of neutral gas, which are finally completely surrounded by the ionised envelope. These condensations are capable of surviving for the lifetime of the nebula (about  $10^4$  years) although they will be ionised, to some extent, by the stellar radiation.

Gurzadian (95) has suggested that both the large-scale and small-scale structure of planetaries can be explained in terms of magnetic fields. He estimates the required nebular field at about  $10^{-3}$  gauss, by equating the magnetic energy of the nebula to its thermal energy. Isophotes can be constructed by assuming equilibrium at all parts in the nebula. (That is, the sum of the thermal and magnetic energies is a constant.) By comparing these calculated contours with isophotes such as those produced by Aller (121) a value of approximately  $10^{-3}$  gauss is again obtained for the nebular magnetic field. Several nebular forms

can be explained in this manner and the knots and condensations are considered to be the results of fragmentation of the dipole field of the nebula.

#### 3.4.2 Monochromatic Photometry

It can be seen that a knowledge of the morphology of planetary nebulae is required to clarify the theoretical calculations of both element abundances and three-dimensional structure. Quantitative as well as qualitative data is required in order to assess, for example, the effective contribution of radiation from high density regions to the overall flux from the nebula.

To obtain this sort of data it is necessary to isolate the important emission lines and to take an exposure of the nebula in each one. For the smaller objects the use of a slitless spectrograph (121) produces a series of images in the different spectral lines. This method suffers from two main drawbacks. First, the images will be distorted due to the width of the lines, and secondly the images of the larger nebulae will tend to overlap even at high dispersion. Therefore, in most cases, it is preferable to isolate the emission lines using narrow-band filters. In the case of the weaker emission lines or those nebulae of low surface brightness it is also necessary to have an efficient detector.

Feibelman (128) has described a system which has been optimised for narrow-band photometry using photographic plate. The mirrors of the telescope are coated for high reflectivity. Other workers have used the combination of an image intensifier with a photographic plate to obtain exposures of faint nebulae in the forbidden lines of [NII] and [SII] which fall at the red end of the spectrum (Ford and Rubin (129), Capriotti, Cromwell and Williams (130)).

Table 3.4.1

## Telescopes used for Observations of Planetary Nebulae

Telescope	Aperture	Focus/f/no	Plate scale
Isaac Newton Herstmonceux	2.5m	Cassegrain f/14	6"/mm
Rochefeller Reflector Boyden Observatory South Africa	1.5m	Cassegrain f/16	8.8"/mm
Mons Tenerife	50cm	Cassegrain f/15	28"/mm

The electronographic process offers certain advantages in having virtually no threshold (only that set by the fog level of the emulsion), a large dynamic range and a linear density versus exposure response. The latter property makes the investigation of relative fluxes across the nebula a fairly straightforward process, while the reciprocity and dynamic range should allow investigation of both bright and faint regions of the nebula from the same exposure. A low tube background is also required, since the sky background, which in broad-band photometry usually sets the limit to the smallest observable signal, is greatly reduced.

Obviously, to undertake full documentation of representative nebulae in all the different emission lines necessary for a full understanding of their structure, an extensive research programme is required. Exposures to reveal filaments and condensations must be taken in the low excitation lines of OI, [NII] and [SII] which fall longward of  $6000\text{\AA}$ ; thus a tube with a S-20 response is needed. The latter device has only recently become readily available. So far contour maps have been obtained from observations restricted to the spectral range defined by the S-11 photocathode.

### 3.4.3 Spectracon Observations

Spectracon observations of planetary nebulae have been undertaken on three telescopes (see Table 3.4.1). Generally the Cassegrain focus is utilised, since a highly convergent light beam will broaden the pass-band and reduce the transmission of the interference filter used to isolate the emission-line. The typical filter pass-bands have a half-power width of  $10\text{\AA}$  to  $15\text{\AA}$ , with the exception of the filter used for observations of the combined emissions of the N1 and N2 lines of [OIII] which has a width of  $50\text{\AA}$ .

Table 3.4.2

## Planetary Nebulae Observed Using the Spectracon

Northern Hemisphere	Southern Hemisphere
NGC 40	H*1 (MNK 3-2)
2022	H7
3587	H19 (IC2448)
6210	H74 (NGC3918)
6543	H89 (IC4191)
6720	H98 (NGC5307)
6826	H110 (IC4406)
7009	H122 (NGC5882)
7027	H150 (VV 78)
7662	

\* Henize catalogue published in  
Ap.J. supplement, 14, 1967.

The observations taken in South Africa were limited to exposures in H $\beta$  and [OIII] (N1 + N2). On the other telescopes electronographs also were obtained in emission from He I, He II, [OIII]  $\lambda$  4363 $\overset{\circ}{\text{A}}$  and the nearby continuum. A list of the objects that have been observed is given in Table 3.4.2.

Much of the data reduction was held up until the microdensitometer and the associated software were in reliable working order. Hand scans were used for a preliminary inspection of the exposures. When scanning the whole nebula an area is chosen that is somewhat larger than the visible extent of the object. Note is also taken of dimensions quoted in the literature to ensure that the complete object is measured. In some cases this is not possible; for example NGC 6543 possesses a giant halo that has been shown to be about  $6\frac{1}{2}'$  in diameter (Millikan (131)) and thus extends off the edge of the photocathode.

Some of the results of this work have been reported elsewhere (76, 132) and there follows a discussion of a selection of the data that illustrates the general quality that has been obtained.

#### 3.4.3.1 Nebular Dimensions

In order to find the maximum observed dimensions of the nebulae it is necessary to assess the limitations set by the detection process. Preliminary plotting with 15 equispaced contours very often reveals an outer contour which is quite smooth and is obviously well above the noise level of the plate. In order to set the "limiting" outer contour an assessment of the background level and the noise on that background is made at several points round each object. These figures are used to set contour levels at multiples of the standard deviation above the general background. It is found that, for most of the data, an outer contour at two standard deviations above background



Table 3.4.3

Object	Dimensions <sup>a</sup>	Outer Contour Level <sup>b</sup>	Dimensions <sup>c</sup>	Level <sup>d</sup>
NGC 6210	25 <sup>''</sup> x 23 <sup>''</sup>	0.8%	20 <sup>''</sup> x 13 <sup>''e</sup>	~ 5%
NGC 6543	38 <sup>''</sup> x 35 <sup>''</sup>	0.2%	23 <sup>''</sup> .4 x 19 <sup>''</sup> .7 <sup>f</sup> (300) <sup>g</sup>	~15% <0.2
NGC 6826	36 <sup>''</sup> x 36 <sup>''</sup>	1.6%	25 <sup>''</sup> .7 x 24 <sup>''</sup> .4 <sup>h</sup> (110) <sup>i</sup>	~18% <1.6
NGC 7009	36 <sup>''</sup> x 30 <sup>''</sup>	2.3	30 <sup>''</sup> x 26 <sup>''e</sup> (110) <sup>j</sup>	~ 6% <2.3
NGC 7027	25 <sup>''</sup> x 22 <sup>''</sup>	0.4	18 <sup>''</sup> x 11 <sup>''e</sup>	~ 6%
NGC 7662	35 <sup>''</sup> x 30 <sup>''</sup>	1.5	30 <sup>''</sup> .2 x 26 <sup>''</sup> .2 <sup>f</sup> (130) <sup>j</sup>	12% <1.5

a Major and minor <sup>axes</sup> ~~areas~~ of region enclosed by outer contour

b Level of outer contour expressed as percentage of peak surface brightness in image

c Maximum recorded dimensions, not necessarily for monochromatic H $\beta$  observations. The figures in brackets refer to faint outer halos only found in long broadband exposures

d Approximate percentage of peak surface brightness at boundary defined by previous studies

e Perek L., Kohoutek L., Catalogue of Galactic Planetary Nebulae (Prague Academic Publishing House) 1967

f Feibelman, W.A., R.A.S.C. Journal, 65 no.1, 25, 1971

g Gurzadian, G.A., D.A.N. 133, 1053, 1960

h Feibelman, W.A., R.A.S.C., Journal, 65, no.6, 251, 1971

i Duncan, J.C., Ap.J. 86, 496, 1937

j Kaler, J.B., A.J. 79, 594, 1974

provides a good guide to the maximum observed dimensions of the nebula.

It has been found that when these measurements are compared with those from previous studies there is a general trend to larger images from the electronographic data. It is simple enough to check for systematic effects by comparing separations of recognisable features. These distances measured from the electronographs are found to be in good agreement with those from other sources. Thus the increased dimensions are a real effect. As Baum (133) has pointed out, with the improvement of detection techniques the observed size of an object tends to increase. Therefore, in order to make the inter-comparison of results easier it is useful to give a flux level at the defined boundary in terms of a fraction of the peak surface brightness; this also serves as a guide to the dynamic range of the exposure.

Table 3.4.3 gives details of the dimensions found from a study of H $\beta$  emission from six nebulae (132). The general background level is predominantly due to plate fog. The noise on this background has two components, one from the emulsion and the other from any dirt or defects picked up during processing. Obviously, with care, this noise can be very low as compared with the peak density of the image.

#### 3.4.3.2 NGC 6543

A prime example of the large dynamic range that can be obtained is shown in the plot of NGC 6543 (see Fig. 3.4.3) where the outer contour is at 0.2% of the peak surface brightness. The print at the top shows the typical visible extent of the object on the electronograph. This nebula has a large faint halo which is several arcminutes in diameter. It can be seen from the cross-sectional plot that there is a tail-off from the central core of the nebula into this outer envelope. Details of the exposure are given at the bottom of Fig. 3.4.3.

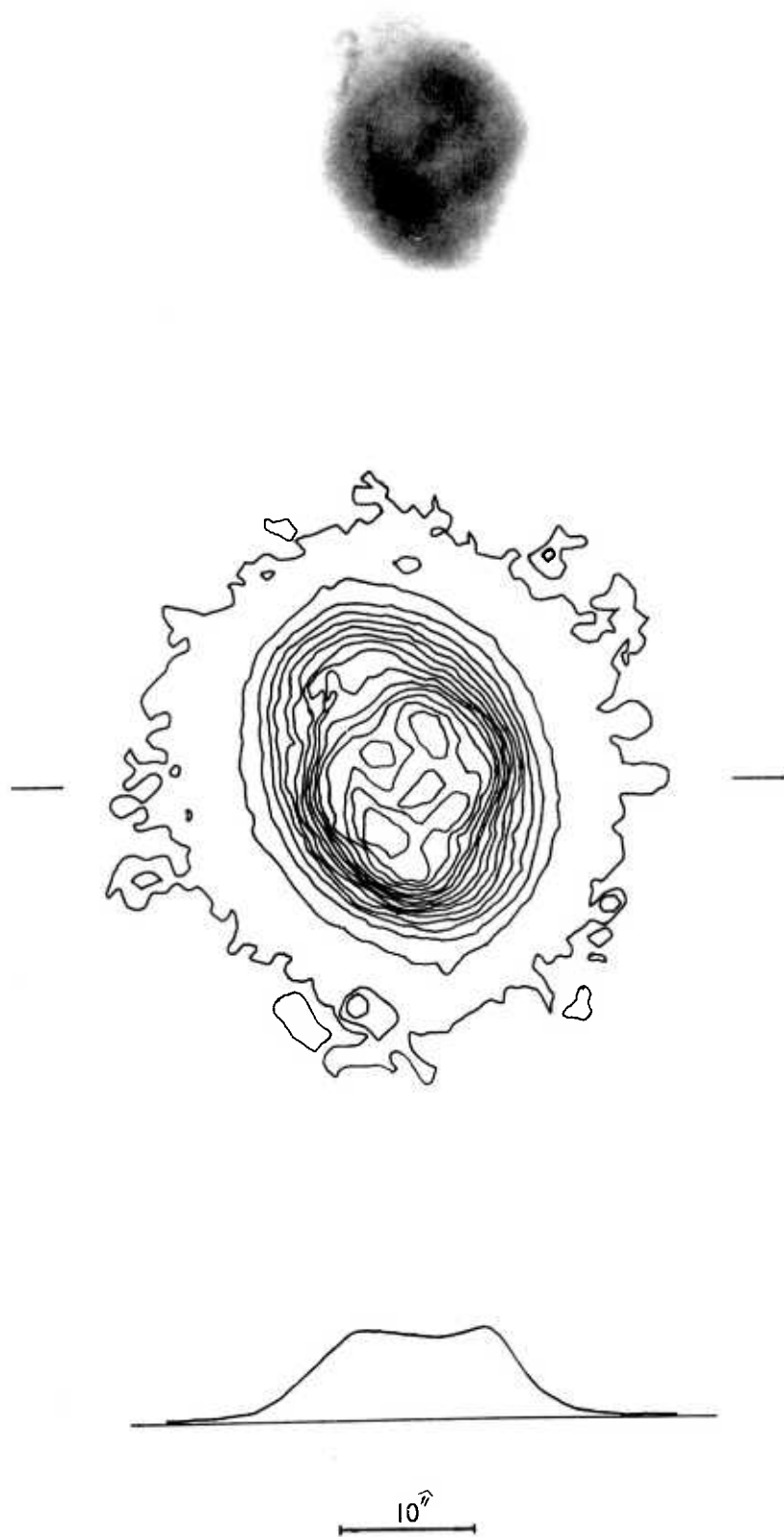
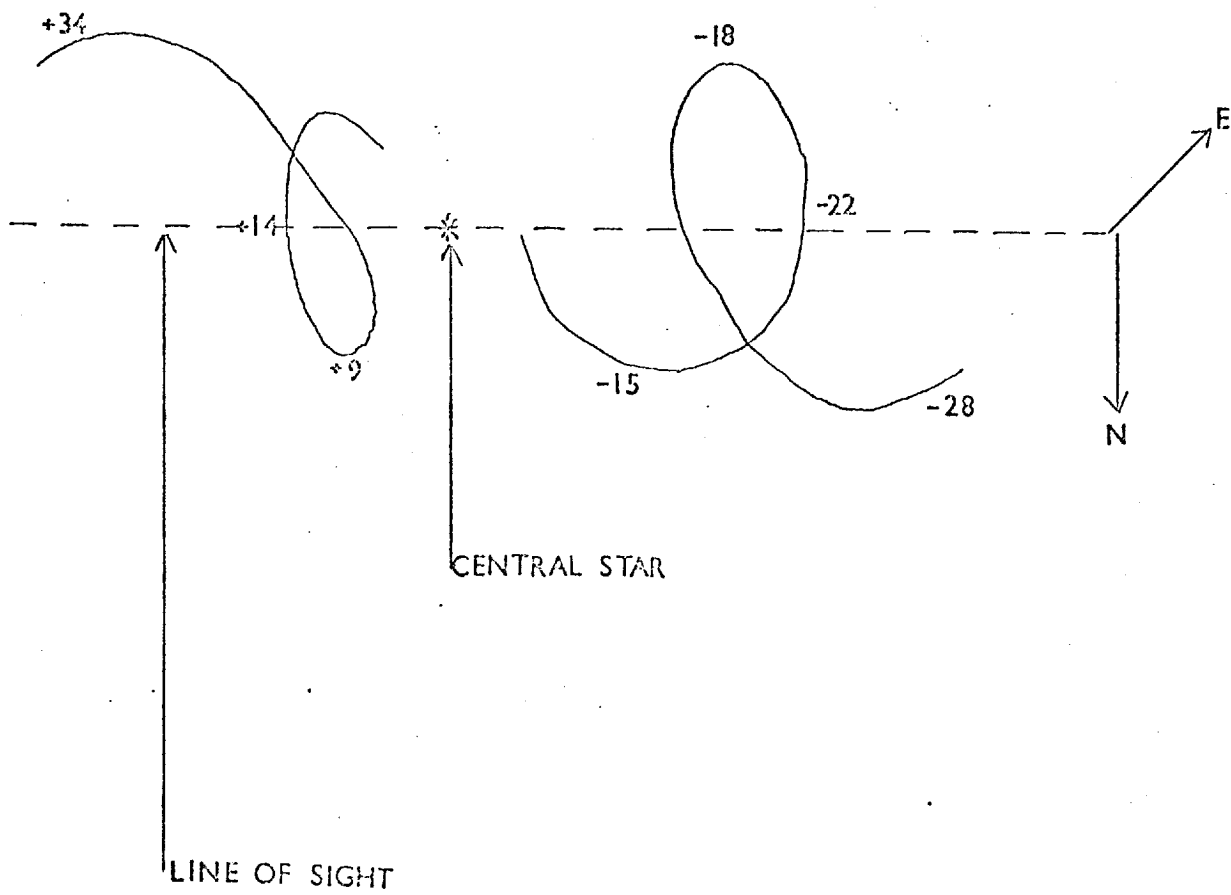


FIGURE 3.4.3: NGC 6543 H $\beta$  CONTOURS

15 minutes L4 50cm telescope

FIGURE 3-4-4: STRUCTURE OF NGC 6543



Velocities in km/sec relative to the central star  
obtained from the emission lines of  $[OIII]$ .

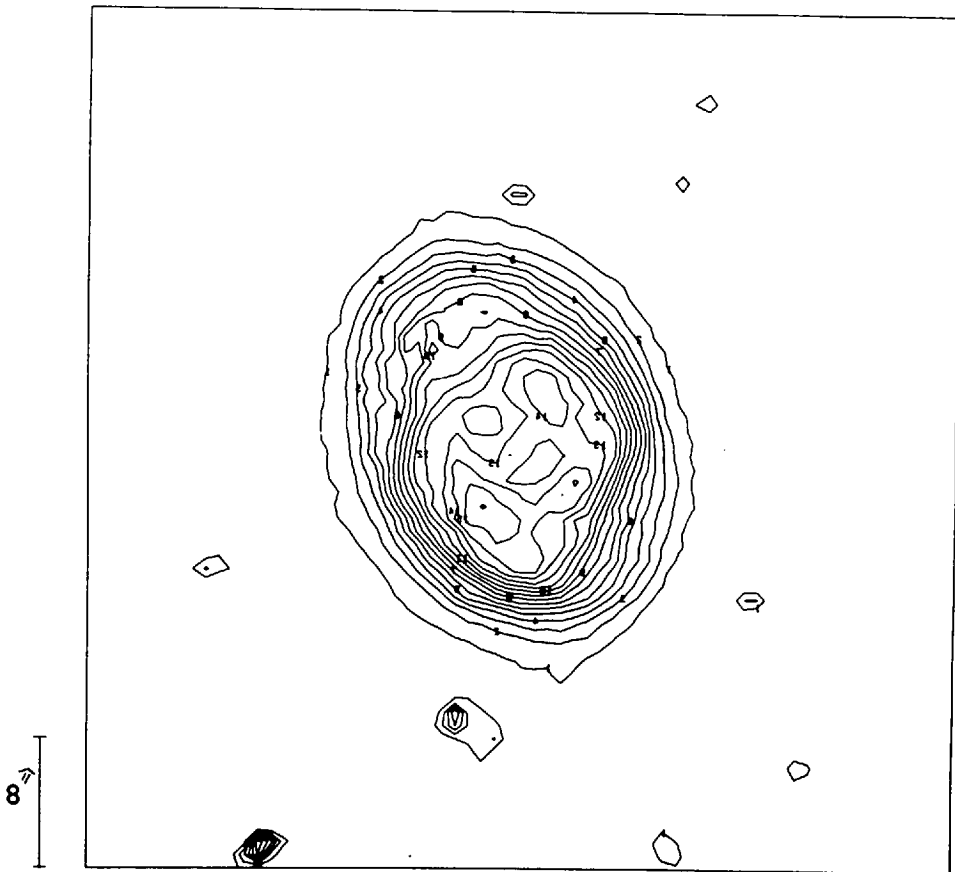
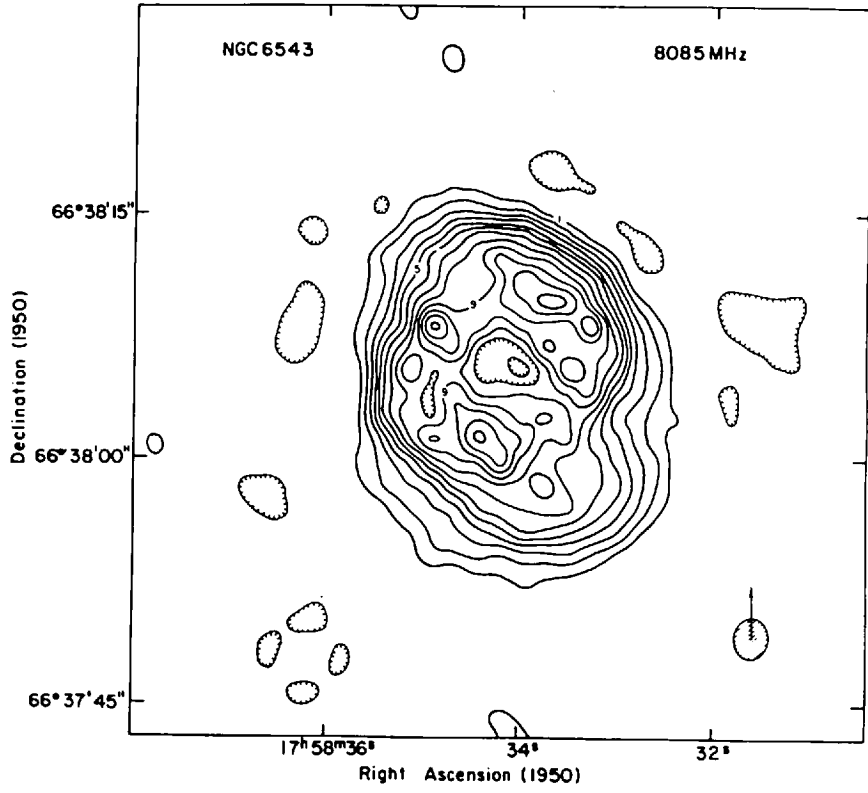


FIGURE 3·4·5: NCC 6543 RADIO AND H $\beta$  CONTOURS

The central part of the nebula presents a complex structure which Münch (134) has interpreted, using radial velocity data, as two helical surfaces with the generatrix passing through the central star and forming an angle of  $55^\circ$  with the line of sight (see Fig. 3.4.4). Terzian et al (135) have produced a high resolution radio map at 8,085 MHz for this object. A comparison of this with the  $H\beta$  contours for the central region of the nebula (see Fig. 3.4.5) shows that there is substantial agreement between the two sets of data. The central depression found in radio measurements is also present in the  $H\beta$  contours. By a comparison of the radio flux with that from  $H\beta$  it is possible to search for effects of differential extinction across the nebula; the good agreement between the two sets of contours implies that there is no localised dust concentration. Therefore, if continuum emission from dust is to be invoked to explain the large infrared flux from this object (Woolf (136)) the grains must be fairly evenly distributed throughout the nebula.

#### 3.4.3.3 NGC 7662

This object is an example of a double envelope nebula. The  $H\beta$  contours (Fig. 3.4.6) show the elongated core surrounded by a more circular outer-envelope. When a comparison is made between radio-contours (Terzian et al) and the  $H\beta$  map there seems to be little evidence for differential obscuration.

Kaler (96) has reported that this nebula has a third shell that is just visible on the Palomar Sky Survey plates. He estimates the diameter of this halo to be about  $130''$ . The outer shell does not appear on the relatively short exposure  $H\beta$  electronograph (see Fig. 3.4.6 for details). However, scans of a fairly long exposure taken with the  $[OIII]$  ( $N1 + N2$ ) filter show some evidence for this feature. Repeated scans were made across the central region of the nebula and a rise in emission was found to the east of the planetary at a distance of about  $60''$  to  $70''$  from the

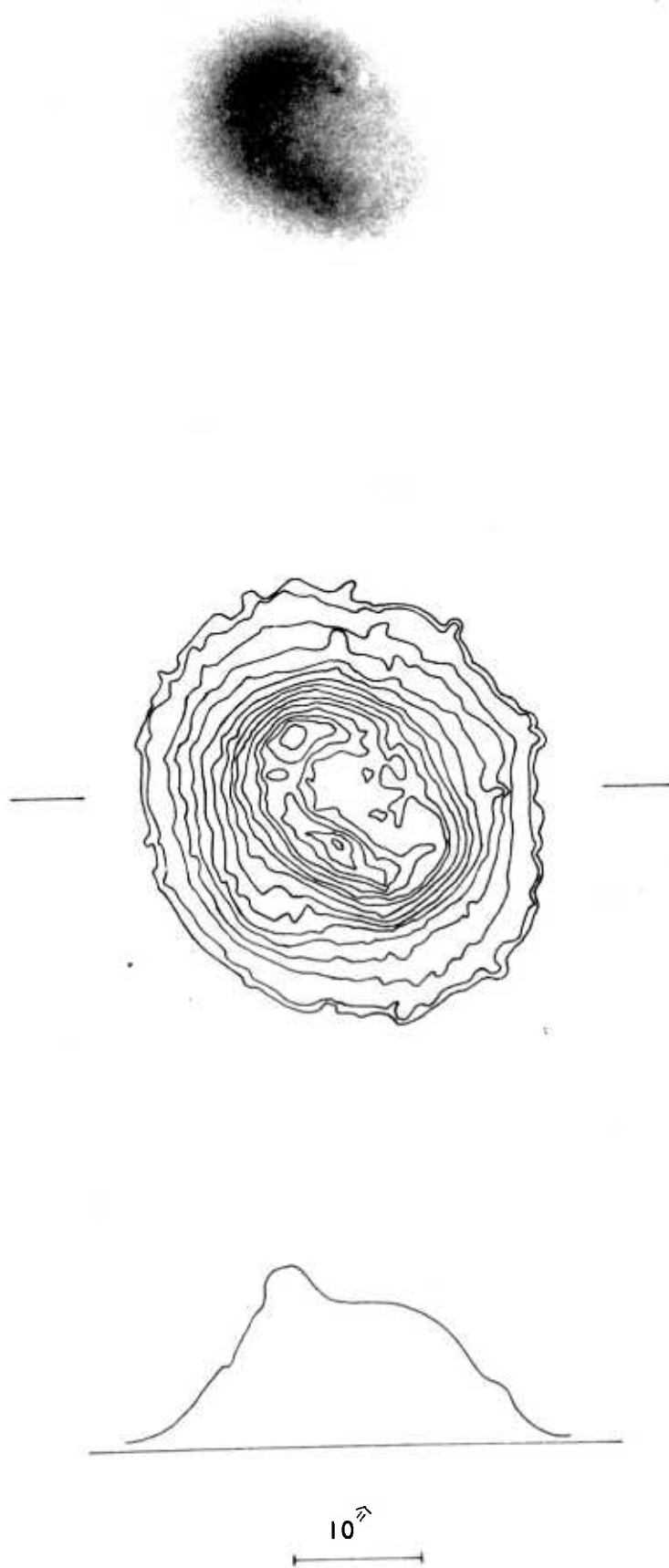
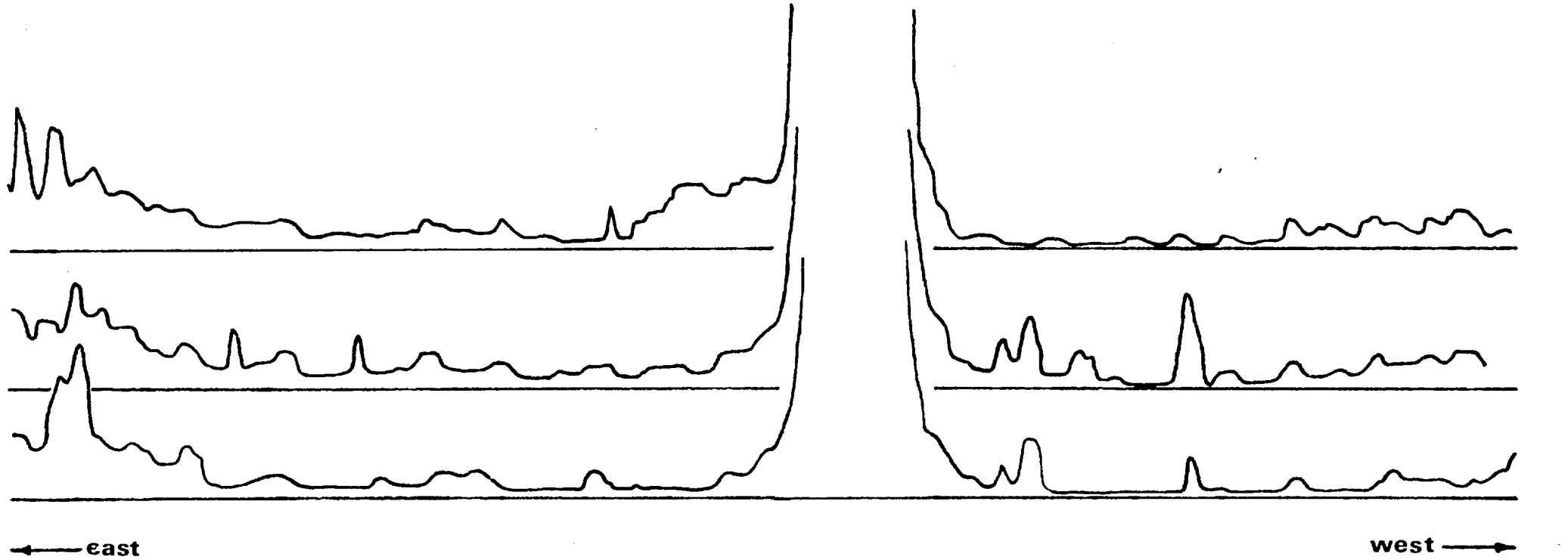


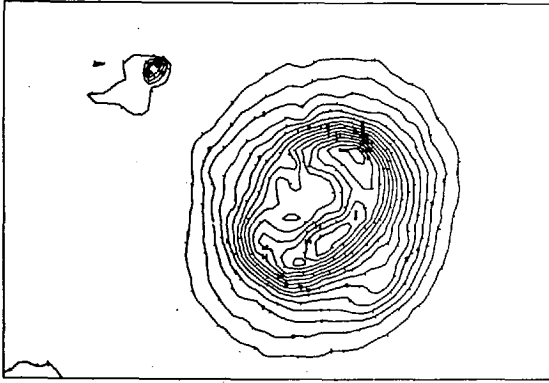
FIGURE 3·4·6: NGC 7662 H $\beta$  CONTOURS

15minutes L4 50 cm telescope

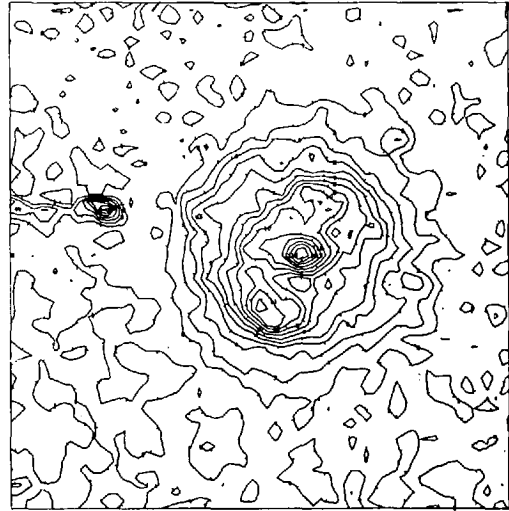


NGC 7662. FILTER [OIII] 5007+4959Å  
 Scans through central region showing  
 rise at eastern edge.  
 FIGURE 3·4·7

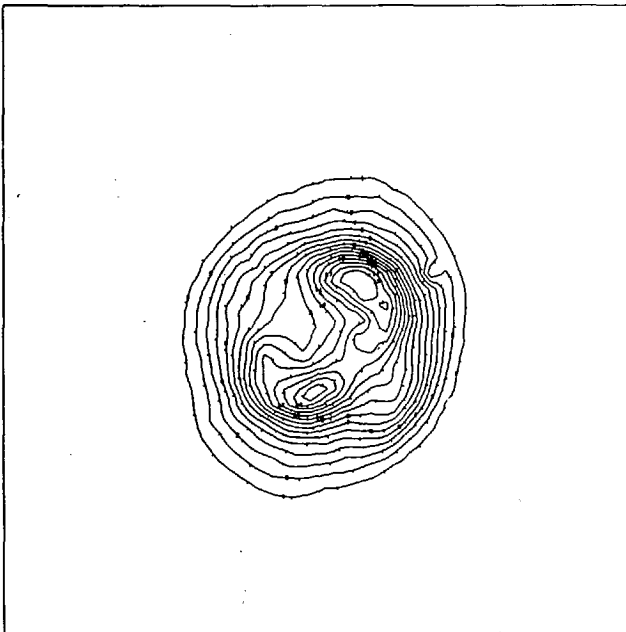




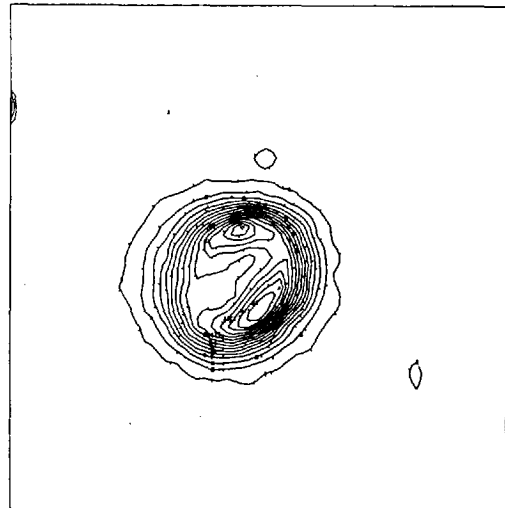
a



c



b



d

a) H $\beta$   $\lambda$  4861c) He I  $\lambda$  4921b) [O III]  $\lambda\lambda$  4959+5007d) He II  $\lambda$  4686

FIGURE 3·4·8: NGC 7662

Table 3.4.4

ION/WAVELENGTH (Å)	EXPOSURE DETAILS				POSITION <sup>a</sup> ANGLE (DEG)	DIMENSIONS (ARCSEC)			
	TELESCOPE	EMULSION	EXP. TIME (MINS)	PRESENT STUDY <sup>b</sup>		PREVIOUS STUDIES			
				50% level		6¼% level	Dimensions	Level (%) <sup>c</sup>	
Hβ 4861	MONS	L4	15	37	20 x 15	34 x 30	13.9 <sup>d</sup>	80	
							14.6x8.7 <sup>e</sup>	70	
							30.2x26.2 <sup>f</sup>	13	
HeI 4922	MONS	G5	30	35	20 x 13	35 x 32	14.8 <sup>d</sup>	77	
HeII 4686	MONS	L4	30	37	15 x 13	23 x 24	12.1 <sup>d</sup>	69	
							13.8x10.0 <sup>e</sup>	56	
[OIII] (5007+4959)	MONS	L4	5	35	22 x 17	36 x 31	14.1 <sup>d</sup>	>75	
							14.8x10.0 <sup>e</sup>	>75	

a Accurate to  $\pm 5^\circ$

b Major and minor axes of regions enclosed by contour at 50% and 6¼% peak surface brightness levels

c Approximate contour levels in the new data (expressed as percentage of peak surface brightness) that would correspond to these previously measured dimensions

d Wilson, O.C., Ap.J., 111, 279, 1950

e Wright, W.H., Publ.Lick.Obs., 13, 191, 1918

f Feibelman, W.A., R.A.S.C. Journal 65, No.1, 25, 1971

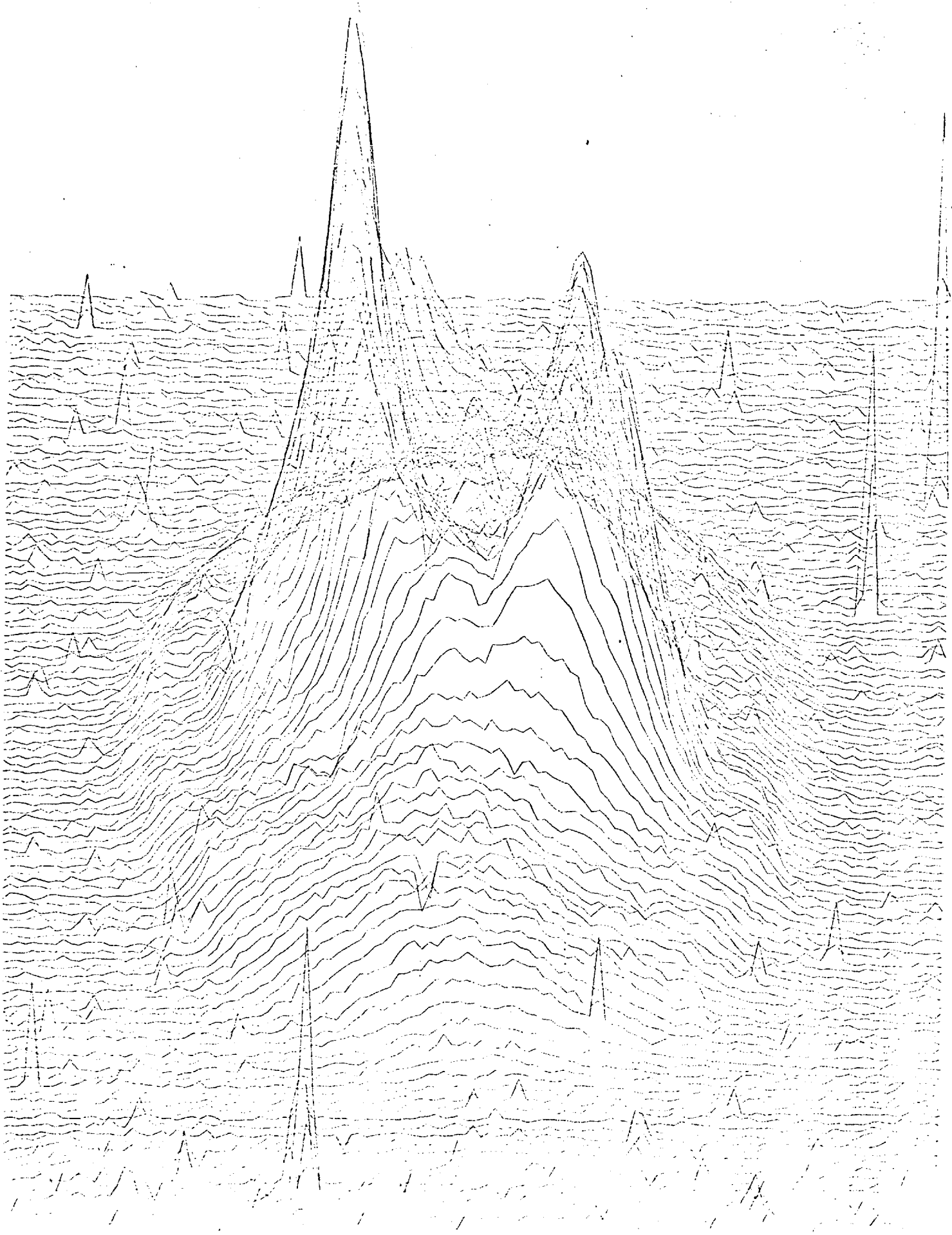
centre of the nebula (see Fig. 3.4.7). This exposure was taken at the Cassegrain focus of the Isaac Newton Telescope and the image scale is such that the westerly end of the shell does not fall on the exposure; nevertheless there is evidence of a general rise in intensity in this direction. An upper limit of about 0.5% of the peak  $[\text{OIII}]$  surface brightness of the nebula can be taken for the surface brightness of the halo.

The structure of this nebula in different emission lines is shown in Fig. 3.4.8. The contour maps are for  $\text{H}\beta$ ,  $[\text{OIII}]$  ( $\text{N1} + \text{N2}$ ), He I ( $4922\text{\AA}$ ) and He II ( $4686\text{\AA}$ ) and consist of a series of 15 contour levels equispaced between the background level and the brightest part of the image. The data has also been smoothed in the computer to remove the effects of small defects on the film (Youll (137)). The outermost contour is at about 6.25% of the peak surface brightness.

There is a striking similarity between the general features of the  $\text{H}\beta$  and  $[\text{OIII}]$  isophotes despite the difference in ionisation potentials for He I (13.6 eV) and OII (35.1 eV). The map of He I emission is noisy due to the intrinsic weakness of the line, but the extent of the nebula is seen to be similar to that found from the  $\text{H}\beta$  exposure. The central star is also visible. The structure in the He II line is more compact due to the high ionisation potential of He I (246 eV) and the two bright spots seem "twisted" with respect to those in the  $[\text{OIII}]$  map. Table 3.4.4 summarises the data for these maps and compares the results with previous measurements.

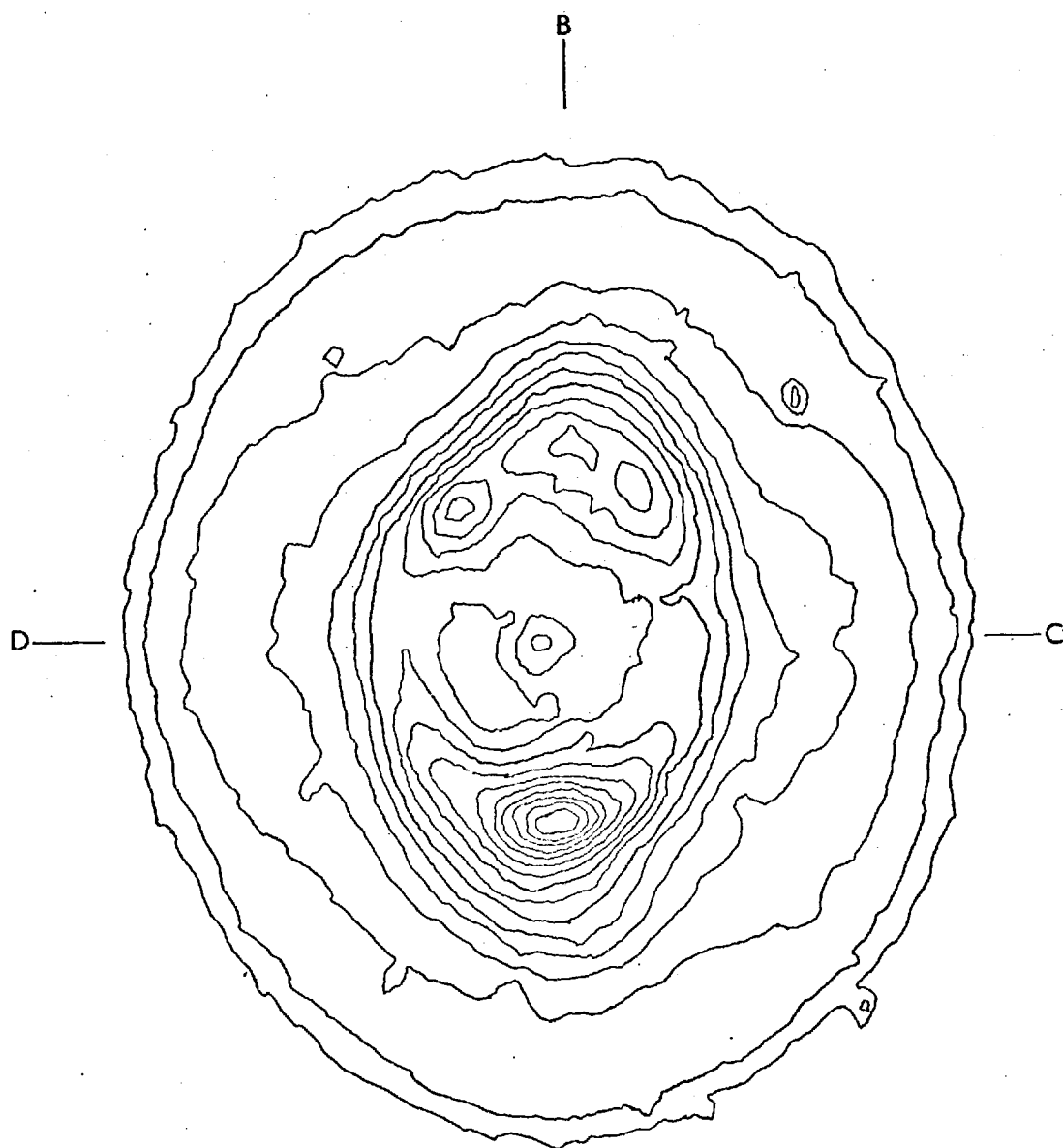
#### 3.4.3.4 NGC 3242

This nebula is an example of a bi-polar structure with an outer halo. The cross-sectional display of the complete scan (Fig. 3.4.9) of an  $[\text{OIII}]$  exposure shows clearly the halo, the two peaks and the



NGC 3242 is a barred spiral galaxy located in the constellation Coma Berenices. It is a member of the NGC 3242 group, which is a compact group of galaxies. The [O III] emission line is a strong indicator of ionized oxygen, which is commonly found in the interstellar medium of galaxies. The emission from NGC 3242 is particularly strong, suggesting a high level of ionization and a significant amount of ionized oxygen in the galaxy's interstellar medium. The emission is primarily concentrated in the central region of the galaxy, with some smaller, isolated peaks scattered throughout the field of view.

FIGURE 3-4-10: [O III] CONTOURS OF NGC 3242



1 = 1.6%

2 = 5.0%

↓ equispaced

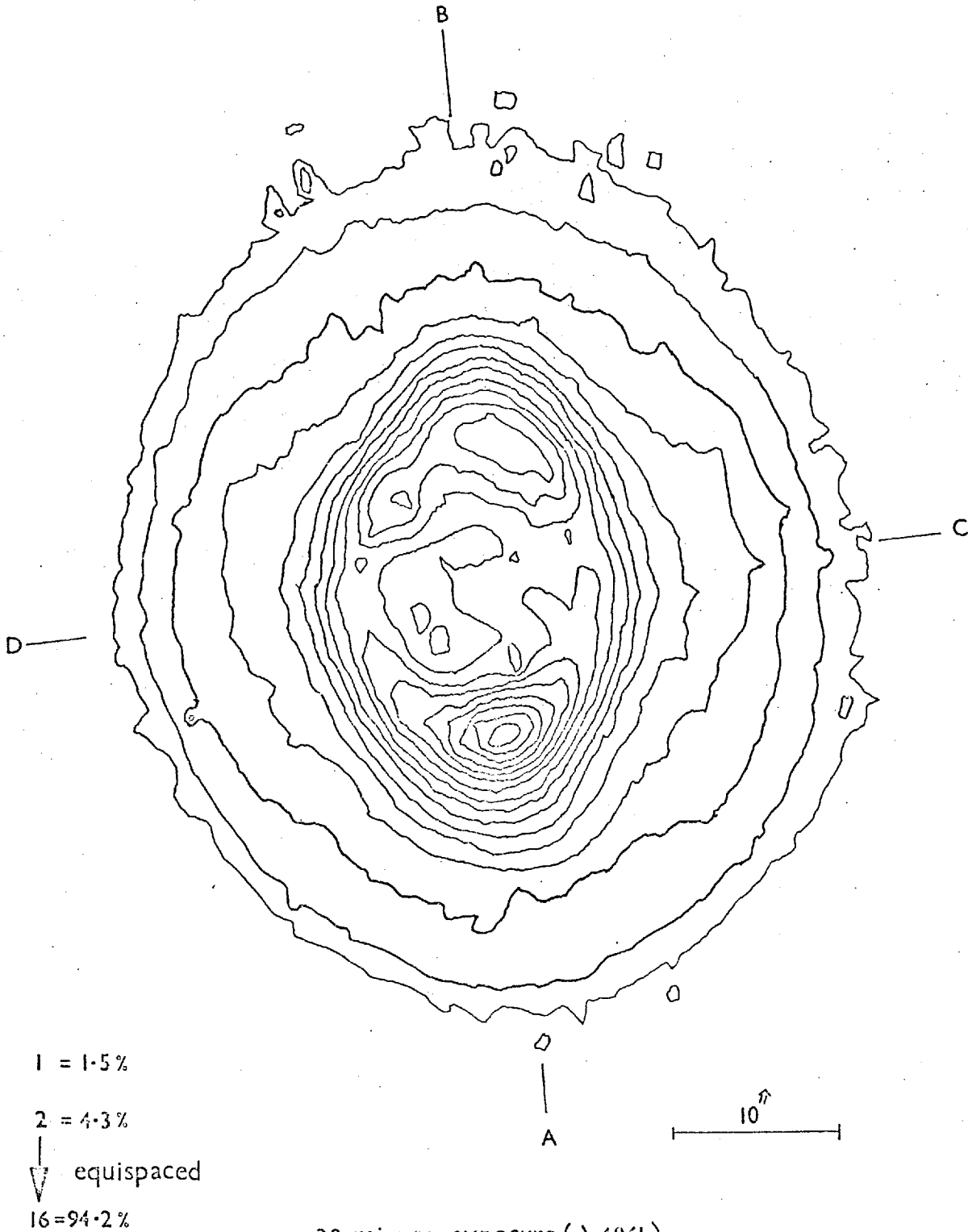
16 = 93.8%

10<sup>''</sup>

A

5 minute exposure ( $\lambda \lambda 4959+5007$ )

Boyd 60 inch telescope

FIGURE 3-4-11: H $\beta$  CONTOURS OF NGC 3242.30 minute exposure ( $\lambda 4861$ )

60 inch Boyden telescope

star. Figures 3.4.10 and 3.4.11 show [OIII] (N1 and N2) and H $\beta$  contours respectively. There are 16 contours in all, the first being  $3\sigma$  above the background; this corresponds to about 1.5% of the peak surface brightness of the nebula. The heights of the other contour levels are listed in the figures.

A B and C D denote the major and minor axes of the nebula along which the profiles of the object have been plotted (fig. 3.4.12). It can be seen that the general shape of the nebula is the same in both [OIII] and H $\beta$ , although the absolute flux is much <sup>higher</sup> brighter for the [OIII] emission. Taking the profile along the major axis it is found that, when the fluxes are related to the peak flux in the nebula, the [OIII] is lower than H $\beta$  in the centre of the nebula and in the smaller peak, while there is good agreement in the higher peak and the halo. Taking the minor-axis profile, there is good agreement again in the halo, but a lower flux from [OIII] towards the central star.

Hromov and Kohoutek (119) have produced a model which they believe can be applied to a large proportion of nebulae. It is possible to consider it qualitatively with respect to the central structure of NGC 3242. The model consists of a hollow cylinder of gas which can have different orientation of its axis with respect to the line of sight (fig. 3.4.13). Using this distribution of gas, various sets of isophotes can be produced for different orientations. Hromov and Kohoutek have found that some of the nebular forms observed in the hydrogen lines resemble the calculated isophotes quite closely.

It can be seen that this model can be used to produce a bi-polar structure. As a simple test, the calculated isophotes were scaled to match the H $\beta$  contours of NGC 3242 and profiles along the major and minor axes of the model were taken. For the cylinder at  $45^\circ$  to the

FIGURE 3-4-12: PROFILES ACROSS NGC 3242

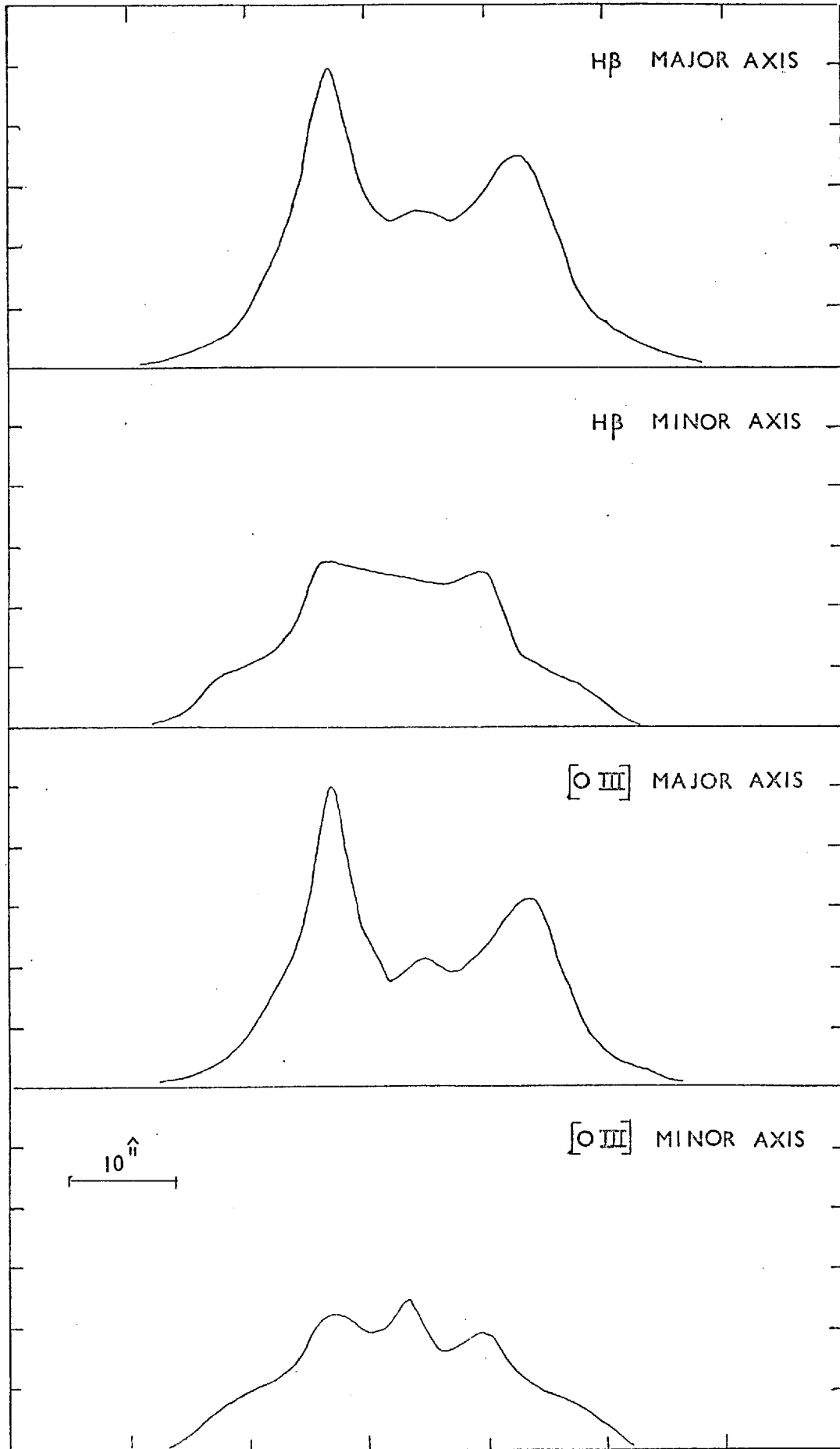
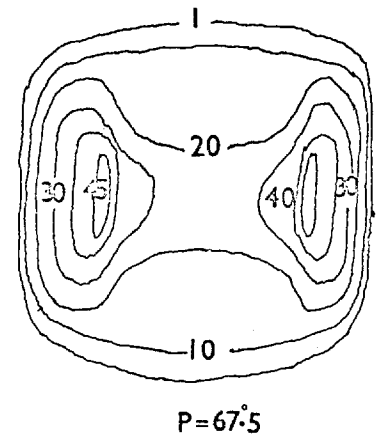
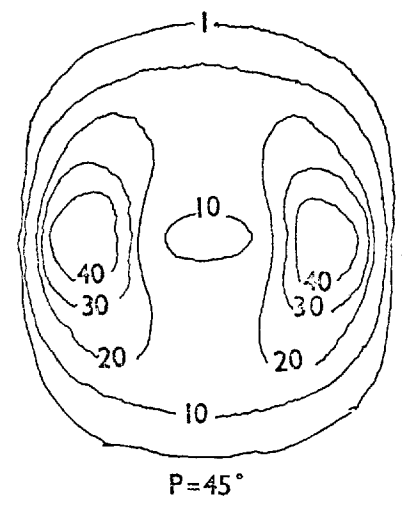
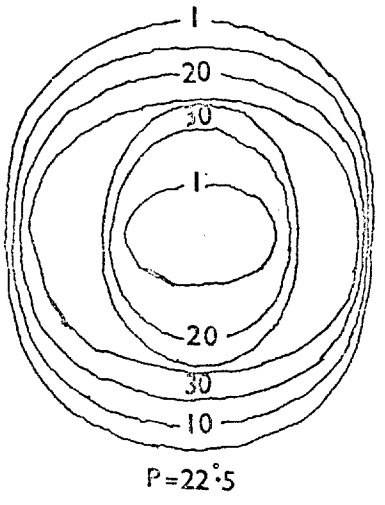
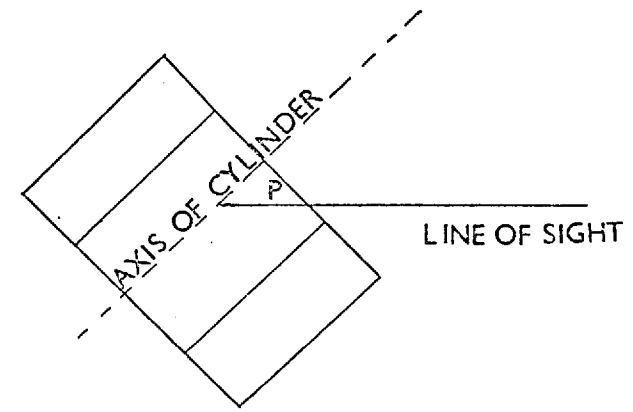
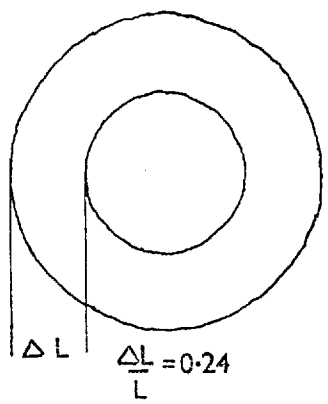
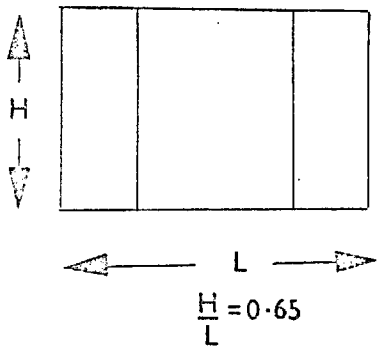


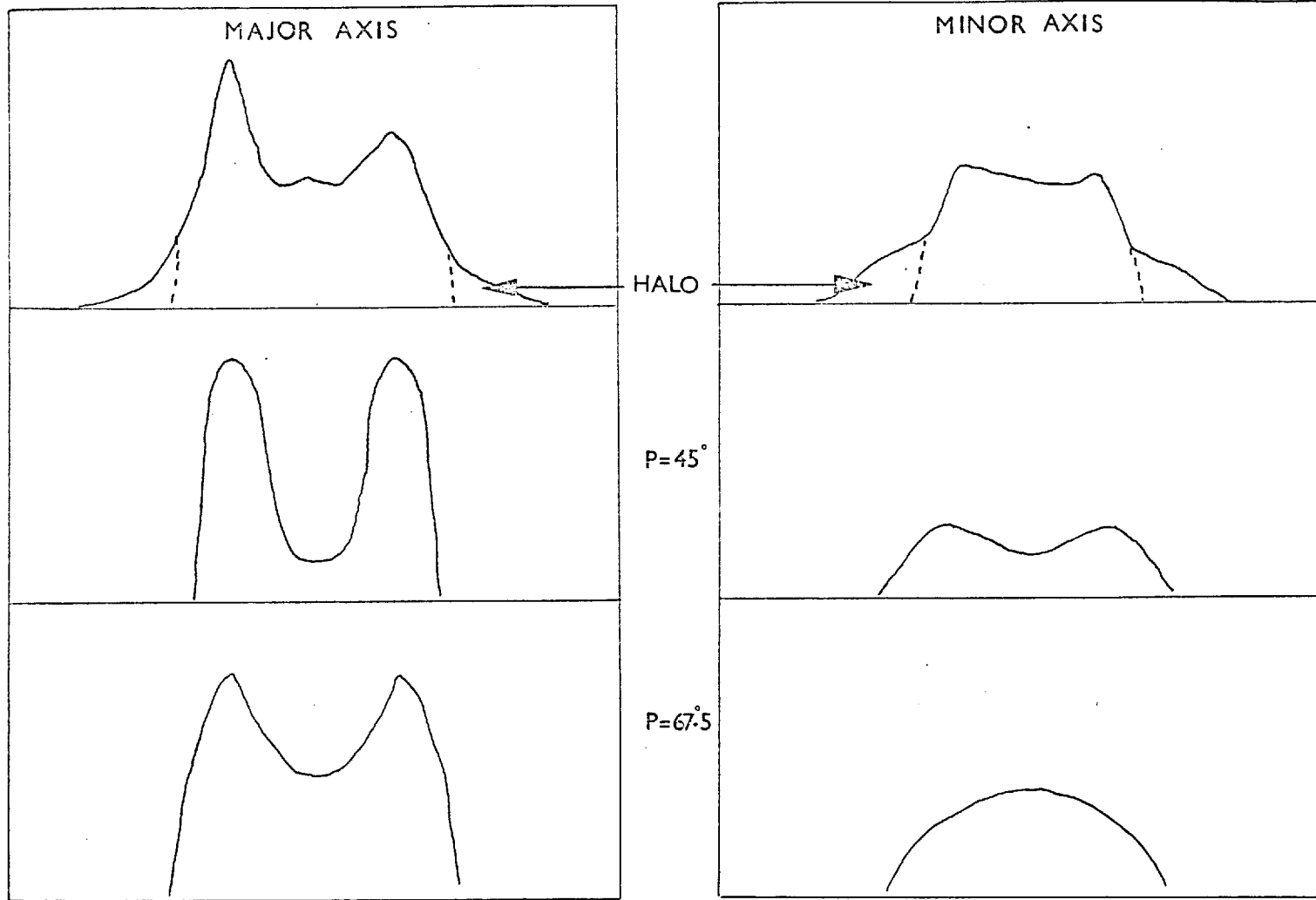


FIGURE 3-4-13: HROMOV MODEL FOR PLANETARY NEBULAE



ISOPHOTES FOR DIFFERENT VALUES OF P

FIGURE 3-4-14: NGC 3242 H $\beta$  PROFILES COMPARED WITH HROMOV MODEL



line of sight the peaks are somewhat too broad along the major axis, while the general distribution along the minor axis gives peaks that are too far apart. This would imply that a larger angle between the axis of the cylinder and the line of sight is necessary. Checking the isophotes for the angle of  $67.5^\circ$  the peaks along the major axis are in better agreement, although the centre of the nebula, when viewed along the minor axis, is almost completely filled in (Fig. 3.4.14).

Of course there is an involved interaction between the observed form of isophotes and the angle to the line of sight, but if the foreshortening effect of tilt is considered for the bi-polar isophotes produced for the  $45^\circ$  orientation, one would get the correct space between the peaks along the minor axis for an angle of about  $56.5^\circ$ . At the same time there would obviously be some associated filling-in of the central depression and a narrowing of the bi-polar peaks along the major axis.

This is only a qualitative discussion of the form of the central region of this nebula, the effects of the halo having been ignored. However, it can be seen that the observed isophotes can be explained in terms of a cylinder of gas. It is obviously possible to interpret the two-dimensional brightness distribution as a projection of a three-dimensional structure. With a knowledge of the dynamics of the nebula it would be possible to produce a much clearer idea of the actual distribution of gas in the object.

The use of the Spectracon for observations of planetary nebulae can yield high quality data which, for the brighter objects, can be obtained on a fairly small telescope. One problem that has not been mentioned in this chapter is the effects of photocathode non-uniformity. Most of the images presented here are of fairly small extent, and the variations across typical image areas are about 2% to 7% of the overall sensitivity

for the tubes used. However, larger images have shown distortions in contours due to both dead spots and sensitivity changes, and therefore it was necessary to set up a system for removing these variations. The results of this investigation are discussed in the next chapter.

## CHAPTER IV

### LIMITATIONS SET BY PHOTOCATHODE NON-UNIFORMITIES

"Out, out.....accursed spot!"

Robert Southey (1774-1843)

In Chapter I some of the different approaches that have been taken to the removal of photocathode sensitivity variations were outlined. The ease with which these effects can be compensated is highly dependent on the form that the processed electronographic data takes. Maps of exposures to a uniform light source can provide a general idea of the shape of the function but, for ease of manipulation, numerical data is required.

Since the predominant application of the electronographic system, described in Chapter II, is to the surface photometry of extended objects, the use of sky background as a measure of local sensitivity (Wlérick et al (38)) did not seem the best approach. It was decided to set up a method whereby an exposure to a uniform light source could be used as the "calibration" data for the correction of an astronomical exposure. Limitations to the process have been investigated.

#### 4.1 The Calibration Process

The process of removing the photocathode non-uniformities can be divided into three main steps.

- 1) Location of the same area of photocathode in both the calibration data and the exposure to be corrected.

- 2) The production of two sets of data which are matched in spatial orientation.
- 3) The production of the corrected data.

#### 4.1.1 Location

To be able to match two scans, produced from electronographic exposures, the same features must be located in both sets of data. These features should define an unambiguous set of co-ordinates with a fairly high spatial accuracy. Ideally, some form of fiducial mark should be provided on the photocathode but, in the absence of this facility, the small areas of zero sensitivity known as dead spots provide the reference points. To locate these spots a clearly visible background-density is required to throw them into relief. The measuring machine can be set up so that roughly the same areas are scanned on both exposures. The positions of the dead spots are then fixed in each scan.

The location of the centre of each dead spot is undertaken manually. Plots of the complete scans are produced and the same features are located in both. Data from the areas around each spot are used to obtain an estimate of the centre point. The dead spots are a few tens of microns in diameter - thus the accuracy of location of the centre will depend on the sampling aperture and the step length used. For the smallest table step length of  $5\mu\text{m}$  the limiting accuracy on a single position should be about  $\pm 2.5\mu\text{m}$ .

Having located the positions of these fiducial features in both scans it is possible to produce two sets of data that have the same spatial orientation.

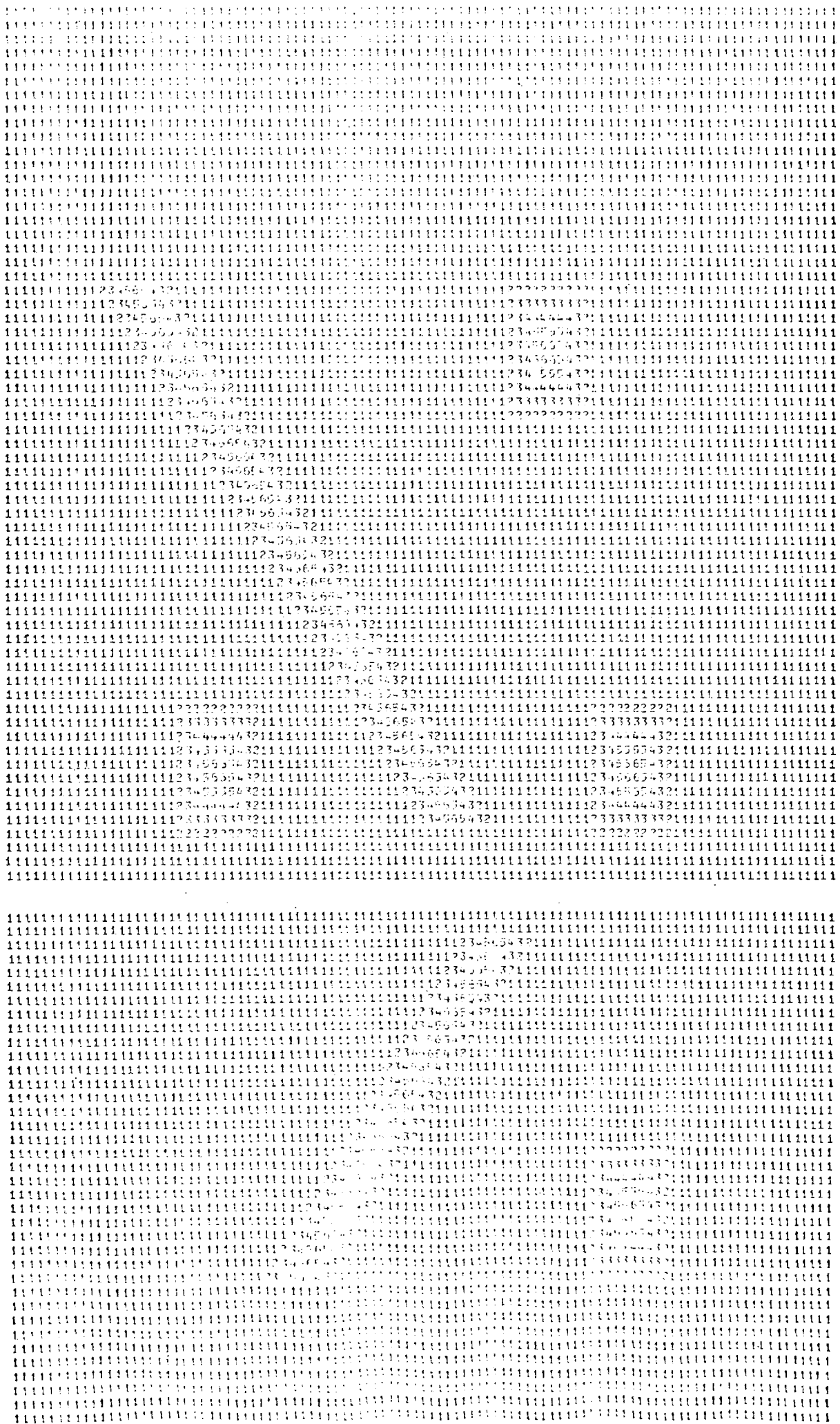


FIGURE 4.1-1: ARRAY OF DUMMY DATA





#### 4.1.2 Matching

For ease in the further processing of the data one of the scans should be translated and rotated so that the resultant array matches the other scan point for point. Having set up a co-ordinate system from the positions of the dead spots it is a fairly straightforward process to produce the required data for such a transformation.

A program has been written which, using the positions of three or more features in each scan, will rotate and translate one scan so that it matches the other. The listing of the program (MATCH) can be found in Appendix II. The co-ordinates are taken from an origin at the top left-hand corner of the array. A section in the program to take care of a change of scale between the two scans was put in so that the program could be used for matching two astronomical exposures from different telescopes. It has no application in the calibration process. A check has also been put in for any anomalous changes in scale arising from the matching of two points that are not, in fact, the same features.

The densities in the new array are found by linear interpolation between adjacent points since the small sampling distance required for accurate matching is usually very much less than the resolution element of the astronomical exposure and the size of the typical scale of photocathode sensitivity variations. If an application is found which requires a polynomial fit, a different subroutine can be inserted.

As a check of the program a dummy tape was written and the scan rotated through  $45^{\circ}$ . Figures 4.1.1 and 4.1.2 show the two maps produced, on the line printer, of the original and rotated arrays. The letters in the second map represent the interpolated numbers. Allowance must be made for the 8 by 5 matrix of the line printer which stretches the array in the 'Y' direction.



FIGURE 4-2-1 : PHOTOCATHODE NON-UNIFORMITIES

#### 4.1.3 Correction of Data

Having produced the two arrays of data that match, the calibration of the exposure can be undertaken with a simple program which obtains the ratio of the data point by point and forms a new array, on magnetic tape, in the standard archive format. This corrected array can then be processed using any of the routines already described in Chapter III.

#### 4.2 Practical Limitations of the Calibration Process

In order to check the limitations of the calibration process a series of laboratory exposures were made. A Spectracon tube was selected which exhibited as wide a collection as possible of the various defects. These included dead spots, a general drift in sensitivity along the length of the photocathode and a step in sensitivity where there was a change in thickness of the mica window (see Fig. 4.2.1).

The photocathode was illuminated by light reflected from a sheet of white card. The uniformity was checked using a photomultiplier with a 500 $\mu$ m aperture placed in front of it. The whole assembly was scanned across the region of the photocathode and measurements were taken every mm. The illumination was found to be uniform to better than 1%.

Exposures were taken using L4 emulsion in a 5 $\mu$ m layer on a 25 $\mu$ m Melinex backing. All the strips of emulsion used for this work came from three plates in the same batch. The electronographs were processed using the techniques outlined in Appendix I. The intensity of the light source was adjusted so that exposure times were between one and ten minutes, producing a range of densities from 0.25 D to 2.5 D.

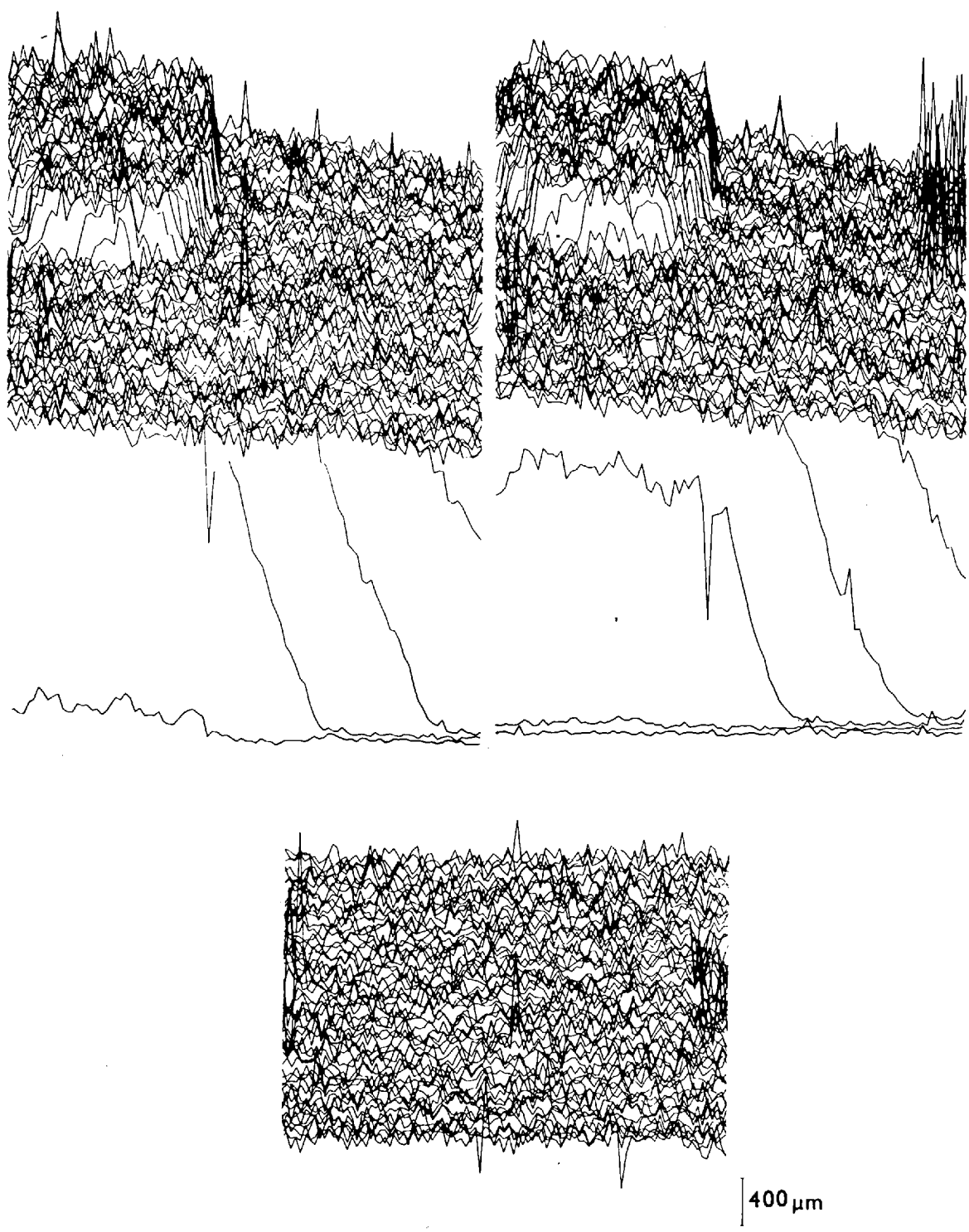


FIGURE 4-2-2: DIVISION OF TWO EXPOSURES

Areas of the exposures were sampled at  $10\mu\text{m}$  intervals using a  $10\mu\text{m}$  x  $10\mu\text{m}$  measuring aperture. A region of the photocathode was chosen that had easily recognisable dead spots and also contained the step in sensitivity due to the mica window. This latter feature was used as a check of the matching process since any edge mis-alignment would show up. Fig. 4.2.2 shows both the original scans and the calibrated scan for the 0.25 D exposures. The data has been "blocked up" so that each plotting point represents an element  $40\mu\text{m}$  x  $40\mu\text{m}$ . On the two originals the intensity step is about 14% of the overall level, while the emulsion noise at this density is about 2% for a  $40\mu\text{m}$  aperture. The feature in the top right-hand corner of the right-hand scan was a small fibre picked up on the emulsion during processing. There is also a general drift downwards in sensitivity along the length of the scan.

The two scans were matched and divided in the computer, the fog level of the emulsion being assessed and subtracted. The resultant array of data is shown at the bottom of Fig. 4.2.2. The step has been removed to the overall level of the noise of the plot, which is about 3%, as has the general drift in sensitivity.

To obtain a measure of the emulsion noise on the uncorrected data a rough fit to the varying sensitivity was made by taking the average background level at several points along a line and interpolating between them. Areas free of dead spots were chosen for this measurement. Using this process a factor of  $\sqrt{2}$  was found between the noise of the calibrated scan and the emulsion noise of the originals for resolution elements up to  $40\mu\text{m}$  x  $40\mu\text{m}$  and a background density of 0.25 D - that is for noise levels on the calibrated data down to about 3%.

FIGURE 4-2-3: L4 EMULSION NOISE FOR A 10μm APERTURE

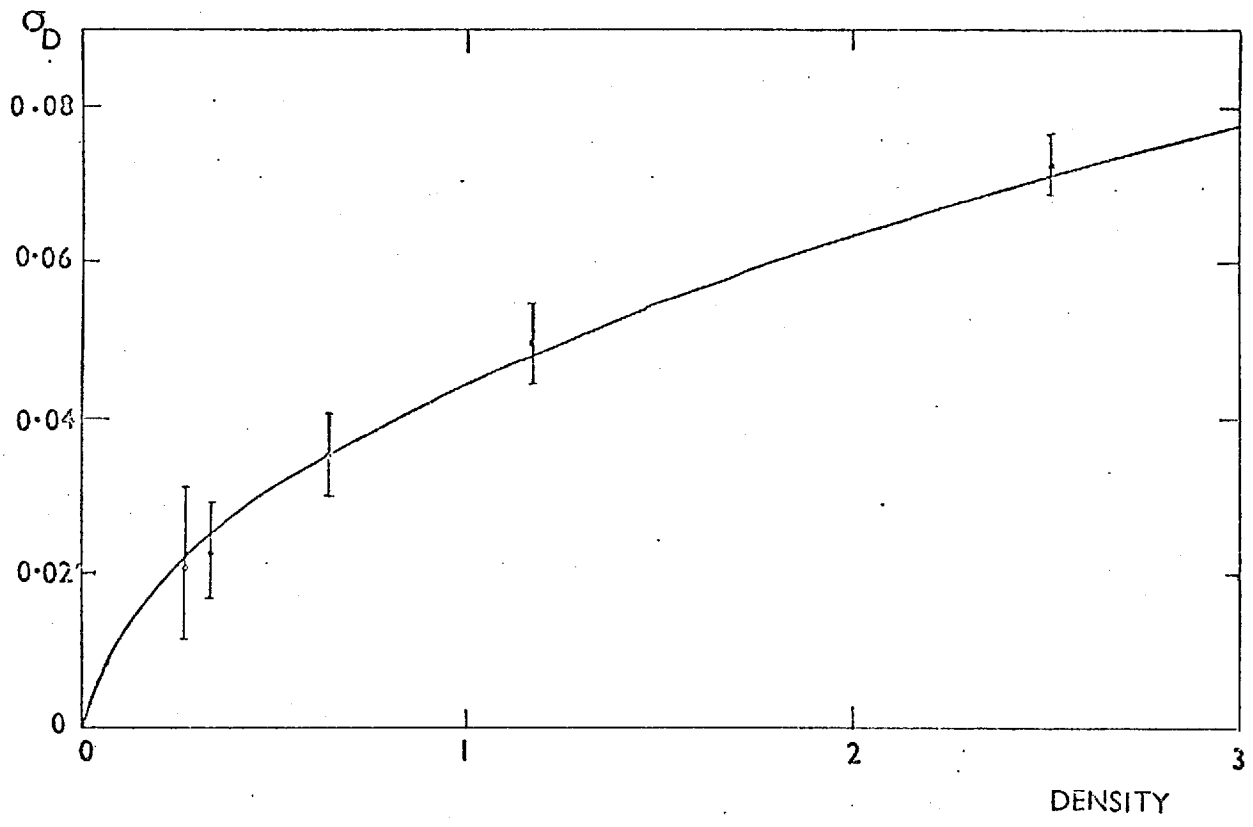
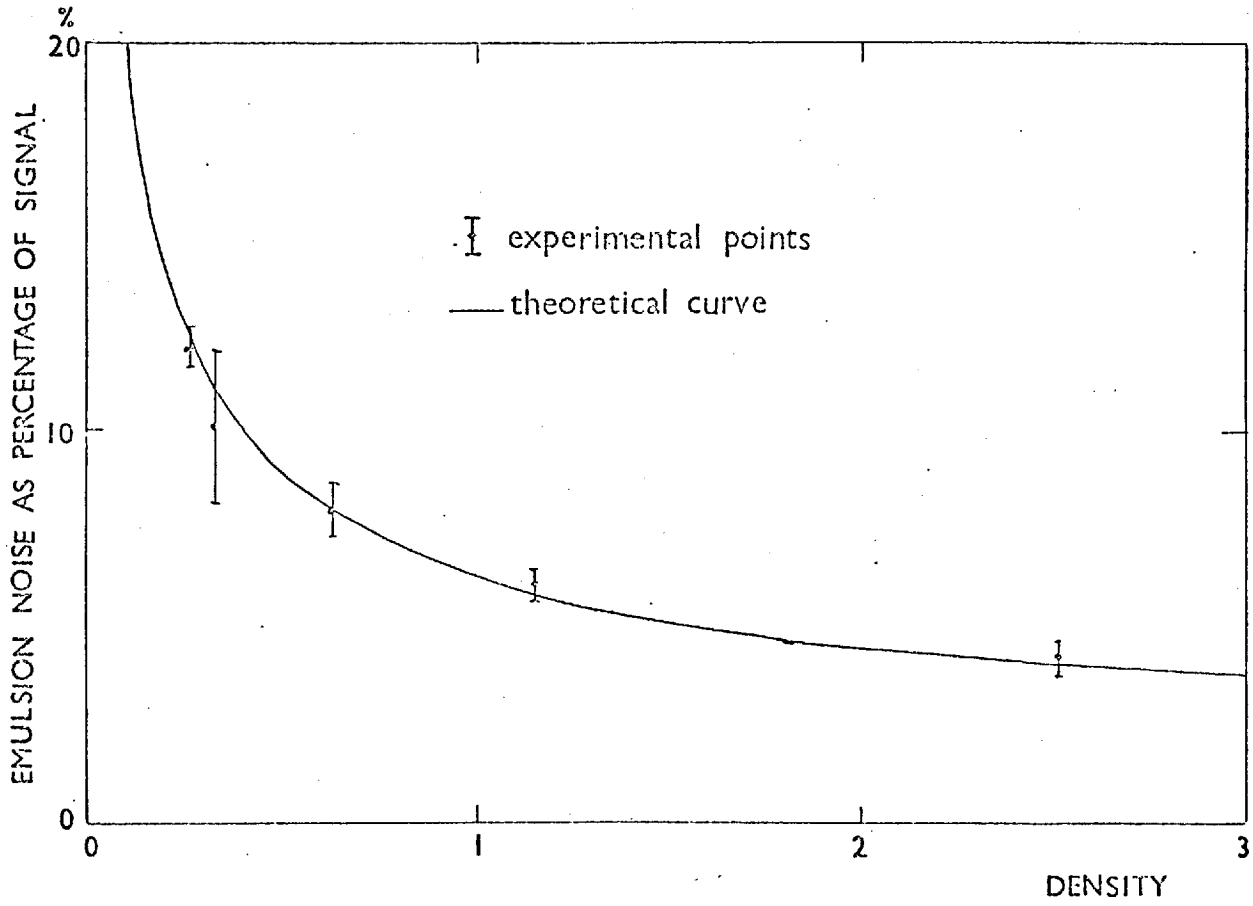


FIGURE 4-2-4: NOISE ON CALIBRATED EXPOSURE AS A FUNCTION OF DENSITY  
FOR A 10 $\mu$ m ANALYSING APERTURE



Using exposures taken to a higher density it is possible to check the relationship between the noise on the corrected data and that on the original scans for a single measuring aperture. Emulsion noise figures obtained from this work tie in well with the estimates that can be made using Coleman's (6) figures for the detective quantum efficiency and sensitivity of the Spectracon combined with L4 emulsion (see Fig. 4.2.3). The emulsion noise for a given density and measuring aperture can be roughly estimated by treating the emulsion as a detector that registers 5 events per square micron per unit density. Using these figures it is possible to check measured values of the noise on the corrected data with that which would be expected if there was just the straightforward addition of the two sets of emulsion noise. Fig. 4.2.4 shows just such a plot for a  $10\mu\text{m} \times 10\mu\text{m}$  measuring aperture and different background densities. On the whole the agreement is quite good to the level of the noise at the highest density, which is about 4%.

Therefore from the measurements made so far both with a single resolution element and varying density and a single density and varying analysing aperture, residual effects of photocathode non-uniformities do not seem to be present. The noise levels of the calibrated data (3% to 4%) can be explained purely in terms of addition of emulsion noise. In order to find the limiting accuracy of the process the emulsion noise must be further reduced until a point is reached where the noise on the corrected data cannot be explained in terms of emulsion statistics.

One such method is to block up the data from a corrected scan so that larger resolution elements are obtained. This was done for data taken from two exposures with a density of 0.62 D. The resultant noise obtained from elements ranging in size from  $10\mu\text{m} \times 10\mu\text{m}$  to  $100\mu\text{m} \times 100\mu\text{m}$  was compared with that which would be expected from emulsion grain statistics alone. The comparison is shown in Fig. 4.2.5. It can be seen



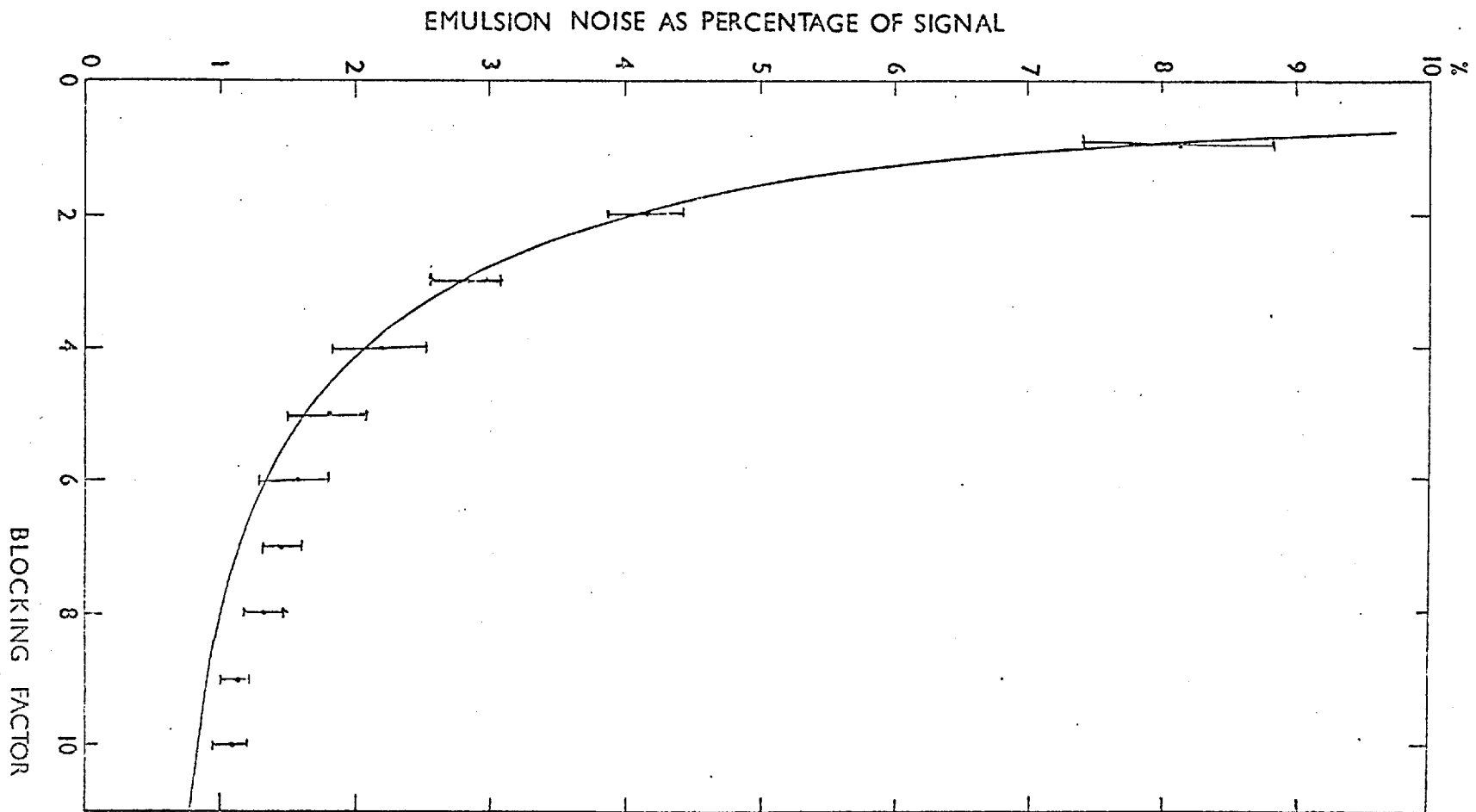


FIGURE 4-2-5

that there is a general trend to a higher value for the measured noise as the overall accuracy increases. In the region of 1 to 1.5% the predicted noise from the emulsion is well outside the errors of the measurements. Thus it would seem that, in the region of one to two percent, the residual effects of non-uniformities become apparent. However, by blocking up this data to resolution elements  $100\mu\text{m} \times 100\mu\text{m}$  the effects of dead spots must be smoothed out to a certain extent since each element will be of the same size or somewhat larger than the average dead spot. Therefore noise figures are required that have been obtained from areas that are clear of dead spots to see if there is any correlation between the measured noise of the calibrated data and the visible defects on the photocathode.

For the two exposures at a density of 2.5 D the corrected data should have a contribution of 1% from the emulsion to the noise for an analysing aperture  $40\mu\text{m} \times 40\mu\text{m}$ . Therefore, taking this data and obtaining noise figures from those areas free of dead spots, it should be possible to assess whether there is still an increase in noise from some other source or whether the observed noise levels can be explained in terms of the presence of dead spots. From regions carefully selected to be clear of visible defects on the originals (that is only areas with a slow drift in sensitivity) noise levels of the order of  $1.03 \pm 0.08\%$  have been obtained. However, in the areas where there are several dead spots, and thus no systematic relationship between the density within them and that over the rest of the exposure the overall noise level of strips  $40\mu\text{m}$  wide and about 2.5 mm long sampled at  $40\mu\text{m}$  intervals can rise to 1.5 to 2%. Obviously these results are only true for a specific distribution of dead spots, but it would seem to point to these features providing the most troublesome source of noise as far as the calibration of the system for a

uniform surface-response is concerned. This would also point to the necessity of keeping the mica window dust-free, since areas of zero sensitivity on the emulsion due to the screening effect of dust particles would have the same effect of reducing the performance of the system.

#### 4.3 Noise Power Spectrum

The spatial frequency distribution of the noise on both the uncalibrated exposures and the corrected data serves as a guide to the frequency at which the slowly varying sensitivity changes of the photosensitive surface become important. The noise power spectrum of the L4 emulsion has been shown to be sensibly flat up to 80 cy/mm (64); thus any substantial peaking in the raw and calibrated data should not stem from this source.

The calculation of noise power or Wiener spectra from digital data is fully described in several references (Bendat and Piersol (138), Dainty and Shaw (139), Blackman and Tukey (140)). Only those features relevant to the particular calculations made for this work will be outlined.

The Wiener spectrum for the electronographic exposures was obtained from the Fourier transform of the auto-correlation function of the data. Given a density record  $N$  samples long with values  $D_1 \dots \dots D_N$ , the first stage was to obtain the mean value of the sample  $\bar{D}$ . The data was then transformed to an array of numbers with a zero mean-value, i.e.  $X_1 \dots \dots X_N$ , where  $X_N = D_N - \bar{D}$ . From this set of data the auto-correlation function ( $R$ ) could be obtained for displacements which were an integer ( $r$ ) multiple of the sample length  $h$ .

The auto-correlation function for this displacement is given by

$$R_r = \frac{1}{N-r} \sum_{n=1}^{N-r} X_n X_{n+r}$$

$r$  can have a value between zero and  $m$ , where  $m$  is the maximum lag number and gives the largest displacement of the data with respect to itself. This maximum displacement will set the resolution bandwidth ( $B_e$ ) of the resulting noise power density estimate, these two quantities being related in the following manner

$$B_e = \frac{1}{mh} \text{ cycles/mm}$$

For continuous data the noise power spectrum ( $S$ ) which is a function of the spatial frequency ( $f$ ) can be related to the auto-correlation function which is a function of the lag distance ( $\ell$ ). Thus

$$S(f) = \int_{-\infty}^{\infty} R(\ell) e^{-j2\pi f \ell} d\ell$$

The auto-correlation function is an even function of  $\ell$ , therefore

$$S(f) = 2 \int_0^{\infty} R(\ell) \cos 2\pi f \ell d\ell$$

and

$$S(f) = S(-f)$$

A one-sided noise power spectrum  $G(f)$  may also be defined where  $f$  only varies from 0 to  $+\infty$ ,  $G(f)$  is twice  $S(f)$  over this region and is otherwise zero. Thus

$$G(f) = 4 \int_0^{\infty} R(\ell) \cos 2\pi f \ell d\ell$$

For digital calculations the maximum length of  $\ell$  is given by  $mh$ . The integration can be replaced by a summation using the following substitution

$$\begin{aligned}\ell &= rh \\ d\ell &= dr h \quad dr = 1 \\ f_c &= \frac{1}{2h} \quad (\text{Nyquist or cut-off frequency})\end{aligned}$$

This leads to a raw estimate of  $G(f)$ , known as the periodogram ( $\tilde{G}(f)$ )

$$\tilde{G}(f) = 2h \left[ R_0 + 2 \sum_{r=1}^{m-1} R_r \cos \frac{\pi r f}{f_c} + R_m \cos \frac{\pi m f}{f_c} \right]$$

However, this value approximates to taking the integral of the continuous function  $R$  over a finite range given by  $\ell = mh$ . Therefore

$$G(f) = 2 \int_{-mh}^{mh} R(\ell) \cos 2\pi f \ell \, d\ell$$

which is equivalent to modifying the auto-correlation function by a top hat function of width  $2mh$ . Therefore the true noise power spectrum, will in turn be convoluted with a sinc function to yield the raw estimate  $\tilde{G}(f)$ . To reduce the effects of this process some form of smoothing is required. First, the function is only calculated at  $m + 1$  discrete frequencies, given by

$$f = \frac{kf_c}{m} \quad k = 0, 1, 2, \dots, m$$

This will yield  $m/2$  independent estimates since it has already been

shown that the resolution bandwidth is set at  $\frac{1}{mh}$ , which is equal to  $\frac{2f_c}{m}$ . At these discrete frequency points the periodogram is given by

$$\tilde{G}_k = 2h \left[ R_0 + 2 \sum_{r=1}^{m-1} R_r \cos \frac{\pi rk}{m} + (-1)^k R_m \right]$$

where  $k$  is the harmonic number.

A final smooth estimate of the noise power spectrum at the harmonic  $k$  is given by a procedure known as Hanning. This value results in an averaging process which is as follows

$$G_0 = 0.5 \tilde{G}_0 + 0.5 \tilde{G}_1$$

$$G_k = 0.25 \tilde{G}_{k-1} + 0.5 \tilde{G}_k + 0.25 \tilde{G}_{k+1} \quad k=1, \dots, m-1$$

$$G_m = 0.5 \tilde{G}_{m-1} + 0.5 \tilde{G}_m$$

The smoothing is carried out during calculation using a Hanning lag weighting function  $C_r$  which is given by

$$C_r = \frac{1}{2} \left( 1 + \cos \frac{\pi r}{m} \right) \quad r = 0, 1, 2, \dots, m$$

$$C_r = 0 \quad r > m$$

Thus the smoothed noise power spectrum may be calculated using the following expression

$$G_k = 2h \left[ R_0 + 2 \sum_{r=1}^{m-1} C_r R_r \cos \left( \frac{\pi rk}{m} \right) \right]$$

A program (POW) was written to perform these calculations on data stored on the standard archive tapes; it is listed in Appendix II.

These techniques for analysing data have been developed for stationary random processes. Strictly speaking the uncalibrated data is not random or isotropic since the emulsion noise is superimposed on a fixed noise-pattern due to the changes in sensitivity of the photocathode. However, the figures from these data are only to be used to obtain qualitative information. In particular the area around the large step in density due to the change in thickness of the mica window was avoided since this will swamp the low frequency contributions from the true photocathode variations.

When an aperture is used to scan an emulsion the measured noise power spectrum ( $S'$ ) can be related to the real function ( $S$ ) in the following manner

$$S'(u,v) = S(u,v) | T(u,v) |^2$$

where  $u$  and  $v$  are spatial frequencies related to the two directions  $x$  and  $y$  and  $T$  is the transfer function of the aperture. For a scan along one line of data the relationship between the one-dimensional information and the two-dimensional power spectrum must be found. The auto-correlation function and the power spectrum are a Fourier pair, thus

$$R(\ell,p) = \int_{-\infty}^{\infty} \int_{-\infty}^{\infty} S(u,v) e^{i2\pi(u\ell + vp)} du dv$$

Therefore the measured auto-correlation function  $R'$  for a one-dimensional scan (where  $p = 0$ ) is given by

$$R'(\ell) = \int_{-\infty}^{\infty} \left( \int_{-\infty}^{\infty} S(u,v) |T(u,v)|^2 dv \right) e^{i2\pi u\ell} du$$

Equally well

$$R'(\ell) = \int_{-\infty}^{\infty} S'(u) e^{i2\pi u\ell} du$$

Thus

$$S'(u) = \int_{-\infty}^{\infty} S(u,v) |T(u,v)|^2 dv$$

If the transfer function of the measuring optics can be ignored, then  $T(u,v)$  can be expressed in terms of the filter function of the slit.

If the slit has a width  $a$  and a height  $b$

$$S'(u) = \int_{-\infty}^{\infty} S(u,v) \text{sinc}^2(au) \text{sinc}^2(bv) dv$$

$$S'(u) = \text{sinc}^2(au) \int_{-\infty}^{\infty} S(u,v) \text{sinc}^2(bv) dv$$

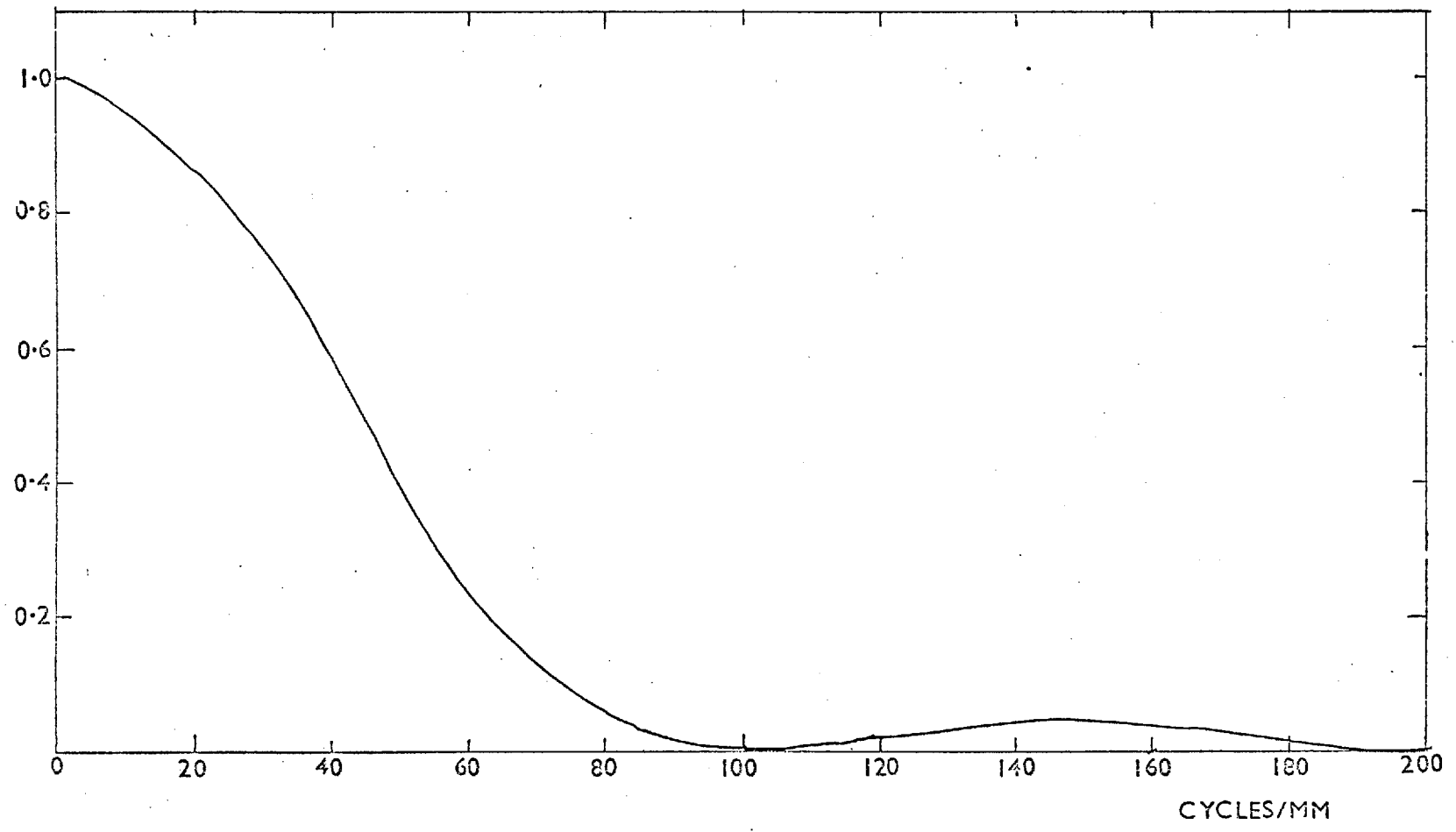
If  $S(u,v)$  is constant over the region that  $\text{sinc}^2(bv)$  is appreciably non-zero, then this relationship reduces to

$$S'(u) = \text{sinc}^2(au) S(u,0) \int_{-\infty}^{\infty} \text{sinc}^2(bv) dv$$

$$S'(u) = \frac{\text{sinc}^2(au)}{b} S(u,0)$$



FIGURE 4-3-1: FILTER FUNCTION OF 10 $\mu$ m SLIT

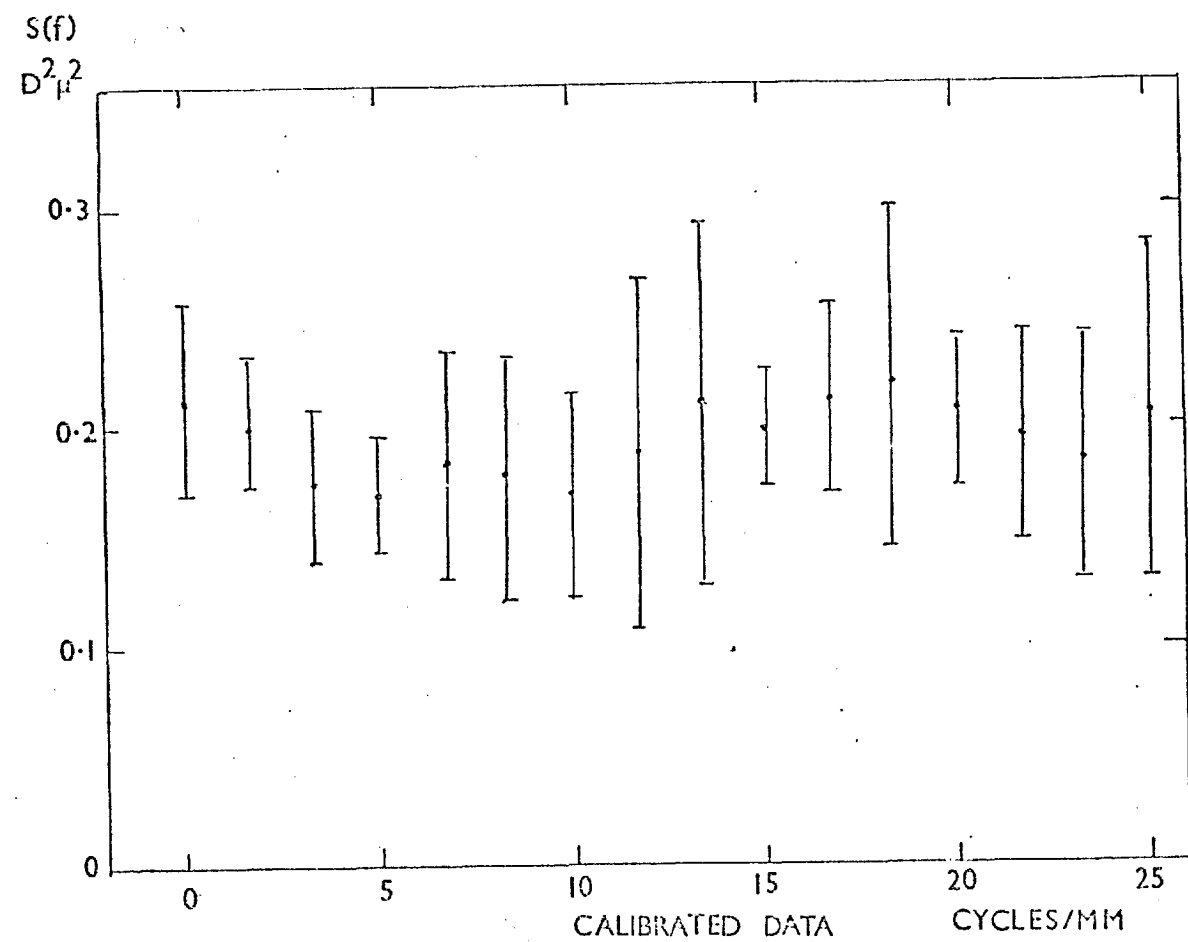
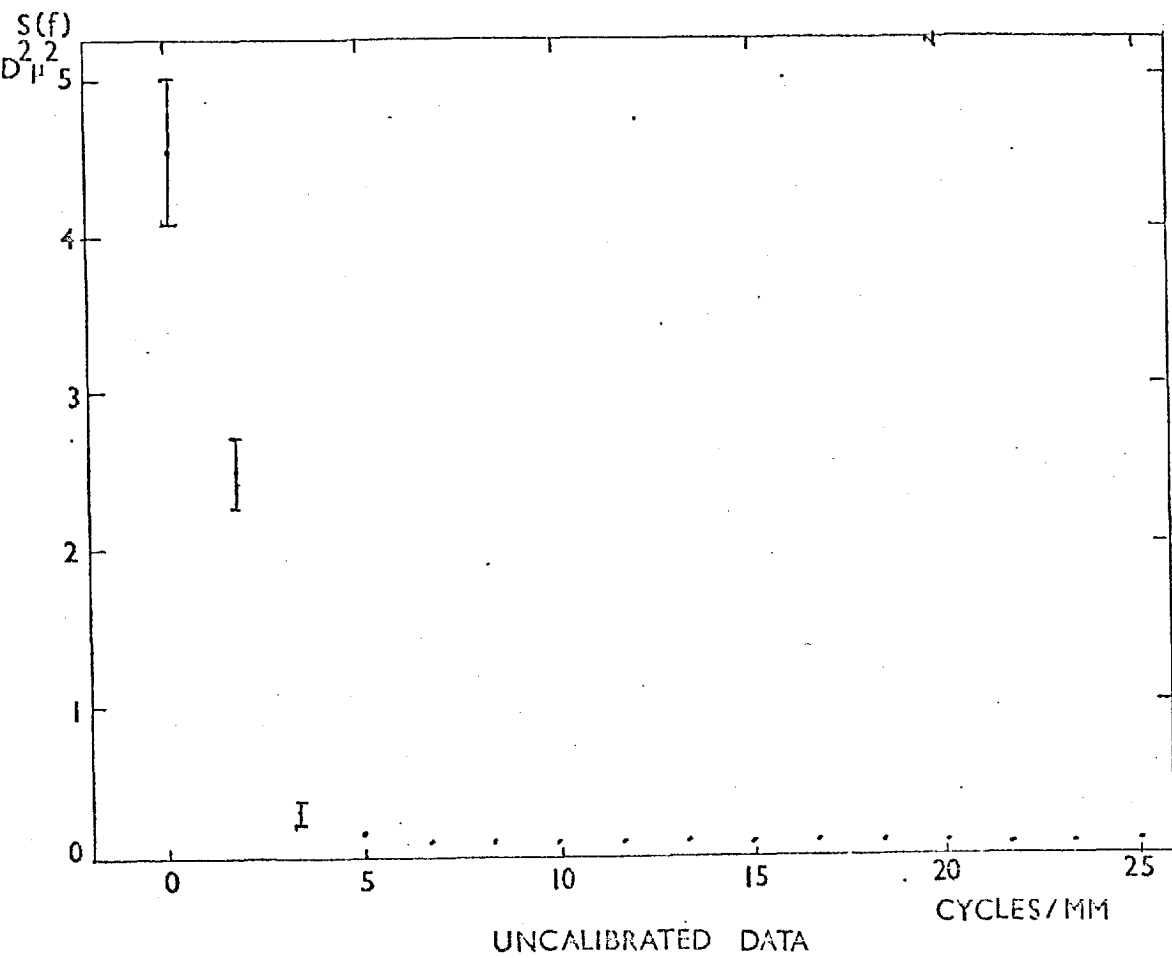


If  $S(u,v)$  varies over the range of spatial frequencies defined by the slit length  $b$  then the measured one-dimensional spectrum is an integration over the  $v$  spatial frequency of the two-dimensional function weighted by the transfer function of the slit.

The scans which were obtained for the investigation of the calibration process were measured using a  $10\mu\text{m} \times 10\mu\text{m}$  slit with samples taken every  $10\mu\text{m}$ . This leads to a folding frequency ( $f_c$ ) of 50 cycles/mm. However, the emulsion noise power is known to be flat out to 80 cycles/mm and the power in the frequencies above 50 cycles/mm will be folded into the calculated spectrum, producing an aliased spectrum. For any frequency  $f$  in the range  $0 < f < f_c$  the higher frequencies that are aliased with  $f$  are given by  $(2n f_c \pm f)$   $n = 1, 2, \dots$ . Thus the power at 60 cycles/mm will be folded into the calculated spectrum at 40 cycles/mm.

To avoid these effects the spectrum should only be calculated up to a frequency such that the power which might be folded in is small. The  $10\mu\text{m}$  measuring slit serves as a filter which attenuates the higher spatial frequencies, dropping to zero at 100 cycles/mm and only reaching a peak of about 5% in its second lobe (fig. 4.3.1). Taking 10% as the highest accuracy one is likely to obtain in these calculations the filter has dropped to this level at about 75 cycles/mm. This frequency will be aliased with 25 cycles/mm in the calculated spectrum so that the function from 0 to 25 cycles should be substantially correct.

The resolution bandwidth ( $B_e$ ) of the final spectrum had to be fairly small since the interest lay in the region round the low frequency end of the spectrum. The maximum number ( $m$ ) of lag values for the calculation of the auto-correlation function was chosen such that  $B_e$  was 3.33 cycles/mm. For a string of  $N$  samples the normalised standard error



for the noise-power calculations is given by

$$e = \sqrt{\frac{m}{N}}$$

Therefore for a fixed length of scan the error goes up with the number of lag values, i.e. as the resolution increases. For the typical scan lengths of about 300 points this leads to an error of about 30% on the individual noise-power estimates.

To compare the results before and after calibration the same areas of scan had to be selected and processed in the same way. A fairly narrow strip well clear of the main step in density due to the change in mica window thickness was chosen. The calculated spectrum was corrected for the effects of the measuring slit which produces an attenuation at 25 cycles/mm of 0.81. The two sets of power spectra both before and after calibration are shown in Fig. 4.3.2. It can be seen that the low frequency components of the noise in the uncalibrated data fall off by about 5 to 6 cycles/mm while the calibrated data produces a fairly flat spectrum. The emulsion noise at the density of these exposures (0.6 D) should yield a noise power of  $0.12 D^2 \mu^2$  for the uncalibrated data and  $0.24 D^2 \mu^2$  for the corrected scan. The average levels from the two sets of data are  $0.11 D^2 \mu^2$  and  $0.22 D^2 \mu^2$  respectively.

These figures were obtained from a fairly restricted area of the scan which was free of dead spots. Another spectrum was calculated for the corrected data but taking in a fairly large area. The lines were added together to form a set of data which was equivalent to measuring the exposures with a slit 600 $\mu$ m long and 10 $\mu$ m wide. This spectrum

FIGURE 4-3-3 : NOISE POWER SPECTRA FROM LARGE AREA OF PHOTOCATHODE

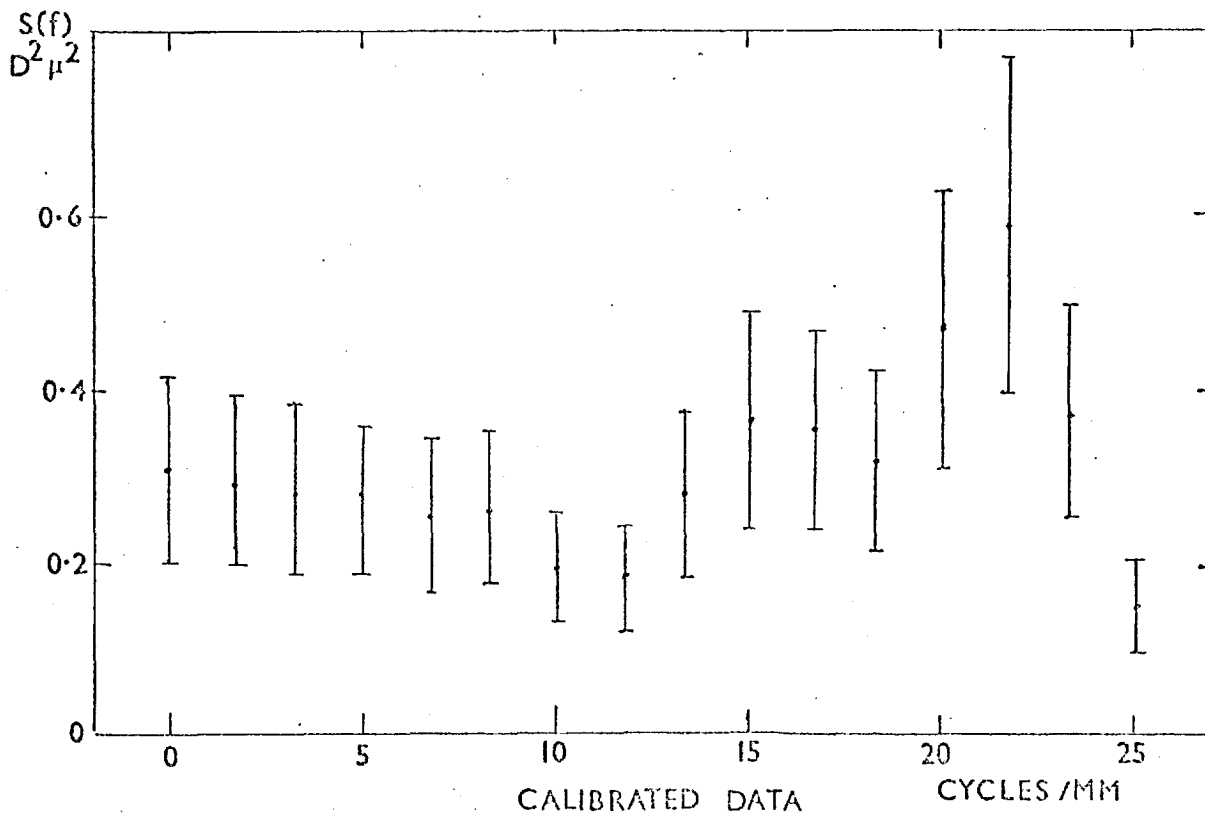
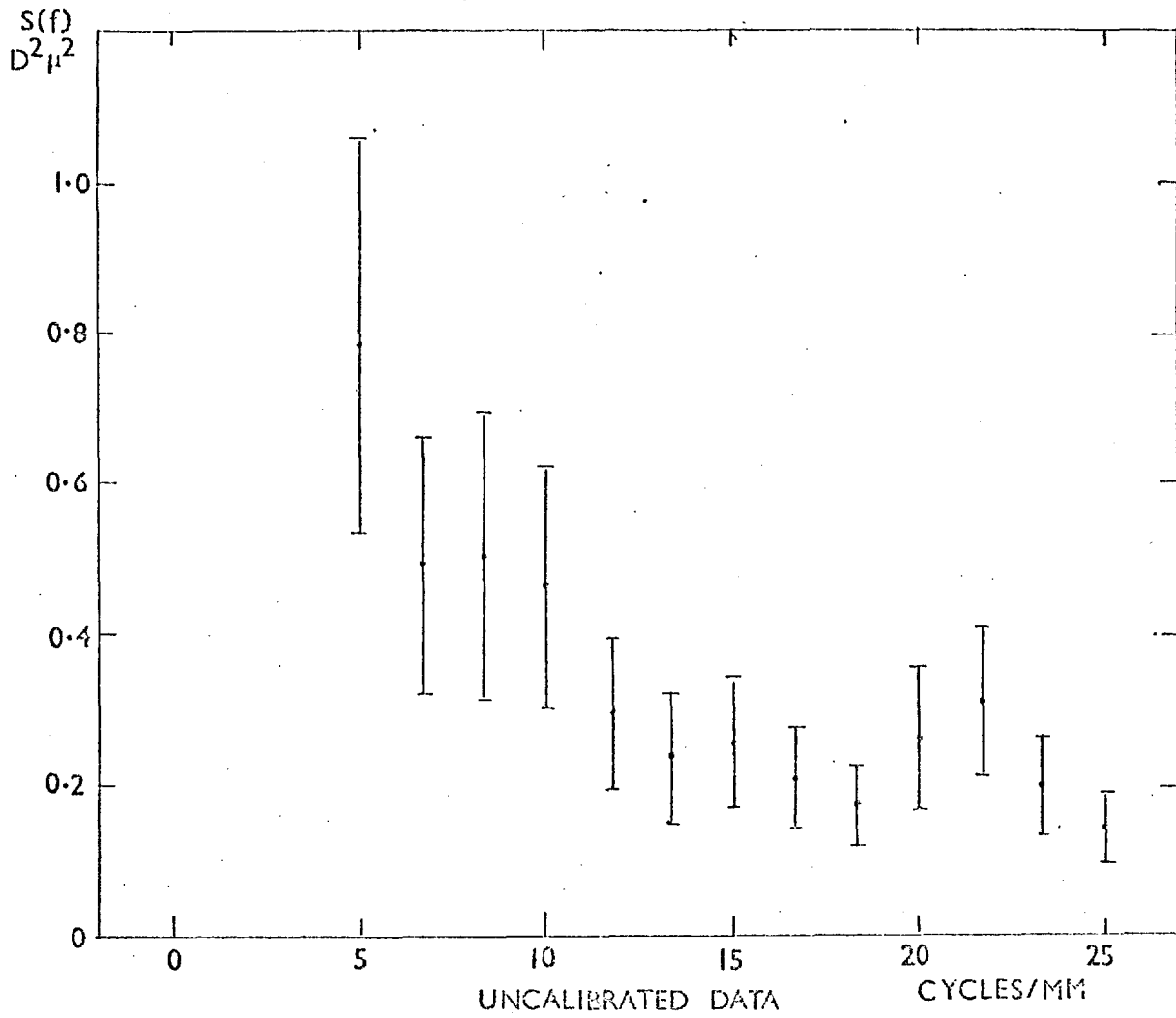
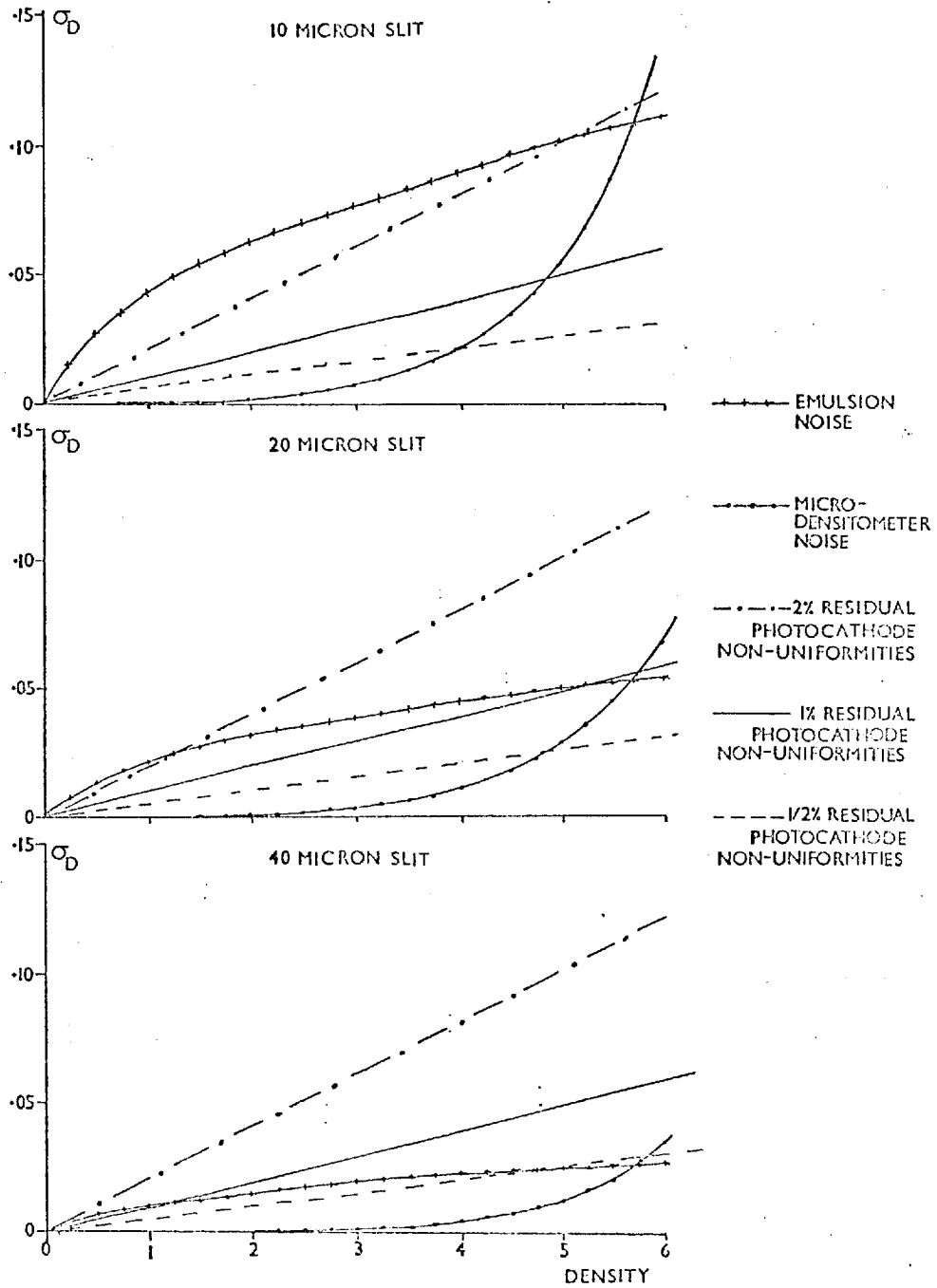


FIGURE 4.4-1: SOURCES OF LIMITATIONS TO PHOTOMETRY



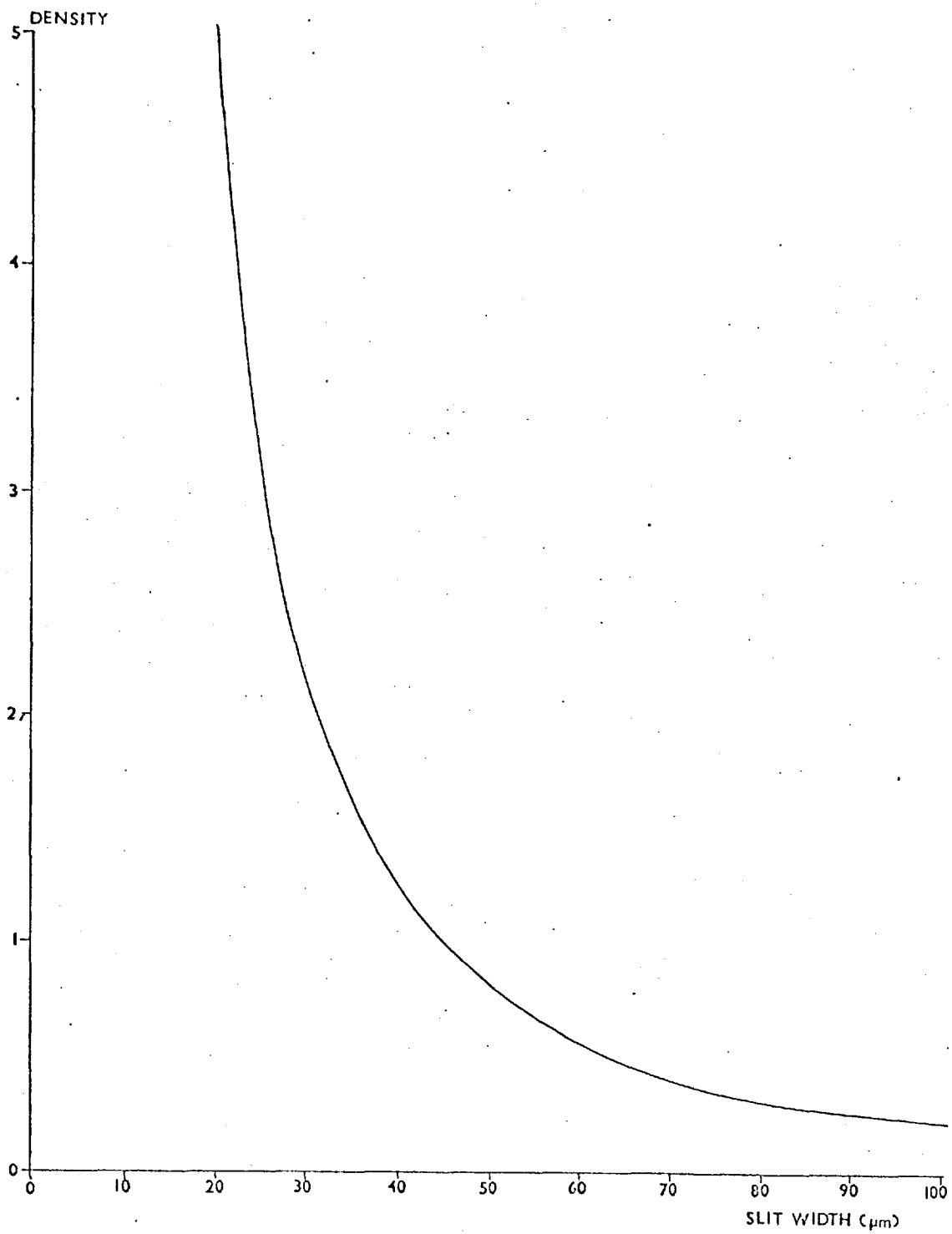
(Fig. 4.3.3) again shows a reduction in the low frequency noise components. The overall noise power has risen slightly in the calibrated data; this might be expected if dead spots are taken in with the emulsion noise. There is a peak in the spectrum around 20 cycles/mm which is also present in the uncalibrated data. This would imply that there is some periodic variation which is not being calibrated out.

From these power spectra it can be seen that the low frequency components of the noise due to sensitivity changes of the photocathode can be removed. These effects seem to be restricted to spatial frequencies lower than about 6 cycles/mm, i.e. they are of the order of 200 $\mu$ m in size or greater.

#### 4.4 Limitation to Photometric Accuracy

It has been shown that emulsion noise-limited performance can only be obtained in areas of the photocathode that are free from dead spots. Therefore when studying objects which extend over substantial areas of photocathode photometric accuracy is limited by these features to the region of 1% to 2% of the background level, depending on the concentration of these areas of zero sensitivity. Figure 4.4.1 shows a summary of the contributions arising from different sources of noise, as a function of background density. It can be seen for the case of emulsion and microdensitometer noise alone that the same limiting density, that is the density at which the microdensitometer noise exceeds that of the emulsion, is reached for all the different sizes of measuring aperture. This would seem reasonable since the improvement in machine noise due to the increased photon flux from a larger slit will be matched by the drop in emulsion noise due to grain statistics. A straight line indicating 1% residual photocathode non-uniformities after calibration shows that these do not severely limit the measurements made using 10 $\mu$ m or 20 $\mu$ m

FIGURE 4.4.2: DENSITY REQUIRED FOR 1% EMULSION NOISE





slits, but for the 40 $\mu$ m analysing aperture they prevent full use being made of the possible storage of the emulsion. The two broken lines show the effects 2% and  $\frac{1}{2}$ % residual non-uniformities would have.

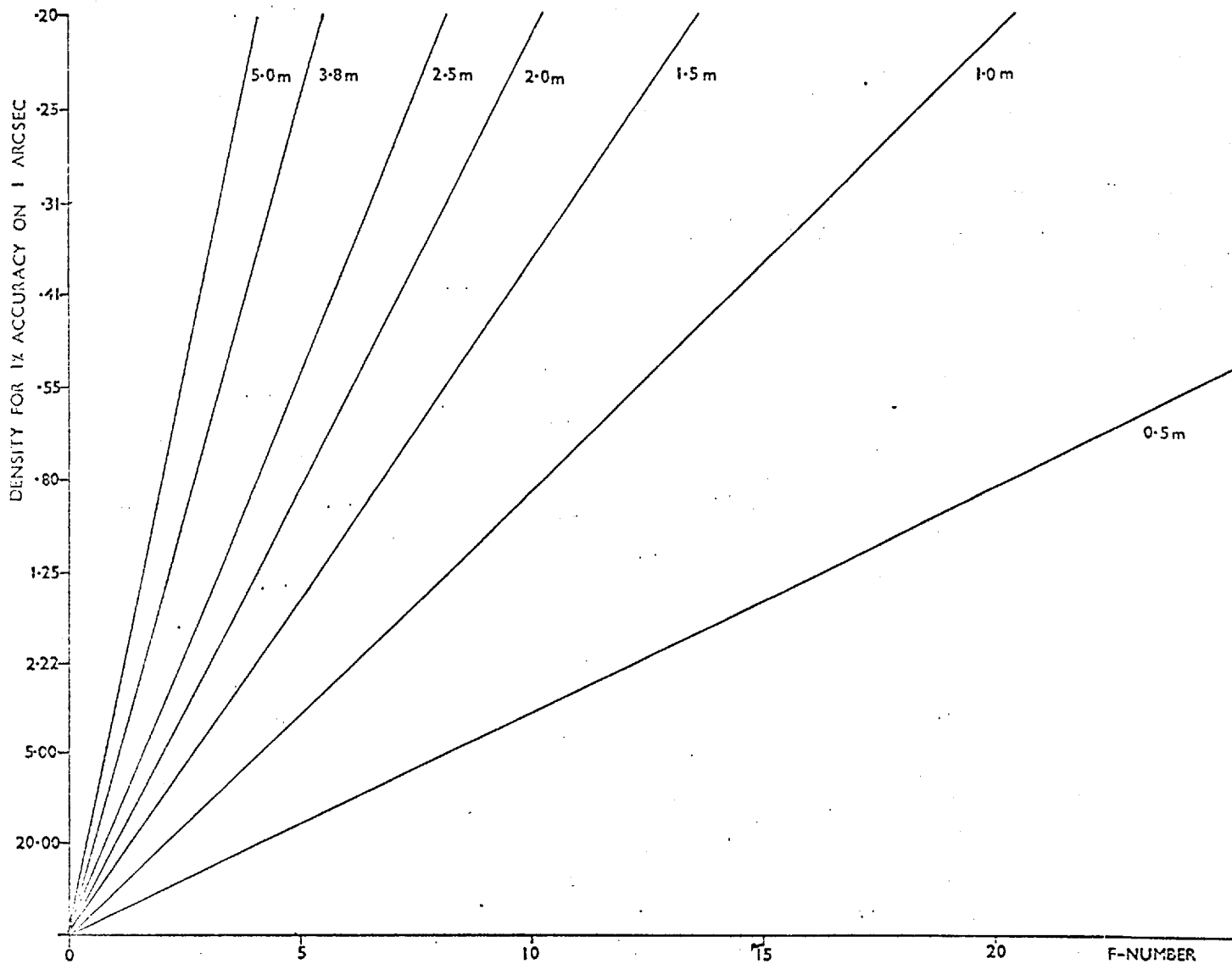
One way of reducing the effect of dead spots would be to use some form of interpolation routine. However, this will only be possible if they are of a size that is small compared with the resolution element in the exposure.

Since the emulsion noise on the calibration exposure is added to that of the astronomical data, the scan used for correction purposes should ideally have a substantially lower noise value than that required of the final processed image. Thus the astronomical exposure need only be long enough to reach a density which gives an emulsion noise of the order of the final accuracy required. The noise of the calibration data can be reduced by either taking it to higher density or by some form of artificial smoothing, provided this does not limit the correction of the slow changes in sensitivity.

Taking 1% as the best limiting accuracy, it is possible to calculate the emulsion density required for 1% photometry and different sizes of analysing aperture. Figure 4.4.2 shows that for slits smaller than 20 $\mu$ m the microdensitometer noise will limit the performance of the system and of course the higher the background density required the smaller the dynamic range of the exposure. That is to say if  $D_B$  is the background density and  $D_L$  is the limiting density fixed by microdensitometer noise the dynamic range is given by

$$\frac{D_L - D_B}{0.01D_B}$$

FIGURE 4-4-3



when the photocathode is limiting the photometric accuracy. If it is the emulsion noise that is providing the limitation then the dynamic range is given by

$$\frac{D_L - D_B}{\sigma_{D_B}}$$

Thus for a 40 $\mu$ m aperture with the emulsion noise reduced to the level of 1% (background density 1.25 D) the dynamic range available is about 350:1. The maximum dynamic range is set by the smallest and largest density that the microdensitometer can measure; Cohen (64) has calculated that this is at least three orders of magnitude.

Figure 4.4.3 shows the densities required for 1% emulsion accuracy on a 1 arcsec resolution element for telescopes of different apertures and f-numbers. If better image resolution is required, in terms of the number of samples per arcsecond, then a trade-off must be made between photometric accuracy, field, dynamic range and exposure time. For example, if the resolution element is increased to  $\frac{1}{2}$  arcsec then the density must be increased by a factor of 4. Also, as the f-number increases so the relative exposure goes up by the square of that quantity. Thus there is a difference in exposure time of 25 between an f/16.25, 0.5m telescope and a f/3.25, 2.5m telescope, although the image scale and the required background density are the same in both cases.

The limitation of 1% to 2% photometry set by the photocathode means that features 4 to 5 magnitudes down on the sky background should be discernible. This limitation is important for broad band photometry where one is trying to distinguish faint features against a high sky background. The accuracy of measurement of relative fluxes across an object is set by the dynamic range of the electronograph and although

each individual measurement may be accurate to the order of a few percent the smallest measurable flux may be only a few tenths of a percent of the peak flux from the object. Therefore in stellar photometry, although the flux from each star can only be obtained to an accuracy of 1% to 2%, the dynamic range and linearity allow the estimation of relative brightness over more than five stellar magnitudes.

Therefore it would seem that the extra effort required to reduce the effects of photocathode non-uniformities is still recompensed by the linearity and dynamic range of the electronographic process.

Some of the work described in this chapter was presented at the Sixth Symposium on Photoelectronic Imaging Devices, London (1974).

CHAPTER VCONCLUSIONS AND FUTURE WORK

"From the end spring new beginnings"

Pliny the Elder (23-79)

The foregoing pages have served as a documentation of three years postgraduate research. Perhaps they represent an unbalanced picture in that much of the routine can be written off in a short sentence while the thoughts of a day may be expanded to several pages. However, it can probably be said that the routine provides the building blocks that enable one occasionally to make a quick advance.

What, then, is the general picture that has emerged from the drawing together of all the different parts of the photometric system? Clearly, it can be seen that except when sampling with a very small aperture, where emulsion noise is large, the limit to photometric accuracy is set by the quality of the photocathode. The slowly varying sensitivity changes due to uneven deposition of the photosensitive surface are easily dealt with, but a large concentration of dead spots serves to drastically lower the performance. If these spots are small, as compared with the resolution element within the image, then a certain improvement could be obtained by interpolation across the area of zero sensitivity. If this procedure is used it might be possible to obtain a close approximation to the emulsion-limited noise across the photocathode.

It has been shown, for apertures ranging from  $10\mu\text{m} \times 10\mu\text{m}$  upwards, that the point at which the microdensitometer noise becomes comparable with that from the emulsion is a constant value between 5D and 6D. This "limiting" density leads to a value for the highest accuracy that

can be obtained for each measuring aperture and thus for a given spatial resolution. The residual effects of photocathode non-uniformities have been shown to overtake the emulsion noise in the region of 1% to 2% of the signal level; therefore they set the practical limit to photometry for analysing apertures larger than  $10\mu\text{m} \times 10\mu\text{m}$ .

These limitations to the accuracy of a single measurement must not be confused with the criteria which set the dynamic range of the device. The latter are basically the smallest and largest densities which can be taken as a true representation of an incoming flux. The lower density level is set at 1% to 2% of the general background (provided it can be resolved by the microdensitometer) while the upper value is simply the "limiting" density set by the microdensitometer noise. Cohen (64) has calculated the dynamic range to be about three orders of magnitude and practically a range of just over 500 to 1 has been obtained (Chapter III). This large dynamic range, coupled with the linearity of the electronographic process, certainly compensates for the extra care that must be taken to remove the effects of photocathode non-uniformities.

Taking the present system as being somewhat less than perfect, what would be the general areas for improvement?

1) The Image Tube

Obviously attention must be given to the production of high quality photocathodes. Defects such as dead spots should be removed as far as possible while an improvement in the general uniformity would also be useful.

Fiducial marks of some sort should be provided. At the moment all of the matching procedures are undertaken using dead spots as location points. For the slowly-varying surface-sensitivity a positional accuracy of about  $10\mu\text{m}$  is perfectly sufficient. The marks

should define an unambiguous set of co-ordinates for ease in matching exposures.

The reproduction of such marks on the exposure is no problem when there is a sufficiently high background density to throw them into relief. However, for narrow-band photometry, where the background is very low, a means must be found of providing illumination to the areas of the photocathode around the fiducial marks. Probably a simple mask which leaves just the extreme ends of the photocathode uncovered would be sufficient, but the effects of light scattered into the image area would have to be taken into account.

## 2) Emulsion

The results presented in this thesis have been explained on the basis that the L4 emulsion used for the experiments had a fairly uniform surface-sensitivity. In fact there has been no evidence to the contrary.

Recently the quality of nuclear track emulsion has been criticised (McKay (141), Wlérick (142)) and clearly in some respects this is a less easily-handled problem than photocathode non-uniformity. The sensitivity of the emulsion (in terms of the density for a given exposure) will be dependent on the thickness of the emulsion layer up to the point that this exceeds the electron range. Therefore if there is a change in the depth of the emulsion across the exposure a variation in sensitivity will be found that cannot be calibrated out. Coleman (6) has given the range for 40 KV electrons as about  $8\mu\text{m}$  to  $10\mu\text{m}$  in nuclear track emulsion.

The uniformity of the emulsion layer will be dependent on the flatness of the surface onto which it is deposited. For glass plates this should be no problem, provided they are kept level, but the Melinex backing used with the Spectracon must first be attached to a glass plate before it is coated with emulsion. If this process is not properly done the Melinex may lift and cause the emulsion to flow unevenly.

Therefore, to obtain repeatable results, the uniformity of the emulsion layer must be good and it is probably necessary to increase its thickness to exceed the electron range. Coleman (6) has shown that an increase of this sort would also improve the detective quantum efficiency of the process.

### 3) The Measuring Machine

By far the longest part of the production of astronomical information from this system is taken up in the retrieval of data from the electronographs and its processing into the required form. Because of the nature of the machine presently used for plate measurement, most of the manipulation of the data (spatial as well as photometric) is undertaken using a fairly large computer. For instance the matching of two sets of data is undertaken by handling large arrays, one being rotated with respect to the other. This process will work quite well for a small number of picture elements, but if whole exposures are to be handled then it very rapidly becomes cumbersome.

Obviously one still wants the scan in digital form so that both photometric and spatial information can be obtained from the same set of data, but if the measuring machine is more flexible one can obtain the specific measurements required.



The electronograph itself presents the most compact method of storing the astronomical data on it. If it is considered as a read-only memory then it should be possible to transfer from it to some other storage medium (such as tape or disc) only that information that is required for a specific job. To do this a microdensitometer with a table of high positional accuracy, operated under computer control, is necessary. With sufficient interaction between the operator and the machine it should be possible to use fiducial marks to define a fixed set of co-ordinates and to position the table so that, for example, the same areas of photocathode are measured from an astronomical exposure and a calibration exposure. The subsequent data handling to obtain the calibrated scan then is trivial and fairly fast since the two sets of data can be superimposed point by point or line by line.

As stated in Chapter I, machines capable of this type of operation have been produced for work on aerial surveys. They are also fast but, as has been pointed out, their very speed limits their photometric accuracy. However, for work on single objects, rather than star fields, a very high scanning rate is not particularly necessary. If the photometric performance can be improved by slowing the machine down, the loss in speed will probably be negligible as compared with the time saved in obtaining data with the correct spatial orientation.

The problems of producing a method of measuring high densities during fast scanning are extensive. If the high density (greater than 2D) content of the electronographs is low an improvement might be achieved by a selective slowing of the scanning rate above a certain density level, without greatly increasing the total scan time. This would be important for stellar photometry where the high density images will represent the bright standard stars which will be used to estimate the magnitudes of the rest of the objects in the field. It

remains to be seen if measures such as these can improve the photometric performance of fast, single-beam scanners to the stage that they are comparable, over the whole density range, with the very much slower two-beam system such as that used in the Joyce-Loebl.

The combination of image tube, emulsion and microdensitometer is as much a photometric system as television-type sensors or photon-counting systems which produce digital data on the telescope. Some thought must be given to the optimisation of the whole so that the routine production of data is straightforward. Obviously in the future the photometry of extremely faint sources of limited angular extent (less than  $10^5$  picture elements) will be undertaken using two-dimensional photon-counting detectors. However, electronography will still have certain advantages which are not to be ignored. Electronographic devices potentially will have available a much larger number of picture elements, and despite the problems of microdensitometry, the nuclear emulsion represents a very compact and stable form of information storage. For example, to digitise a complete Spectracon exposure 3 cm x 1 cm a 7-track magnetic tape 1,200 feet long is required. If the digital image of an object is to be preserved for any length of time a more compact form of storage than tape must be used. Thus for two-dimensional photoelectric photometry of larger fields and for the storage of this data in an archival form electronography must be considered as a prime candidate for some time to come.

APPENDICES

"This concludes the supplement, with the exception of forty pages of illustrative and mathematical notes, which could greatly enhance the size and price of this work, without commensurably adding to its general interest. Ed. Sun."

Richard Adams Locke

Note at the end of:

Great Astronomical Discoveries Lately Made by  
Sir John Herschel at the Cape of Good Hope.

"Supplement to the Edinburgh Journal of Science"

Published in the New York Sun, August 21st-31st 1835.

APPENDIX IProcessing of Electronographic Emulsions

- 1) 2 minute soak in distilled water.

This serves to swell the emulsion and reduces the diffusion time of the developer by a factor of about 100.

- 2) 5 minutes development in Kodak D-19.

A nitrogen bubble burst system is used to maintain a continuous exchange of developer and reaction products within the emulsion.

- 3) 1 minute stop bath in  $\frac{1}{2}$ % acetic acid.
- 4) Fix for  $1\frac{1}{2}$  times the clearing time in Hypam fixer plus hardener.
- 5) Wash for  $\frac{1}{2}$  an hour in running filtered water.
- 6) 2 minutes rinse in 50% alcohol, 50% distilled water.
- 7) 1 minute rinse in 95% alcohol, 5% distilled water.

The last two processes help to shrink the gelatin and to aid in quick drying.

APPENDIX IIComputer Programs

This appendix contains the listings of the computer programs described in Chapters III and IV .

<u>Program</u>	<u>Page</u>
JLTRAN(ZTRAN)	168
LARD	173
MICSIT	175
DSPLY	179
VOL	192
MATCH	196
POW	201

```

PROGRAM ZTRAN ( JLDATA, SCAN, INPUT, OUTPUT, TAPE1=JLDATA,
1 TAPE3=SCAN, TAPE5=INPUT, TAPE6=OUTPUT, TAPE7 )
DIMENSION IBUF(256),DATA(512),ASOT(18),SCOT(18),DENS(9),DENH(9)
COMMON IPAR
INTEGER ZZCH
IPAR=0
IPAR=1

(
**** THIS PROGRAM TRANSLATES A DATA TAPE FROM THE MICRODENSITOMETER
**** INTO A STANDARD FORMAT READABLE BY FORTRAN PROGRAMS
(
**** IBUF IS THE AREA INTO WHICH INFORMATION IS READ
* IDATA IS THE AREA INTO WHICH COMPLETE DENSITIES WILL BE PUT
* NDATA IS A COUNT OF THE WORDS IN IDATA
* I IS INDEX OF WORD CURRENTLY BEING DECODED
* J IS INDEX OF CHARACTER CURRENTLY BEING DECODED
* NF = FILE NUMBER
* NR = RECORD NUMBER
* ITS = 0 THEN SIMULTANEOUS PRINT OF DATA FILE
(
18 READ (5,2) ISW, NOF, ITS
2 FORMAT ( 9I10 )
IF ( NOF.LT.0 ) STOP
(
**** ISW INDICATES PROCESSING TO BE DONE FOR EACH OF NOF FILES
* NOF=0 OR 1 THEN 1 FILE, NOF =IVE STOP 2
* ISW=-IVE READ AND PRINT FILE
* 0 DATA IN STANDARD ELECTROGRAPHIC FORMAT
* 1 NO INITIAL DATA HEADER
(
IF ( ISW ) 3,4,4
(
**** PRINT ALL FILES
(
3 NF=0
17 NF=NF+1
NR=0
WRITE (6,6) NF
6 FORMAT ( 1H1, 30X, 6HFILE , I2 )
15 NR=NR+1
BUFFER IN (1,IPAR) ( IBUF(1), IBUF(256) )
7 CALL XRCL
IF ( UNIT,1 ) 7,8,9,10
10 WRITE (6,11) NF,NR
11 FORMAT ( 24H0 PARITY ERROR AT FILE , I3, 10H RECORD , I5 )
STOP 1
(
**** PRINT EACH RECORD
(
8 WRITE (6,12) NR
12 FORMAT ( 10H0 RECORD , I5, / )
DO 13 KK=1,254,5
13 WRITE (6,14) KK, IBUF(KK), IBUF(KK+1), IBUF(KK+2), IBUF(KK+3),
1 IBUF(KK+4)
KK=254
WRITE (6,14) KK, IBUF (KK)
14 FORMAT ( 1X, I5, 5(5X,020) )
GO TO 15
(
**** EOF FOR SIMPLE PRINT
(
9 IF ( NOF-NF ) 16,18,17
16 STOP
(
**** WHAT TO DO WITH FIRST RECORD NB IFLAG=ISW+1 FOR EASE OF GOTO
(
4 IFLAG=ISW+1
GO TO (5,5),IFLAG
(
**** RECORD TRANSLATED TO TAPE7
(
5 NF=0
57 NF=NF+1
NR=0
ML=0
NR=0
NR=0
NR=0
NR=1
34 I=1
I=1
J=1
NR=0

```

```

000154          NDAT=1
C
C**** NP=COUNT OF WORDS IN LINE
C * NPX=MAX WORDS IN LINE
C * NL=LINE NUMBER
C
000155          BUFFER IN (1,IPAR) (IBUF(1),IBUF(256))
000161          19 CALL XRCL
000162          IF (UNIT,1) 19,54,21,10
000167          21 WRITE (5,22) NP
000175          22 FORMAT (18H0 NO DATA IN FILE , I3 )
000175          STOP 3
C
C**** GET A DATA WORD
C
000177          20 CALL ZZRWD (IBUF, I, J, IM, IER, NR)
000213          GO TO (81,82,83,83,10,35) , IER
000215          82 IF (NL.NE.0) GO TO 84
000216          NL=1
000217          81 DATA(NDAT)=IM
000222          NDAT=NDAT+1
000222          NP=NP+1
000223          IF (NDAT.LT.S13) GO TO 20
C
C**** OUTPUT A BLOCK
C
000229          WRITE (7) DATA
000233          IF (ITS.NE.0) WRITE (6,40) DATA
000242          40 FORMAT (1H0, 52(10F13.0,/,X))
000243          NDAT=1
000243          GO TO 20
C
C**** TEST END OF LINE
C
000264          84 IF (NL.NE.1) GO TO 83
000266          NPX=NR
000267          NPX=NP-1
000268          GO TO 85
000269          83 IF (NPX.NE.NP) GO TO 86
000274          85 NL=NL+1
000275          NL=NL-1
000275          NP=0
000276          NDAT=NDAT-1
000280          IF (NDAT.EQ.0) GO TO 87
C
C**** FLUSH BUFFER
C
000281          WRITE (7) (DATA(KK),KK=1,NDAT)
000287          IF (ITS.NE.0) WRITE (6,40) (DATA(KK), KK=1,NDAT)
000287          NDAT=1
000300          GO TO (81,81,32,80) , IER
000310          86 CONTINUE
000310          NWRITE
000311          28 WRITE(6,28) NP, NPX, NL, NR, NF
000327          28 FORMAT(1H0, IS, 21H POINTS WHEN NORM IS, IS, 6H LINE, IS,
000327          1 6H RECORD, IS, 6H FILE, IS)
000327          NL=NL
000331          GO TO (85,85,32,80), IER
C
C**** GET PAST FILE MARK
C
000341          80 BUFFER IN (1,IPAR) (IBUF(1),IBUF(256))
000346          33 CALL XRCL
000347          IF (UNIT,1) 33,39,32,10
000354          32 GO TO (53,39),IFLAG
C
C**** FILE FINISH FOR SIMPLE TRANSLATE
C
000362          39 NF=NF+1
000364          END FILE 7
000366          IF (NOF=NF) 16,18,34
C
C**** ILLEGAL CHARACTER
C
000371          35 NP=NP-1
000373          WRITE (6,36) NL, NP, NF, NR, I, J
000412          36 FORMAT (7H0 LINE, IS, 6H POINT, IS, 29H ILLEGAL CH -1000 SUBSTITU
000412          1TED, /, 8H IN FILE, IS, 8H RECORD, IS, 6H WORD, IS, 4H CH.,
000412          2 22)
000422          IF (NR.EQ.NR.AND.NF.EQ.NF) GO TO 38
000423          DO 37 KK=1,251.5
000442          37 WRITE (6,14) KK, IBUF(KK), IBUF(KK+1), IBUF(KK+2), IBUF(KK+3),
000445          1 IBUF(KK+4)
000445          KK=256
000445          WRITE (6,14) KK, IBUF(KK)

```

```

001455 NRR=NR
001456 NRF=NF
001460 38 IM=-1000
001461 IER=1
001462 GO TO 61

C**** GET RECORD HEADER AND READ CARDS
C
001463 54 GO TO (41,20), IFLAG
001471 41 READ (5,41) ASDT,SCDT,IUR,ISC,DENS
001507 42 FORMAT(21SA10,71,110/110/9FS,3)
001507 WRITE (6,42)
001513 44 FORMAT (7111)
001513 WRITE (6,43) IUR,ISC
001523 43 FORMAT(14H USER I.D. ,IS,20X,JURSCAN I.D.,I10)
001523 WRITE (6,45) ASDT,SCDT
001533 45 FORMAT ( /, X, 4A10, 5X, 9HEXPOSURE ,A10,5X,7HFILTER ,A10,5X,
1 4HDATE ,A10,5X,5HPLATE ,A10
2 5X,5HTUBE ,A10,5X,5HFELM ,A10 )
JJ=2ZCH(IBUF,1,1)*10+2ZCH(IBUF,1,2)
KK=2ZCH(IBUF,1,3)*10000+2ZCH(IBUF,1,4)*1000+2ZCH(IBUF,1,5)*100
+2ZCH(IBUF,1,6)*10+2ZCH(IBUF,1,7)
1 IF ( JJ.EQ.102.AND.KK.EQ.100 ) GO TO 46
WRITE (6,47)
001604 47 FORMAT (19H ID'S DO NOT AGREE )
001607 WRITE (6,43) JJ, KK
001617 STOP 5

C**** PICK UP DENSITIES AND OUTPUT
C
001621 46 J=9
001622 M=1
001623 JJ=2ZCH(IBUF,1,8)
001626 NOM=JJ
001627 IF (JJ.EQ.0) GO TO 60
001631 DO 48 KK=1, JJ
001632 CALL ZWLD (IBUF, J, J, IM, IER, NR )
001636 GO TO (48,50,50,10,50), IER
001651 48 DENH(KK)=IM
001655 WRITE (6,48) (DENS(KK), KK=1, JJ)
001655 49 FORMAT (110,10X,24H CALIBRATION DENSITIES 1, /,
1 20H STANDARD DENSITIES, 9F10,2)
WRITE (6,51) (DENH(KK), KK=1, JJ)
001672 51 FORMAT (20H MEASURED DENSITIES, 9F10,2)

C**** SKIP REST OF RECORD
C
001672 60 BUFFER IN (1,IPAR) (IBUF(1),IBUF(256))
001677 61 CALL XCALL
001700 62 IF (UNIT,1) 61,62,63,10
001705 62 I=1
001707 J=1
001711 NE=NR+1
001711 GO TO 20
001711 63 WRITE (6,64)
001715 64 FORMAT (14H UNEXPECTED EOF )
001715 STOP 2

C**** NO STANDARD RECORD
C
001717 50 WRITE (6,52) IER
001725 52 FORMAT (31H0 ERROR IN INITIAL RECORD IER=, I10)
STOP 6

C**** FILE FINISH FOR STANDARD TAPE
C
001727 53 IF (NRR.EQ.0) GO TO 160
001731 WRITE (6,200)
001734 200 FORMAT(1H ,X,55H SCAN NOT WRITTEN TO ARCHIVE DUE TO NON STANDARD
1 LINE )
001734 REWIND 7
001736 IF (NRF=NF) 16,18,57
001741 160 WRITE (3) IUR, ISC, NL1, NPX, ASDT, SCDT, NOM, (DENS(JJ), DENH(JJ), JJ=1, NOM)
001743 29 WRITE (6,31) NL1, NPX
001743 31 FORMAT ( 310 , IS, 10H LINES OF, I6, 6H POINTS )
001743 REWIND 7
001745 DO 58 JJ=1, NL1
001747 K=NPX/512
001747 IF (K.EQ.0) GO TO 55
001747 DO 56 KK=1, K
001747 READ (7) DATA
001747 56 WRITE (3) DATA
001747 55 K=NPX-K*512
001747 IF (K.EQ.0) GO TO 58

```



```

001036 READ (7) (DATA(KK),KK=1,K)
001037 WRITE (3) (DATA(KK),KK=1,K)
001038 CONTINUE
001039 END FILE 3
001040 REWIND 7
001041 IF (NOF-NF) 16,18,57
001042 END
    
```

UNDEFD LUN(1) SHUL  
11001

```

SUBROUTINE Z2WRD (IBUF, I, J, IM, JER, NR)
DIMENSION IBUF(256), IDT(4)
INTEGER Z2CH
COMMON IPAR
    
```

```

L**** SUBROUTINE TO OBTAIN DECODED WORDS
L
L IER=1 NORMAL RETURN
L IER=2 END OF LINE
L IER=3 RLF
L IER=4 DATA WAS ZERO
L IER=5 PARITY ERROR
L IER=6 ILLEGAL CHARACTER
    
```

```

L**** SEARCH FOR START
L
L IER=1
L KK=1
L IF (IM.EQ.0) GO TO 2
L JJ=Z2CH (IBUF, I, J)
L IF (JJ.EQ.11.OR.JJ.EQ.15) GO TO 8
L IF (JJ.EQ.31.OR.JJ.EQ.27) GO TO 8
L J=J+1
L IF (J.LT.11) GO TO 3
L J=1
L I=I+1
L IF (I.LT.257) GO TO 3
L I=1
L NR=NR+1
L BUFFER IN (1,IPAR) (IBUF(1),IBUF(256))
L CALL XRL
L IF (UNIT,1) 4,3,6,7
L IER=3
L RETURN
L IER=5
L RETURN
    
```

```

L**** PACK CHARACTERS
L
L IER=1
L KK=1
L JJ=Z2CH (IBUF, I, J)
L IDT(KK)=JJ
L J=J+1
L IF (J.LT.11) GO TO 9
L J=1
L I=I+1
L IF (I.LT.257) GO TO 9
L I=1
L NR=NR+1
L BUFFER IN (1,IPAR) (IBUF(1),IBUF(256))
L CALL XRL
L IF (UNIT,1) 10,11,6,7
L IER=1
L KK=KK+1
L IF (KK.LT.5) GO TO 14
    
```

```

L**** TEST FOR ZEROS
L
L DO 12 JJ=1,4
L IF (IDT(JJ).NE.0) GO TO 13
L IER=4
L IM=0
L RETURN
    
```

```

L**** DECODE CHARACTERS
L
L IS=0
L IF (IDT(4).LT.16) GO TO 16
    
```

```

L**** REMOVE OVERFLOW BIT
L
L DO 17 JJ=1,4
L IF (IDT(JJ).GT.32) GO TO 15
L IDT(JJ)=IDT(JJ)-16
    
```

```

00215 IS=1000
L**** TEST VALIDITY
L
L DO 18 JJ=2,4
L IF (IDT(JJ).GT.9.OR.IDT(JJ).LT.0) GO TO 15
L CONTINUE
L IF (IDT(1).EQ.15) IER=2
L IM=IS+IDT(2)*100+IDT(3)*10+IDT(4)
L RETURN
L IER=6
L IM=1
L RETURN
L END
    
```

UNDEFD LUN(1) SHUL  
11701

73H  
SYMBOLIC ALLOCATION TABLE.

COMPASS 3.74248.

74/11/80. 14.45.00.

PAGE 1

ADDRESS LENGTH

BINARY CONTROL LABELS.

IDENT ZCH  
EIO

ENTRY POINTS.

ZZCH 1+

73H

COMPASS 3.74248.

74/10/80. 14.45.00.

PAGE 2

IDENT ZCH  
ENTRY ZZCH

\* \* \* \* \* THIS INTEGER FUNCTION OBTAINS THE J TH. CHARACTER  
\* \* \* \* \* FROM THE I TH. WORD OF THE ARRAY IBCF  
\* \* \* \* \* JJ=ZZCH (IBCF, I, J)  
\*

1 3922 31555158 1  
2 5033 5622 80421  
3 511-77777 714000012  
4 37243 7232 2 2 20301  
5 36232 8042 23141  
6 7:2.00077 11612  
7 100 10000 +  
11

VFD 42/7HZZCH , 18/2  
BSS 1  
SA3 B3 GET J  
SA2 B3 GET I  
SA4 B1+X2 CALCULATE INDEX  
SA1 B4-1 GET INCREASED VALUE  
SX4 10  
IX1 X4-X3 CHS. TO BE REMOVED  
SX3 X2  
LX2 2  
LX3 1  
IX2 X3+X2  
SA4 X2 PUT IN B REG  
SA1 B4,X1 SHIFT  
SX2 G3 SET UP MASK  
SX6 X1+X2 MASK OUT  
EQ  
END

017000 CH STORAGE USED 25 STATEMENTS 1 SYMBOLS  
MODEL 73 ASSEMBLY 0.128 SECONDS 3 REFERENCES

73H  
SYMBOLIC REFERENCE TABLE.

COMPASS 3.74248.

74/11/80. 14.45.00.

PAGE 3

ZZCH 1 PROGRAM\* 2/02-E 2/09 L 2/24

```

PROGRAM LARD (INPUT, OUTPUT, SCAN, TAPE 3=SCAN, TAPES=INPUT,
1 REAL LINE TAPE 6=OUTPUT, TAPE 4, TAPE 25, TAPE 27, TAPE 82)
DIMENSION LINE (2000), PBUF (2000), DATA (SI 2), ASDT (6), SCDT (8), PLDT (8)
3 EXTERNAL ENPLOT
CALL ENTRAP (ENPLOT)

C
C**** INITIALISE
C
000004 CALL START
000005 NT=0
000006 66 REWIND 3
000011 REWIND 4
000012 NT=NT+1

C
C**** READ HEADER DATA AND CHECK SCAN ID
000014 31 READ (3) IUR, ISC, M, NPX, ASDT, SCDT, NDM, (DENS (JJ), DENM (JJ))
1 2, JJ=1, NDM)
1 IF (NT.GT. 4) GO TO 30
READ (5, 101) ISCP, NCP
101 FORMAT (110X, I10)
WRITE (6, 102) IUR, ISC, ASDT, SCDT
102 FORMAT (1H1, 14H USER I.D., IS, 20X, 10HSCAN I.D., IS, /,
1 X, 4A10, 5X, 9H EXPOSURE, A10, 5X, 7HFILTER, A10, 5X
2 AHDATE, A10, 5X, 5HPLATE, A10
3 //, 1X, 4A10, 5X, 5HSLIT, A10, 5X, 10HTELESCOPE, A10,
4 5X, 5HTWICE, A10, 5X, 5HPFILM, A10)
000075 IF (ISCP.EQ.ISC) GO TO 30
000077 WRITE (6, 103) ISC, ISCP
000087 103 FORMAT (/, X, 23H SCAN ID'S DON'T AGREE, /, X, 9HTAPE ID =, I6,
1 10X, 9HCARD ID =, I6)
000117 CALL ENPLOT (0.0)
000118 STOP

C
C**** READ IN CARD DATA TO SELECT AREA OF SCAN REQUIRED
C
C MFST,NFST*****MFST,NLST
C * *
C * *
C NLST,NFST*****NLST,NLST
C
C**** CONSIDER SCAN AS AN ARRAY WITH M ROWS AND N COLUMNS
C**** MFST,NFST DEFINE START OF SELECTED AREA
C**** NLST,NLST DEFINE END OF SELECTED AREA
C**** IBLK IS THE NUMBER OF POINTS IN ROW OR COLUMN
C**** TO BE ADDED TO GIVE ONE PLOTTING POINT
000113 30 READ (5, 100) MFST, NFST, NLST, NLST, IBLK, PLDT
000133 100 FORMAT (SIIC / 8A10)

C
C**** CHECK THAT AREA FOR PLOTTING LIES WITHIN SCAN
C**** AND CALCULATE SIZE OF PLOTTING ARRAY
000133 IF (NLST.GT.NL) NLST=NL
000134 IF (NLST.GT.NP) NLST=NP
000141 JBST=(NLST-MFST+1)/IBLK
000142 KLST=(NLST-NFST+1)/IBLK

C
C**** POSITION SCAN
000152 IF (NFST.EQ.1) GO TO 2
000154 MFHI=NFST-1

C
C**** READ IN UNUSED SCANS
000155 DO 3 J=1, MFHI

C
C**** NOTE. DATA BLOCK CONSISTS OF 512 WORDS WHEN FULL
000156 NB=NPX/512
000161 IF (NB.EQ.0) GO TO 60
000162 DO 41 MNB=1, NB
000164 41 READ (3) DATA
000174 40 NB=NPX-NB*512
000177 IF (NB.EQ.0) GO TO 3
000211 READ (3) (DATA (MNB), MNB=1, NB)
000217 3 CONTINUE

C
C**** FOR EACH VALUE OF J

```

```

001212      2 DO 4 J=1, JLST
      L
      L**** ZERO THE PLOTTING ARRAY
001214      DO 5 K=1, KLST
001220      5 PBUF(K)=0.0
      C
      L**** REDUCE IN J DIRECTION
      C
001222      DO 6 I=1, IBLK
001223      NR=NPA/SI2
001226      ML=NPA-NJ4SI2
001230      IF (NR-1) 43, 44, 45
001233      44 READ(3) (LINE(K), K=1, SI2)
001241      GO TO 46
001241      45 DO 51 II=1, NB
001243      KK=II*SI2
001245      KJ=KK-SI1
001247      51 READ(3) (LINE(K), K=KJ, KK)
001249      KJ=KK+1
001249      KK=KK+KL
001249      IF (KL-1) 46, 52, 52
001249      43 KJ=1
001249      KK=KL
001249      52 READ(3) (LINE(K), K=KJ, KK)
001250      46 IKI=NFST-1
001250      DO 6 K=1, KLST
001314      STOT=0.0
      C
      L**** REDUCE IN K DIRECTION
      C
001315      DO 7 IK=1, IBLK
001312      IKI=IKI+1
001313      7 STOT=STOT+LINE(IKI)
000316      6 PBUF(K)=PBUF(K)+STOT
      C
      L**** INITIAL VALUE OF LIMITS
      C
001325      IF (J.GT.1) GO TO 8
001330      XMAX=PBUF(1)
000330      XMIN=XMAX
      C
      L**** FIND XMAX-XMIN
      C
001332      8 DO 9 K=1, KLST
001340      IF (PBUF(K).GT.XMAX) XMAX=PBUF(K)
001343      IF (PBUF(K).LT.XMIN) XMIN=PBUF(K)
001347      4 WRITE(4) (PBUF(K), IQ=1, KLST)
      C
      L**** PLOTTING CONSTANTS, HIGH IS DISTANCE IN INCHES
      C**** CORRESPONDING TO XMAX-XMIN
      C
001361      READ (5, 104) HIGH
001365      104 FORMAT(F10.2)
001365      SCALE=(XMAX-XMIN)/HIGH
001371      DIST=(2.0-S+HIGH)/FLOAT(JLST)
001373      IF (DIST.GT.0.1) DIST=0.1
      C
      L**** PLOT HEADER UNDER MAIN PLOT
      L**** TL=TITLE LENGTH IN INCHES
      L**** PL=PLOT LENGTH IN INCHES
      C
      L**** FIND MAXIMUM OF PLOT AND HEADER LENGTHS
      C
001377      PL=FLOAT(KLST)*ADIST
001411      TL=8.0
001413      IF (TL-PL) 60, 61, 62
001415      60 PL2=PL/2
000407      X2=PL/2-4.0
001413      CALL SYMBOL (X2, 0.0, 0.1, PLDT, 00.0, 80)
001417      CALL SYMBOL (X2, 0.5, 0.1, SCDT, 00.0, 80)
001423      CALL SYMBOL (X2, 1.0, 0.1, ASDT, 00.0, 80)
001427      CALL PLOT (0.0, 1.5, -3)
001432      GO TO 63
001433      61 CALL SYMBOL (0.0, 0.0, 0.4, PLDT, 00.0, 80)
001437      CALL SYMBOL (0.0, 0.5, 0.1, SCDT, 00.0, 80)
001443      CALL SYMBOL (0.0, 1.0, 0.1, ASDT, 00.0, 80)
001447      CALL PLOT (0.0, 1.5, -3)
001452      GO TO 63
001453      62 PL2=PL/2
001455      X2=4.0-PL/2
000461      CALL SYMBOL (0.0, 0.0, 0.1, PLDT, 00.0, 80)
000465      CALL SYMBOL (0.0, 0.5, 0.1, SCDT, 00.0, 80)
001471      CALL SYMBOL (0.0, 1.0, 0.1, ASDT, 00.0, 80)
      C
001475      CALL PLOT (X2, 1.5, -3)
001500      63 Y=DIST*FLOAT(JLST)
001502      X=0.0
001503      XINC=DIST
001504      IFST=1
001505      INC=1
001506      ILST=KLST
001510      REMIND 4
      C
      L**** PLOT ARRAY LINE BY LINE
      C
001512      DO 10 J=1, JLST
001514      WRITE (6, 13) J
001515      13 FORMAT('A LINE', I6)
001521      READ (4) (PBUF(IJ), IQ=1, KLST)
001527      CALL PLOT (X, Y+(PBUF(IJ)*ST)-XMIN)/SCALE, 3)
001529      I=IFST
001531      I=I+INC
001532      X=X+XINC
001544      11 CALL PLOT (X, Y+(PBUF(I)-XMIN)/SCALE, 2)
001543      IF (E.NE.ILST) GO TO 14
001545      IST=ILST
001545      ILST=IFST
001547      IFST=IST
001547      INC=-INC
001547      XINC=-XINC
001547      10 Y=Y-DIST
001547      IF (NI.GE.ND) GO TO 80
001547      CALL PLOT (4.0+X2*2.0, 0.0, -3)
001547      GO TO 64
001547      60 CALL ENPLOT (2.0+FLOAT(KLST)*DIST)
001547      STOP
001547      END

```

```

PROGRAM MIOSIT(INPUT,OUTPUT,SCAN,TAPE3=SCAN,TAPE5=INPUT,TAPE6=
1      OUTPUT,TAPE8,TAPE(2))
000002 REAL LINE
000002 DIMENSION LINE(2000),PRUF(2000),DATA(512),ASDT(6),SCDT(6),PLOT(6)
1      ,DENS(9),DENM(9)
000002 EXTERNAL ENPLOT
000002 CALL OINTRAP (ENPLOT)

C
C**** INITIALISE
C
000004 READ(5,100) ICAL
000012 100 FORMAT(I10)

C
C**** ICAL IS FLAG FOR DIFFERENT CALL TO START
C
000012 IF(ICAL-1) 10,11,12
000015 10 CALL START(3)
000017 GO TO 13
000020 11 CALL START(1)
000022 GO TO 13
000023 12 CALL START(2)
000025 13 NT=0
000026 WRITE(6,200)
000032 200 FORMAT(1H1)
000032 65 REWIND 3
000034 REWIND 4
000036 NT=NT+1

C
C**** READ HEADER DATA AND CHECK SCAN ID
C
000040 14 READ(3) IUR ,ISC,NL,NPX,ASDT,SCDT,NOM,(OE IS(JJ),DENM(JJ)
1      ,JJ=1,NOM)
000072 IF(NT.GT.1) GO TO 15
000076 READ(5,101)ISCP,NCP
000105 101 FORMAT(I10/I10)
000105 WRITE(6,201) IUR,ISC,ASDT,SCDT
000121 201 FORMAT(1H,1-H USER I.D. ,I5,20X,10HSCAN I.D. ,I5,/,
1      X,4A10,5X,5H EXPOSURE,A10,1X,7HFILTER ,A10,5X
2      4HDATE,A10,5X,5HPLATE,A10
3      ,//,1X,4A10,5X,5HSLIT ,A10,5X,10HTELESCOPE,A10,
4      5X,5HTUBE ,A10,5X,5HFILM ,A10)
000121 IF(ISCP.EQ.ISC) GO TO 15
000123 WRITE(6,202) ISC,ISCP
000133 202 FORMAT(/,X,25H SCAN ID'S DON'T AGREE ,/,X,9HTAPE ID =,I5,
1      10X,9HCARD ID =,I5)
000133 CALL ENPLOT
000134 STOP 1

C
C**** READ IN CARD DATA TO SELECT AREA OF SCAN REQUIRED
C
C      MFST,MFST*****MFST,NLST
C      * *
C      * *
C      * *
C      NLST,MFST*****NLST,NLST
C
C**** CONSIDER SCAN AS AN ARRAY WITH M ROWS AND N COLUMNS
C**** MFST,MFST DEFINE START OF SELECTED AREA

```

```

C***** NLST,NLST DEFINE END OF SELECTED AREA
C**** IBLK IS THE NUMBER OF POINTS IN ROW OR COLUMN
C**** TO BE ADDED TO GIVE ONE PLOTTING POINT
C
000136 15 READ(E,102) MFST,MFST,NLST,NLST,IBLK,PLOT
000156 10? FORMAT(5I10/EA10)
C
C**** CHECK THAT AREA FOR PLOTTING LIES WITHIN SCAN
C**** AND CALCULATE SIZE OF PLOTTING ARRAY
C
000156 IF (NLST.GT.NL)NLST=NL
000161 IF (NLST.GT.NPX)NLST=NPX
000164 JLST=(NLST-MFST+1)/IBLK
000171 KLST=(NLST-MFST+1)/IBLK
C
C**** POSITION SCAN
C
000175 IF (MFST.EQ.1)GO TO 2
000177 MFMI=MFST-1
C
C**** READ IN UNUSED SCANS
C
000200 DO 3 J=1,MFMI
C
C**** NOTE. DATA BLOCK CONSISTS OF 512 WORDS WHEN FULL
C
000201 NB=NPX/512
000204 IF (NB.EQ.0) GO TO 40
000205 DO 41 MNB=1,NB
000207 41 READ (3) DATA
000217 40 MB=NPX-NB*512
000222 IF (MB.EQ.0)GO TO 3
000224 READ(3) (DATA(MB),MNB=1,NB)
000232 3 CONTINUE
C
C**** FOR EACH VALUE OF J
C
000235 2 DO 4 J=1,JLST
C
C**** ZERO THE PLOTTING ARRAY
C
000237 DO 5 K=1,KLST
000243 5 PBUF(K)=0.0
C
C**** REDUCE IN J DIRECTION
C
000245 DO 6 I=1,IBLK
000246 NB=NPX/512
000251 KL=NPX-NB*512
000253 IF (NB-1)43,44,45
000256 44 READ(3) (LINE(K), K=1,512)
000263 GO TO 46
000264 45 DO 51 II=1,NB
000266 KK=II*512
000270 KJ=KK-511
000272 51 READ(3) (LINE(K),K=KJ,KK)
000304 KJ=KK+1
000305 KK=KK+KL

```

```

000307      IF (KL-1) 46,52,52
000311      43 KJ=1
000312      KK=KL
000314      52 READ(7) (LINE(K),K=KJ,KK)
000323      46 IKI=NFST-1
000325      DO 6 K=1,KLST
000327      STOT=0.0
C
C**** REDUCE IN K DIRECTION
C
000330      DO 7 IK=1,IBLK
000335      IKI=IKI+1
000336      7 STOT=STOT+LINE(IKI)
000341      6 PBUF(K)=PBUF(K)+STOT
C
C**** INITIAL VALUE OF LIMITS
C
000350      IF (J.GT.1) GO TO 8
000353      XMAX=PBUF(1)
000353      XMIN=XMAX
C
C**** FIND XMAX-XMIN
C
000355      8 DO 9 K=1,KLST
000363      IF (PBUF(K).GT.XMAX) XMAX=PBUF(K)
000366      9 IF (PBUF(K).LT.XMIN) XMIN=PBUF(K)
000372      4 WRITE(4) (PBUF(IQ),IQ=1,KLST)
000403      REWIND 4
C
C**** SCALE THE PLOT
C
000405      IF (ICAL-1) 20,21,22
000410      20 X=41.9
000411      X=31.5
000413      GO TO 23
000414      21 X=28.6
000415      Y=21.4
000417      GO TO 23
000420      22 X=20.6
000421      Y=15.3
000423      23 DIST1=(X-1.5)/FLOAT(KLST)
000426      DIST2=(Y-2.5)/FLOAT(JLST)
000432      DIST=AMIN1(DIST1,DIST2)
C
C**** TAKE DIST TO THE NEAREST 1/100TH INCH
C
000435      DIST=DIST*100.0
000436      NDIST=NDIST
000440      OIST=NDIST
000441      DIST=OIST/100.0
000442      IF (DIST.GT.0.1) OIST=0.1
C
C**** CENTRE PLOT IN FRAME
C
000446      PL=DIST*FLOAT(KLST)
000450      TL=0.0
000452      XL=AMAX1(TL,PL)
000455      YL=1.5+DIST*FLOAT(JLST)

```

```

000460      XX=X-1.5-XL
000463      XN=XX/2.0
000464      YY=YY-1.0-YL
000467      YN=YY/2.0
000471      CALL PLOT(XN,YN,-3)
C
C**** PLOT HEADER UNDER MAIN PLOT
C**** TL=TITLE LENGTH IN INCHES
C**** PL=PLOT LENGTH IN INCHES
C
C**** FIND MAXIMUM OF PLOT AND HEADER LENGTHS
C
000473      PL=FLOAT(KLST)*DIST
000475      TL=5.0
000477      IF (TL-PL)50,61,62
000501      60 PL2=PL/2
000503      X2=PL/2-4.0
000507      CALL SYMBOL (X2,0.0,0.1,PLDT,00.0,50)
000513      CALL SYMBOL (X2,0.5,0.1,SCDT,00.0,50)
000517      CALL SYMBOL (X2,1.0,0.1,ASDT,00.0,50)
000523      CALL PLOT (0.0,1.5,-3)
000525      GO TO 63
000527      61 CALL SYMBOL (0.0,0.0,0.1,PLDT,00.0,50)
000533      CALL SYMBOL (0.0,0.5,0.1,SCDT,00.0,50)
000537      CALL SYMBOL (0.0,1.0,0.1,ASDT,00.0,50)
000543      CALL PLOT (0.0,1.5,-3)
000546      GO TO 63
000547      62 PL2=PL/2
000551      X2=4.0-PL/2
000555      CALL SYMBOL (0.0,0.0,0.1,PLDT,00.0,50)
000561      CALL SYMBOL (0.0,0.5,0.1,SCDT,00.0,50)
000565      CALL SYMBOL (0.0,1.0,0.1,ASDT,00.0,50)
000571      CALL PLOT (X2,1.5,-3)
C
C**** DRAW BOX AND SCALE INDICATOR 10 PLOT STEPS LONG
C
000574      63 CALL PLOT(0.0,0.0,3)
000577      CALL PLOT(0.0,DIST*FLOAT(JLST),2)
000604      CALL PLOT(DIST*FLOAT(KLST),DIST*FLOAT(JLST),2)
000613      CALL PLOT(DIST*FLOAT(KLST),0.0,2)
000620      CALL PLOT(DIST*FLOAT(KLST+3),0.0,3)
000626      CALL PLOT(DIST*FLOAT(KLST+2),0.0,2)
000634      CALL PLOT(DIST*(FLOAT(KLST)+2.5),0.0,3)
000642      CALL PLOT(DIST*(FLOAT(KLST)+2.5),10.0*DIST,2)
000652      CALL PLOT(DIST*FLOAT(KLST+3),10.0*DIST,3)
000661      CALL PLOT(DIST*FLOAT(KLST+2),10.0*DIST,2)
000670      CALL PLOT(DIST*FLOAT(KLST),0.0,3)
000675      CALL PLOT(0.0,0.0,2)
C
C**** CALCULATE GREY LEVELS (NG IS NUMBER OF GREY LEVELS)
C
000700      READ(5,100) NG
000706      DX=(XMAX-XMIN)/FLOAT(NG)
C
C**** PLOT ARRAY LINE BY LINE
C
000712      DO 70 JJ=1,JLST
000713      READ(4) (PBUF(K),K=1,KLST)

000721      DO 70 KK=1,KLST
000723      DEN=PBUF(KK)
000725      DL=(DEN-XMIN)/DX
000727      LV=DL
000730      L=LV+1
000732      PL=L
000733      R2=PL/2.0
000734      L2=L/2
000735      R2=L2
000737      R=R2-PL2
000740      IF (PBUF(0,0)) GO TO 70
000743      XP=DIST*FLOAT(KK)-DIST/2.0
000746      YP=DIST*FLOAT(JJ-1)+DIST/2.0
000751      CALL SYMBOL (XP,YP,DIST,4,0.0,-1)
000755      70 CONTINUE
000762      IF (GT.3E.HIP) GO TO 80
000765      CALL NEWPAGE
000766      GO TO 56
000767      80 CALL PLOT
000770      STOP 2
000772      END

```

UNUSED COMPILER SPACE  
014700



```

          PROGRAM DSPLY (INPUT,OUTPUT,SCAN,TAPES=INPUT,TAPES=OUTPUT,
1          TAPE3=SCAN,TAPE25,TAPE26,TAPE27,TAPE2)
000002 DIMENSION ASDT(8),SCDT(8),PLOT(8),HT(100)
          ,DENS(9),DENM(9)
000002 COMMON A(5000)
          C
          C**** READ FILE DATA AND CHECK SCAN ID
          C
000002 REWIND 3
000004 READ(3)IUR,ISC,NL,NPX,ASDT,SCDT,NOM,(DENS(JJ),DENM(JJ),JJ=1,
1          NOM)
000036 WRITE(6,100)
000042 100 FORMAT(1H1)
000042 WRITE(6,101)ASDT,SCDT
000052 101 FORMAT(/,X,4A10,5X,9H EXPOSURE ,A10,5X,7H FILTER ,A10,5X,
1          4H DATE,A10,5X,5H PLATE,A10,
2          //,1X,4A10,5X,5H SLIT ,A10,5X,10H TELESCOPE ,A10,
3          5X,5H TUBE ,A10,5X,5H FILM ,A10)
000052 READ(5,200) ISCP
000060 200 FORMAT(I10)
000060 IF (ISCP.EQ.ISC) GO TO 2
000062 WRITE(6,102)ISC,ISCP
000072 102 FORMAT(/,X,22H SCAN ID'S DONT'T AGREE ,/,5X,10H TAPE ID =,I10,/,
1          5X,13H PLOT ID = ,I10)
000072 STOP
          C
          C**** READ IN CARD DATA FOR SUBROUTINE WHICH FORMS PLOTTING ARRAY A
          C
          C
          C MFST,NFST****MFST,NLST
          C * *
          C * *
          C * *
          C * *
          C MLST,NFST****NLST,NLST
          C
          C**** CONSIDER DATA TO BE SELECTED AS A BLOCK DEFINED BY
          C****MFST,NFST AND NLST,NLST. IBLK IS THE NUMBER OF POINTS
          C**** IN A ROW OR COLUMN WHICH ARE ADDED TOGETHER TO GIVE
          C**** ONE PLOTTING POINT IN ARRAY A.
          C**** PLOT IS AN ALPHAMERIC SUMMARY OF ABOVE FOR PUTTING ON PLOT
          C
000074 2 READ(5,201)MFST,NFST,MLST,NLST,IBLK,PLOT
000114 201 FORMAT(9I10/8A10)
000114 M=(NLST-MFST+1)/IBLK
000121 N=(NLST-MFST+1)/IBLK
000125 CALL SECTN(MFST,NFST,MLST,NLST,IBLK,A,NL,NPX,M,N)
          C
          C**** INITIALISE PLOTTING PACKAGE
          C
000137 CALL START
          C
          C**** CALCULATE PLOT LENGTH FOR USE IN LABELLING PLOT
          C
000140 PL=FLOAT(N)*0.1
000142 TL=8.0
000144 IF (TL-PL)50,61,62
000146 50 PL2=PL/2
000150 X2=PL/2-4.,0
000154 CALL SYM20L (X2,0.0,0.1,PLOT,00.0,50)

```

```

000160      CALL SYMBOL (X2,0.0,0.1,SOOT,00.0,80)
000164      CALL SYMBOL (X2,1.0,0.1,ASOT,00.0,80)
000170      CALL PLOT (0.0,1.0,-3)
000173      GO TO 63
000174      01 CALL SYMBOL (0.0,0.0,0.1,PLOT,00.0,80)
000200      CALL SYMBOL (0.0,0.0,0.1,SOOT,00.0,80)
000204      CALL SYMBOL (0.0,1.0,0.1,ASOT,00.0,80)
000210      CALL PLOT (0.0,1.0,-3)
000213      GO TO 63
000214      02 XL=PL/2
000216      XZ=4.0-PL/2
000222      CALL SYMBOL (0.0,0.0,0.1,PLOT,00.0,80)
000226      CALL SYMBOL (0.0,0.0,0.1,SOOT,00.0,80)
000232      CALL SYMBOL (0.0,1.0,0.1,ASOT,00.0,80)
000236      CALL PLOT (X2,1.0,-3)
C
C**** READ IN CARD DATA FOR INSTRUCTIONS FOR PLOTTING
C**** WHEN FLAG=1 THEN THAT PART OF THE PROGRAM IS USED
C**** ICON=FLAG FOR EQUALLY SPACED CONTOURS
C**** IFIX=FLAG FOR SPECIFIED HEIGHT CONTOURS.
C****      ICON=1 IS ALSO REQUIRED FOR THIS PROCESSING
C**** ICLOG=FLAG FOR LOG CONTOURS
C
C**** NCON=NUMBER OF CONTOURS FOR BOTH EQUALLY SPACED
C****      AND FIXED HEIGHT CONTOURS
C**** HT IS THE ARRAY CONTAINING THE HEIGHTS OF THE FIXED CONTOURS
C**** NCLOG=NUMBER OF LOG CONTOURS
C**** ZRO=ZERO POINT FOR LOG CONTOURS
C
000241      63 READ(5,202)ICON,IFIX,ICLOG
000253      202 FORMAT(3I10)
000253      READ(5,203) NCON,NCLOG,ZRO
000265      203 FORMAT(2I10,F10.5)
000265      IF(IFIX.NE.1) GO TO 3
000267      GO 4 KLE=1,NCON
000271      4 READ (5,204)LL,HT(LL)
000303      204 FORMAT(I10,F10.4)
000303      3 REWIND 3
000305      RN=N
C
C**** PLOT LINEAR CONTOURS
C
000306      IF(ICON.NE.1) GO TO 5
000311      CALL CONTHR(A,M,N,NCON,IFIX,HT)
000315      RLN=RN/10.0
000317      IF (RLN.LT.8.0) GO TO 6
000321      XL=RLN+1.0
000323      CALL PLOT (XL,-0.4,-3)
000325      GO TO 5
000326      6 CALL PLOT (9.0,-0.4,-3)
C
C**** PLOT LOG CONTOURS
C
000331      5 IF (ICLOG.NE.1) GO TO 7
000333      CALL CONHLOG (A,M,N,NCLOG,ZRO)
000337      RLN=RN/10.0
000341      IF (RLN.LT.8.0) GO TO 8
000343      XL=RLN+1.0

000345      CALL PLOT (XL,-0.4,-3)
000347      GO TO 7
000350      8 CALL PLOT (9.0,-0.4,-3)
000353      7 CONTINUE
000353      CALL ENPLOT (2.0)
000355      STOP
000357      END

UNUSED COMPILER SPACE
030300

```

```

C
C**** THIS SUBROUTINE SELECTS AND DECODES DATA FROM A FILE
C**** AND FEEDS IT INTO THE PLOTTING ARRAY.
C
000014 REAL LINE
000014 DIMENSION A(JLST, KLST), LINE(2000), DATA(512)
C
C**** CHECK THAT AREA FOR PLOTTING LIES WITHIN SCAN
C**** AND CALCULATE SIZE OF PLOTTING ARRAY
C
000014 IF (NLST.GT.NL) NLST=NL
000017 IF (NLST.GT.NPX) NLST=NPX
000022 JLST=(NLST-MFST+1)/IBLK
000026 KLST=(NLST-NFST+1)/IPLK
C
C**** POSITION SCAN
C
000032 IF (MFST.EQ.1) GO TO 2
000034 MFMI=MFST-1
C
C**** READ IN UNUSED SCANS
C
000035 DO 3 J=1, MFMI
C
C**** NOTE DATA BLOCK ON STANDARD ARCHIVE TAPE CONSISTS OF
C**** 512 WORDS WHEN FULL
C
000036 NB=NPX/512
000041 IF (NB.EQ.0) GO TO 42
000043 DO 41 NNB=1, NB
000044 41 READ (3) DATA
000057 42 NB=NPX-NB*512
000063 IF (NB.EQ.0) GO TO 3
000064 READ (3) (DATA(MNB), MNB=1, NB)
000076 3 CONTINUE
C
C**** ZERO PLOTTING ARRAY
C
000101 2 ILST=JLST*KLST
000104 DO 5 I=1, ILST
000111 5 A(I)=0.0
C
C**** FOR EACH VALUE OF J
C
000113 DO 4 J=1, JLST
C
C**** REDUCE IN J DIRECTION
C
000120 DO 6 IZ=1, IBLK
000121 NB=NPX/512
000124 KL=NPX-NB*512
000127 IF (NB-1) 43, 44, 45
000132 44 READ (3) (LINE(K), K=1, 512)
000137 GO TO 46
000143 45 DO 47 II=1, NB
000145 KK=II*512
000147 KJ=KK-511
C
000151 47 READ (3) (LINE(K), K=KJ, KK)
000156 KJ=KK+1
000170 KK=KK+KL
000171 IF (KL-1) 46, 46, 48
000173 43 KJ=1
000174 KK=KL
000176 48 READ (3) (LINE(K), K=KJ, KK)
000211 46 IKI=NFST-1
000213 DO 6 K=1, KLST
000214 STOT=0.0
C
C**** REDUCE IN K DIRECTION
C
000215 DO 7 IK=1, IBLK
000222 IKI=IKI+1
000223 7 STOT=STOT+LINE(IKI)
000226 I=J+JLST*(K-1)
000232 6 A(I)=A(I)+STOT
000245 4 CONTINUE
000250 RETURN
000250 END

```

UNUSED COMPILER SPACE  
031000

```

SUBROUTINE CONT ( A, M, N, VAL )
  A( I-1, J ) 3 A( I-1, J+1 )
  *****
  *           *
  *           *
  *           *
  *           *
  *           *
  *           *
  *           *
  *           *
  *           *
  *           *
  *****
  A( I, J ) 1 A( I, J+1 )
  THIS SUBROUTINE CALLS NINSEC, NEDG, DIST, WXY AND ARCI2T
000006 DIMENSION A(M,N), X(500), Y(500), IXY( 1500), CX(4), CY(4),
1      JA(3), IH(4)
000006 LOGICAL NINSEC, NEDG
000006 COMMON /COMMON/ LAB(4)
000006 DATA IH/ 3,4,1,2 /
000006 KA=0
000006 KD=1
000007 RIN=FLOAT(N)*0.1-0.1
000012 RIM=FLOAT(I)*0.1-0.1
000014 NIK=N-1
000016 KLOOK=1
000017 KF=1
000020 00 51 I=1,1500
000024 61 IXY(1)=0
C
C      MAIN LOOP WITH INITIAL CONDITIONS SET UP
C
000026 DO 2 IK=2,M
000032 DO 2 JK=1,NIK
000033 II=IK
000034 JJ=JK
000036 3 IF ( KD-1500 ) 46,46,47
000041 47 WRITE ( 6,48) IK,JK , KD, KA
000055 46 FORMAT ( 50H EXIT FROM CONT DUE TO LACK OF STORAGE SPACE AT ,2I4,
1      9H KD IS , I4, 9H KA IS , I3 )
000060 RETURN
000060 46 IF( KA-500 ) 74,74,75
000063 75 WRITE (6,48) IK, JK, KD, KA
000077 RETURN
000100 74 DO 4 IZ=1,4
000106 CX(IZ)=0.0
000107 CY(IZ)=0.0
000107 4 LAB(IZ)=0
000110 K4=3
000111 KSEC=1
000112 IF ( KA.EQ.0 ) I=4
000117 KOUNT=1
C
C      EXAMINS FOR INTERSECTION OF CONTOUR AND BOX
C
000120 IF ( NINSEC ( A(II,JJ), A(II,JJ+1), VAL ) ) GO TO 5
000135 LAB(KOUNT)=1
000137 CY(1)=FLOAT(M-II)*0.1
000141 CX(1)=FLOAT(JJ)*0.1+DIST(A(II,JJ), A(II,JJ+1),VAL )-0.1
000157 KOUNT=KOUNT+1
000161 5 IF ( NINSEC( A(II,JJ+1), A(II-1,JJ+1), VAL ) ) GO TO 6

```

```

CONT0002
CONT0003
CONT0004
CONT0005
CONT0006
CONT0007
CONT0008
CONT0009
CONT0010
CONT0011
CONT0012
CONT0013
CONT0014
CONT0015
CONT0016
CONT0017
CONT0018
CONT0019
CONT0020
CONT0021
CONT0022
CONT0023
CONT0024
CONT0025
CONT0026
CONT0027
CONT0028
CONT0029
CONT0030
CONT0031
CONT0032
CONT0033
CONT0034
CONT0035
CONT0036
CONT0037
CONT0038
CONT0039
CONT0040
CONT0041
CONT0042
CONT0043
CONT0044
CONT0045
CONT0046
CONT0047
CONT0048
CONT0049
CONT0050
CONT0051
CONT0052
CONT0053
CONT0054
CONT0055
CONT0056
CONT0057
CONT0058
CONT0059

```

```

000177          LAB(KOUNT)=2          CONT 0060
000201          CX(2)=FLOAT(JJ+1)*0.1-0.1    CONT 0061
000204          CY(2)=FLOAT(M-II)*0.1+DIST( A(II,JJ+1), A(II-1,JJ+1), VAL ) CONT 0062
000222          KOUNT=KOUNT+1          CONT 0063
000224          6 IF ( MINSEC( A(II-1,JJ+1), A(II-1,JJ), VAL ) ) GO TO 7    CONT 0064
000241          LAB(KOUNT)=3          CONT 0065
000243          CY(3)=FLOAT(M-II+1)*0.1      CONT 0066
000246          CX(3)=FLOAT(JJ)*0.1+DIST( A(II-1,JJ), A(II-1,JJ+1), VAL )-0.1 CONT 0067
000264          KOUNT=KOUNT+1          CONT 0068
000266          7 IF ( MINSEC( A(II-1,JJ), A(II,JJ), VAL ) ) GO TO 8      CONT 0069
000302          LAB(KOUNT)=4          CONT 0070
000304          CX(4)=FLOAT(JJ)*0.1-0.1      CONT 0071
000306          CY(4)=FLOAT(M-II)*0.1+DIST( A(II,JJ), A(II-1,JJ), VAL ) CONT 0072
000323          KOUNT=KOUNT+1          CONT 0073
000325          8 IF ( KOUNT .EQ. 1 ) GO TO 2  CONT 0074

C
C          SEE IF THIS BOX HAS BEEN PLOTTED ALREADY          CONT 0075
C
000327          KC=2          CONT 0076
000330          IF ( KD .EQ. 1 ) GO TO 44    CONT 0077
000332          IT=KD-1          CONT 0078
000333          DO 9 K3=1,IT          CONT 0079
000334          KW=IXY(K3)/100000          CONT 0080
000337          IF ( KW .NE. JJ ) GO TO 9    CONT 0081
000341          KW1=100000*KW          CONT 0082
000342          KX=( IXY(K3)-KW1 )/100      CONT 0083
000346          IF ( KX .NE. II ) GO TO 9    CONT 0084
000352          KX1=100*KX          CONT 0085
000353          KF=( IXY(K3)-KW1-KX1 )/10  CONT 0086
000357          K4=IXY(K3)-KW1-KX1-KF*10  CONT 0087
000362          KC=1          CONT 0088
000363          GO TO 44          CONT 0089
000364          9 CONTINUE          CONT 0090
000367          44 IF ( KA .EQ. 0 .AND. KC .EQ. 1 .AND. K4 .GE. 3 ) GO TO 2    CONT 0091
000402          KA=KA+1          CONT 0092
000403          IF ( KA .EQ. 1 ) GO TO ( 2, 2, 10, 62, 52 ), KOUNT          CONT 0093
000415          GO TO ( 2, 2, 14, 63, 11 ),KOUNT          CONT 0094

C
C          3 OR 4 INTERSECTIONS          CONT 0095
C
000426          62 K4=3          CONT 0100
000427          I=4          CONT 0101
000430          IF ( LAB(3).EQ.3 ) I=3      CONT 0102
000433          X(1)=CX(I)          CONT 0103
000435          Y(1)=CY(I)          CONT 0104
000436          KF=I          CONT 0105
000437          KA=2          CONT 0106
000440          IF ( X(1).EQ.0.0 .OR. X(1).EQ.RIN .OR. Y(1).EQ.0.0 .OR. Y(1).EQ. CONT 0107
1          RIN ) GO TO 67          CONT 0108
000455          JJSTR=JJ          CONT 0109
000456          IISTR=II          CONT 0110
000460          ISTR=I          CONT 0111
000461          KLOOK=2          CONT 0112
000463          GO TO 67          CONT 0113
000463          63 K4=3          CONT 0114
000464          I=IW(I)          CONT 0115
000466          67 DO 64 IZ=1,3          CONT 0116
000470          IZ=LAB(IZ)          CONT 0117

```

```

000471          IF (I2) 65,64,61
000472      65 IF ( ABS( CX(I2)-CX(I) ) .GT. .000001 .OR. ABS( CY(I2)-CY(I) ).GT.
1          .000001 ) GO TO 66
000511      64 CONTINUE
000513      66 I=I2
000515          GO TO ( 50,49 ),KC
000523      50 IF ( KA.EQ.1 ) GO TO 72
000525          GO TO 17
C
000526      52 GO TO ( 53, 54 ), KC
C
000534      54 I=2
000535          IF ( II.EQ.M ) I=4
000540          IF ( II.EQ.2 ) I=3
000543          X(1)=CX(I)
000545          Y(1)=CY(I)
000546          KA=2
000547          IF ( X(1).EQ.0.0 .OR. X(1).EQ.RIN .OR. Y(1).EQ.0.0 .OR. Y(1).EQ.
1          RIA ) GO TO 45
000564          ISTR=I
000565          IISTR=II
000567          JJSTR=JJ
000570          KLOOK=2
000572      45 KF=I
000573          K4=2
000575          CALL WAY ( CX, CY, KF, I, KM2, KM3 )
000601          GO TO 49
C
000604      53 CALL WAY ( CX, CY, KF, KM1, I, KM3 )
000610          X(1)=CX(I)
000612          Y(1)=CY(I)
000615          KA=2
000616          IF ( X(1).EQ.0.0 .OR. X(1).EQ.RIN .OR. Y(1).EQ.0.0 .OR. Y(1).EQ.
1          RIA ) GO TO 71
000635          ISTR=I
000636          JJSTR=JJ
000640          IISTR=II
000641          KLOOK=2
000643      71 IXY(K3)=IXY(K3)+2-10*KF+10*I
000651          KB=-7
000652          I=KM3
000653          GO TO 49
C
000654      11 GO TO ( 55, 56 ), KC
C
000662      55 I=IW(I)
000664          IF ( KF .EQ. I ) GO TO 17
000665          CALL WAY ( CX, CY, KF, KM1, KM2, KM3 )
000671          KC=I
000672          IF ( KM2.NE.KC ) I=KM2
000677          IF ( KM3.NE.KC ) I=KM3
000702          IXY(K3)=IXY(K3)+2
000704          KB=-7
000705          GO TO 49
C
000706      56 I=IW(I)
000710          CALL WAY ( CX, CY, I, KM1, KM2, KM3 )
000714          KF=I

```

```

CONT0118
CONT0119
CONT0120
CONT0121
CONT0122
CONT0123
CONT0124
CONT0125
CONT0125
CONT0127
CONT0129
CONT0129
CONT0130
CONT0131
CONT0132
CONT0133
CONT0134
CONT0135
CONT0135
CONT0137
CONT0138
CONT0139
CONT0140
CONT0141
CONT0142
CONT0143
CONT0144
CONT0145
CONT0145
CONT0147
CONT0148
CONT0149
CONT0150
CONT0151
CONT0152
CONT0153
CONT0154
CONT0155
CONT0156
CONT0157
CONT0158
CONT0159
CONT0160
CONT0161
CONT0162
CONT0163
CONT0164
CONT0165
CONT0166
CONT0167
CONT0168
CONT0169
CONT0170
CONT0171
CONT0172
CONT0173
CONT0174
CONT0175

```

000715	I=KM1	CONT 0175
000717	K4=2	CONT 0177
000720	GO TO 49	CONT 0178
		CONT 0179
		CONT 0180
		CONT 0181
		CONT 0182
		CONT 0183
		CONT 0184
		CONT 0185
		CONT 0186
		CONT 0187
		CONT 0188
		CONT 0189
		CONT 0190
		CONT 0191
		CONT 0192
		CONT 0193
		CONT 0194
		CONT 0195
		CONT 0196
		CONT 0197
		CONT 0198
		CONT 0199
		CONT 0200
		CONT 0201
		CONT 0202
		CONT 0203
		CONT 0204
		CONT 0205
		CONT 0206
		CONT 0207
		CONT 0208
		CONT 0209
		CONT 0210
		CONT 0211
		CONT 0212
		CONT 0213
		CONT 0214
		CONT 0215
		CONT 0216
		CONT 0217
		CONT 0218
		CONT 0219
		CONT 0220
		CONT 0221
		CONT 0222
		CONT 0223
		CONT 0224
		CONT 0225
		CONT 0226
		CONT 0227
		CONT 0228
		CONT 0229
		CONT 0230
		CONT 0231
		CONT 0232
		CONT 0233
		CONT 0234
		CONT 0235
		CONT 0236
		CONT 0237
		CONT 0238
		CONT 0239
		CONT 0240
		CONT 0241
		CONT 0242
		CONT 0243
		CONT 0244
		CONT 0245
		CONT 0246
		CONT 0247
		CONT 0248
		CONT 0249
		CONT 0250
		CONT 0251
		CONT 0252
		CONT 0253
		CONT 0254
		CONT 0255
		CONT 0256
		CONT 0257
		CONT 0258
		CONT 0259
		CONT 0260
		CONT 0261
		CONT 0262
		CONT 0263
		CONT 0264
		CONT 0265
		CONT 0266
		CONT 0267
		CONT 0268
		CONT 0269
		CONT 0270
		CONT 0271
		CONT 0272
		CONT 0273
		CONT 0274
		CONT 0275
		CONT 0276
		CONT 0277
		CONT 0278
		CONT 0279
		CONT 0280
		CONT 0281
		CONT 0282
		CONT 0283
		CONT 0284
		CONT 0285
		CONT 0286
		CONT 0287
		CONT 0288
		CONT 0289
		CONT 0290
		CONT 0291
		CONT 0292
		CONT 0293
		CONT 0294
		CONT 0295
		CONT 0296
		CONT 0297
		CONT 0298
		CONT 0299
		CONT 0300
		CONT 0301
		CONT 0302
		CONT 0303
		CONT 0304
		CONT 0305
		CONT 0306
		CONT 0307
		CONT 0308
		CONT 0309
		CONT 0310
		CONT 0311
		CONT 0312
		CONT 0313
		CONT 0314
		CONT 0315
		CONT 0316
		CONT 0317
		CONT 0318
		CONT 0319
		CONT 0320
		CONT 0321
		CONT 0322
		CONT 0323
		CONT 0324
		CONT 0325
		CONT 0326
		CONT 0327
		CONT 0328
		CONT 0329
		CONT 0330
		CONT 0331
		CONT 0332
		CONT 0333
		CONT 0334
		CONT 0335
		CONT 0336
		CONT 0337
		CONT 0338
		CONT 0339
		CONT 0340
		CONT 0341
		CONT 0342
		CONT 0343
		CONT 0344
		CONT 0345
		CONT 0346
		CONT 0347
		CONT 0348
		CONT 0349
		CONT 0350
		CONT 0351
		CONT 0352
		CONT 0353
		CONT 0354
		CONT 0355
		CONT 0356
		CONT 0357
		CONT 0358
		CONT 0359
		CONT 0360
		CONT 0361
		CONT 0362
		CONT 0363
		CONT 0364
		CONT 0365
		CONT 0366
		CONT 0367
		CONT 0368
		CONT 0369
		CONT 0370
		CONT 0371
		CONT 0372
		CONT 0373
		CONT 0374
		CONT 0375
		CONT 0376
		CONT 0377
		CONT 0378
		CONT 0379
		CONT 0380
		CONT 0381
		CONT 0382
		CONT 0383
		CONT 0384
		CONT 0385
		CONT 0386
		CONT 0387
		CONT 0388
		CONT 0389
		CONT 0390
		CONT 0391
		CONT 0392
		CONT 0393
		CONT 0394
		CONT 0395
		CONT 0396
		CONT 0397
		CONT 0398
		CONT 0399
		CONT 0400

001112	34	CALL ARCSIT ( X, Y, 1, KA, 35, 1.0, 1.0, 0.0, 0.0, 2 )	CONT0234
001113	13	IXY(KD)=K4+10*KF+100*II+100000*JJ	CONT0235
001113		KD=KD+1	CONT0236
001141	72	KC=2	CONT0237
001142		KA=0	CONT0238
001143		KLOOK=1	CONT0239
001144		GO TO 2	CONT0240
	C		CONT0241
	C	ACTION FOR SEARCH-BACK	CONT0242
	C		CONT0243
001145	35	KSTOR=KA	CONT0244
001146		IXY(KD)=K4+10*KF+100*II+100000*JJ	CONT0245
001157		KD=KD+1	CONT0246
001160	37	KLOOK=4	CONT0247
001161		II=IISTR	CONT0248
001162		JJ=JUSTR	CONT0249
001164		I=ISTOR	CONT0250
001166		GO TO 51	CONT0251
001166	36	REWIND 2	CONT0252
001170		DO 39 ITC=1,KSTOR	CONT0253
001172		IT=KSTOR+1-ITC	CONT0254
001174	39	WRITE (2) X(IT), Y(IT)	CONT0255
001210		ITS=KSTOR+1	CONT0256
001212		DO 41 IT=ITS,KA	CONT0257
001213	41	WRITE (2) X(IT), Y(IT)	CONT0258
001227		REWIND 2	CONT0259
001231		DO 40 IT=1,KA	CONT0260
001233	40	READ (2) X(IT), Y(IT)	CONT0261
001247		KLOOK=1	CONT0262
001250		GO TO 34	CONT0263
	C		CONT0264
	C	CONTINUOUS CONTOUR	CONT0265
	C		CONT0266
001251	29	GO TO ( 17, 30 ), KC	CONT0267
001257	17	KA=KA-1	CONT0268
001261		CALL ARCSIT ( X, Y, 1, KA, 35, 1.0, 1.0, 0.0, 0.0, 1 )	CONT0269
001272		KLOOK=1	CONT0270
001273		KA=0	CONT0271
001274		GO TO 2	CONT0272
	C		CONT0273
	C	ORDER IN WHICH THE POINTS ARE TO BE PLOTTED AND NEW II,JJ CALCULATED	CONT0274
	C		CONT0275
001277	30	I=LAB(1)	CONT0276
001300		I2=LAB(2)	CONT0277
001302		IF ( X(KA-1) .EQ. CX(I) .AND. Y(KA-1) .EQ. CY(I) ) GO TO 32	CONT0278
001316		X(KA)=CX(I)	CONT0279
001317		Y(KA)=CY(I)	CONT0280
001321		GO TO 19	CONT0281
001321	32	I=LAB(2)	CONT0282
001325	49	X(KA)=CX(I)	CONT0283
001326		Y(KA)=CY(I)	CONT0284
001330		IF ( KD .EQ. -7 ) GO TO 51	CONT0285
001332	19	IXY(KD)=K4+10*KF+100*II+100000*JJ	CONT0286
001342		KD=KD+1	CONT0287
001344	51	IF ( I .EQ. 1 ) II=II+1	CONT0288
001347		IF ( I .EQ. 2 ) JJ=JJ+1	CONT0289
001353		IF ( I .EQ. 3 ) II=II-1	CONT0290
001356		IF ( I .EQ. 4 ) JJ=JJ-1	CONT0291
001351		IF ( II.LT.2.OR.II.GT.4 ) GO TO ( 34, 35, 34, 36 ), KLOOK	CONT0292
001401		IF ( JJ.LT.1.OR.JJ.GT.4 ) GO TO ( 34, 35, 34, 36 ), KLOOK	CONT0293
001421		GO TO 3	CONT0294
001422	2	CONTINUE	CONT0295
001427		RETURN	CONT0296
001427		END	

UNUSED COMPILER SPACE  
025300



```

SUBROUTINE ARCIST ( X, Y, I1, I2, NDF, XM, YM, XA, YA, ISVICH )   ARC
DIMENSION X(1), Y(1)                                           ARC
000014 C**** TO BE USED IN PLACE OF THE FULL ARCIST TO JOIN POINTS WITH STRAIGHT   ARC
C**** LINES                                                    ARC
000014 CALL PLOT ( X(I1), Y(I1), 3 )                               ARC
000026 I3=I1+1                                                    ARC
000027 DO 2 J=I3,I2                                              ARC
000030 CALL PLOT ( X(J), Y(J), 2 )                               ARC
000042 2 CALL LINUM ( X(J), Y(J), -1 )                          ARC
000056 IF ( ISVICH.EQ.1 ) CALL PLOT ( X(I1), Y(I1), 2 )       ARC
000072 RETURN                                                    ARC
000073 END                                                        ARC

```

UNUSED COMPILER SPACE  
031700

```

SUBROUTINE LINUM ( X, Y, I )                                     LINUM0000
COMMON /CONCOM/ LAB(4),RIVAL,J                                LINUM0001
000005 C IN ORDER NOT TO PUT A NUMBER ONTO THE GRAPH PUT RIVAL= 0.5   LINUM0002
DATA ID/41/                                                    LINUM0003
000005 IF ( ABS(RIVAL) .LT. 1.0 ) RETURN                          LINUM0004
000011 IF ( I ) 2,3,5                                             LINUM0005
000013 2 J=J+1                                                    LINUM0006
000015 IF (ID-J) 4,5,4                                           LINUM0007
000016 5 CALL NUMBER ( X-.025, Y-.025, .05, RIVAL, 0.0, -1 )   LINUM0008
000025 CALL PLOT ( X, Y, 3 )                                     LINUM0009
000033 3 J=J                                                     LINUM0010
000034 4 RETURN                                                  LINUM0011
000035 END                                                        LINUM0012

```

UNUSED COMPILER SPACE  
032000

```

SUBROUTINE CONLOG (A,M,N,IVAL,ZRO)
000007   DIMENSION A(M,N)
000007   COMMON/CONCOM/LAB(4),RIVAL,K
C****
C****   THIS SUBROUTINE PLOTS IVAL CONTOURS
C****
000007   DO 57 IZ=1,M
000010   DO 57 IQ=1,N
000017   57 IF (A(IZ,IQ).LE.ZRO) &(IZ,IQ)=ZRO
000031   WRITE(6,5)
000034   5 FORMAT(1H1)
C****
C****   DRAW BOX
C****
000037   RNIK=FLOAT(M-1)/10.0
000042   RMIK=FLOAT(N-1)/10.0
000044   CALL PLOT(0.0,0.0,3)
000046   CALL PLOT(1.0,RNIK,2)
000051   CALL PLOT(RMIK,RNIK,2)
000054   CALL PLOT(RMIK,0.0,2)
000057   CALL PLOT(0.0,0.0,2)
C****
C****   SCALE THE ARRAY
C****
000065   13 CALL RANGE(A,M,N,RMAX,RMIN)
000067   SCALV=ALOG(RMAX-RMIN)/FLOAT(IVAL+1)
C****
C****   PLOT CONTOURS WITH VAL AS HEIGHT
C****
000102   DO 58 J=1,IVAL
000106   RIVAL=J
000107   VAL=RMIN+EXP(SCALV*RIVAL)
000114   CALL CONT(A,M,N,VAL)
000124   58 WRITE(6,59) J,VAL
000142   59 FORMAT(20H CONTOUR WITH NUMBER,I3,11H HAS HEIGHT,5X,F9.4)
000142   RETURN
000142   ENDO

UNUSED COMPILER SPACE
031400

```

```

SUBROUTINE CONTOUR ( A, N, D, IVAL, IFIX, HT)
DIMENSION A(D, D), HT(IVAL)
COMMON /CONTOUR/ LAB(4), RIVAL, K
THIS SUBROUTINE PLOTS IVAL CONTOURS.
000010 WRITE (6,5)
000010
000013 5 FORMAT ( '1H1' )
C
C
C DRAW BOX
000017 RNIK=FLOAT(N-1)/10.0
000021 RNIK=FLOAT(N-1)/10.0
000024 CALL PLOT ( 0.0, 0.0, 3 )
000026 CALL PLOT ( 0.0, RNIK, 2 )
000031 CALL PLOT ( RNIK, RNIK, 2 )
000034 CALL PLOT ( RNIK, 0.0, 2 )
000037 CALL PLOT ( 0.0, 0.0, 2 )
C DRAWING CONTOURS AT FIXED HEIGHTS
000042 IF(IFIX.NE.1) GO TO 13
000047 DO 40 L=1,IVAL
000051 VAL=HT(L)
000053 CALL CONT(A,N,H,VAL)
000060 40 WRITE(6,41)L,VAL
000075 41 FORMAT(20H CONTOUR WITH NUMBER, I3,11H HAS HEIGHT, 5X,F9.4)
000075 RETURN
C
C FOR IVAL EQUALLY SPACED CONTOURS
C SCALE THE ARRAY
C
000075 13 CALL RANGE ( A, M, N, RMAX, RMIN )
000077 SCV=(RMAX-RMIN)/FLOAT(IVAL+1)
C
C PLOT CONTOURS WITH VAL AS HEIGHT
C
000107 DO 58 J=1,IVAL
000110 RIVAL=J
000111 VAL=RMIN+FLOAT(J)*SCV
000114 CALL CONT ( A, M, N, VAL )
000122 53 WRITE (6,53) J,VAL
000137 53 FORMAT (20H CONTOUR WITH NUMBER, I3,11H HAS HEIGHT, 5X, F9.4 )
000137 RETURN
000137 END

```

UNUSED COMPILER SPACE  
031400

```

SUBROUTINE RANGE ( A, M, N, RMAX, RMIN )
C
C THIS SUBROUTINE FINDS THE LARGEST VALUE (RMAX), AND THE SMALLEST
C VALUE (RMIN) OF AN ARRAY A(M,N)
000007 DIMENSION A(M,N)
000007 B=A(1,1)
000007 C=3
000011 DO 2 I=1,M
000012 DO 2 J=1,N
000021 C=AMAX1( C, A(I,J) )
000024 2 R=AMIN1( R, A(I,J) )
000034 RMAX=C
000035 RMIN=R
000036 RETURN
000037 END

```

UNUSED COMPILER SPACE  
032300

```

REAL FUNCTION DIST(A,B,VAL)
IF (A.LE.1) GO TO 1
C=(VAL-A)/(2-A)*0.1
Z=C
GO TO 2
1 Z=1.05
2 DIST=Z
RETURN
END

```

UNUSED COMPILER SPACE  
032100

```

SUBROUTINE WAY ( CX,CY, KF, KM1, KM2, KM3 )
DIMENSION CX(4), CY(4), DIS(2), LOC(7), N(2)
DATA LOC / 4,1,2,3,4,1,2 /
DO 2 I=1,3,2
J=(I+1)/2
K=KF+I-1
K=LOC(K)
N(J)=K
2 DIS(J)=( CX(K)-CX(KF) )**2+( CY(K)-CY(KF) )**2
IF ( DIS(1)-DIS(2) ) 3,3,4
3 KM1=N(1)
KM2=N(2)
GO TO 5
4 KM1=N(2)
KM2=N(1)
5 DO 7 I=1,4
IF ( KF.EQ.I ) GO TO 7
IF ( KM1.EQ.I ) GO TO 7
IF ( KM2.EQ.I ) GO TO 7
KM3=I
GO TO 5
7 CONTINUE
6 CONTINUE
RETURN
END

```

WAY0002  
WAY0003  
WAY0004  
WAY0005  
WAY0006  
WAY0007  
WAY0008  
WAY0009  
WAY0010  
WAY0011  
WAY0012  
WAY0013  
WAY0014  
WAY0015  
WAY0016  
WAY0017  
WAY0018  
WAY0019  
WAY0020  
WAY0021  
WAY0022  
WAY0023  
WAY0024  
WAY0025  
WAY0026

UNUSED COMPILER SPACE  
031600

```

LOGICAL FUNCTION NINSEC( A, B, V )
LOGICAL G
G=.TRUE.
IF ( A.GE.V.AND.V.GE.B ) G=.FALSE.
IF ( A.LE.V.AND.V.LE.B ) G=.FALSE.
NINSEC=G
RETURN
END

```

NINSEC0  
NINSEC1  
NINSEC2  
NINSEC3  
NINSEC4  
NINSEC5  
NINSEC6  
NINSEC7  
NINSEC8  
NINSEC9

UNUSED COMPILER SPACE  
032000

```
000005 LOGICAL FUNCTION NEDG ( I, IVAL, LVAL ) NEDG 2
000005 LOGICAL G NEDG 3
000005 COMMON /COMMON/ LAB(4) NEDG 4
000005 G=.TRUE. NEDG 5
000005 IF ( I .EQ. IVAL .AND. LAB(1) .EQ. LVAL ) G=.FALSE. NEDG 6
000016 IF ( I .EQ. IVAL .AND. LAB(2) .EQ. LVAL ) G=.FALSE. NEDG 7
000026 NEDG=G NEDG 8
000030 RETURN NEDG 9
000030 END NEDG 10

UNUSED COMPILER SPACE
032000
```

```

000002 PROGRAM VOL INPUT, OUTPUT, SCAN, TAPE5=INPUT, TAPE6=OUTPUT, TAPE3=SCAN)
DIMENSION J1(10), J2(10), K1(10), K2(10), A(2000), AMAX(10), AMIN(10),
1 DATA(S12), ALINE(1000), BUF(1000), SUML(1000), ASDT(S),
1 SCOT(8), DENS(9), DENM(9), GK(10), RNS(10)
C --- READ IN IDENTITY OF SCAN, NUMBER OF AREAS OVER WHICH BACKGROUND
C --- IF TO BE ASSESSED AND BLOCKING FACTOR TO BE USED THROUGHOUT
C *** N.B. A BLOCKING FACTOR OF ONE MUST BE USED WITH THE CIRCULAR
C *** APERTURE SUBROUTINE
000002 WRITE(6, 200)
000006 200 FORMAT(1H1)
000006 READ(5, 100) ISC1, N, IBLK
000002 100 FORMAT(I10/I10/I10)
C --- READ IN CO-ORDINATES OF AREAS TO BE USED FOR BACKGROUND
000020 READ(5, 101) (J1(I), K1(I), J2(I), K2(I), I=1, N)
000041 101 FORMAT(4IS)
C --- READ DATA HEADER OF TAPE
000041 READ(3) IUR, ISC, NL, NPX, ASDT, SCOT, NDM, (DENS(JJ), DENM(JJ), JJ=1, NDM)
000073 IF (ISC1.EQ.ISC) GO TO 20
000075 WRITE(6, 201) ISC1, ISC
000105 201 FORMAT(25H SCAN I.D.'S DON'T AGREE /15H REQUEST I.D. =, 15,
1 21H TAPE I.D.=, 15, )
000105 STOP 1
C --- ASSESS SEPARATE BACKGROUND LEVELS AND RMS NOISE VALUES
000107 20 DO 1 J=1, N
000112 IF (J2(J).GT.NL) J2(J)=NL
000115 IF (K2(J).GT.NPX) K2(J)=NPX
000120 JL=(J2(J)-J1(J)+1)/IBLK
000125 KL=(K2(J)-K1(J)+1)/IBLK
000131 CALL SECTN (J1(J), K1(J), J2(J), K2(J), IBLK, A, NL, NPX, JL, KL)
000143 IA=JL*KL
000145 SUN=0.0
000147 DO 2 I=1, IA
000150 IF (I.GT.1) GO TO 21
000154 AMAX(J)=A(I)
000156 AMIN(J)=AMAX(J)
000163 21 IF (A(I).GT.AMAX(J)) AMAX(J)=A(I)
000163 IF (A(I).LT.AMIN(J)) AMIN(J)=A(I)
000175 2 SUN=SUN+A(I)
000175 RIA=FLOAT(IA)
000175 BK(J)=SUN/RIA
000210 CALL NOYS(A, IA, BK(J), RNS(J))
000213 REWIND 3
000215 1 READ(3) IUR, ISC, NL, NPX, ASDT, SCOT, NDM, (DENS(JJ), DENM(JJ), JJ=1, NDM)
000242 SB=0.0
000242 SNS=0.0
000243 DO 3 L=1, N
000252 SNS=SNS+RNS(L)
000253 3 SB=SB+BK(L)
000256 RN=FLOAT(N)
000257 ANS=SNS/RN
000260 BAK=SB/RN
C --- BAK IS THE AVERAGE BACKGROUND LEVEL TAKEN OVER N AREAS
C *** NOVOL IS FLAG FOR VOLUME ASSESSMENT TO BE OMITTED
C *** IDA IS FLAG FOR CIRCULAR DIAPHRAGM
000262 READ(5, 102) NOVOL
000270 102 FORMAT(I10)
000270 IF (NOVOL.EQ.1) GO TO 30
000272 READ(5, 102) IDA
000300 IF (IDA.EQ.1) GO TO 30
C --- NOW PROCESS THE MAIN OBJECT LINE BY LINE
000302 READ(5, 101) MFST, MFST, MLST, NLST
000316 IF (MLST.GT.NL) NLST=NL
000321 IF (NLST.GT.NPX) NLST=NPX
000324 JLST=(MLST-MFST+1)/IBLK
000331 KLST=(NLST-MFST+1)/IBLK
000335 IF (MFST.EQ.1) GO TO 4
000337 MFMI=MFST-1
000340 DO 5 JJ=1, MFMI

```

```

000341      NB=NPX/512
000344      IF(NB.EQ.0)GO TO 40
000345      DO 41 NNG=1,NB
000347      41 READ(3)DATA
000347      40 NB=NPX-NB*512
000347      IF(NB.EQ.0)GO TO 5
000348      READ(3) (DATA(MNB),MNB=1,NB)
000372      5 CONTINUE

C *** FOR EACH VALUE OF J ZERO THE LINE ARRAY
000375      4 DO 6 J=1,JLST
000377      DO 7 K=1,KLST
000403      7 BUF(K)=0.0

C *** REDUCE IN J DIRECTION
000405      DO 8 I=1,IJLK
000406      NB=NPX/512
000411      KL=NPX-NB*512
000413      IF(NB-1) 43,45,45
000416      45 DO 51 II=1,NB
000420      KK=II*512
000422      KJ=KK-511
000424      51 READ(3) (LINE(K),K=KJ,KK)
000435      KJ=KK+1
000437      KK=KK+KL
000441      43 IF(KL-1)46,52,52
000443      KJ=1
000444      KK=KL
000446      52 READ(3) (ALINE(K),K=KJ,KK)
000455      46 IKI=NFST-1
000457      DO 9 K=1,KLST
000461      STOT=0.0

C *** REDUCE IN K DIRECTION
000462      DO 9 IK=1,IJLK
000467      IKI=IKI+1
000470      9 STOT=STOT+ALINE(IKI)
000473      8 BUF(K)=BUF(K)+STOT

C *** SORT MAX AND MIN OF OBJECT
000502      IF(J.GT.1)GO TO 10
000505      XMAX=BUF(1)
000505      XMIN=XMAX
000507      10 DO 11 K=1,KLST
000515      IF(BUF(K).GT.XMAX) XMAX=BUF(K)
000521      11 IF(BUF(K).LT.XMIN) XMIN=BUF(K)
000524      SUML(J)=0.0
000525      DO 12 K=1,KLST
000534      12 SUML(J)=SUML(J)+BUF(K)-BAX
000537      6 CONTINUE

C *** FIND TOTAL VOLUME OF OBJECT
000542      TSUM=0.0
000543      DO 13 N=1,JLST
000550      13 TSUM=TSUM+SUML(N)

C *** OUTPUT THE BACKGROUND AND TOTAL VOLUME
000552      30 WRITE(6,202) ASPT,SCDT,IJLK
000564      202 FORMAT(2(SA10/),3SH BLOCKING FACTOR USED THROUGHOUT = ,I2/,1,2GX,
1 24H BACKGROUND LEVEL ASSESSMENT ,1/,5SH AREA CO-ORDINA
ITES OF AREA MAX OF MIN OF BACKGROUND LEVEL RMS
1 1/,5SH FROM THIS AREA J1 K1 J2 K2 AREA
000564      WRITE(6,203) ((I, J1(I), K1(I), J2(I), K2(I), AMAX(I), AMIN(I), BK(I),
1 124H RMS(I)), I=1,N)
000616      203 FORMAT(4X, I2, 6X, I4, 1X, I4, 1X, I4, 1X, I4, 10X, F8.1, 2X, F8.1, 6X, F9.2, 4X,
1 F8.3)
000615      WRITE(6,204) BAX, ANS
000626      204 FORMAT(1H ,3SH BACKGROUND ASSESSED ON ALL AREAS = ,F8.2/
1 32H NOISE ASSESSED ON ALL AREAS = ,F8.3/)
000626      IF(NCVDL.EQ.1) GO TO 31
000631      IF(ADP.EQ.2) GO TO 32
000632      WRITE(6,205) NFST, NLST, NFST, NLSST, XMAX, XMIN, TSUM
000653      205 FORMAT(/, 53H AREA OF ARRAY USED FOR ASSESSING VOLUME OF OBJECT
1/7X, 4HNFST, 6X, 4HNLST, 6X, 4HNFST, 6X, 4HNLST/7X, I4, 6X, I4, 6X, I4, 6X, I4//
124H LIMITS OF ARRAY USED, /24X, 5HHIGH=,F7.1,5H LOW=,F7.1//
123H VOLUME OF OBJECT = ,F10.1)
000653      GO TO 31
000654      32 READ(5,(03)I,J,ND

```

```
000666      103 FORMAT(3I10)
000667      CALL OLE(I,J,NO,NPX,BAK)
000672      31 STOP 2
000674      END
```

UNLS:0 COMPILER SPACE  
L15116

```
000006      SUBROUTINE NOVS (A,IA,BK,RNS)
000006      DIMENSION A(IA)
000006      DEV=0.0
000007      DO 1 N=1,IA
000013      1 DEV=DEV+(A(N)-BK)*#2
000015      RP=IA-1
000022      RNS=SQRT(DEV/RP)
000031      RETURN
000032      END
```

UNLS:0 COMPILER SPACE  
E20200

```
000007      SUBROUTINE OLE(I,J,N,NPX,BK)
000007      DIMENSION ALINE(1000),DATA(S12)
000007      C * * THIS SUBROUTINE FINDS THE VOLUME OF AN OBJECT
000007      C * * CONTAINED WITHIN A CIRCULAR DIAPHRAGM CENTRE I,J DIAMETER 2N-1
000007      C * * * READ IN UNUSED LINES OF ARRAY
```

```
000007      L=I-N
000010      IF(L.EQ.0) GO TO 1
000011      DO 1 JJ=1,L
000012      NB=NPX/S12
000015      IF (NB.EQ.0) GO TO 3
000015      DO 4 NN=1,NB
000017      4 READ(3) DATA
000032      3 NB=NPX-NB*S12
000035      IF (NB.EQ.0) GO TO 1
000037      READ(3) (DATA(KK),KK=1,NB)
000051      1 CONTINUE
000053      IA=0
000053      SUM=0.0
```

C \* \* FIND VOLUME OF OBJECT AND AREA OF DIAPHRAGM

```
000054      NN=2*N-1
000057      DO 5 NL=1,NN
000061      RN=NL
000061      RL=NL
000062      RK=SQRT(0.1*(2*NL-RL))
000073      AX=RK+0.5
000074      NX=AX
000076      LX=2*NK-1
000101      NB=NPX/S12
000104      KL=NPX-NB*S12
000106      IF (NB=1) 43,45,45
000112      45 DO 51 II=1,NB
000112      KK=II*S12
000114      KJ=KK-S11
000116      51 READ(3) (ALINE(K),K=KJ,KK)
000133      KJ=KK+1
000134      KK=KK+KL
000136      IF (KL=1) 46,52,52
000141      43 KJ=1
000141      KK=KL
000143      52 READ(3) (ALINE(K),K=KJ,KK)
000155      46 IF (LX.EQ.0) GO TO 5
000156      DO 5 LX=1,LX
000163      Z=ALINE(J-NX+L)
000163      IF (NL.NE.1.AND.L.NE.1) GO TO 6
000171      XMAX=Z
000171      XMIN=XMAX
000173      6 IF (Z.LT.XMIN) XMIN=Z
000176      IF (Z.GT.XMAX) XMAX=Z
000176      SUM=SQRT(Z-BK)
000201      IA=IA+LX
000205      5 CONTINUE
000212      WRITE(6,300) I,J,NN,IA,SUM,XMAX,XMIN
000234      300 FORMAT(115H APERTURE DATA //,5H CENTRE //,4H IE //,4H JE //,
14, //,4H DIAMETER //,14,6H STEPS //,5H AREA //,16,8H SAMPLES //,
20H VOLUME OF OBJECT = ,F10.1 //,20H MAX OF DATA USED = ,F7.1 //,
320H MIN OF DATA USED = ,F7.1)
000237      RETURN
```



000240           END  
 UNUSED COMPILER SPACE  
 017300

```

SUBROUTINE SECTN (MFST,NFST,MLST,NLST,IBLK,A,NL,NPX,JLST,KLST)
C *** THIS SUBROUTINE SELECTS AND BLOCKS DATA FROM A FILE
C *** AND FEEDS IT INTO THE PLOTTING ARRAY A
000014           REAL LINE
000014           DIMENSION A(JLST,KLST), LINE(2000), DATA(512)
C *** CHECK THAT AREA FOR PLOTTING LIES WITHIN SCAN
C *** AND CALCULATE SIZE OF PLOTTING ARRAY
000014           IF (MLST.GT.NL) MLST=NL
000017           IF (NLST.GT.NPX) NLST=NPX
000022           JLST=(MLST-MFST+1)/IBLK
000026           KLST=(NLST-NFST+1)/IBLK
C *** POSITION SCAN
000032           IF (MFST.EQ.1) GO TO 2
000034           MFST=MFST-1
C *** READ IN UNUSED SCANS
000035           DO 3 J=1,MFST
C *** NOTE DATA BLOCK ON STANDARD ARCHIVE TAPE CONSISTS OF
C *** 512 WORDS WHEN FULL
000036           NB=NPX/512
000041           IF (NB.EQ.0) GO TO 42
000043           DO 41 NN=1,N
000044           41 READ (3) DATA
000057           42 NB=NPX-NB+512
000063           IF (NB.EQ.0) GO TO 3
000064           READ (3) (DATA(MNB),MNB=1,MB)
000076           3 CONTINUE
C *** ZERO PLOTTING ARRAY
000101           2 JLST=JLST*KLST
000104           DO 5 I=1,JLST
000111           5 A(I)=0.0
C *** FOR EACH VALUE OF J
000113           DO 4 J=1,JLST
C *** REDUCE IN J DIRECTION
000120           DO 6 IZ=1,IBLK
000121           NB=NPX/512
000124           KL=NPX-NB+512
000127           IF (NB-1) 43,45,45
000131           45 DO 47 II=1,NB
000133           KK=II*512
000135           KJ=KK-511
000137           47 READ (3) (LINE(K),K=KJ,KK)
000154           KJ=KK+1
000156           KK=KK+KL
000157           IF (KL-1) 46,48,48
000161           43 KJ=1
000162           KK=KL
000164           48 READ (3) (LINE(K),K=KJ,KK)
000177           46 IKI=NFST-1
000201           DO 6 K=1,KLST
000202           STOT=0.0
C *** REDUCE IN K DIRECTION
000203           DO 7 IK=1,IBLK
000210           IKI=IKI+1
000211           7 STOT=STOT+LINE(IKI)
000214           I=J+JLST+(K-1)
000223           6 A(I)=A(I)+STOT
000233           4 CONTINUE
000236           RETURN
000236           END
  
```

UNUSED COMPILER SPACE

```

PROGRAM MATCH (INPUT,OUTPUT,SCAN,ROTA,TAPES=INPUT,TAPC6=OUTPUT,
1 TAPE3=SCAN,TAPE4=ROTA,TAPE7)
000002 DIMENSION DATA(512),ALINE(1000),XA(10),YA(10),X2A(10),Y2A(10),
1 A(1000),ASDT(8),RSDF(3),SCDT(3),DENS(9),DENH(9)
C
C**** THIS PROGRAMME TAKES KNOWN CO-ORDINATES OF FIDUCIAL
C**** FEATURES IN TWO ARRAYS AND USES THEM TO PUT THE DATA
C**** FROM ONE ARRAY INTO A NEW ONE WITH THE SAME X,Y ORIENTATION
C**** AS THE ARRAY YOU ARE TRYING TO MATCH
C
000002 WRITE(6,200)
000006 200 FORMAT(1H1)
000006 READ(5,100)IUR,ISC1,ISC2
000020 100 FORMAT(I10/I10/I10)
C
C**** IUR IS USER ID, ISC1 SCAN TO WHICH ONE IS MATCHING
C**** ISC2 SCAN WHICH IS TO BE TRANSFORMED
C
000020 READ(3)IUR,ISC,NL,NPX,ASDT,SCDT,NOM,(DENS(JJ),DENH(JJ),JJ=1,NOM)
000052 IF(ISC.EQ.ISC2)GO TO 2
000054 WRITE(6,201)ISC,ISC2
000064 201 FORMAT(1H ,19H I.D.'S DON'T AGREE/X,10HTAPE ID = ,I10/
1 X,13HREQUEST ID = ,I10)
000064 STOP 1
000066 2 WRITE(6,202)ASDT,SCDT
000076 202 FORMAT(/,X,4A10,5X,9HEXPOSURE ,A10,5X,7HFILTER ,A10,5X,
1 4HDATE,A10,5X,5HPLATE,A10
1 //,1X,4A10,5X,5HSLIT ,A10,5X,10HTELESCOPE ,A10,
1 5X,5HTUBE ,A10,5X,5HFILM ,A10)
000076 READ(5,101)MFST,NFST,MLST,NLST,IBLK
000114 101 FORMAT(5I10)
000114 M=(MLST-MFST+1)/IBLK
000121 N=(NLST-NFST+1)/IBLK
000125 CALL SECTN(MFST,NFST,MLST,NLST,IBLK,A,NL,NPX,M,N)
C
C**** THIS SUBROUTINE FORMS THE ARRAY A IN MEMORY
C
000137 READ(5,102) IX,((XA(IJ),YA(IJ),X2A(IJ),Y2A(IJ)),IJ=1,IX)
000162 102 FORMAT(I10/(4F10.4))
000162 READ(5,103)IFST,LFST,ILST,LLST,ISCALE
000200 103 FORMAT(5I10)
C
C**** I AND L REFER TO THE Y AND X CO-ORDINATES OF THE ARRAY
C**** TO WHICH ONE IS MATCHING
C
000200 ISTOP=0
000201 CALL STRECH(XA,YA,X2A,Y2A,R,SC,IX,ISTOP,ISCALE)
000212 IF(ISTOP.NE.1)GO TO 4
000214 STOP 2
000216 4 REWIND 7
C
C**** EACH LINE OF THE FIRST ARRAY IS LOCATED POINT BY POINT
C**** IN THE SECOND AND A NEW ARRAY IS FORMED AND WRITTEN
C**** ON TO TAPE 7 LINE BY LINE
C
000220 IEND=ILST-IFST+1
000222 LEND=LLST-LFST+1
000224 II=IFST-1

```

```

000226      DO 10 I=1,IEND
000227      II=II+1
000230      RI=II
C
C**** BLANK THE LINE OF THE NEW ARRAY
C
000232      DO 12 KK=1,LEND
000236      12 ALINE(KK)=0.0
000240      CL=LFST-1
000242      DO 11 L=1,LEND
000243      LL=LL+1
000244      RL=LL
000246      CALL CARRY(XA,YA,X2A,Y2A,R,SC,RI,RL,X,Y)
000257      CALL FUDGIT(X,Y,Z,A,M,N)
000263      11 ALINE(L)=Z
000270      IL=LEND/512
000272      IF(IL.EQ.0)GO TO 42
000274      DO 41 IIL=1,IL
000275      KIL=IL*512
000277      KIL=KIL-511
000301      41 WRITE(7)(ALINE(LI),LI=KIL,KIL)
000313      42 ILI=LEND
000314      ILL=IL*512+1
000320      WRITE(7)(ALINE(LI),LI=ILL,ILI)
000327      10 CONTINUE
000332      END FILE 7
000334      REWIND 7
C
C**** PUT NEW ARRAY ON TO TAPE WITH IDENTIFICATION IN HEADER
C**** REPLACE SCOT WITH A NEW ARRAY RSOT WHICH CONTAINS INFORMATION
C**** ON WHICH SCAN THE NEW ARRAY HAS COME FROM AND TO WHICH ONE
C**** IT IS BEING MATCHED
C
000336      READ(5,104)RSOT
000344      104 FORMAT(8A10)
000344      REWIND 4
000346      WRITE(4) IUR,ISC,IEND,LEND,ASDT,RSOT,NDM,(DENS(JJ),DENM(JJ),
1          JJ=1,NDM)
000400      DO 14 MN=1,IEND
000402      NI=LEND/512
000405      IF(NI.EQ.0)GO TO 50
000406      DO 51 NII=1,NI
000410      READ(7) DATA
000415      51 WRITE(4) DATA
000425      50 INI=LEND-NI*512
000430      IF(INI.EQ.0)GO TO 14
000432      READ(7)(DATA(NN),NN=1,INI)
000440      WRITE(4)(DATA(NN),NN=1,INI)
000446      14 CONTINUE
000451      END FILE 4
000453      STOP 3
000455      END

UNUSED COMPILER SPACE
030100

```

```

SUBROUTINE STRECH(XA,YA,XB,YB,R,SC,IX,ISTOP,ISCALE)
DIMENSION (A(10),YA(10),XB(10),YB(10),RR(10),SCALE(10))
PI=3.1415926536
C
C**** IT WILL CALCULATE THE ROTATION AND CHECK FOR
C**** A VARIATION GREATER THAN ONE PERCENT
C
000014      P2=PI/2.0
000015      II=IX-1
000020      DO 1 I=1,II
000021          XZ=XA(I+1)-XA(1)
000023          YZ=YA(I+1)-YA(1)
000026          G=ATAN(XZ/YZ)
000037          XX=XB(I+1)-XB(1)
000041          YX=YB(I+1)-YB(1)
000044          B=ATAN(XX/YX)
000047          RR(I)=B-G
000051          IF(RR(I).GT.P2)RR(I)=RR(I)-PI
000063          IF(RR(I).LT.-P2)RR(I)=RR(I)+PI
000070          IF(I.GT.1)GO TO 2
000073          RMAX=RR(I)
000074          RMIN=RMAX
000076          2 IF(RR(I).GT.RMAX)RMAX=RR(I)
000102          1 IF(RR(I).LT.RMIN)RMIN=RR(I)
000111          RN=RMAX-RMIN
000112          VRN=(RN/(RMIN+RN/2.0))*100.0
000115          IF(VRN.LE.1.0)GO TO 3
000120          WRITE(6,30)RMAX,RMIN,(RR(JJ),JJ=1,II)
000133          30 FORMAT(1H ,16H MAX OF ANGLE = ,F7.4,16H MIN OF ANGLE = ,F7.4/
1              13H ARRAY ANGLE,/, (1H ,F10.4))
000137          ISTOP=1
000140          RETURN
000141          3 ISTOP=0
000142          RSUM=0.0
000143          DO 4 L=1,II
000150          4 RSUM=RSUM+RR(L)
000156          RI=II
000157          R=RSUM/RI
C
C**** CALCULATE SCALING FACTOR
C**** AND CHECK FOR LARGE VARIATION
C
000160      DO 5 J=1,II
000162          SCALE(J)=SQRT(((XB(J+1)-XB(J))**2+(YB(J+1)-YB(J))**2)/
1              ((XA(J+1)-XA(J))**2+(YA(J+1)-YA(J))**2))
000203          IF(J.GT.1)GO TO 5
000207          SCALEX=SCALE(1)
000207          SCALEN=SCALEX
000211          6 IF(SCALE(J).GT.SCALEX)SCALEX=SCALE(J)
000215          5 IF(SCALE(J).LT.SCALEN)SCALEN=SCALE(J)
C
C**** CHECK VARIATION IN SCALE IS LESS THAN TWO PERCENT
C
000224      SCAR=SCALEX-SCALEN
000225      VARN=(SCAR/(SCALEN+SCAR/2.0))*100.0
000230      IF(VARN.LE.2.0)GO TO 7
000233      WRITE(6,31)SCALEX,SCALEN,(SCALE(JJ),JJ=1,II)
000246      31 FORMAT(1H ,15H MAX OF SCALE =,F7.4,15H MIN OF SCALE =,F7.4/
1              12H ARRAY SCALE,/, (1H ,F10.4))
000252          ISTOP=1
000253          RETURN
000254          7 ISTOP=0
000255          IF(ISCALE.EQ.1)GO TO 8
000257          SUM=0.0
000260          DO 9 L=1,II
000266          9 SUM=SUM+SCALE(L)
000274          RIX=II
000275          SC=SUM/RIX
000276          GO TO 10
000277          8 SC=1.0
000300          10 RETURN
000301          END

```

UNUSED COMPILER SPACE  
030600

SUBROUTINE CARRY(XA,YA,XB,YB,R,SC,RI,RL,X,Y)

```

C
C**** THIS SUBROUTINE PERFORMS THE TRANSFORMATION OF THE
C**** CO-ORDINATES RI,RL, TO Y AND X RESPECTIVELY
C
000014      DIMENSION XA(10),YA(10),XB(10),YB(10)
000014      XN=RL-XA(1)
000016      YN=RI-YA(1)
000020      VN=(XN*COS(R)+YN*SIN(R))*SC
000037      WN=(YI*COS(R)-XN*SIN(R))*SC
000057      X=VN+XB(1)
000060      Y=WN+YB(1)
000063      RETURN
000064      END

```

UNUSED COMPILER SPACE  
031700

SUBROUTINE FUGGIT (X,Y,Z,A,M,N)

```

C
C**** THIS SUBROUTINE INTERPOLATES TO FIND THE NUMBER AT POINT
C**** X,Y OF THE ARRAY BEING TRANSFORMED
C
C          J1,K1*****J1,K2
C          *           *
C          *           *
C          *           *
C          *           *
C          J2,K1*****J2,K2
C
000010      DIMENSION A(M,N)
000010      J1=Y
000011      K1=X
000013      J2=J1+1
000015      K2=K1+1
000016      RJ1=J1
000017      RK1=K1
000017      Y1=A(J1,K1)+(A(J2,K1)-A(J1,K1))*(Y-RJ1)
000032      Y2=A(J1,K2)+(A(J2,K2)-A(J1,K2))*(Y-RJ1)
000044      Z=Y1+(Y2-Y1)*(X-RK1)
000050      Z=Z*0.5
000051      IZ=Z
000052      Z=IZ
000053      RETURN
000054      END

```

UNUSED COMPILER SPACE  
031700

```

SUBROUTINE SECTN (MFST,HFST,HLST,HLST,IBLK,A,NL,NPX,JLST,KLST)
C
C**** THIS SUBROUTINE SELECTS AND BLOCKS DATA FROM A FILE
C**** AND FEEDS IT INTO THE PLOTTING ARRAY A
C
000014 REAL LINE
000016 DIMENSION LINE(2000),DATA(512),A(JLST,KLST)
C
C**** CHECK THAT AREA FOR PLOTTING LIES WITHIN SCAN
C**** AND CALCULATE SIZE OF PLOTTING ARRAY
C
000014 IF (HLST.GT.NL)KLST=NL
000017 IF (HLST.GT.NPX)HLST=NPX
000022 JLST=(HLST-MFST+1)/IBLK
000026 KLST=(HLST-HFST+1)/IBLK
C
C**** POSITION SCAN
C
000032 IF (MFST.EQ.1) GO TO 2
000034 MFHI=MFST-1
C
C**** READ IN UNUSED SCANS
C
000035 DO 3 J=1,MFHI
C
C**** NOTE DATA BLOCK ON STANDARD ARCHIVE TAPE CONSISTS OF
C**** 512 WORDS WHEN FULL
C
000036 NB=NPX/512
000041 IF (NB.EQ.0) GO TO 42
000043 DO 41 NNB=1,NB
000044 41 READ (3) DATA
000057 42 NB=NPX-NB*512
000063 IF (NB.EQ.0) GO TO 3
000064 READ (3) (DATA(NNB),NMB=1,NB)
000076 3 CONTINUE
C
C**** ZERO PLOTTING ARRAY
C
000101 2 ILST=JLST*KLST
000104 DO 5 I=1,ILST
000111 5 A(I)=0.0
C
C**** FOR EACH VALUE OF J
C
000113 DO 4 J=1,JLST
C
C**** REDUCE IN J DIRECTION
C
000120 DO 6 IZ=1,IBLK
000121 NB=NPX/512
000124 KL=NPX-NB*512
000127 IF (NB-1)43,44,45
000132 44 READ (3) (LINE(K),K=1,512)
000137 GO TO 46
000143 45 DO 47 II=1,NB
000145 KK=II*512
000147 KJ=KK-511
C
000151 47 READ (3) (LINE(K),K=KJ,KK)
000166 KJ=KK+1
000170 KK=KK+KL
000171 IF (KL-1)46,48,48
000173 43 KJ=1
000174 KK=KL
000176 48 READ (3) (LINE(K),K=KJ,KK)
000211 46 IKI=MFST-1
000214 DO 6 K=1,KLST
000216 STOT=0.0
C
C**** REDUCE IN K DIRECTION
C
000216 DO 7 IK=1,IBLK
000222 IKI=IKI+1
000223 7 STOT=STOT+LINE(IKI)
000226 I=JLST*(K-1)
000230 6 A(I)=A(I)+STOT
000245 4 CONTINUE
000250 RETURN
000250 END

```

```

PROGRAM FOW INPUT, OUTPUT, SCAN, TAPE5=INPUT, TAPE6=OUTPUT, TAPE3=SCAN)
DIMENSION ALINE(2000), X(2000), R(100), GX(100), FX(100), DATA(512),
1 ASDT(8), SCDT(8), DENS(9), DENH(9)
1 BLINE(500)
WRITE(6, 200)
200 FORMAT(1H1)
DO 30 IJ=1, 500
BLINE(IJ)=0.0
READ(3) IOR, ISC, NL, NFX, ASDT, SCDT, NDH, (DENS(JJ), DENH(JJ), JJ=1, NDH)
WRITE(6, 201) ASDT, SCDT
201 FORMAT(2(5A10/))
READ(5, 100) ISCP
180 FORMAT(I10)
IF(ISC.EQ.ISCP) GO TO 1
WRITE(6, 211) ISC, ISCP
211 FORMAT(1H, 23H FILE IDIS DON'T AGREE, /, 11H TAPE ID = , I5, 5X,
1 11H CARD ID = , I5)
STOP 1
1 READ(5, 101) N, M, K, H, D
101 FORMAT(3L10/F10.2, F10.6)
K1=K+1
M1=M+1
RN=N
RM=M
FC=1000.0/(2.0*M1)
BE=1000.0/(2.0*M1)
E=SQRT(RN/RM)
WRITE(6, 210) N, M, H, FC, BE, E
210 FORMAT(1H, 10X, 4H AUTO-CORRELATION AND NOISE POWER CALCULATIONS,
1 //, 25H NUMBER OF POINTS USED = , I4, //,
2 45H MAX NUMBER OF CORRELATION LAG VALUES USED = , I3, //,
3 21H SAMPLING INTERVAL = , F3.0, 8H MICRONS, //,
4 20H CUTOFF FREQUENCY = , F4.0, 8H CYCLES/INH, //,
5 34H EQUIVALENT RESOLUTION BANDWIDTH = , F5.2, 10H CYCLES/INH,
6 //, 36H UNANALYSED STANDARD ERROR ON NPS = , F5.3, //)
NR=0
READ(5, 100) IX
14 READ(5, 100) IY
NR=NR+IY
NB=NPK/ST2
NNB=NPK-NB*ST2
DO 2 I=1, IY
IF(NB.EQ.0) GO TO 4
DO 3 L=1, NB
3 READ(3) DATA
4 IF(NNB.EQ.0) GO TO 2
READ(3) (DATA(KK), KK=1, NNB)
2 CONTINUE
READ(5, 100) IYI
IYI=IYI
DO 5 J=1, IYI
NR=NR+1
IF(NNB.EQ.0) GO TO 6
DO 7 LL=1, NB
KK=LL*ST2
KJ=KK-ST1
7 READ(3) (ALINE(KL), KL=KJ, KK)
GO TO 8
8 IF(NNB.EQ.0) GO TO 9
KJ=KK+1
KK=KK+NB
READ(3) (ALINE(KL), KL=KJ, KK)
DO 31 IZ=1, KK
31 BLINE(IZ)=BLINE(IZ)+ALINE(KL)
9 CONTINUE
6 CONTINUE
DO 32 IT=1, KK
32 BLINE(IT)=BLINE(IT)/REYI
CALL NEWA(BLINE, N, A, IX, D)
CALL AUTO(X, M, N, R, M1)
CALL NPS(R, GX, GXS, K, H, M, M1, K1)
WRITE(6, 202) NR, IX
202 FORMAT(1H, 14H LINE NUMBER = , I4, 5X, I3,
1 27H POINTS HITTED AT BEGINNING .)
CALL CHK(GX, R, K, M1, K1, H)
DO 11 KA=1, K1
F=FLOAT(KA-1)*FC/FLOAT(M)
GN=GX(KA)/GX(1)
GNS=GXS(KA)/GXS(1)
11 WRITE(6, 205) F, GX(KA)
205 FORMAT(1H, 21H SPATIAL FREQUENCY = , F6.2, 10H CYCLES/INH, //,

```

```

000001      1 X, 18H SMOOTHED NPS = , F9.6, / 1)
000002      READ(5, 100) IEND
000003      IF (IEND.EQ.3) GO TO 12
000004      GO TO 14
000005  12 STOP
000006      END

```

```

UNLSDF (C) 1965
000000

```

```

000007      SUBROUTINE NEWX(A, N, X, M, D)
000008      DIMENSION A(N), X(N)
000009      RMN=0.0
000010      DO 1 I=1, N
000011      1 RMN=RMN+A(M+I)
000012      RN=N
000013      RMN=RMN/RN
000014      DO 2 J=1, N
000015      2 X(J)=(A(M+J)-RMN)*D
000016      RETURN
000017      END

```

```

UNLSDF (C) 1965
000000

```

```

000018      SUBROUTINE NPS(R, QX, QXS, K, H, M, MI, KK)
000019      DIMENSION R(M), QX(KK), QXS(KK)
000020      PI=3.14159265

```

```

C ***** K IS HARMONIC VALUE UPPER LIMIT
C

```

```

000021      DO 1 L=1, KK
000022      1 LK=L-1
000023      QX(L)=R(1)
000024      QXS(L)=R(1)
000025      DO 2 J=2, M
000026      2 RJ=FLOAT(J-1)
000027      RK=LK
000028      RM=M
000029      AN=PI*RJ/RM
000030      ANG=AN+RK
000031      D=(1.0+COS(AN))/2.0
000032      QX(L)=QX(L)+2.0*R(J)*COS(ANG)
000033      QXS(L)=QXS(L)+2.0*D*R(J)*COS(ANG)
000034      QX(L)=QX(L)+(1.0-LK)*R(M)
000035      QX(L)=QX(L)*2.0*H
000036      1 QXS(L)=QXS(L)+2.0*H
000037      RETURN
000038      END

```

```

UNLSDF (C) 1965
000000

```

```

000039      SUBROUTINE AUTO(X, M, N, R, MH)
000040      DIMENSION X(N), R(MH)
000041      (****) SET UP LOOP FOR DIFFERENT DISPLACEMENTS

```

```

000042      RN=N
000043      DO 1 I=1, MH
000044      1 R(I)=0.0
000045      II=I-1
000046      NN=N-II
000047      DO 2 J=1, NN
000048      2 R(I)=R(I)+X(J)*X(J+II)
000049      RNN=NN
000050      1 R(I)=R(I)/RNN
000051      RETURN
000052      END

```

```

UNLSDF (C) 1965
000000

```

```

000053      SUBROUTINE CUR(CX, R, K, MM, KE, H)
000054      DIMENSION R(MM), CX(KK)
000055      M=MM-1
000056      K=K
000057      SUM=0.0
000058      DO 20 I=2, K
000059      20 SUM=SUM+CX(I)
000060      SUM=(SUM+CX(1)+CX(KE))/2.0

```

```

000061      COM=SUM/(2.0*H*MM)
000062      RSUM=SUM/R(1)
000063      WRITE(6, 220) R(1), SUM, RSUM
000064      220 FORMAT(14, '18H CHECK OF PROGRAM , 1, X, 9H R(1) = , F10.7, /,
000065      1 X, 9H QSUM = , F10.7, /, X, 10H RATIO = , F6.3, / 1, /)
000066      RETURN
000067      END

```

```

UNLSDF (C) 1965
000000

```



References

A.E.E.P. represents Advances in Electronics and Electron Physics  
(Academic Press).

1. Kiepenheuer, K.O., Die Sterne, 9, 190 (1934).
2. Kron, G.E., Ables, H.D., Hewitt, A.V., A.E.E.P., 28 A, 1 (1969).
3. Lallemand, A., A.E.E.P., 22A, 1 (1966).
4. McGee, J.D., Bacik, H., Coleman, C.I., Morgan, B.L., A.E.E.P., 33A,  
13 (1972).
5. McMullan, D., Powell, J.R., Curtis, N.A., A.E.E.P., 33A, 37 (1972).
6. Coleman, C.I., Ph.D Thesis, University of London (1974).
7. Kahan, E., Cohen, M., A.E.E.P., 28B, 725 (1969).
8. Griboval, P., Griboval, D., Marin, M., Martinez, J., A.E.E.P., 33A,  
67 (1972).
9. Walker, M.F., Proceedings of the Conference on Electronography and  
Astronomical Applications, Austin, Texas, 1 (1974).
10. Aller, L.H., Walker, M.F., Ap.J., 161, 917 (1970).
11. Walker, M.F., Chincarini, G., Ap.J., 154, 157 (1968).
12. Lallemand, A., Comptes Rendues, 203, 243 and 990 (1936).
13. Lallemand, A., Duchesne, M., Walker, M.F., Pub.A.S.P., 72, 76 (1960).
14. Walker, M.F., Ap.J., 136, 695 (1962).
15. Walker, M.F., Ap.J., 151, 71 (1968).
16. Chincarini, G., Walker, M.F., Proceedings of the Conference on  
Electronography and Astronomical Applications, Austin, Texas,  
249 (1974).

17. Walker, M.F., *Astronomical Journal*, 73, 854 (1968).
18. Walker, M.F., *Ap.J.*, 175, 89 (1972).
19. Aller, L.H., Walker, M.F., *Ap.J.*, 141, 1318 (1965).
20. Aller, L.H., Walker, M.F., *Ap.J.*, 161, 917 (1970).
21. McGee, J.D., Khogali, A., Baum, W.A., Kraft, R.P., *M.N.R.A.S.*, 137, (1967).
22. Walker, M.F., *Proceedings of the Conference on Electronography and Astronomical Applications*, Austin, Texas, 221 (1974).
23. Palmer, D., Milson, A.S., *A.E.E.P.*, 33B, 769 (1972).
24. Wynne, C.G., Kidger, M.J., *A.E.E.P.*, 28B, 759 (1969).
25. Fosbury, R., *M.N.R.A.S.*, 169, 147 (1974).
26. Tritton, K.P., Henbest, S.N., Penston, M.V., *M.N.R.A.S.*, 162, 31p (1973).
27. Reay, N.K., Private communication (1975).
28. Walker, M.F., *Ap.J.*, 161, 385 (1970).
29. Walker, M.F., *Ap.J.*, 167, 1 (1971).
30. Walker, M.F., *M.N.R.A.S.*, 156, 459 (1972).
31. Walker, M.F., *M.N.R.A.S.*, 159, 379 (1972).
32. Walker, M.F., *M.N.R.A.S.*, 169, 199 (1974).
33. Walker, M.F., Kron, G.E., *Pub.A.S.P.*, 79, 551 (1967).
34. Hewitt, A.V., *Pub.A.S.P.*, 81, 541 (1969).
35. Ables, H.D., Hewitt, A.V., Kron, G.E., *Pub.A.S.P.*, 81, 530 (1969).
36. Walker, M.F., *Proceedings of ESO/CERN Conference on Auxiliary Instrumentation for Large Telescopes*, 339 (1972).
37. Whitford, A.E., *Handbuch der Physik*, 54, 240 (1962).

38. Wlérick, G., Michet, D., Labeyrie, C., Proceedings of the Conference on Electronography and Astronomical Applications, Austin, Texas, 117 (1974).
39. Cullum, M.J., Stephens, C.L., A.E.E.P., 33B, 757 (1972).
40. Zinn, R.J., Newell, E.B., A.A.S. Photobulletin, 2, 6 (1972).
41. Newell, E.B., O'Neill, E.J., Proceedings of the Conference on Electronography and Astronomical Applications, Austin, Texas, 153 (1974).
42. Newell, E.B., Proceedings of ESO/CERN Conference Research Programmes For New Large Telescopes, 347 (1974).
43. Heckathorn, H., Chincarini, G., Proc. S.P.I.E., 42, 147 (1973).
- 44a. Purgathofer, A.Th., Proceedings of the Conference on Electronography and Astronomical Applications, Austin, Texas, 199 (1974).
44. Ables, H.D., Kron, G.E., Ap.J., 181 (1973).
45. Walker, M.F., A.E.E.P., 33B, 697 (1972).
46. Ables, H.D., Ables, P.G., Astronomical Journal, 77, 642 (1972).
47. Ables, H.D., Ables, P.G., A.A.S. Photobulletin, 2, 8 (1972).
48. Kron, G.E., Ables, H.D., Hewitt, A.V., Pub.A.S.P., 84, 303 (1972).
49. Wlérick, G., Proceedings of the Conference on Electronography and Astronomical Applications, Austin, Texas, 323 (1974).
50. Lelièvre, G., Proceedings of the Conference on Electronography and Astronomical Applications, Austin, Texas, 323 (1974).
51. Wray, J.D., Benedict, G.F., Proc. S.P.I.E., 44, 137 (1974).
52. Benedict, G., Chincarini, G., Heckathorn, H., Wray, J., Proceedings of the Conference on Electronography and Astronomical Applications, Austin, Texas, 205 (1974).

53. Chincarini, G., Heckathorn, H., Proceedings of the Conference on Electronography and Astronomical Applications, Austin, Texas, 343 (1974).
54. Jones, W., Obitts, D., Gallet, R., de Vaucouleurs, G., Pub.Dept. Astron.Univ.of Texas, Series 11, 1, 8. (1967).
55. Gull, T.R., Proceedings of the Conference on Electronography and Astronomical Applications, Austin, Texas, 273 (1974).
56. Bacik, H., Ph.D Thesis, University of London (1973).
57. McGee, J.D., Vistas in Astronomy, 15, 61 (1973).
58. McGee, J.D., Coleman, C.I., Phillips, E.G., Nature, 241, 264 (1973).
59. Coleman, C.I., Presented at Sixth Symposium on Photoelectronic Imaging Devices, London (1974). To be published in A.E.E.P.
60. Smyth, M., Brand, P., A.E.E.P., 28B, 737 (1969).
61. Oliver, M., A.E.E.P., 33A, 27 (1972).
62. Oliver, M., Ph.D Thesis, University of London (1970).
63. Brand, P.J.L.W., Ph.D Thesis, University of Edinburgh (1967).
64. Cohen, M., Ph.D Thesis, University of London (1972).
65. Harwood, J.A., Ph.D Thesis, University College of North Wales, Bangor (1972).
66. Cohen, M., Kahan, E., A.E.E.P., 33A, 53 (1972).
67. Kron, G.E., Papiashvili, I.I., Pub.A.S.P., 79, 9 (1967).
68. Ables, H.D., Kron, G.E., Pub.A.S.P., 79, 423 (1967).
69. Valentine, R.C., Advances in Optical and Electron Microscopy, 1, 180 (1966).
70. Silberstein, L., Trivelli, A., J.O.S.A., 28, 441 (1938).

71. Shaw, R., J.Phot.Sci., 17, 141 (1969).
72. Pilkington, J.D.H., Interim report on requirements of measuring machines at R.G.O. (1972).
73. Cullum, M.J., Private Communication (1973).
74. Scott, E., Scott, R.M., Schack, R.V., Phot.Sci.Eng., 7, 345 (1963).
75. McGee, J.D., McMullan, D., Bacik, H., Oliver, M., A.E.E.P., 28A, 61 (1969).
76. Coleman, C.I., Reay, N.K., Worswick, S.P., Presented at Sixth Symposium on Photoelectronic Imaging Devices, London (1974).  
To be published in A.E.E.P.
77. Reay, N.K., Ring, J., Scaddan, R.J., J.Phys.E:Sci.Inst., 7, 673 (1974).
78. Walker, M.F., Sky and Telescope, 40, 132 (1970).
79. Dainty, J.C., Scaddan, R.J., M.N.R.A.S., 167, 69p (1974).
80. Stephens, C.L., Private Communication (1974).
81. Osterbrock, D.E., 18th Liège Astrophys. Symposium, 391 (1973).
82. Cahn, J.H., Kaler, J.B., Ap.J. Supplement, 189, no.22, 319 (1971).
83. Weidemann, V., Zs fur Ap., 67, 286 (1967).
84. Weidemann, V., I.A.U. Symposium no.34 "Planetary Nebulae", 423 (1968).
85. Miller, J.S., Ann.Rev.Astron. and Astrophys. (1974).
86. Perek, L., I.A.U. Symposium no.34 "Planetary Nebulae", 9 (1968).
87. Aller, L.H., Liller, W., Nebulae and Interstellar Matter, ed.  
B.H. Middlehurst and L.H. Aller (Chicago: University of Chicago Press) (1968).
88. Lucy, L.B., Astronomical Journal, 72, 813 (1967).

89. Paczynski, B., Ziolkowski, J., I.A.U. Symposium no.34 "Planetary Nebulae", 396 (1968).
90. Wilson, O.C., Ap.J., 111, 279 (1950).
91. Rose, W.K., I.A.U. Symposium no.34 "Planetary Nebulae", 390 (1968).
92. Smith, R.L., Rose, W.K., Ap.J., 176, 395 (1972).
93. Faulkner, D.J., Ap.J., 162, 573 (1970).
94. Finzi, A., Woolf, R.A., Astronomy and Astrophys., 11, 415 (1971).
95. Gurzadian, G.A., Planetary Nebulae, Gordon and Breach (1967).
96. Kaler, J.B., Astronomical Journal, 79, 594 (1974).
97. Faulkner, D.J., Bessel, M.S., Pub.A.S.P., 82, 1333 (1970).
98. Herbig, G.H., Boyarchuk, A.A., Ap.J., 152, 397 (1968).
99. Herbig, G.H., Boyarchuk, A.A., I.A.U. Symposium no.34 "Planetary Nebulae", 383 (1968).
100. Flannery, B.P., Herbig, G.H., Ap.J., 183, 491 (1973).
101. Seaton, M.J., Reports of Progress in Physics, 23, 113 (1960).
102. Bowen, I.S., Pub.A.S.P., 46, 146 (1934).
103. Mayer, M.G., Ann.d'Phys., 9, 273 (1931).
104. Spitzer, L., Greenstein, J.L., Ap.J., 114, 407 (1951).
105. Aller, L.H., Czyzak, S., 18th Liège Symposium, 285 (1973).
106. Williams, R.E., I.A.U. Symposium no.34 "Planetary Nebulae", 190 (1968).
107. Flower, D.R., M.N.R.A.S., 146, 243 (1969).
108. Harrington, J.P., Ap.J., 156, 903 (1969).
109. Kirkpatrick, R.C., Ap.J., 176, 381 (1972).
110. Boeshaar, G.O., Ap.J., 187, 238 (1974).

111. Curtis, H.D., Lick Observatory publication, 13, 57 (1918).
112. Stoy, R., Observatory, 56, 269 (1933).
113. Vorontsov-Velyaminov, B.A., Astronomical Journal (U.S.S.R.), 11,  
40 (1934).
114. Thackeray, A.D., Evans, D.S., M.N.R.A.S., 10, 429 (1950).
115. Westerlund, B.E., Henize, K.G., Ap.J. Supplement Series Volume XIV,  
154 (1967).
116. Hromov, G.S., Kohoutek, L., B.A.C., 19, 1 (1968).
117. Duncan, J.C., Ap.J., 86, 496 (1937).
118. Wilson, O.C., Rev.Mod.Phys., 30, 1025 (1958).
119. Hromov, G.S., Kohoutek, L., B.A.C., 19, 81 (1968).
120. Wilson, O.C., Aller, L.H., Ap.J., 114, 421 (1951).
121. Aller, L.H., Gaseous Nebulae (London. Chapman Hall) (1956).
122. Minkowski, R., Osterbrock, D., Ap.J., 131, 537 (1970).
123. Evans, D.S., M.N.R.A.S., 110, 37 (1950).
124. Zanstra, H., Brandenburg, W.J., B.A.N., 11, 350 (1951).
125. Scott, P.F., M.N.R.A.S., 161, 35p (1971).
126. Van Blerkom, P., Arny, T.T., M.N.R.A.S., 156, 91 (1972).
127. Capriotti, E.R., Ap.J., 179, 495 (1973).
128. Feibelman, W.A., R.A.S.C. Journal, 64, 305 (1970).
129. Ford, W.K., Rubin, V.C., Astrophysical Letters, 8, 67 (1971).
130. Capriotti, E.R., Cromwell, R.H., Williams, R.E., Astrophysical Letters,  
7, 241 (1971).
131. Millikan, A.G., Astronomical Journal, 79, 1259 (1974).

132. Coleman, C.I., Reay, N.K., Worswick, S.P., M.N.R.A.S., In Press (1975).
133. Baum, W.A., Astronomical Techniques ed. W.A. Hiltner, (Chicago: University of Chicago Press) (1968).
134. Münch, G., I.A.U. Symposium no.34 "Planetary Nebulae", 259 (1968).
135. Terzian, Y., Balick, B., Bignell, C., Ap.J., 188, 251 (1974).
136. Woolf, N.J., Ap.J. (Letters), 157, L37 (1969).
137. Youll, D.P., Private Communication (1975).
138. Bendat, J.S., Piersol, A.G., Random Data: Analysis and Measurement Procedures, Wiley (1971).
139. Dainty, J.C., Shaw, R., Image Science, Academic Press (1974).
140. Blackman, R.B., Tukey, J.W., The Measurement of Power Spectra, Dover (1968).
141. McKay, C.D., Private Communication (1974).
142. Wlérick, G., Private Communication (1974).